Nano-agglomerated capillary polymer monoliths for applications in micro-catalysis and separation science

By

Patrick Gerard Floris

Under the supervision of

Dr. Damian Connolly (PMBRC, WIT),

Prof. Apryll Stalcup (ISSC, DCU) and

Prof. Brett Paull (ACROSS, University of Tasmania)

A thesis submitted to Dublin City University for consideration for the degree of:

Doctor of Philosophy

Dublin City University

School of Chemical Sciences

August 2013

I hereby certify that this material, which I now submit for assessment on the programme of study leading to the award of *Doctor of Philosophy* is entirely my own work, that I have exercised reasonable care to ensure that the work is original, and does not to the best of my knowledge breach any law of copyright, and has not been taken from the work of others save and to the extent that such work has been cited and acknowledged within the text of my work.

Signed: _____

ID No.: 59108151

Date: 06/09/2013

Table of Contents

List of Abbreviations

AIBN	Azobisisobutyronitrile
AMPS	2-acrylamide-2-methyl propane sulfonic acid
AuNP	Gold nano-particle
BET	Brunauer, Emmett and Teller
BGE	Background electrolyte
BuMA	Butyl methacrylate
CE	Capillary electrophoresis
CEC	Capillary electro-chromatography
CIM	Convective interaction media
COC	Cyclic olefin copolymer
CZE	Capillary zone electrophoresis

DAP	2,2-dimethoxy-2-phenylacetophenone
DHDAB	dihexadecyldimethyl ammonium bromide
DVB	Divinylbenzene
EDMA	Ethylene dimethacrylate
EDX	Energy dispersive x-ray spectroscopy
FE-SEM	Field emission-scanning electron microscopy
GMA	Glycidyl methacrylate
HIS	L(-)-histidine
I.D	Internal diameter
IC	Ion-exchange
LC	Liquid chromatography
LMA	Lauryl methacrylate
MES	2-(N-morpholino)ethanesulfonic acid
NP	Nano-particle
NF	Nano-flower
NSA	N-Succinimidyl acrylate
O.D.	Outer diameter
PAA	Poly(acrylic acid)
PEGDA	Poly(ethylene glycol) diacrylate
PDADMAC	Polydiallyldimethylammonium chloride
PdNPs	Palladium nano-particles
PSS	Poly(sodium 4-styrene sulfonate)
RP	Reversed-phase

sC^4D	Scanning capacitively coupled contactless conductivity detection
SEMA	Sulfoethylmethacrylic acid
SEM	Scanning electron microscopy
SiNP	Silica nano-particle
SPE	Solid-phase extraction
SPM	3-sulfopropylmethacrylate
TRIS	Tris(hydroxymethyl)aminomethane
UHPLC	Ultra high performance liquid chromatography
VAL	Vinyl azlactone

List of Figures

Figure 1.6: *Common functional monomers used for the preparation of polymer monoliths. A: acrylamide, B: 2-acrylamido-2-methyl-1-propanesulphonic acid, C: glycidyl methacrylate, D: 2-vinyl-4,4-dimethylazlactone, E: styrene, F: butyl methacrylate.*

Figure 1.7: *Effects of porogens on pore size in (a) a GMA-co-EDMA monolith with a cyclohexanol-dodecanol ratio of (1) 60/0, (2) 57/3, (3) 54/6, (4) 45/15 and (b) a PS-co-DVB monolith with a dodecanol/toluene ratio of (1) 60/0, (2) 50/10, (3) 45/15, (4) 40/20.*

Figure 1.8: *Examples of commonly used cross-linkers, A: ethylene dimethacrylate, B: divinyl benzene.*

Figure 1.9: *Effects of temperature on porous structure of (a) a GMA-co-EDMA monolith at (1) 80, (2) 70 and (3) 55 °C and (b) a PS-co-DVB monolith at Pore size distrubution of GMA-co-EDMA prepared at (1) 80, (2) 70 and (3) 60 °C.*

Figure 1.10*: Free-radical initiators (a) AIBN and (b) DAP commonly used for the preparation of polymer monoliths.*

Figure 1.11: *Schematic showing the reaction of a monolith with azlactone moieties with the amine groups on trypsin.*

Figure 1.12: *Schematic of the grafting process illustrating (a) the formation of polymer chains on the pre-formed monolith, (b) an intermediate stage where extensive branching occurs and (c) termination stage where inter-branching connections occur.*

Figure 1.13: *Image showing the photoreduction reactivity order for 5 different types of hydrogens.*

Figure 1.14: *Schematic illustrating the 2-step grafting process of a reactive monomer in the presence of benzophenone as the photoinitiator. (1) In a first step, photoinitiator is immobilised on the pore surface by UV irradiation of a polymer monolith that is in contact with the benzophenone solution. (2) In a second step, UV-initiated grafting is carried out with a solution containing a monomer only.*

Figure 1.15: *(a) silanol groups present on the inner surface of fused silica capillaries and (b) modification of silanol groups with 3-methacryloyloxypropyl trimethoxysilane.*

Figure 1.16: *CEC separations of alkylbenzenes on polymer monoliths prepared with an average pore size of (a) 4000 nm, (b) 1230 nm and (c) 670 nm. Peaks: thiourea (1), benzyl alcohol (2), benzaldehyde (3), benzene (4), toluene (5), ethylbenzene (6), propylbenzene (7), butylbenzene (8), and amylbenzene (9). Mobile phase, 80:20 v/v mixture of acetonitrile and 5 mM phosphate buffer pH 7; UV detection at 215 nm.*

Figure 1.17: *Image showing (a) the separation of alkylbenzenes on a methacrylate capillary column (139 x 0.32 mm) and (b) a column packed with Biosphere C_{18} beads (141 x 0.32 mm). Mobile phase: 70% aqueous acetonitrile, flow rate 2.0-2.2 µL/min, UV detection at 254 nm. Peaks: (1) uracil, (2) benzyl alcohol, (3) benzaldehyde, (4) benzene, (5) toulene, (6) propylbenzene, (7) butylbenzene, (8) amylbenzene.*

Figure 1.18: *Schematic showing the integration of a on-line SPE monolithic device with a separation column.*

Figure 1.19: *Polymer monoliths in pipette tips in a 96-well format.*

Figure 1.20*: Images of (a) ProSwift column from Thermo Scientific and (b) monolithic CIM disk from Bia Separations.*

Figure 1.21*: Images showing (a) SEM of a BuMA-co-EDMA-co-AMPS monolith, (b) SEM of a similar monolith with latex nano-particles attached, (c) a chromatogram showing the separation of 7 carbohydrates using a latex nano-particle modified monolith. Peaks: (1) d(+)galactose , (2) d(+)glucose, (3) d(+)xylose, (4) d(+)mannose, (5) maltose, (6) d(−)fructose, (7) sucrose. Injection volume 100 nL; sample concentration 1 mg/mL.*

Figure 1.22: *Chromatograms showing the separation of a 7-anion mixture using latex nano-particle functionalised GMA monoliths which had been modified with (a) 4-hydroxybenzenesulphonic acid and (b) sodium sulphite. Analytes: (1) IO_3^-, (2) BrO_3^-, (3) NO_2^-, (4)Br^-, (5)NO_3^-, (6) I^- and (7) benzenesulphonate. Concentrations: 0.14 mM.*

***Figure 1.23**: Images showing (a) a SEM of the uncoated silica monolithic, (b) a SEM of the latex nano-particle silica monolithic structure and (c) IE-CEC separations of inorganic anions on a latex-coated silica monolith when the concentration of perchlorate as competing anion was varied. Detection was performed on-column using a 33.4 cm × 50 µm i.d. latex nano-particle coated silica monolith. BGE: Tris/ClO_4 at varying concentrations; voltage: −15 kV; temperature: 25 °C; UV detection: 195 nm.*

***Figure 1.24**: Chromatograms showing the retention of m-nitroaniline on GMA-co-EDMA monoliths in (a) the absence and (b) the presence of 30 wt % MWCNTs Mobile phase: 0.1 mM Tris–HCl buffer pH 7.4, 10 mM $MnCl_2$. Flow rate: 0.4 mL/min. Column temperature: 25 °C. Detection wavelength: 372 nm.*

***Figure 1.25**: Chromatograms showing the separation of small molecules on (top) a carbon nano-tube modified silica monolith and on (bottom) a bare C_{18} Chromolith column. Analytes: (1) Phenol, (2) aniline, (3) cathecol, (4) 4-methoxy-phenol, (5) 4-ethoxy-phenol, (6) 4-propioxy-phenol, (7) 3-nitro-phenol, (8) 2,3-dihydroxynaphthalene, (9) 1,3-dihydroxynaphthalene, (10) 2,3-dinitronaphthalene and (11) 1,3 dinitronaphthalene. Mobile phase: ACN/H_2O (60/40)(v/v). Flow rate: 8.5 mL/min. Column temperature: 25 °C. UV detection at 254 nm.*

***Figure 1.26**: SEM micrographs of monolithic columns containing hydroxyapatite nano-particles at a nano-particle/monomer ratio of (A) 0/50, (B)30/50, and (C) 60/50 (magnification 10,000x) and corresponding energy-dispersive X-ray spectroscopy (EDX) spectra.*

***Figure 1.27**: SEM images of a silica monolith modified with BSA-AuNPs.*

***Figure 1.28**: Image showing a polymer monolith functionalised with AgNPs for SERS applications.*

***Figure 1.29**: Image showing (a) a DVB monolith in tip format with immobilised TiO2/ZrO2 nano-particles, (b) and (c) the automated system developed for optimising the enrichment of phosphopeptides.*

***Figure 1.30**: Silica monoliths (a) before and (b) after modification with PdNPs.*

***Figure 1.31**: Schematic showing a PASSflow* (*Polymer Assisted Solution-Phase Synthesis flow-through mode) system. A monolith is placed in a glass rod which can be integrated with a HPLC system.*

***Figure 1.32**: Schematic showing the immobilisation of PdNPs on a PASSflow (Polymer Assisted Solution-Phase Synthesis flow-through mode) system.*

***Figure 1.33**: (left) Raschig rings and (right) a Raschig ring inserted in a PASSflow (Polymer Assisted Solution-Phase Synthesis flow-through mode) reactor.*

***Figure 1.34**: Schematic illustrating a series of coupling reactions. Suzuki-Miyaura reactions involve the reaction between an aryl-vinyl boronic acid with an aryl-vinyl halide. Sonogashira reactions involving terminal alkyne and aryl/vinyl halide. Heck coupling involve the reaction of a unsaturated halide with an alkene. * All reactions performed in the presence of a base, a Pd/Pt based calyst and at elevated temperatures.*

***Figure 1.35**: Schematic showing the immobilisation of nano-particles on (a) a monolith prepared by ROMP polymerisation of (Z)-9 oxabicyclo[6.1.0]non-4-ene (OBN) and tris(cyclooct-4-en-1-yloxy)methylsilane and (b) a glycidyl methacrylate monoliths cross-linked with trimethylolpropan triacrylate (TMPTA) prepared using electro beam-triggered polymerisation.*

***Figure 1.36**: Glass discs 20 x 10 mm i.d. used as housings for monoliths prepared by ROMP and subsequent loading with PdNPs.*

***Figure 1.37**: Image showing the schematic of C^4D electrodes with l: electrode length and d: distance gap between electrodes.*

***Figure 1.38:** Schematic showing the circuitry of a C^4D cell where C: cell capacitance formed by the 2 electrodes, R: resistance from electrolyte inside capillary, C_0: stray capacitance, R_f: feedback resistor on the pick-up amplifier.*

***Figure 1.39:** (left) Bode plot illustrating the effect of electrode length (l) on operating frequency, (right) Bode plot illustrating the effect of detection gap (d) on operating frequency. The dotted lines indicate the frequency settings at which a Tracedec operates.*

***Figure 1.40**: Image showing the operating principles behind scanning electron microscopy (SEM) and energy-dispersive x-ray spectroscopy (EDX).*

***Figure 1.41:** Determination of pore size distribution by mercury porosimetry in three polymer monoliths. The average pore sizes were reported to be: (1) 0.97 μm, (2) 2.30 μm and (3) 4.07 μm.*

***Figure 2.1:** Schematic showing the principles of Successive Multiple Ionic Layers (SMIL) inside capillaries.*

***Figure 2.2**: Plot showing the sC^4D profiles of a silica monolith after coating with sodium dioctyl sulphosuccinate (DOSS) initially from inlet to outlet and in a second step in the reverse direction.*

***Figure 2.3:** Overlay showing (a) a digital image of a monolith modified with GFP in 3 zones and (b) the corresponding sC^4D profile illustrating an increased conductive response due to the presence of GFP.*

***Figure 2.4**: Image showing the experimental set up for the C^4D characterisation of monoliths and fused silica capillaries.*

***Figure 2.5**: Schematic representations of the immobilisation of Pd on CMS-co-DVB monoliths modified with (a) 1-methylimidazole (Monolith A) and (b) 5-amino-1,10-phenanthroline (monoliths B and C).*

***Figure 2.6:** sC^4D profile of a 1-methylimidazole/palladium modified polymer monolith (Monolith A) in a 250 μm i.d. fused silica capillary (a) before and (b) after metal removal by flushing with EDTA. Settings: frequency medium, -12dB, gain 50%.*

***Figure 2.7:** sC^4D profile of a 5-amino-1,10-phenanthroline/palladium modified polymer monolith (Monolith B) prepared in 100 μm i.d. fused silica capillary (a) before and (b) after metal removal by flushing with EDTA. Settings: frequency 2x high, 0dB, gain 50%.*

***Figure 2.8:** sC^4D profile of a 5-amino-1,10-phenanthroline/palladium modified polymer monolith (Monolith C) prepared in 250 μm i.d. fused silica capillary (a) before, (b) after metal removal by rinsing with EDTA and (c) a blank unmodified*

monolith (Monolith D) of similar porosity. Settings: frequency 2x high, -6 dB, gain 50%.

Figure 2.9: *Chemical structures of (a) the surfactant dihexadecyldimethyl ammonium bromide (DHDAB), (b) polydiallyldimethylammonium chloride (PDADMAC) and (c) poly(sodium 4-styrenesulphonate) (PSS).*

Figure 2.10: *Schematic showing a typical bi-layer configuration of positively charged surfactants bearing two alkyl chain substituents within a negatively charged fused silica capillary.*

Figure 2.11: *sC^4D profile for a surfactant coated fused silica capillary (a) after modification with NaOH, (b) immediately after modification with DHDAB, (c) after pumping water for 10 minutes, (d) 20 minutes and (e) 30 minutes. Detector settings: 2x high, 0dB, gain 50%, offset 0, n=3.*

Figure 2.12: *sC^4D profile overlay showing the decrease in conductivity along the length of a capillary: (a) before modification with a polyelectrolyte solution, (b) immediately after coating, (c) after a 10 minutes water wash, (d) after 20 minutes and (e) after 50 minutes. Detector settings: 2x high, 0dB, gain 50%, offset 0.*

Figure 2.13: *sC^4D profile showing the decrease in conductivity at a fixed point along the length of the capillary (a) after the polyelectrolyte modification step and (b) conductivity of a capillary which was not modified with polyelectrolytes. Detector settings: 2x high, 0dB, gain 50%, offset 0.*

Figure 2.14*: Structure of a polymer monolith grafted with sulphopropyl methacrylate (SPM) chains, leading to negatively charged sulphonate groups on the surface.*

Figure 2.15*: Image describing the the grafting process using photo-masking. (1) A monolith is prepared in UV transparent housing, (2) the monolith is filled with a solution containing the desired monomer and (3) masks are applied (such as black vinyl paper) to prevent the passage of UV light in undesired regions of the monolith. Extensive branching of polymer chains forms in the regions were UV light was allowed through.*

Figure 2.16: *(top) Image showing the applications of photomasks on a monolith prior to performing the grafting procedure and (bottom) conductivity profile of a BuMA-co-EDMA monolith grafted with SPM using a photo-masking technique: (a) a 1 cm region of the monolith exposed to 0.25 J/cm^2 UV irradiation and (b) a similar monolith which was not exposed to UV irradiation. Settings: 2x high, 0dB, gain 50%, offset 0. All readings obtained using 2mM sodium benzoate.*

Figure 3.1*: Image showing the two-step synthesis for the formation of Pd/Pt nano-flowers.*

Figure 3.2*: Images showing (a) a blank BuMA-2 monolith in capillary format, (b) a similar monolith functionalised with Pd/Pt nano-flowers, (c) a blank GMA-co-EDMA CIM disc and (d) a similar CIM disc modified functionalised with Pd/Pt nano-flowers.*

Figure 3.3: *Schematic showing the experimental set up for the flow-through catalytic oxidation of NADH to NAD$^+$ via the Pd/Pt nano-flower functionalised monolithic micro-reactor*.

Figure 3.4*: Schematic showing the reduction in Gibbs energy of a supersaturated solution as a solid phase forms. (i): concentration at equilibrium in solution, (ii): concentration of a supersaturated solution and (iii): concentration of a formed solid phase.*

Figure 3.5: *Image showing the nucleation process. A stable nucleus forms when a minimum size of r is present. If the nucleus size is below the critical size r_c, it will dissolve back into solution while if it is larger, it will continue to grow.*

Figure 3.6: *FE-SEM image of Pd/Pt NFs (~ 26 nm) (magnification 300,000x).*

Figure 3.7: *UV-Vis spectra of PVP capped Pd seeds and Pd/Pt nano-flowers.*

Figure 3.8*: FE-SEM images of (a) monolith GMA-1 (magnification 80,000x), (b) monolith GMA (2%) (magnification 60,000x), (c) monolith GMA (6%) (80,000x), (d) monolith GMA (12%) (magnification 80,000x), (e) monolith GMA (24%) (magnification 100,000x) and (f) monolith BuMA-2 (magnification 80,000x).*

***Figure 3.9**: Schematic showing the covalent immobilisation of Pd/Pt nano-flowers via lone-pair interactions with primary NH_2 groups on (a) BuMA-2 monoliths photografted with VAL and (b) BuMA-1 monoliths photografted with GMA.*

***Figure 3.10**: FE-SEM images of (a) a blank GMA-co-EDMA CIM disc and (b) a similar disc modified with Pd/Pt nano-flowers.*

***Figure 3.11:** Retention of perchlorate ions (100 ppm) on (b) a BuMA-2 monolith before nano-flower attachment. No retention was observed on (a) which was a BuMA-2 monolith functionalised with Pd/Pt nano-flowers. Conditions: 0.5 mM phthalic acid pH 4.5, injection volume 0.4 µL, non-suppressed conductivity detection. Flow rate: 3 $\mu L.min^{-1}$, length of column (a): 14 cm, length of column (b): 12 cm.*

***Figure 3.12**: Image showing the effects of a catalyst on the activation energy (E_a) of a reaction.*

***Figure 3.13:** Calibration plot relating absorbance (at 340 nm) versus concentration of NADH in the range 0-0.6 mM.*

***Figure 3.14**: Plot of concentration versus time for the oxidation of NADH to NAD^+ catalysed in the presence of Pd/Pt nano-flowers (100µL) as a colloidal suspension.*

***Figure 3.15:** (a) UV spectra showing the catalytic oxidation of NADH to NAD^+ in the presence of (100 µL) Pd/Pt nano-flowers as a colloidal suspension using an initial 0.56 mM concentration. Time intervals: (—) 0, (—) 5, (—)10 , (—) 40, (—) 50, (—) 70, (—) 90 minutes. (b) The same reaction when using 0.11 mM initial NADH concentration and the same amount of Pd/Pt nano-flowers. Time intervals: (—) 0, (—) 5, (—)10 , (—) 15, (—) 20, (—) 40 minutes.*

***Figure 3.16:** UV profile at 340 nm of a 0.5mM NADH solution pumped through (a) a blank BuMA-2 monolith, (b) a BuMA-2 monolith modified with Pd/Pt nano-flowers demonstrating the effects of contact time on the catalytic reaction. The flow was stopped at various time intervals such as 5, 10, 15, 30, 60, 90 minutes and the height of the negative peak observed was proportional to the amount of NAD^+ formed.*

***Figure 3.17:** Plot illustrating the effects of contact time on peak height between the*

Figure 4.6: *Images of (a) a EDMA-Tip-16 monolith visualised from the bottom of the tip and (b) FE-SEM image showing the presence of 16 nm AuNPs on the surface of a EDMA-Tip-16 monolith (magnification 5,000x).*

Figure 4.7*: EDX spectra of (a) a blank EDMA-Tip and (b) a EDMA-Tip-16 modified with 16 nm AuNPs.*

Figure 4.8: *FE-SEM images of (a and b) monolith LMA-GMA-16 which had been aminated by flushing ethylenediamine for 1 hour and placing the column in a water bath for 24 hours at 70 °C (magnification 50,000x and 100,000x), (c and d) monolith LMA-GMA-16 which had been aminated by constantly pumping ethylenediamine for 24 hours in a column oven at 70°C (magnification 50,000x and 100,000x), (e and f) monolith LMA-NSA-16 which had been photografted with 15% NSA and aminated in constant flow mode over 24 hours at room temperature.*

Figure 4.9: *FE-SEM images of (a) monoliths LMA-GMA-7 functionalised with 7 nm citrate stabilised AuNPs (magnification 220,000x) and (b) monoliths LMA-GMA-4 functionalised with 4 nm THPC capped AuNPs (magnification 100,000x).*

Figure 4.10: *Scanning capacitively coupled contactless conductivity (sC^4D) profiles of (a) a blank LMA-GMA monolith, (b, c and d) after modification with 1, 5, and 7 cm of 16 nm AuNPs for the preparation of monoliths LMA-GMA-16. sC^4D settings: frequency 2x high, voltage 0dB. All measurements were obtained in water.*

Figure 4.11*: Scanning capacitively coupled contactless conductivity (sC^4D) profiles of (a) a blank LMA-GMA monolith, (b) same monolith after amination and (c) after modification with 7 nm AuNPs for the preparation of monoliths LMA-GMA-7. sC^4D settings: frequency 2x high, voltage 0dB. All measurements were obtained in water.*

Figure 4.12: *Schematic showing the reduction of ferrocyanate from Fe(III) to Fe(II) on a monolith in a pipette tip modified with 16 nm AuNPs (shown in red on top). A blank monolith which did not contain Au NP (bottom) is shown for comparative purposes. The colourless product obtained from flushing the ferrocyanide (III) solution (in yellow) through the AuNP-modified monolith was indicative of the successfull catalytic reduction of Fe(III) to Fe(II).*

Figure 4.13: *UV spectra showing the reduction of ferrocyanide(III) to ferrocyanide(II) performed on monoliths in pipette-tip format by monitoring the absorbance at 420 nm of (a) an original ferrocyanide(III) with sodium borohydride solution at time 0, (b) the same solution flushed through a blank EDMA-Tip and (c) the solution collected from pumping through monolith EDMA-Tip-16.*

Figure 4.14: *Calibration plots at (a) 1 µL/min and (b) 3 µL/min relating peak height versus concentration for ferrocyanide(III) at 420 nm (0-17.5 mM).*

Figure 4.15: *Reduction of ferrocyanide(III) to (II) performed by injecting 100 nL amounts of a ferrocyanide/borohydride mixture at (i) 3 µL/min and (ii) 1 µL/min on (a) a blank LMA-GMA monolith, (b) a LMA-GMA-16 monolith functionalised with 16 nm citrate capped AuNPs, (c) LMA-GMA-4 monolith which contained 4 nm THPC capped AuNPs and (d) LMA-GMA-7 monolith which was functionalised with 7 nm citrate capped AuNPs. UV-Vis detection at 420 nm. Column lengths: 13 cm. Eluent: water.*

Figure 5.1*: Separation of aromatic compounds using (A) ODS and (B) C18-Au columns. Samples: uracil* (t_0)*, benzene, naphthalene, phenanthrene, and anthracene. ODS column: i.d. 0.15 mm, length 100 mm; C18-Au column: i.d. 0.15 mm, length 130 mm. Eluent: acetonitrile/water (50:50, v/v). UV detection at 254 nm.*

Figure 5.2*: Reversed-phase separation of proteins using generic monolithic poly(glycidyl methacrylate-co-ethylene dimethacrylate) column (a), poly(glycidyl methacrylate-co-ethylene dimethacrylate) column with attached gold nanoparticles (b), and the latter modified with 1-octadecanethiol (c). Conditions: column 10 cm × 100 µm i.d., mobile phase A 0.1% aqueous formic acid, mobile phase B 0.1% formic acid in acetonitrile, gradient from 0 to 35% B in A in 5.2 min, flow-rate 2.5 mL/min, injection volume 100 nL, UV detection at 210 nm. Peaks: ribonuclease A (1), cytochrome c (2), myoglobin (3).*

Figure 5.3: *Structure of PAA-grafted SiNPs.*

Figure 5.4: *Image showing the phase transfer of citrate-stabilised AuNP (present in the top aqueous layer) to an organic layer (at the bottom) via ligand exchange with octadecanethiol (on the left) and octadecylamine (on the right).*

Figure 5.5: *Separation of alkylbenzenes on AuNP-agglomerated polymer monoliths before and after modification with alkyl chains (column length: 12 cm). Mobile phase: 50/50 ACN:H_2O at a flow-rate of 2µL/min (3.4 mm/sec). Injection volume: 100 nL. UV detection at 220 nm. Analytes: 100 ppm (1) uracil (unretained marker), (2) ethylbenzene, (3) propylbenzene, (4) butylbenzene and (5) pentylbenzene.*

Figure 5.6*: Van Deemter curves for 100 ppm mixture of ethylbenzene, propylbenzene, butylbenzene and pentylbenzene. V_{opt}: optimal linear velocity.*

Figure 5.7: *Determination of the ion-exchange capacity of an AuNP-agglomerated monolith before and after modification with sulphonate groups. Eluent: 0.5 mM $CuSO_4$, UV detection at 210 nm, flow-rate 1µL/min. Column length: 12 cm.*

Figure 5.8: *Image showing the retention of 2.5 mM Ca^{2+} on a AuNP functionalised monolith modified with sulphonate groups. Eluent: 0.5 mM to 5.0 mM $CuSO_4$, UV detection at 210 nm, flow-rate 1 µL/min, 100 nL injections. Column length: 12 cm.*

Figure 5.9: *Plot showing the relationship between the log of the retention factor (k') and the log of $CuSO_4$ concentration for the separation of Ca^{2+} on the sulphonated AuNP-agglomerated monolith.*

Figure 5.10: *SEM image of a PAA-grafted SiNP (magnification: 200,000x).*

Figure 5.11: *FE-SEM images showing (a) a blank quaternary ammonium functionalised monolith (magnification: 100,000x) and (b) immobilised PAA-grafted SiNPs on the surface of a quaternary ammonium functionalised polymer monolith (magnification: 45,000x).*

Figure 5.12*: sC^4D profiles showing the immobilisation of PAA-grafted SiNPs on the surface of a quaternary ammonium functionalised (NR_4^+) polymer monolith (a) before any modification, (b) after 2 cm, (c) 6 cm and (d) 10 cm. Conductive responses of (i) bare LMA monolith, (ii) NR_4^+ functionalised monolith and (iii) the same monolith as the modification with PAA-grafted SiNPs occurred are shown.*

Figure 5.13: *Retention of 10 ppm Cl^- and $H_2PO_4^-$ on a quaternary ammonium functionalised monolith using a phthalic acid eluent (0.25 mM) adjusted to pH 6.5 using ethylenediamine. Conditions: on-column conductivity detection with settings:*

List of Tables

List of Publications

Connolly, D.; Floris, P.; Nesterenko, P. N.; Paull, B. Non-invasive characterization of stationary phases in capillary flow systems using scanning capacitively coupled contactless conductivity detection (sC(4)D). , *Trac-Trends in Analytical Chemistry* **2010,** *29* (8), 870-884.

Floris, P.; Twamley, B.; Nesterenko, P. N.; Paull, B.; Connolly, D. Agglomerated polymer monoliths with bimetallic nano-particles as flow-through micro-reactors. *Microchimica Acta* **2012,** *179* (1-2), 149-156.

Nesterenko, E. P.; Nesterenko, P. N.; Connolly, D.; He, X.; Floris, P.; Paull, B. Nano-particle modified stationary phases for high-performance liquid chromatography. *Analyst*, **2013**, *138*, 4229-4254.

Floris, P.; Twamley, B.; Nesterenko, P. N.; Paull, B.; Connolly, D. Gold nano-particle modified polymer monoliths for flow-through catalytic reactions. *Microchimica Acta*, **July 2013,** submitted.

List of Poster Presentations

1. **Immobilisation of gold nanoparticles on a polymer monolith in a pipette tip for catalytic activity in redox reactions,** *Patrick Floris, Damian Connolly, Hassan Alwael and Brett Paull.* RSC Analytical Research Forum, Loughborough University, UK 26-28th July 2010.

2. **High capacity gold gano-particle modified monolithic stationary phases for flow-through catalysis of selected redox reactions**, *Patrick Floris, Damian Connolly, Hassan Alwael and Brett Paull.* International Symposium on Chromatography, Valencia, Spain, 12-16th September 2010.

3. **Capillary scale micro-reactors incorporating immobilised palladium/platinum nanodendrites on porous polymer monoliths for selected coupling reactions**, *Patrick Floris, Damian Connolly and Brett Paull.* Conference on Analytical Sciences Ireland, 21-22nd February 2011.

4. **Monolithic micro-reactors with covalently attached palladium/platinum nano-flowers for selected redox reactions,** *Patrick Floris, Damian Connolly, Pavel N. Nesterenko and Brett Paull.* HPLC, Budapest, 19-23rd June 2011.

5. **Development of metal nano-particle agglomerated polymer monoliths for capillary LC applications**, *Patrick Floris, Damian Connolly and Brett Paull.* RSC Analytical Research Forum, Durham University, UK, 2-4th July 2012.

6. **Modification of porous polymer monoliths with functional nano-materials for applications in capillary ion chromatography,** *Patrick Floris, Marcello Iacono, Andreas Heise, Pavel N. Nesterenko, Brett Paull and Damian Connolly.* 2nd International Symposium on Functional Nano-materials, Dublin City University, 6-7th of September 2012.

7. **Development of nano-particle agglomerated polymer monoliths for capillary IC applications,** *Patrick Floris, Pavel N. Nesterenko, Brett Paull and Damian Connolly.* 24th International Ion Chromatography Symposium, Berlin, 17-20th September 2012.

List of Oral Presentations

1. **Development of metal nano-particle agglomerated polymer monoliths for capillary LC applications,** *Patrick Floris, Damian Connolly and Brett Paull.* Chemistry Colloquium, University of Limerick, Ireland, 14-15th of June 2012.

2. **Development of nano-particle agglomerated polymer monoliths for capillary IC applications,** *Patrick Floris, Pavel N. Nesterenko, Brett Paull and Damian Connolly.* 24th International Ion Chromatography Symposium, Berlin, 17-20th September 2012.

List of Honours and Awards

Analytical Chemistry Trust Fund bursary for attendance to the RSC Analytical Research Forum 2010.

Analytical Chemistry Trust Fund bursary for attendance to the RSC Analytical Research Forum 2012.

CASSS Travel Grant for the 24th International Ion Chromatography Symposium, Berlin, Germany, 17-20th September 2012.

Acknowledgments

Firstly I'd like to thank my supervisors Dr. Damian Connolly, Prof. Brett Paull and Prof. Apryll Stalcup for the opportunity to obtain my PhD and all the support throughout the project. I'd like to extend my gratitude to Dr. Brendan Twamley, Prof. Pavel Nesterenko and Dr. Katya Nesterenko for their help and advice during these years. Special thanks also go to all the technical staff in the NCSR and School of Chemical Sciences.

I'd like to acknowledge all my collagues at the ISSC in particular Nicola, Gillian, Lily, Sara, Orla, Dave and Disha. I have really enjoyed working with you all.

Finally special thanks go to my family, in particular my mum and dad for all the encouragement during these years.

Abstract

In this thesis, novel approaches to the preparation and characterisation of nano-agglomerated polymer monoliths are described. Polymer monoliths in various formats were prepared by availing of *in-situ* photopolymerisation techniques, with the modification of surface chemistry achieved via grafting selected amine-reactive monomers, facilitating the subsequent attachment of metal nano-materials. Traditional destructive characterisation methods such as field emission scanning electron microscopy (FE-SEM) and energy-dispersive X-ray spectroscopy provided the qualitative confirmation of the presence of the nano-materials. A very dense coverage of bimetallic Pd/Pt nano-flowers was achieved upon the surface of such polymer monoliths. The macro-porous structure of the monoliths and the high coverage of nano-particles facilitated catalytic applications, such as the oxidation of NADH to NAD^+, in flow-through configuration. The rate of reaction was found to be dependant on the initial NADH concentration. Other polymer monoliths were functionalised with gold nano-particle (AuNPs) of various sizes in order to evaluate the effects of nano-particle size on catalytic efficiency. The catalytic properties of the immobilised AuNPs were retained following immobilisation, as demonstrated by the reduction of ferrocyanide from Fe(III) to Fe(II). A 57 % conversion rate was obtained when the reaction was performed on monolithic surfaces which had been functionalised with 16 nm AuNPs. Higher reaction yields (95 %) were obtained when 7 nm AuNPs were used. Non-invasive and non-destructive scanning capacitively coupled contactless conductivity detection (sC^4D) was applied to monitor the temporal stability of surfactant and polyelectrolyte coatings in capillary columns which would traditionally be applied in capillary electrophoresis. The benefits of this technique were further illustrated by confirming the presence of AuNPs and PAA-grafted silica nano-particles (SiNPs) on previously aminated or quaternary ammonium functionalised monoliths. The movement of the nano-particle's plug was monitored at mm increments as it progressed along the column. Finally, an evaluation of the chromatographic properties of nano-agglomerated stationary phases was performed. Reversed-phase applications of AuNP-functionalised monoliths were demonstrated upon further modification of the nano-particles with alkylthiol and alkylamine chains. However, poor chromatographic

performance was observed with a test mixture of alkylbenzenes due to the limited hydrophobicity of the stationary phase. Ion-exchange applications were also possible upon modification of the immobilised AuNPs with sulphonate groups, which was demonstrated by the retention of Ca^{2+} ions. PAA-grafted SiNPs were immobilised on the surface of a quaternary ammonium-functionalised polymer monolith and the anion-exchange properties of the stationary phase demonstrated by separating a mixture of Cl^- and $H_2PO_4^-$. The immobilisation of negatively charged PAA-grafted SiNPs however, lead to the formation of a cation-exchange stationary phase as confirmed by the retention of Ca^{2+} and Mg^{2+}.

Chapter 1: Literature survey

1.1 Monolithic stationary phases: an overview

Stationary phases based on monolithic materials have been at the centre of great research interest over the last 20 years [1]. A first concept of monolithic material was introduced by Richard Synge who in 1952 documented his intentions to use 'a continuous block of porous gel structure' for the analysis of polysaccharides [2]. The first real shift towards monolithic materials however, was only observed in the 1980s when important developments occurred in the formation of macro-porous polymer discs, columns and silica rods. Silica monoliths currently produced can all be related to the columns first developed by Tanaka and Nakanishi's group [3-6] while Hjertèn [7] and Svec [8, 9] can be considered the pioneers of monoliths prepared from polymers. The main variations between the two materials, which will be discussed in detail below, are based on the different porous structures and the provided surface areas. All monolithic stationary phases can be likened to a large 'particle' that does not contain any inter-particular voids. The possible in-situ fabrication of these stationary phases in miniaturised formats, without the need of retaining frits, eliminates the variability/poor physical stability issues introduced by a traditional packing procedure. Also the high permeability of monoliths due to their high porosity (above 65% relative to 25% of particulate columns) [3], represents a distinctive advantage of these materials relative to particulate stationary phases. Monoliths have a high inter-pore connectivity which allows low resistance to flow and the operation at high flow-rates with efficiencies comparable to traditional 3-3.5 µm silica particles [10]. This is because the nature of the flow is convective rather than diffusive, since the liquid flow is able to go through pores rather than around particles, hence the contribution to the C term of the van Deemter equation (Equation 1.1) is considerably reduced leading to a flatter ascending portion of the curve, as shown in Figure 1.1, relative to packed columns.

$$\mathrm{HETP} = A + B/\nu + C\nu \qquad \text{(Equation 1.1)}$$

Where HETP = height equivalent to a theoretical plate, A = eddy diffusion, B = axial diffusion, ν = reduced velocity and C = mass transfer.

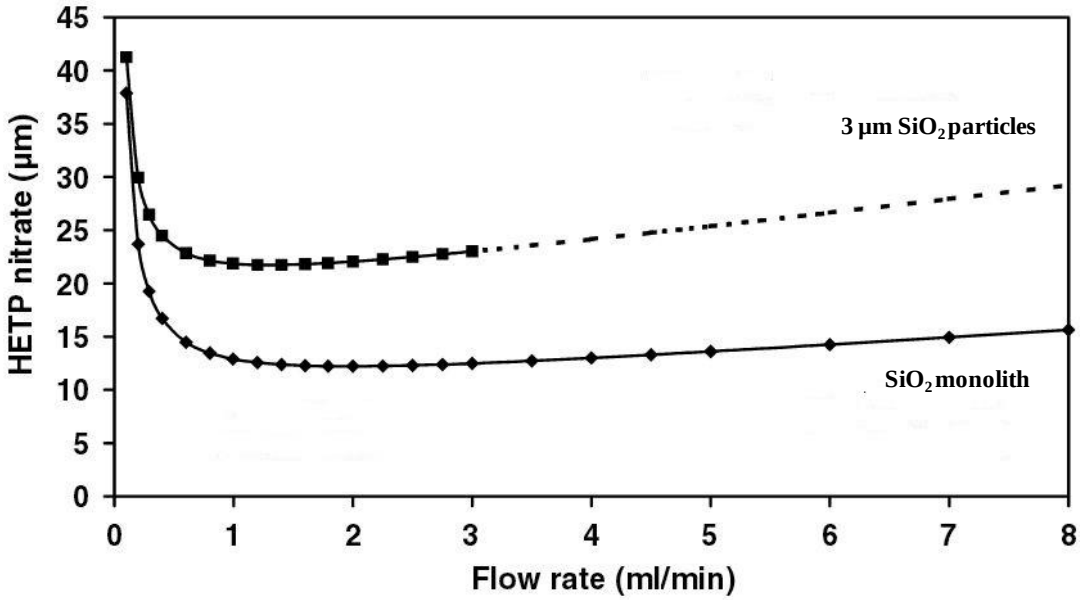

Figure 1.1: *Relationship between HETP and flow-rate on a SiO2 packed column (Kingsorb C18, 3 µm, 30 × 4.6 mm) and a monolithic column (Chromolith RP18). Mobile phase: (97:3) 1.54 mM tetrabutylammonium hydroxide, 0.8 mM phthalic acid, pH 7.25/acetonitrile. Column temperature: 30 °C. Loop volume: 25 µl. Analyte concentrations: 10 mg/l NO_3^- standard was used with flow-rates of 0.2–8.0 mL/min [11].*

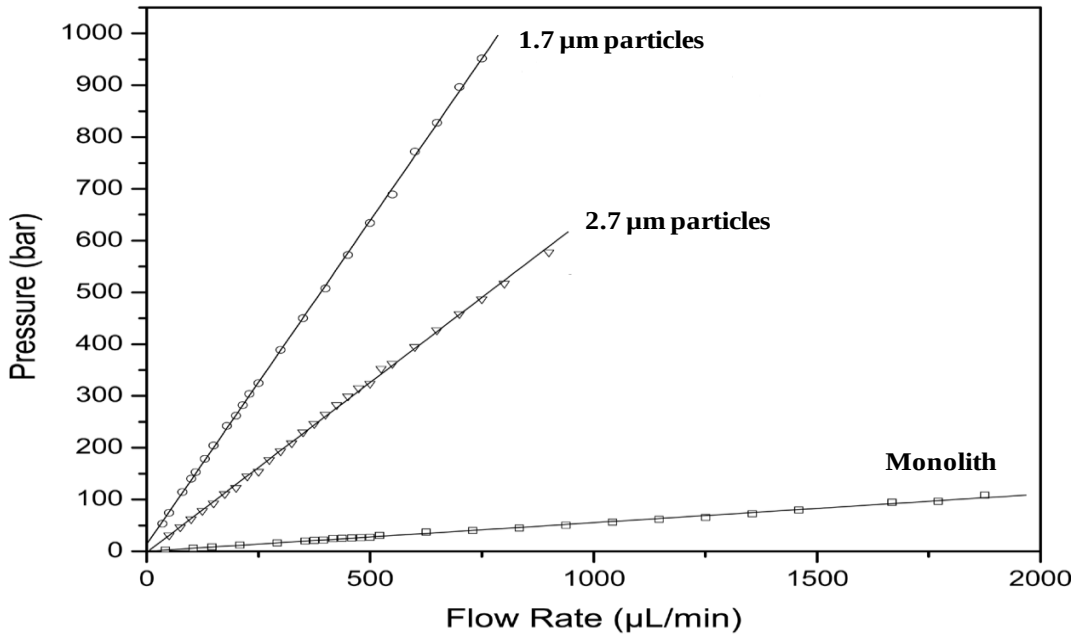

Figure 1.2: *Plot showing the effects of flow rate on pressure for three different columns using an acetonitrile/water mixture mobile phase [12].*

Monolithic columns, because of their high permeability, can also be operated at high velocities without large increases in backpressures as illustrated in Figure 1.2, following the relationship described by Darcy's law:

$$\Delta P = (\eta L u / B_0) \qquad \text{(Equation 1.2)}$$

Where L = column length, u = average mobile phase velocity, η = mobile phase viscosity, and B_0 = column permeability.

By increasing the size of the through-pores, higher permeabilities can be achieved which allows the use of comparatively higher linear velocities of mobile phase, with relatively lower operating backpressures.

1.2 Silica monoliths

1.2.1 Properties of silica monoliths

Silica monoliths are characterised by an ordered distribution of meso-pores (between 2-50 nm in size) and macro-pores (larger than 50 nm), which provide large surface areas (up to 300 m^2/g) [13]. These properties are particularly suitable for small molecules which are capable of diffusing in and out of the pores very rapidly, hence leading to high separation efficiencies (up to 100,000 N/m) that have been achieved with aromatic hydrocarbons [14].

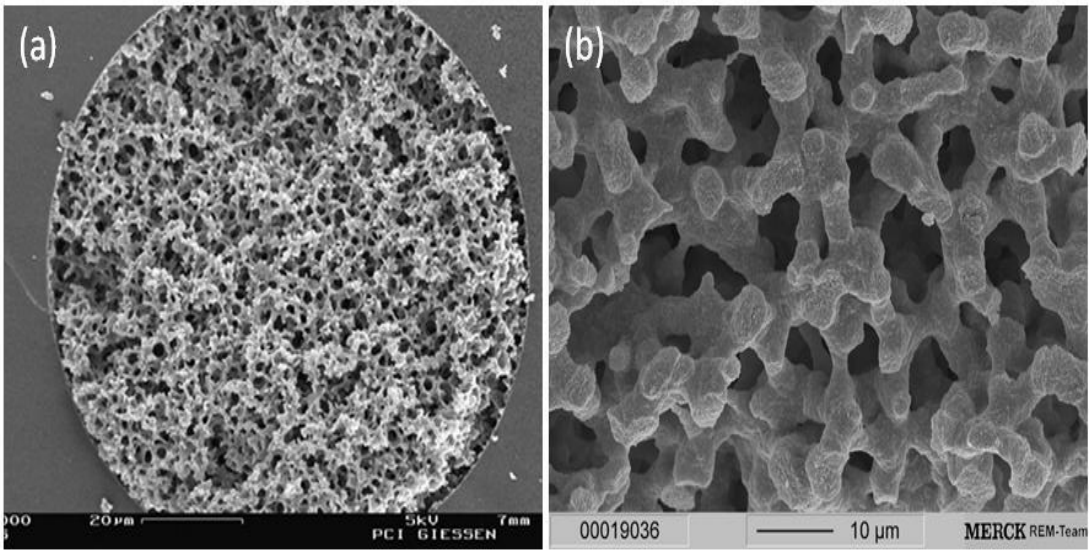

***Figure 1.3**: SEM images showing the typical skeleton structure present in silica monoliths [15, 16].*

The presence of a small meso-porous structure however, represents an obstacle when dealing with large molecules such as proteins or peptides because of the tendency to hinder the movement of such molecules, which can lead to band broadening effects. By altering simple parameters such as time, ageing and temperature of the drying steps during the synthetic process [17], the monolith's skeleton can be finely tuned to form a wider porous structure which has successfully been applied to the separation of proteins [18]. Silica monoliths are also stable only within a p*H* 2-8 range since at p*H* < 2, the bonds of the monolith with organic functional groups are no longer stable and at p*H* > 8 silica hydrolyses [19].

1.2.2 Synthetic procedures

The preparation of silica monoliths was first described by Nakanishi *et al.* [6] and it involves the hydrolytic polymerisation of a silane or a mixture of these with a polymer such as polyethyelene glycol (PEG) in a mold, generally a tube holder of 6-9 mm i.d. [20]. The typical silane compounds include tetramethoxysilane (TMOS), tetraethoxysilane (TEOS), polyethoxysilane (PEOS), aminopropyl-triethoxysilane (APTES) or a mixture of these. Heat is released when tetraalkoxysilane compounds react with water, leading to the alkoxy groups being replaced by silanol groups. As the polymer forms, the rate of reactions slows down to allow for cooling of the product and pouring into a mold before the sol-gel transformation is complete which leads to the formation of the macro-porous structure, the size of which depends on the concentrations of starting materials and porogens. Subsequent post-gelation treatments, such as ageing, affect the formation of meso-pores. The final steps involve the drying and cladding of the monolith. Because considerable shrinkage can occur during the polymerisation stage, it is necessary to enclose the monolith around PTFE tubing or a PEEK resin using the careful application of heat which causes the housing to shrink and close any gaps present [3].

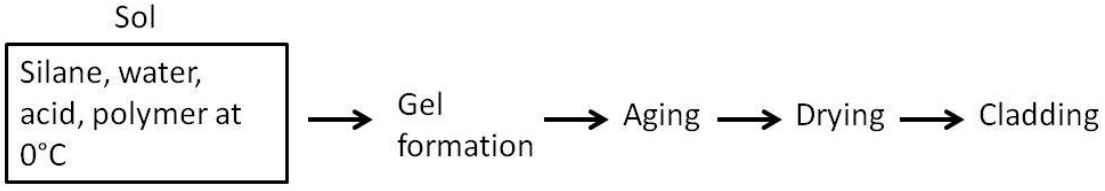

***Figure 1.4**: Schematic showing the steps involved in the preparation of silica monoliths.*

The difficulties observed at the cladding step with columns of large i.d. led to the preparation of silica monoliths in capillary formats and micro-chip devices [21]. Wu *et al*. [22] generated a silica monolith from TMOS in glass micro-chip channels (2 cm long, 60 µm deep and 400 µm wide) for the extraction of DNA from clinical samples and from bacteria. Since similar shrinking issues as mentioned previously by Tanaka [21] were observed, NaOH was flushed through the channels prior to the formation of the monolith to allow hydrolysis of the inner walls which could then bond with the sol-gel material.

1.2.3 Commercially available silica monoliths

Silica monoliths are currently available commercially in a variety of formats as shown in Figure 1.5.

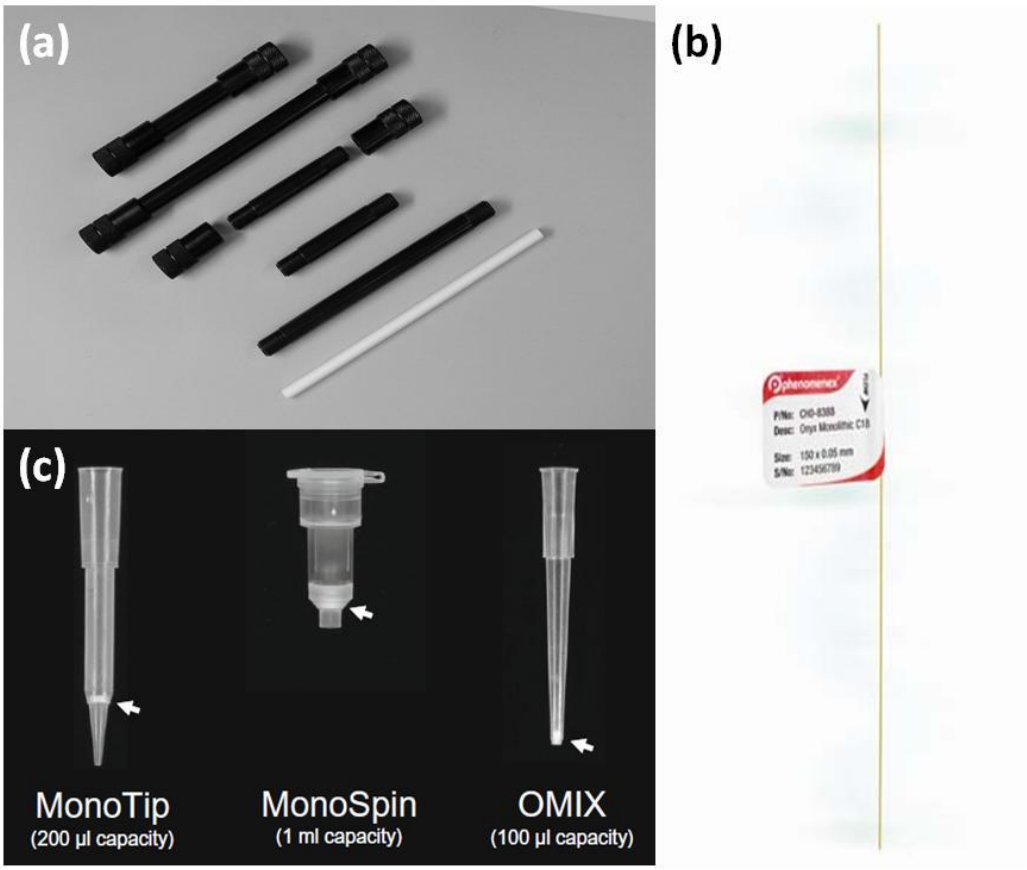

Figure 1.5*: Commercially available silica monoliths. (a) Chromolith in 4.6 mm i.d. column format [15], (b) Onyx in capillary format (0.2 mm i.d.) and (c) monoliths in pipette tip/centrifuge tube formats [23].*

Merck KGaA developed a technology for the precise cladding of 4.6 mm i.d. silica rods with a PEEK polymer. These monoliths, branded as Chromolith, are also available in capillary formats of two different lengths (15 or 30 cm) and various internal diameters (i.d. 50-200 µm), with C_{18} and C_8 functionalities, having macro-pores of 2 µm and meso-pores of 13 nm [24]. Similarly, Phenomenex produces Onyx capillary columns with identical functionalities which are available in varying lengths (0.5-10 cm) and inner diameters (i.d. 100-200µm) followed also by standard bore columns (4.6 mm i.d.). Silica monoliths are also available in pipette-tip or inside micro-centrifuge tubes. These are available with a variety of functional groups attached to the monolithic phase which allow reversed-phase, normal phase and ion-exchange functionalities as summarised in a recent review [23].

1.3 Polymer monoliths

Polymer monoliths can be described as poorly organised globule structured materials with only macro-pores present [25]. Advantages relative to silica monoliths include the stability over the full p*H* range [26, 27], the ease of fabrication in-situ and a higher control over the surface properties of the monolith which can be achieved directly during the synthesis rather than by successive modification. While silica monoliths have high surface areas, which makes them suitable for separating small molecules, the vast majority of reports documenting polymer monoliths highlight the lack of small meso-pores [7, 25, 26] which limits the surface areas present between 10-30 m^2/g [28] and restricts their chromatographic application to mainly large molecules. Recent reports however, illustrate that the achievement of meso-pores in a polymer monolith is possible by early termination of the polymerisation step [29] and hyper-crosslinking of the monolith with Friedal Crafts reactions in a successive step after the monolith preparation [30] achieving surface areas of 600 m^2/g with separation efficiencies of 80,000 N/m for alkylbenzenes.

1.3.1 Types of monomers used

The range of monomers available for preparing monolithic materials is vast, allowing the tailoring of the chemical properties depending on the application required. Some examples are shown in Figure 1.6. Monomers with hydrophobic properties have been used for reversed-phase LC and solid-phase extraction while

monomers with charged functional groups have been used for ion-exchange separations. In contrast with the traditional suspension polymerisation, the choice of monomers available for the production of monoliths is larger since only one phase is present in this case which means that water-soluble or reactive monomers can now be used.

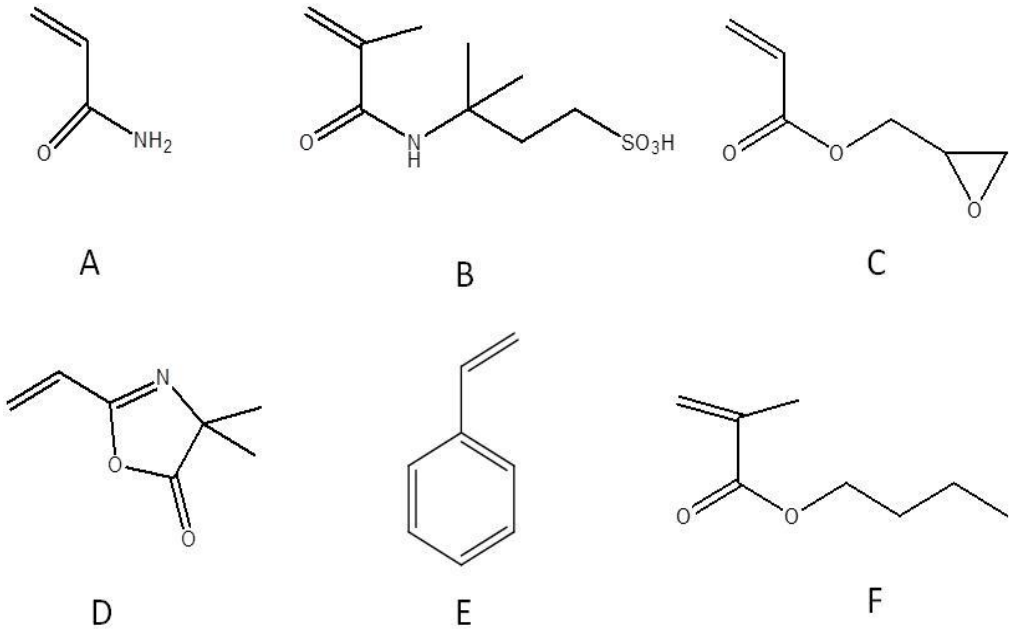

Figure 1.6: *Common functional monomers used for the preparation of polymer monoliths. A: acrylamide, B: 2-acrylamido-2-methyl-1-propanesulphonic acid, C: glycidyl methacrylate, D: 2-vinyl-4,4-dimethylazlactone, E: styrene, F: butyl methacrylate.*

1.3.2 Synthesis of polymer monoliths

The synthesis of polymer monoliths can be broken down into three main steps. The first steps involves modification of the housing's walls so that the monolithic materials will adhere strongly to it. The absence of gaps between the two will ensure that all the liquid phase can flow through the monolithic bed allowing the highest degree of interaction between stationary phase and analytes. Courtois *et al*. [31] evaluated 11 different silanisation procedures based on a vinylic silane, 3-trimethoxysilyl propyl methacrylate (γ-MAPS), and concluded that the best results were obtained using toluene as the solvent. Secondly, the polymerisation of a mixture of components, selected depending on the required chemistry and polymeric

structure, is performed. This consists of a mixture of monomers, a cross-linker, porogens and an initiator, which is required to generate free radicals in order to begin the step-wise polymerisation reaction. Degassing is required via nitrogen purging or sonication in order to remove excess oxygen which prevents the formation of free radicals [32]. A mould, which can be anything from a large bore column to a micro-fluidic channel, is filled with the monomer mixture and sealed. The polymerisation process can then take place by thermal or UV irradiation after which the mold can be connected to a pump for the removal of unreacted material. According to the classical mechanism of the polymerisation reaction [33, 34], free radicals are generated when heat is applied to this solution which generate polymer chains that precipitate out due to their insolubility in the surrounding porogens. Growing polymer chains aggregate into nuclei and the residual monomers in solution then become the ideal solvating agents for the polymers (nuclei) formed, allowing further polymerisation to occur both within the nuclei and also in the remaining monomer solution. As the size and number of nuclei increase, these develop an extended network joined by polymer chains. A final polymer body forms characterised by a fraction of pores proportional to the initial volume fraction of porogen. As the polymerisation continues, the nuclei of this highly porous and fragile structure form numerous inter-connections which cause the disappearance of very large pores. Partial shrinking at this stage of the process is inevitable however, the impact of this is considerably less relative to what is observed with silica monoliths as it tends to occur inside the monolith rather then externally, leading to small changes in the porous structure and little variations in the overall diameter size.

1.4 Control of porous properties in polymer monoliths

The network of large pores which characterises polymer monoliths allows the passage of liquids at moderate pressures even at high flow rates. The morphology of the monolith is dependent on the timing of phase separation of the polymer from the surrounding solution. This can be controlled by tuning parameters such as choice of porogens, concentration of cross-linker used and the amount of energy applied for the polymerisation [35-37].

1.4.1 Effects of porogens

Significantly different porous structures can be achieved by a careful selection of porogens. A thermodynamically unfavourable (poor) porogen will lead to a fast phase separation of polymer formed from the remaining solution. Swelling then occurs with the remaining monomer solution since this represents a much better solvent relative to the porogen. The polymerisation therefore proceeds faster in the growing nuclei rather than in the remaining solution, leading to large globules with high interstitial voids in between forming large pores. If a thermodynamically favourable (good) porogen is chosen, the phase separation of the polymer from the remaining solution is delayed because of the increased solubility of growing polymer nuclei in the porogen. The porogen will then compete with the monomer solution for the solvation of the nuclei formed [35, 36]. The concentration of monomer in the nuclei will therefore be lower hence the globules formed are smaller leading to smaller pores. This can be visualised in Figure 1.7 below where additions of small amounts of dodecanol in the preparation of a GMA-*co*-EDMA monolith led to a drastic increase in pore size since this resulted in an earlier phase separation of the polymer.

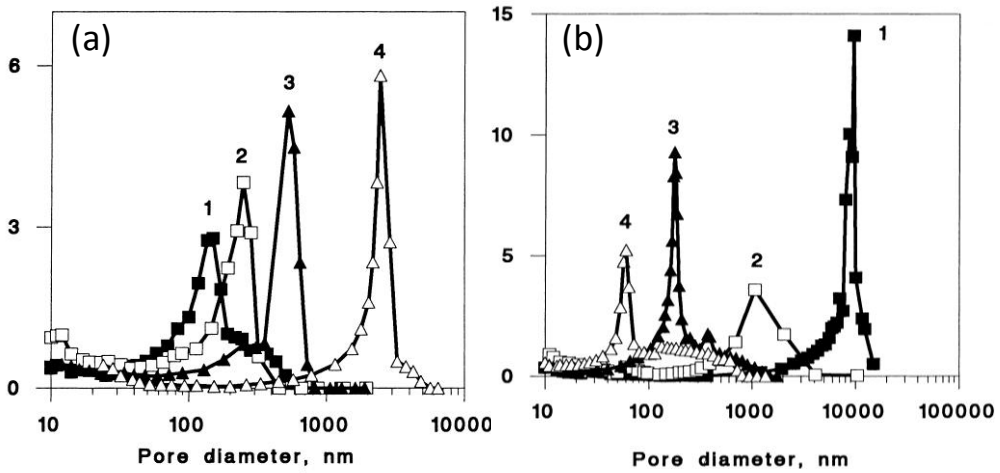

Figure 1.7: *Effects of porogens on pore size in (a) a GMA-co-EDMA monolith with a cyclohexanol-dodecanol ratio of (1) 60/0, (2) 57/3, (3) 54/6, (4) 45/15 and (b) a PS-co-DVB monolith with a dodecanol/toluene ratio of (1) 60/0, (2) 50/10, (3) 45/15, (4) 40/20 [36].*

Similarly, toluene is a more favourable solvent for the preparation of a PS-*co*-DVB monolith hence a shift towards a smaller porous structure is observed upon its addition.

1.4.2 Effects of cross-linkers

Commonly used cross-linkers for the preparation of polymer monoliths are shown in Figure 1.8. Altering the amount of cross-linker changes not only the chemical composition of the monolith but also its porous structure. As the content of the cross-linker is increased, the pore size decreases [38]. Many cross-linked micro-globules are formed and precipitate at an early stage in the reaction. Their highly cross-linked density leads to the low probability of coalescence between globules as they continue to polymerise. A report from Santora *et al.* [39] demonstrated that variations in surface areas can be obtained by altering the amount of cross-linker in PS-*co*-DVB polymer monoliths. When pure divinylbenzene is present as the cross-linker, a surface area of 800 m^2/g was reported which was determined using the BET isotherm technique.

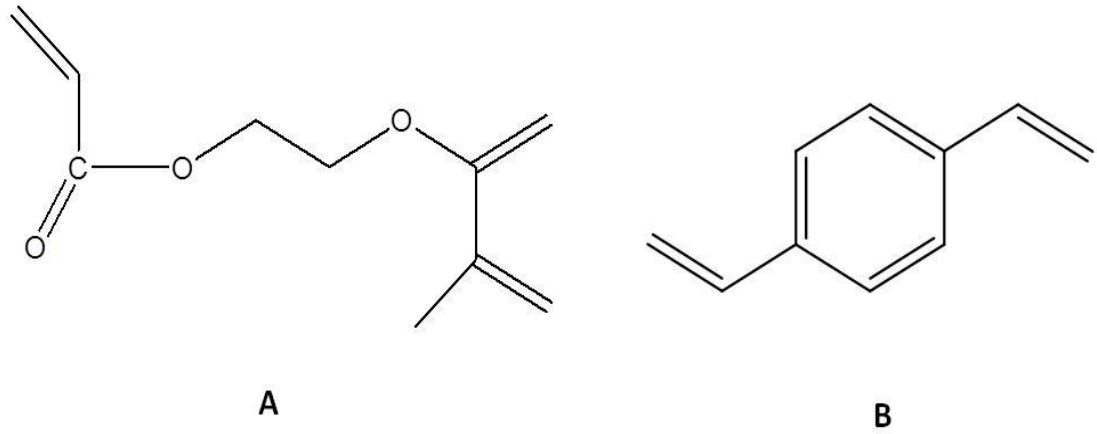

Figure 1.8: *Examples of commonly used cross-linkers, A: ethylene dimethacrylate, B: divinyl benzene.*

1.4.3 Polymerisation techniques

1.4.3.1 Free-radical initiated polymerisation

A good control of the rate of polymerisation allows the tuning of polymer monolith morphology in order to obtain the desired characteristics. The first method that was used for the preparation of polymer monoliths was based on thermally initiated

polymerisation [1, 25] over 24 hours. As shown in Figure 1.9, the porous structures of GMA-*co*-EDMA and PS-*co*-DVB monoliths were highly influenced by changes in polymerisation temperature. By increasing the temperature, a higher rate of nucleation is achieved leading to a larger number of free radicals, and thus, resulting in the formation of a larger number of growing nuclei. Consequently, a larger number of globules form leading to a smaller globule size and smaller pores. In particular, it is the decomposition rate of the initiator that it is highly dependant on temperature. For example, the half-life of a commonly used initiator, azobisisobutyronitrile (AIBN), is 37 hours at 55 ºC but it decreases to 6 hours at 70 ºC [34]. Alternatively, smaller pores can also be achieved by reducing the length of the polymerisation. Trojer *et al.* [40] studied the effects of reaction time, 30 min to 24 hours for the preparation of poly(methylstyrene-*co*-1,2-(4-vinylphenyl) ethane) monoliths.

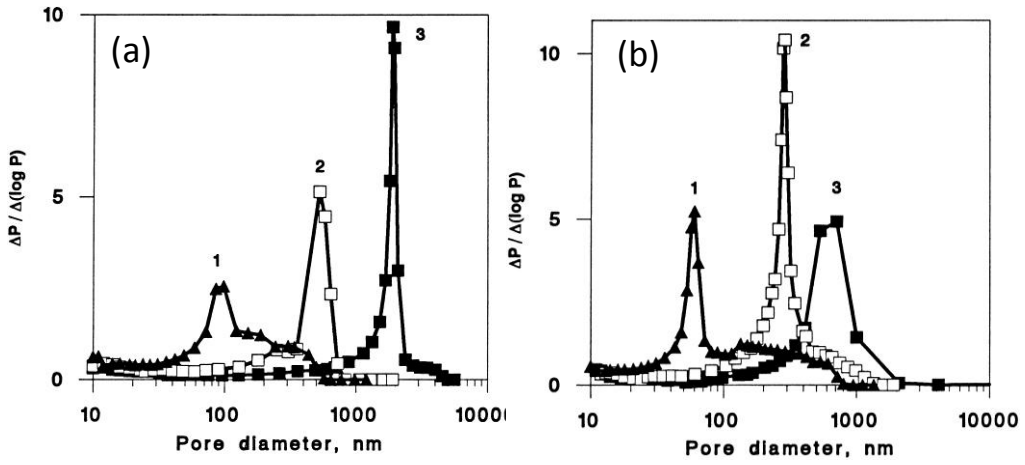

Figure 1.9: *Effects of temperature on porous structure of (a) a GMA-co-EDMA monolith at (1) 80, (2) 70 and (3) 55 °C and (b) a PS-co-DVB monolith at Pore size distrubution of GMA-co-EDMA prepared at (1) 80, (2) 70 and (3) 60 °C [36].*

As the reaction was left for longer, a higher polymerisation of the monomer solution occurred leading to a decrease in surface area from 76 to 23 m^2/g and in porosity from 71% to 42%.

Another possible methodology involves the use of photoinitiated polymerisation. This procedure, which was developed in 1997 [35], has several advantages over the thermally-initiated method. First because this occurs at room temperature, a wider range of solvents are available including low boiling point alcohols and

hydrocarbons such as methanol, ethanol, ethyl acetate and hexane [41]. Another advantage is represented by the highly enhanced rate of polymerisation which leads to reactions to be completed within only a matter of minutes instead of several hours. It also allows the formation of a polymer monolith only in certain desired regions of a housing by availing of masking techniques [42]. As described for thermal polymerisation, AIBN can also be used for photoinitiated polymerisation since it decomposes at 365 nm and some studies have compared its activity under both thermal and photoirradiated conditions [43]. No differences in chromatographic performances between the monoliths prepared under the two procedures were found, however, the photopolymerised monolith exhibited higher backpressures indicating a smaller porous structure. Another type of initiator used is 2,2-dimethoxy-2-phenyl-acetophenone (DAP) which breaks down at a different wavelength (254 nm) [44]. Some disadvantages to photoinitiated polymerisation however, include the fact that only UV transparent housings, such as for example teflon-coated capillaries, can be used and UV absorbing monomers such as styrene and divinylbenzene are no longer possible choices [28]. This issue can be resolved however, by using a light emitting diode at 470 nm as the light source, using compatible initiators that break down at that wavelength such as a mixture of (+)-(*S*)-camphorquinone, methyl-4-dimethylaminobenzoate and *N*-methoxy-4-phenylpyridinium tetrafluoroborate [45].

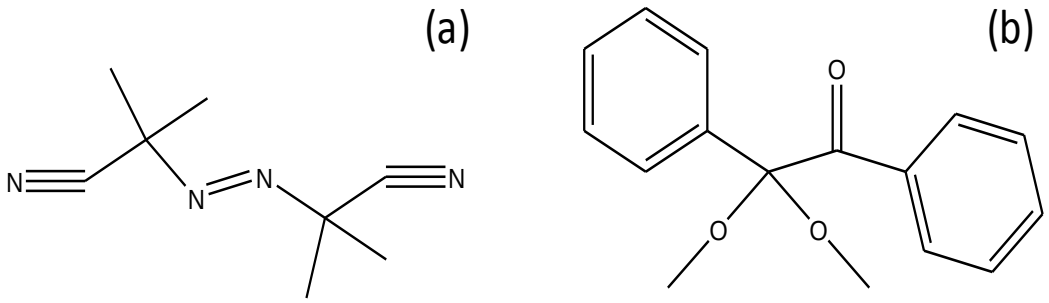

***Figure 1.10**: Free-radical initiators (a) AIBN and (b) DAP commonly used for the preparation of polymer monoliths.*

The issue of light attenuation caused by the absorption from the initiator and other components of the polymerisation mixture (mainly monomers) must be considered when preparing photopolymerised polymer monoliths. It is known that the kinetics of a UV iniated reaction is dependent on the light intensity [46] since the rate of polymerisation is faster at higher intensities. Within a fused-silica capillary in

particular, the polymerisation process occurs from the capillary walls inwards because light intensity will decrease radially toward the center of the capillary. It is possible that the radial homogeneity of monolith density could be adversely affected due to the unintentional presence of a gradient of light intensity across the diameter of the capillary. The obvious way to minimise such issues is to retrict the capillary diameter to < 200 µm i.d.

Some evidence exists in the literature which suggests that for capillaries of 100 µm i.d. the potential of an unwanted gradient across the radius of the capillary are essentially nil. Specifically, in 2003 Rohr *et al.* [42] grafted 2-acrylamido-2-methyl-1-propanesulphonic acid onto a 100 um i.d. methacrylate monolith using similar UV-initiated methods as described in this thesis. Electron-probe microscopy was used to confirm that the radial coverage of grafted monomer (scanning for sulphur) was even and homogeneous. It is reasonable to suggest that the monolith density would be similarly homogeneous for all monoliths described in this work (particularly since all monomers were selected in part due to their low UV absorbance at the wavelengths employed during polymerisation or grafting events (254 nm).

Other approaches involve the use of γ rays [47, 48] or electron beam as initiators [49]. The main advantages of these methodologies are the lack of traditional initiators which led to no functional groups present on the chain ends and the ability to form monoliths at any temperatures and almost in any container. However, not many laboratories have access to the instrumentation required and also safety regulations represent serious drawbacks of these methods.

1.4.3.2 Living polymerisation

In order to improve the control on the porous properties of polymer monoliths, other types of polymerisation techniques have been developed. A type of polymerisation known as ‘living’ is based on the addition of fresh monomer solution which allows to re-start the polymerisation. The absence of termination and chain transfer reactions allows a better control of the nucleation and phase separation stages, leading to the simultaneous growth of the polymer chains and the ability to finely tune the structural properties of the monolith. Living polymerisation procedures can be nitroxide mediated [50], organotellurium mediated [51] and also include atom

transfer radical polymerisation (ATRP) [52] as well as ring-opening methathesis polymerisation (ROMP) [53-57]. These types of polymerisation methods are however, beyond the scope of the material here discussed.

1.5 Tailored chemistry of polymer monoliths

1.5.1 Co-polymerisation

Depending on the desired application, monoliths which exhibit a wide range of surface functionalities can be easily prepared by direct co-polymerisation of a variety of monomers. For example poly(2-vinyl-4,4-dimethylazlactone-*co*-acrylamide-*co*-ethylenedimethacrylate) monoliths have been used efficiently for the immobilisation of enzymes [58] as shown in Figure 1.11.

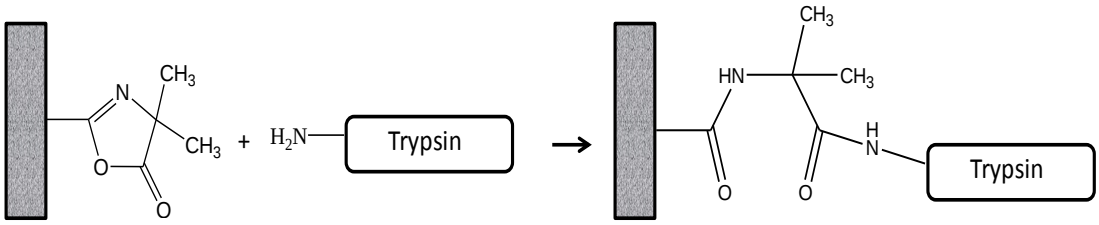

Figure 1.11: *Schematic showing the reaction of a monolith with azlactone moieties with the amine groups on trypsin.*

The presence of such monomers in the polymerisation mixture allows the formation of a monolith which shows both hydrophilic characteristics, introduced by the acrylamide part, combined with the reactivity of azlactone, which can bond easily with the amino groups present on the trypsin molecules. More recently, Chambers *et al*. [59] described the co-polymerisation of traditional methacrylate monoliths combined with a C_{60} functionalised monomer, [9, 9]-phenyl-C_{61}-butyric acid 2-hydroxyethyl methacrylate ester, for the separation of alkylbenzenes showing high separation efficiencies (up to 110,000 N/m) for benzene. One main disadvantage of co-polymerised monoliths is represented by the limited presence of the desired functionalities on the surface of the monolith since the bulk of the reactive monomer is contained within the globule structure.

1.5.2 Chemical modification

Chemical modification is an alternative route for achieving the desired functionalities. This modification does not affect the porous structure of the monolith, since the modification is done at the pore surface. The outcome of the modification is dependent on the number of reactive functionalities originally present on the surface which can be increased by increasing the concentration of reactive monomer in the monomer mixture prior to polymerisation or by availing of grafting techniques. Glycidyl methacrylate is a commonly used reactive monomer which is often exploited to achieve a variety of other functionalities based on the ring opening reaction of epoxy moieties. For example the reaction of GMA with ethylenediamine and trimethylamine has often been reported for applications as weak and strong anion exchangers [60]. The presence of amino groups on the surface, which become activated in the presence of aldehydes, can also be used for the immobilisation of ligands such as trypsin and applications in affinity chromatography [61]. Similarly if a monolith with cation exchange functionalities is required, a reaction between the epoxy group of GMA and sodium sulphide can be used to achieve surface sulphonate groups [62]. Vinyl azlactone (VAL) is also a reactive monomer which can be subsequently chemically modified. Gillespie et *al.* [63] for example reported the modification of monoliths containing grafted azlactone polymer chains with *p*-hydroxyphenylboronic acid, leading to an ion-exchange stationary phase. The ability of epoxy groups to be modified with amino or thiol groups has also been reported for the subsequent attachment of proteins [64].

1.5.3 Grafting

Similar to chemical modification, grafting involves the modification of the chemistry at the surface of a monolith without altering its backbone structure. However, these processes differ significantly. By chemically modifying a monolith, only a small amount of the monolith active sites will be available to be functionalised at the surface since a portion of these will be embedded inside the monolithic structure and thus not available for any reaction to occur. Grafting allows instead the formation of multiple functionalities due to extensive branching at each graft site thus increasing the density of functional groups available at the pore surface. This process requires the presence of free radicals which can be provided by initiators. These are generally

flushed through the pores of a pre-formed monolith either in a single step (along with the graftable monomer) or as a separate step. In 2003 Rohr *et al*. [42] modified polymer monoliths using a grafting methodology originally designed by Rånby for photografting aromatic ketones such as benzophenone onto polymer films [65, 66]. This method involves the excitation of the initiator (benzophenone) by applying UV light between 200-300 nm, which leads to a process of hydrogen abstraction and the formation of free radicals on the monolith's surface. In the presence of a suitable monomer (usually an acrylate or methacrylate bearing a suitable functional group), the surface radicals thus formed, lead to a propagation effect which causes branching of polymer chains to occur as shown in Figure 1.12.

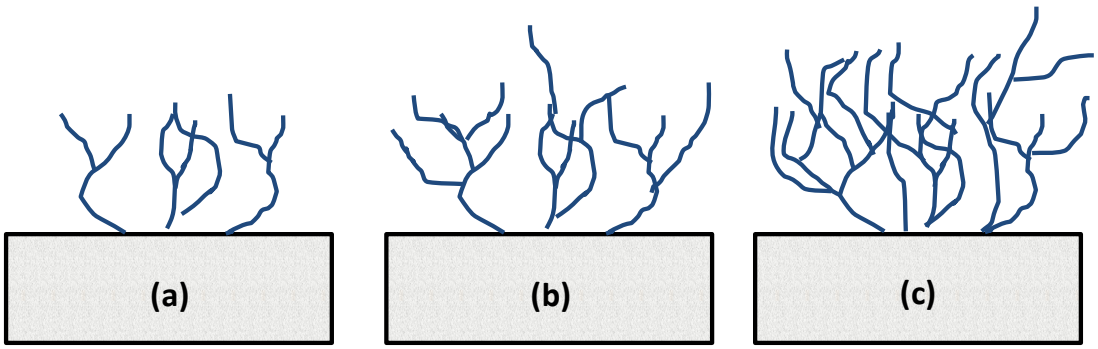

Figure 1.12: *Schematic of the grafting process illustrating (a) the formation of polymer chains on the pre-formed monolith, (b) an intermediate stage where extensive branching occurs and (c) termination stage where inter-branching connections occur.*

These newly formed branches also contained abstractible hydrogens and hence further chains can grow upon these, leading to extensive cross-linking. Rånby observed that acrylate monomers have a higher reactivity than methacrylate monomers since the level of reactivity is related to the type of hydrogens present (see Figure 1.13). The photoreduction process is accelerated with tertiary hydrogens present in acrylates which are not present when methacrylate monomers are used. This single step process (initiator and monomer both present during irradiation) however, limits the efficiency of the grafting, often leaving ungrafted polymer filling the pores of the monolith which is often difficult to remove and could potentially lead to the blocking of the monolith. In order to counteract these limitations, two-step processes have been developed which aim at improving the grafting efficiency. The initiator is immobilised on the surface in the first step in the absence of

monomer, such that when monomer is introduced to the pore volume for the second irradiation cycle, the pre-immobilised initiator promotes surface-initiated grafting of the monomer. The first developed two-step methodologies involved trapping the initiator into the monolith's surface by physical absorption [67] while more advanced methodologies resulted in the covalent attachment of the photoinitiator prior to the introduction of the monomer in the second step [68, 69]. As shown in the example illustrated in Figure 1.14, benzophenone molecules are covalently attached by hydrogens being abstracted from the monolith's surface leading to the formation of a surface bound initiator.

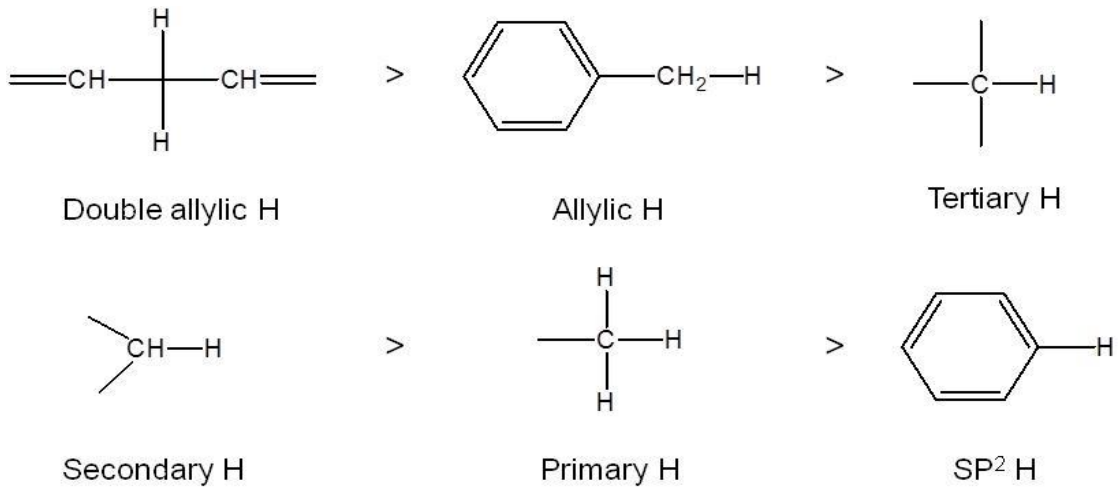

Figure 1.13: *Image showing the photoreduction reactivity order for 6 different types of hydrogens [65].*

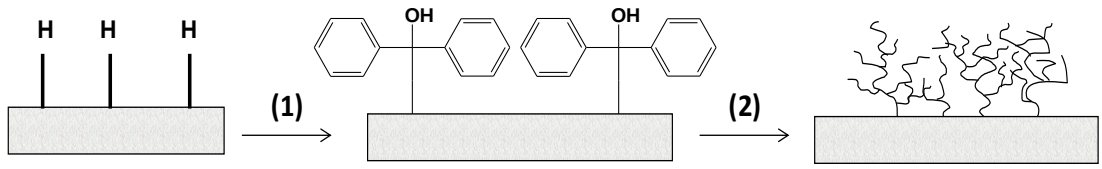

Figure 1.14: *Schematic illustrating the 2-step grafting process of a reactive monomer in the presence of benzophenone as the photoinitiator. (1) In a first step, photoinitiator is immobilised on the pore surface by UV irradiation of a polymer monolith that is in contact with the benzophenone solution. (2) In a second step, UV-initiated grafting is carried out with a solution containing a monomer only.*

When the monomer is subsequently added and UV light is applied for a second time, the free radical previously generated allows the polymerisation to occur directly from the surface. The two-step approach proves to be favorable for a variety of

reasons such as improved grafting efficiency and reduced amounts of non-grafted polymer in solution.

The grafting process can be applied to modify surfaces with a wide variety of polymer films including polymer brushes and dendrimers. Polymer brushes have an extended configuration from the attachment sites. Initially the substrate of choice is functionalised with an initiator which is then exposed to a solution containing catalyst and monomer. Radical polymerisation techniques such as atom transfer free radical polymerisation (ATRP) and ring opening metathesis polymerisation (ROMP) are often used to achieve a controlled growth of grafted polymer brushes [70]. Kim *et al.* [71] for example grew polymer brushes from norbornene-based monomers by ROMP on silicon wafer surfaces using an immobilised ruthenium catalyst, leading to a rapid and controlled growth of brushes up to 90 nm thick. Using a similar process Moon and Swager [72] grew 10 nm thick brushes of poly(p-phenylene ethynylene) for applications as chemical sensors. Methacrylate monomers (in particular MMA) are commonly grafted by ATRP instead. Ejaz *et al.* [73] grafted 80 nm thick PMMA brushes over a period of 12 hours on a porous glass filter using 2-(4-chlorosulphonylphenyl) ethyltrichlorosilane as the initiator which had been intially chemisorbed onto the surface. The concentration of the initiator was found to affect the thickness of the film since lowering the concentration led to the formation of thicker films (presumably, higher concentrations of initiator led to unwanted homopolymerisation of the monomer rather than surface grafting). Furthermore the addition of water as solvent was found to considerably speed the polymer brush formation as reported by Jones *et al.* [74] who grafted 35 nm thick PMMA brushes in only 35 minutes.

Similarly dendrimers have also been grafted on surfaces such as silica. These star-shaped macromolecules have highly controllable structural properties which allow to achieve very narrow molecular weight distributions. Polyamidoamine dendrimers for example were grafted on ultrafine silica following a two-step mechanism which involved the initial Michael addition of methyl acrylate to amino groups as the surface-bound initiator and the terminal amidation of the resulting esters with ethylenediamine [75]. The percentage of grafting was found to increase by increasing generation and reached 576% after the 10^{th} generation. Dendritic polyether has also been grafted on aminopropyltriethoxysilane (APS)-functionalised

silica nano-particles by *N*-*N*'-dicyclohexylcarbo-diimide mediated esterification [76]. The initial modification with APS was found to be crucial for the formation of polymer grafts on the surface and the overall net grafting was maximised (16%) when dichloroethane was used as solvent.

Numerous applications of dendrimers or dendrimer-modified stationary phases in the field of separation science have appeared in the literature. Jackowska *et al.* modified a bare silica gel surface with a drendritic polymer comprised of methylamine and 1,4-butanedioldiglycidyl ether for applications in anion-exchange chromatography [77]. A liquid-crystalline polypropyleneimine dendrimer has been used as a stationary phase in gas chromatography [78] and dendrimers have been used as pseudo-stationary phases in electrophoretic separations; their use is described in a number of excellent reviews [79, 80].

While the modification of monolithic stationary phases with polymer grafts possessing a dendritic conformation has thus far not been described in the literature; there is no obvious reason why this would not be possible. It will not be the focus of the work described in this thesis, but is certainly a noteworthy alternative that merits further investigation in a related study.

One of the main advantages of photografting is the possibility to target and modify specific regions of a monolith rather than the entire surface, allowing different sections of a single monolith to be functionalised with different surface chemistries. Photomasks are applied for this purpose. Peterson *et al*. [81] described the photografting of azlactone onto a specific region (20 cm) of a 25 cm long polymer monolith in capillary format for the immobilisation of trypsin, allowing the formation of a enzymatic micro-reactor while leaving a portion of a monolith unmodified which acted as a micro solid-phase extractor. Different volumes of a myoglobin solution ranging from 2 to 20 μ*L* were then loaded on the device. Very high sequence coverages of almost 80 % were achieved for the highest loading. Connolly *et al.* also reported the use of photomasking for grafting two distinct zones of 2-acrylamido-2-methyl-1-propanesulphonic acid on a polymer monolith [82]. Conductivity detection was used to obtain a profile of the exact spatial location of the charged functional groups along the surface.

1.6 Formats and housings of polymer monoliths

The first approaches in the synthesis of polymer monoliths involved the use of housing similar to standard-bore HPLC columns with internal diameters (i.d.) ranging from 4 to 10 mm [8, 83] . The lack of homogeneous porous structures and the presence of voids between the column inner walls and the monoliths represent the main limitations of monoliths prepared in these formats. The issues present also when dealing with biological samples, often available in limited quantity, required the shift towards smaller formats such as capillaries, micro-chips and pipette-tips.

1.6.1 Fused silica capillary

A vast number of reports illustrate the in-situ preparation of polymer monoliths within the boundaries of fused silica capillaries. Silane chemistry is often used for allowing proper bonding of the stationary phase with the inner capillary walls. Ericson *et al.* [84] for example originally reported the use of 3-methacryloyloxypropyl trimethoxysilane for this purpose. The methoxysilane part allowed bonding with the silanol groups present on the surface of the silica wall while the methacryloyl group is available to react with acrylic groups present in the monomer solution (see Figure 1.15). Polyimide and teflon coatings are present in most fused silica capillaries available commercially.

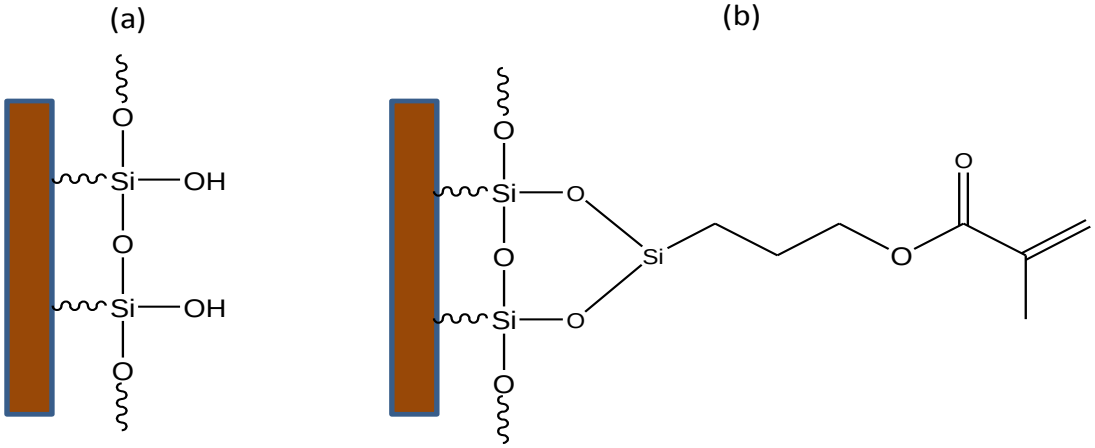

Figure 1.15: *(a) silanol groups present on the inner surface of fused silica capillaries and (b) modification of silanol groups with 3-methacryloyloxypropyl trimethoxysilane [85].*

The teflon coating has decreased flexibility over polyimide [27], hence requiring greater handling care, but it allows UV initiated polymerisation methods. The use of capillaries however, has an impact on the system setup requirements since micro-pumps are required to deliver low flow-rates and to allow minimal gradient delays which can impact chromatographic performance. Numerous applications of monoliths in capillary format are available in CEC, LC and SPE modes.

1.6.1.1 Capillary electro-chromatography (CEC)

CEC is based on a combination of liquid chromatography and capillary electrophoresis since a stationary phase is required to separate analytes but the movement of mobile phase is caused by the application of an electric potential rather than being pressure driven.

Several reports are available illustrating in detail CEC applications using polymer monoliths [86, 87]. Peters *et al.* [88, 89] demonstrated the first CEC application of such materials as shown in Figure 1.16.

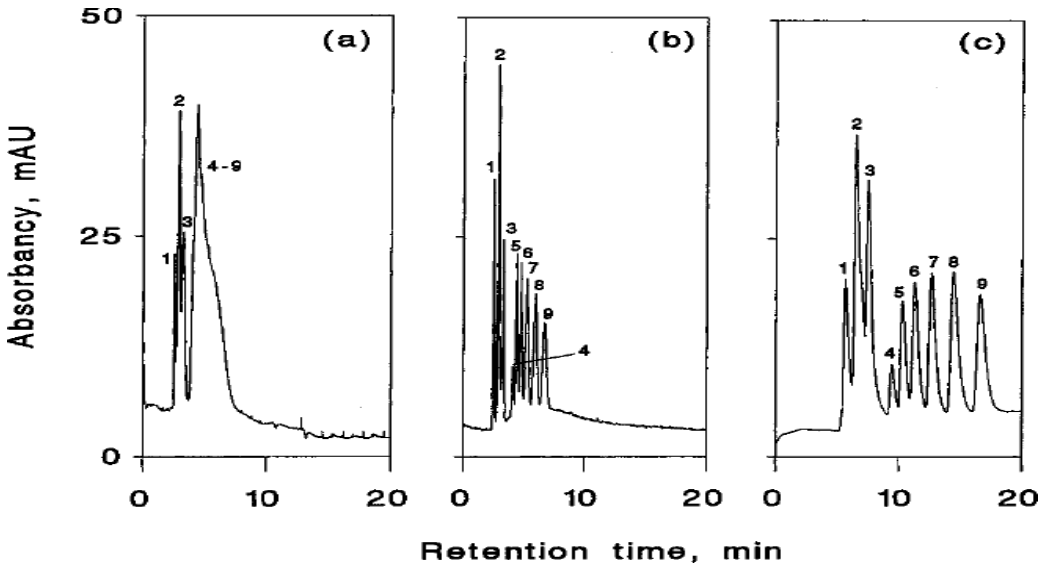

Figure 1.16: *CEC separations of alkylbenzenes on polymer monoliths prepared with an average pore size of (a) 4000 nm, (b) 1230 nm and (c) 670 nm. Peaks: thiourea (1), benzyl alcohol (2), benzaldehyde (3), benzene (4), toluene (5), ethylbenzene (6), propylbenzene (7), butylbenzene (8), and amylbenzene (9). Mobile phase, 80:20 v/v mixture of acetonitrile and 5 mM phosphate buffer pH 7; UV detection at 215 nm [88].*

Monoliths containing both a hydrophobic structure (due to the methacrylate components) and a charged functionality (due to the presence of 2-acrylamido-2-methyl-1-propanesulphonic acid) were prepared and the effects of porosity and chemical composition on chromatographic performance were illustrated.With an average pore size of 4000 nm, the surface area provided to interact with alkylbenzenes is low hence a poor separation was observed. By increasing the hydrophobicity and improving the surface area of the monoliths, high separation efficiencies (up to 120,000 N/m) were obtained. The authors correctly reported that while in LC a stationary phase is only responsible for its effect on the separation, in CEC it is also responsible for enabling the electro-osmotic flow.

1.6.1.2 Liquid chromatography (LC)

The vast range of functionalities offered by the monomers available for the synthesis of monoliths, allowed for a wide range of chromatographic modes, particularly reversed-phase and ion-exchange. The first application in reversed-phase chromatography involving a polymer monolith in capillary format was performed by Liao *et al*. [7] who used a hydrophobic monomer, butyl acrylate, for the preparation of monoliths in a 600 x 0.3 mm capillaries which were applied to the separation of proteins. The main issues with these monoliths were the low robustness, which caused the monolith to break, and poor efficiencies caused by the void volumes which were formed as a consequence of the mechanical issues. Morakovca *et al*. [90] also prepared and showed reversed-phase LC applications (see Figure 1.17) of methacrylate monoliths in 0.32 mm i.d. capillaries based on a porogen system consisting of butanol, propanol and water similar to the monoliths prepared by Svec's group for CEC applications [88]. An increase in butanol as the porogenic solvent led to a decrease in pore volume and size followed by the consequent increase in efficiencies, at the expense of permeability.

A common monomer used for adding cation exchange functionalities is 2-acrylamide-2-methyl propane sulphonic acid (AMPS). For example Gu *et al.* [91] prepared a monolith in a 75 µm i.d. capillary with cation-exchange behaviour from the polymerisation of various sulphonic monomers such as AMPS and sulphoethylmethacrylic acid (SEMA) using poly(ethylene glycol) diacrylate (PEGDA) as the crosslinker and relying on the hydrophilicity of the cross-linker's

ethylene glycol in order to decrease the hydrophobicity of the monolith which could lead to non-specific interactions with biological molecules.

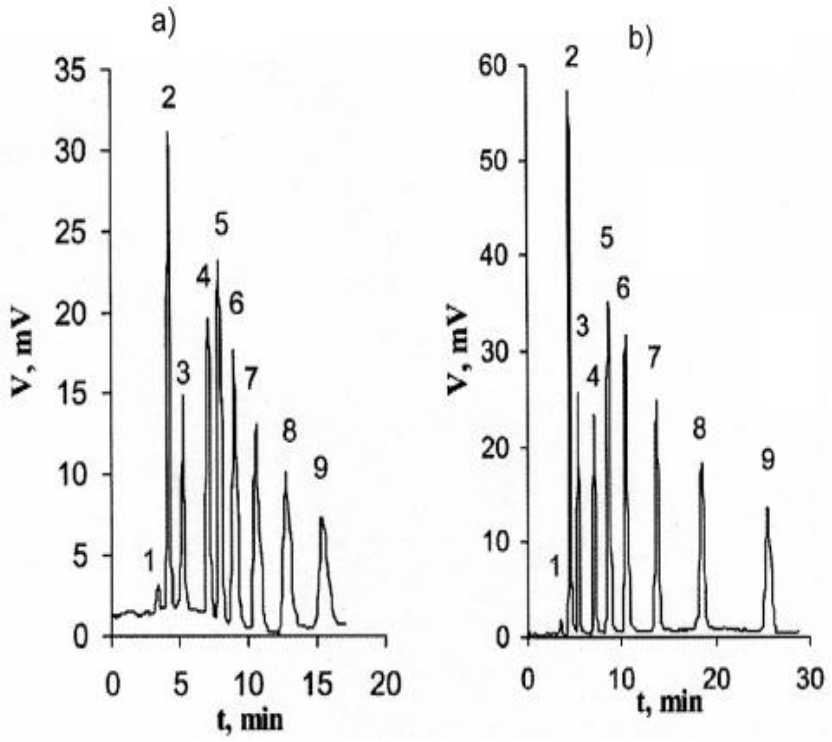

Figure 1.17: *Image showing (a) the separation of alkylbenzenes on a methacrylate capillary column (139 x 0.32 mm) and (b) a column packed with Biosphere C_{18} beads (141 x 0.32 mm). Mobile phase: 70% aqueous acetonitrile, flow rate 2.0-2.2 µL/min, UV detection at 254 nm. Peaks: (1) uracil, (2) benzyl alcohol, (3) benzaldehyde, (4) benzene, (5) toulene, (6) propylbenzene, (7) butylbenzene, (8) amylbenzene [90].*

This ultimately led to very high efficiencies with peak capacities up to 179 for selected peptides. If however, an anion exchange functionality is required, the ring opening reaction involving modification of GMA with an amine containing compound has often being exploited for such purposes [92, 93]. Polymer monoliths have been demonstrated to be particularly useful for such applications due to their high p*H* stability and ability to tolerate hydroxide eluents [94]. The macro-porous structure of polymer monoliths has limited the applications mainly to the separation of large molecules. Poor results are often obtained with small molecules, due to the absence of small meso-pores and the consequent low surface areas present.

1.6.1.3 Solid-phase extraction (SPE)

SPE is based on a process of physisorption hence a large surface area is required for the extraction of analytes from a sample. Capillary monoliths have shown applications in the pre-concentration and extraction of analytes as highlighted in a recent review [95]. With the miniaturisation of analytical devices, sensitivity becomes an issue to consider for proper detection of analytes and consequently the pre-concentration of a sample becomes a very important parameter. Several reports illustrate the application of monolithic capillary columns used for pre-concentration in CEC [96], CE [97] and HPLC [98].

In a typical on-line setup, shown in Figure 1.18, the SPE device and the analytical column are connected to a 6 port injection valve. As demonstrated by Fan *et al*. [98], after the sample is loaded onto the SPE device, (a monolithic column of 15 cm x 0.25 mm i.d. prepared from methacrylic acid and ethylene glycol dimethacrylate), the valve is switched to the inject position for transfering the sample onto the separation column, in this case a C_{18} silica packed column for the analysis of blood serum samples, proving high extraction efficiencies relative to traditional open tubular extraction columns.

The sample capacity for theobromine, theophylline and caffeine was calculated to be 176, 324 and 540 ng. These were extracted from a mixture with a concentration of 1 μg/m*L* at 0.04 m*L*/min. In other instances, the SPE device and the analytical columns can be located on the same structure. Thabano *et al*. [97] for example described the *in situ* photopolymerisation of a poly (MA-*co*-EGDMA) monolith which was used to create the SPE phase in-line with the CE separation capillary.

The adsorption and release of a series of neurotransmitters from urine samples was achieved by simple p*H* adjustments of the elution buffer, availing of the weak cation-exchange properties of the stationary phase. Adsorption of the analytes as protonated, cationic species onto the SPE phase was achieved using an electrolyte of 6 m*M* phosphate and 12 m*M* sodium ion, buffered at p*H* 7.0 while the elution of the analytes from the SPE phase was achieved using an electrolyte of 12 m*M* phosphate and 12 m*M* sodium ion buffered at p*H* 3.0. The sample capacity for dopamine was found at 403 n*M* with a percentage recovery of 97.3 %.

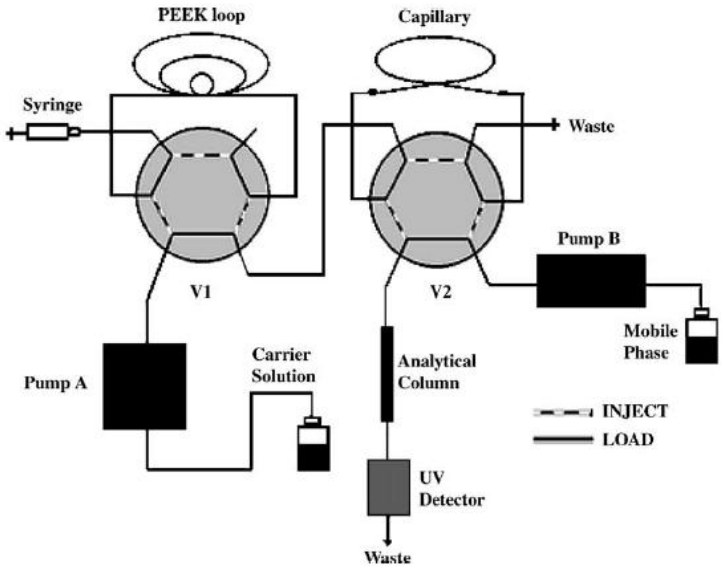

Figure 1.18: *Schematic showing the integration of a on-line SPE monolithic device with a separation column [98].*

1.6.2 Micro-fluidic chip devices

Polymer monoliths have also been prepared within micro-fluidic channels and several reviews have been published on this area [99, 100]. The range of applications is vast ranging from their use as separation columns in LC and CEC modes [101] to SPE [102]. The main advantage of preparing these materials is focused on low sample volume requirements which is a particular advantage when dealing with biological samples. Micro-chip devices are built based on a concept of miniaturisation. A study from He *et al*. [103] evaluated the impact of polymerisation kinetics and surface tension at the capillary inner wall in four capillaries of different i.d. which are considered key factors when downscaling photopolymerised monoliths. The morphology of porous polymer monoliths photopolymerised within capillaries and micro-channels is substantially influenced by the dimensions of confinement. The extent of deformation from the bulk porous structure under confinement strongly depends on the ratio of the i.d. of the housing relative to the monolith pore size. Bulk-like porosity is observed for a confinement dimension to pore size ratio >10, and significant deviation is observed for a ratio < 5. One limitation of this study is caused by the lack of previous treatment of the capillary walls prior to the monolith's formation which could lead to the formation of voids and gaps between the wall and the monolith. When dealing with glass surfaces, a

commonly used reagent for wall modification is 3-(trimethoxysilyl)propyl methacrylate. However, this material is not suitable for polymeric surfaces, representing a limitation when dealing with plastic chips. The grafting of benzophenone was reported by Rohr *et al*. for resolving this issue [104]. Early applications of monolithic micro-chips as separating columns encountered several issues due to pressure limitations. Over the last decade improvements in bonding techniques and the use of high-pressure connections have helped in overcoming these issues. Liu *et al*. [105] have developed a cyclic olefin copolymer (COC) micro-chip based on a BuMA monolith for µLC separations which was able to withstand pressures up to 2900 psi for the separation of peptides and proteins. Of course the pressure limitation is only an issue when dealing with liquid chromatography. µCEC applications have been reported as well [101, 106] which rely on the application of a voltage and do not suffer from this issue since there is no need for pumps or external injectors.

1.6.3 Pipette-tip format

UV transparency makes polypropylene tips another suitable housing for the preparation of photopolymerised polymer monoliths. Other advantages of this material include solvent resistance and the presence of abstractible hydrogens which facilitates photografting. Several reports in the literature have reported the application of polymer monoliths in such formats for the extraction and treatment of biological samples [107-109]. Altun *et al*. [109] reported the preparation of 96 polypropylene tips with chemically bonded methacrylate monolithic stationary phases (see Figure 1.19), handled by a robot in a 96-well format, which have been used for the adsorption of lidocaine and roscovitine from plasma.

The purification of 96 samples in a time frame of 2 minutes was reported. Accuracy values from 95% to 104% (n=24) and RSD values of 3-11 % (n=24) were obtained which are within the international accepted limits [110]. Although, the surface of the tip was not modified to facilitate the anchoring of the monolith, the authors reported that no voids were observed and the monoliths could operate at pressures of up to 4 bar without any structural damage occurring.

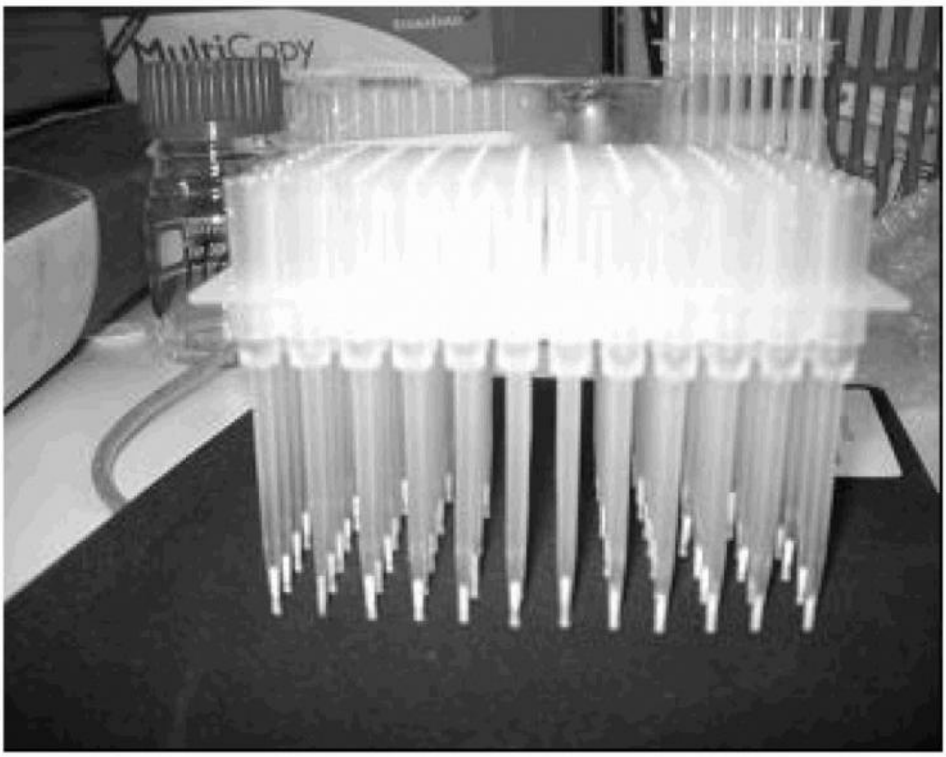

Figure 1.19: *Polymer monoliths in pipette tips in a 96-well format [109].*

1.7 Commercially available polymer monoliths

Polymer monoliths are available commercially in a variety of formats. BIA separations [111] produces monolithic columns in CIM (Convective Interaction Media) format (predominantly GMA-*co*-EDMA monoliths) with various surface chemistries such as weak anion-exchange (WAX), strong cation-exchange (SAX), strong cation-exchange (SCX), in dimensions between 12-16 mm in diameter and 2.5-3 mm width. Thermo Scientific corporation [112] markets several products under the brand names of ProSwift, DNASwift and IonSwift. ProSwift columns are made from polystyrene-*co*-divinylbenzene (PS-*co*-DVB) and are functionalised for both strong and weak cation/anion-exchange applications but also they are also modified with phenyl groups for reversed-phase applications and come in dimensions of 1 mm/4.6 mm i.d. and 50 mm/250 mm in length. DNASwift columns are based on polymethacrylates and come in stuctures of 5 mm i.d./150 mm in length while the IonSwift columns are based on a styrene-DVB backbone. UNO columns from Bio-Rad [113] are based on a polyacrylamide structure instead and are similarly designed for ion-exchange applications.

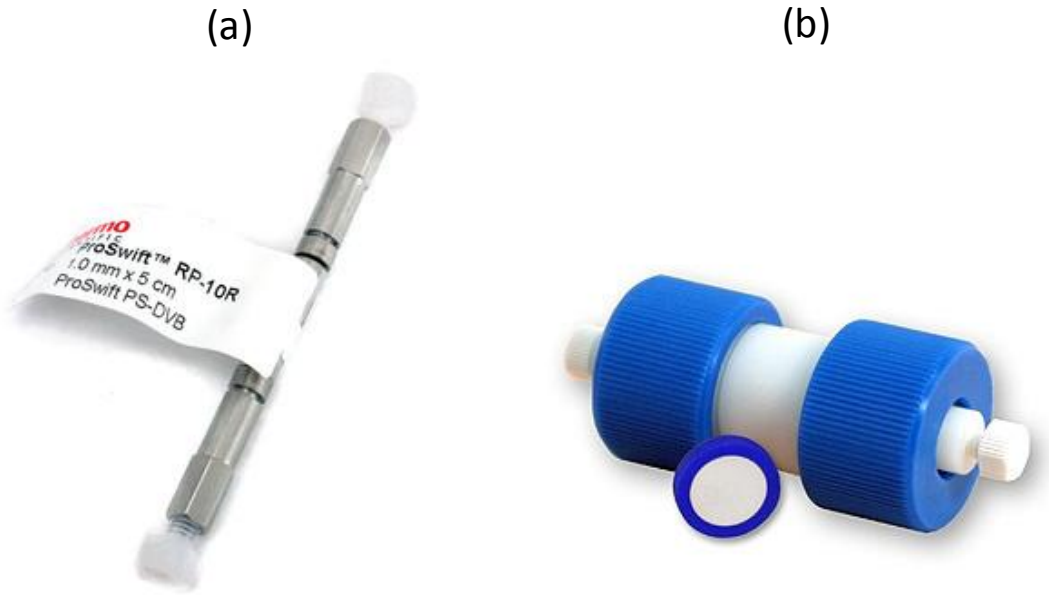

***Figure 1.20**: Images of (a) ProSwift column from Thermo Scientific and (b) monolithic CIM disk from Bia Separations [111, 112].*

1.8 Nano-particle functionalised monolithic stationary phases

Traditionally nano-particles have been immobilised on various micro-porous and meso-porous inorganic supports such as zeolites [114], $Al(OH)_3$ [115], silica [116] and polymers [117] for applications in the areas of catalysis [118] and sensors [119]. More recently, applications of these materials in the areas of separation science have been reported [120]. This led to the fabrication of nano-agglomerated monolithic stationary phase either for functionalisation purposes or, in the case of polymer monoliths, to increase the (limited) surface area present.

1.8.1 Latex nano-particles

Latex nano-particles were originally developed for preparing particulate column packings several decades ago however, only recently they have been used for the functionalisation of polymer monoliths. Hilder *et al.* [121] originally prepared a poly(butylmethacrylate–*co*-ethylenedimethacrylate–*co*-2-acrylamido-2-methyl-1-propanesulphonic acid) (BuMA-*co*-EDMA-*co*-AMPS) monolith modified with 60 nm quaternary ammonium functionalised latex nano-particles via electrostatic bonding, applied for an anion-exchange separation of carbohydrates as shown in Figure 1.21. An increase in surface area from 35.2 to 47.3 m^2/g was observed despite

the very scattered level of coverage which was observed. An efficient separation of 7 saccharides was obtained in less than 10 minutes as shown in Figure 1.22 despite the limited coverage of nano-particles which was related to the low sulphonate functionalities present on the surface. A limited amount of anchoring sites were available for the latex nano-particles and this led to small ion-exchange capacity values (between 0.59-1.58 μequiv.g^{-1}).

Other reports involving the the preparation of similar monolithic stationary phases for ion-exchange were reported. Hutchinson *et al.* [122, 123] prepared sulphonated polymer monoliths modified with quaternary ammonium functionalised Dionex AS10 or AS18 latex particles achieving efficiencies of 1.66 x 10^5 N/m for the separation of 7 inorganic ions in capillary electrochromatography (CEC) mode [122] and of 13,000 N/m for iodate in micro-ion chromatography (μ-IC) mode [123]. In order to increase the ion-exchange capacity of such monoliths Hutchinson *et al*. [94] further investigated the surface modification of reactive GMA monoliths. Seven anions were separated as shown in Figure 1.22. A large increase in ion-exchange capacity, up to 29 μequiv g^{-1}, was observed when the epoxy rings of GMA were reacted with 4-hydroxybenzenesulphonic acid, which is a considerable improvement from the monoliths prepared by co-polymerisation with AMPS [121]. However, heavy peak tailing of benzesulphonate was observed due to π-π interactions of the benzene ring.

The best compromise between ion-exchange capacity and peak resolution was observed when the epoxy ring of GMA was reacted with sodium sulphite due to lower hydrophobic interactions between analytes and the stationary phase. No evaluation on the level of nano-particle coverage achieved on this stationary phase was performed.

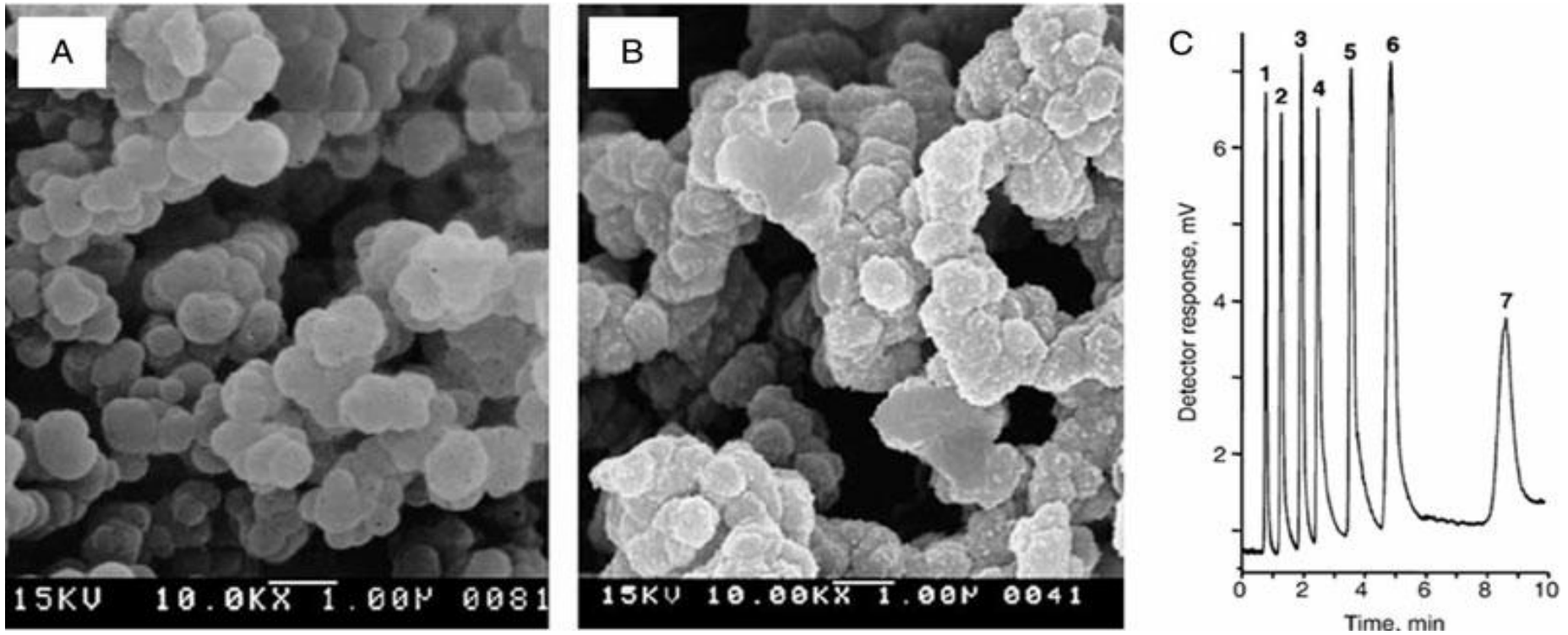

Figure 1.21*: Images showing (a) SEM of a BuMA-co-EDMA-co-AMPS monolith, (b) SEM of a similar monolith with latex nano-particles attached, (c) a chromatogram showing the separation of 7 carbohydrates using a latex nano-particle modified monolith. Peaks: (1) d(+)galactose , (2) d(+)glucose, (3) d(+)xylose, (4) d(+)mannose, (5) maltose, (6) d(−)fructose, (7) sucrose. Injection volume 100 nL; sample concentration 1 mg/mL [121].*

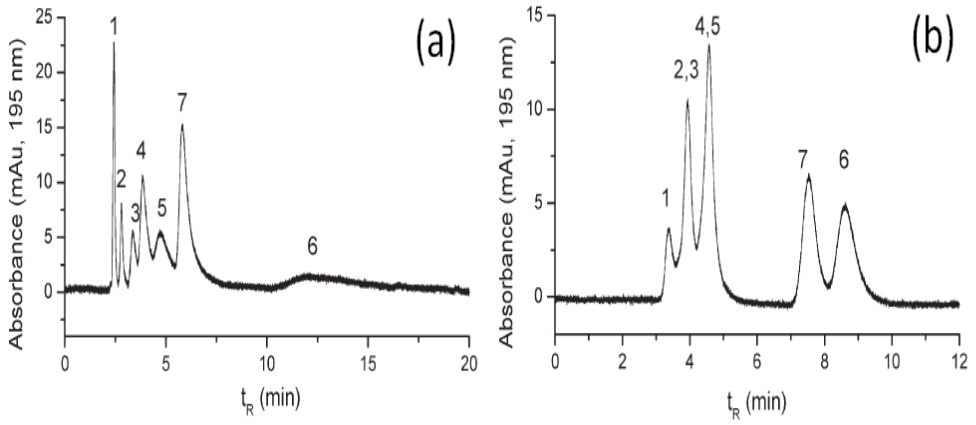

Figure 1.22: *Chromatograms showing the separation of a 7-anion mixture using latex nano-particle functionalised GMA monoliths which had been modified with (a) 4-hydroxybenzenesulphonic acid and (b) sodium sulphite. Analytes: (1) IO_3^-, (2) BrO_3^-, (3) NO_2^-, (4)Br^-, (5)NO_3^-, (6) I^- and (7) benzenesulphonate. Concentrations: 0.14 mM [94].*

The modification of silica monoliths with latex nano-particles was also reported. Hutchinson *et al.* [124] functionalised silica monoliths in 50 and 75 µm i.d. capillaries with quaternary ammonium functionalised latex nano-particles (70 nm) which were immobilised electrostatically to the negatively charged silanol groups, leading to an ion-exchange stationary phase suitable for applications in capillary electrochromatography (CEC) as shown in Figure 1.23. The porosity of the monoliths was found to be 70.4 % and an increase in surface area from 167 to 186 m^2/g was observed upon modification with the nano-particles. The ion-exchange capacity of a 50 µm i.d. / 25 cm long latex-coated silica monolith was found to be 0.342 nano-equivalents and 80,000 theoretical plates per column were typically achieved for weakly retained anions, with lower efficiency being observed for analytes exhibiting strong ion-exchange interactions with the stationary phase. The strong interactions were suppressed only when using large concentrations of competing ions (greater than 1 *M* phosphate or 200 m*M* perchlorate).

Glenn *et al.* [24] described the functionalisation of a commercially available silica monolith (Merck Chromolith 100 mm x 4.6 mm) with Dionex AS9-SC latex nano-particles (110 nm) and its chromatography performace was compared with another silica monolith which had been functionalised with didodecyldimethylammonium bromide (DDAB) to achieve anion-exchange functionalities.

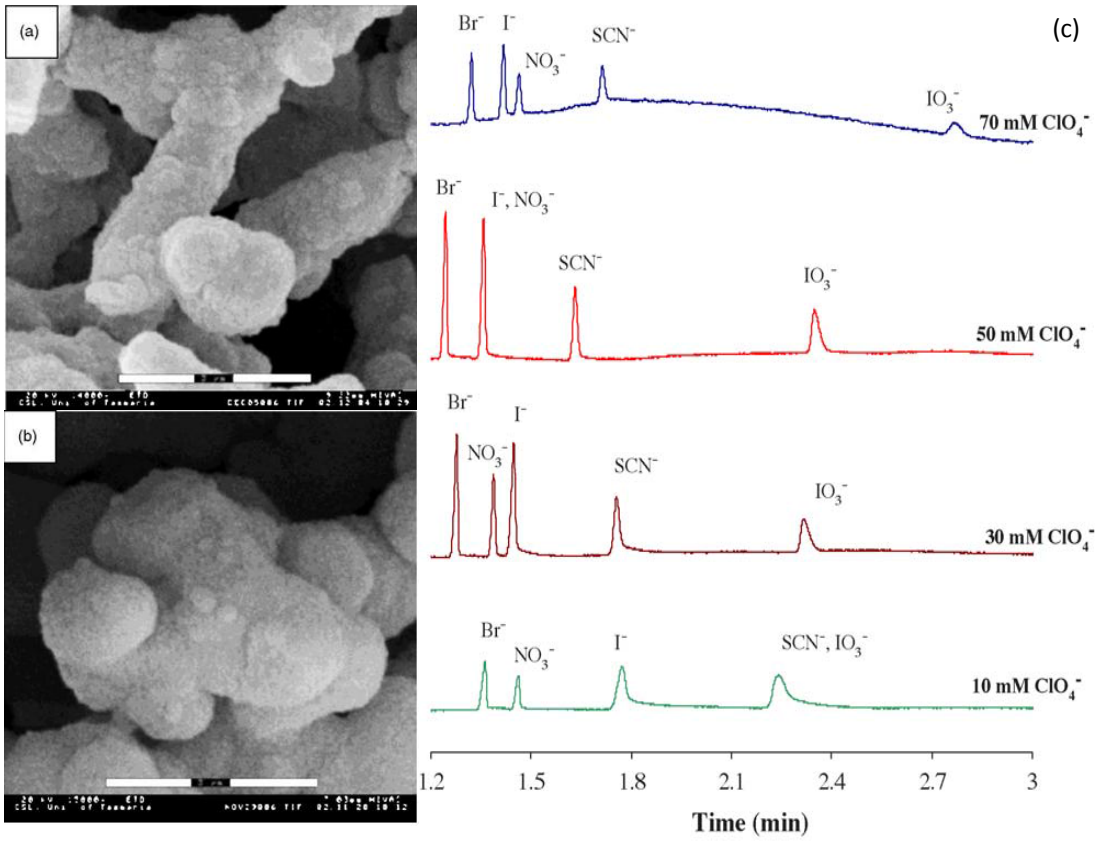

***Figure 1.23**: Images showing (a) a SEM of the uncoated silica monolithic, (b) a SEM of the latex nano-particle silica monolithic structure and (c) IE-CEC separations of inorganic anions on a latex-coated silica monolith when the concentration of perchlorate as competing anion was varied. Detection was performed on-column using a 33.4 cm × 50 µm i.d. latex nano-particle coated silica monolith. BGE: Tris/ClO_4 at varying concentrations; voltage: −15 kV; temperature: 25 °C; UV detection: 195 nm [124].*

The column's selectivity towards inorganic ions was demonstrated using 7.5 or 5.0 m*M* 4-hydroxybenzoic acid (p*H* 7.0) with suppressed conductivity detection. Direct comparisons were then made between the two columns in terms of selectivity, efficiency and stability. The latex-coated column was on average 50 % more efficient than the DDAB-coated column and also more stable since < 1 % change in retention was observed even after 2.5 months of periodic use, relative to a 10 % decrease in retention times which was observed on the DDAB-modified column after constantly pumping the eluent for 11 hours.

Further modification of silica monoliths with latex nano-particles were reported by Ibrahim *et al.* [125, 126] for HILIC and anion-exchange chromatography.

Commercially available silica monoliths, such as Chromolith from Merck and Onyx from Phenomenex, were modified with latex nano-particles of different sizes (105, 140 and 151 nm) and different ion-exchange capacities (44.1 ± 0.2, 4.4 ± 0.1 and 14.0 ± 0.7 μeq/column respectively). As expected, the best separation was obtained with the silica monolith which was coated with the 105 nm latex nano-particles which had the highest capacity, achieving complete separation of acetate, formate, nitrate, bromate, thiocyanate and iodide in under 3.5 minutes with efficiencies between 13,000-50,000 N/m at 3 μ*L*/min. A high acetronitrile content in the mobile phase dramatically increased the efficiency and retention in HILIC mode, where test analytes such as benzoates, nucleotides and amino acids were separated with plate heights of 25–110 μm.

1.8.2. Carbonaceous nano-particles

Carbon nano-tubes (CNTs) have been studied extensively because of their interesting electrical and mechanical properties [127]. More recently, their immobilisation upon monolithic stationary phases has been documented. Li *et al.* [128] originally described the encapsulation of single-walled CNTs in a vinylbenzyl chloride-*co*-ethylenedimethacrylate (VBC-*co*-EDMA) monolith for micro-HPLC and CEC applications. Because of its hydrophobic properties, reversed-phase applications of small neutral molecules were demonstrated with improved retention. Also several peptides were separated in CEC mode with improved efficiencies relative to unmodified stationary phases. Chambers *et al.* [129] also reported the modification of polymer monoliths with multi-walled CNTs (MWCNTs) using two different approaches. The first method was based on the encapsulation of the nano-tubes within a GMA-*co*-EDMA monolith by adding the CNTs to the monomer mixture prior to polymerisation. Although improved retention and efficiencies were obtained for small organic molecules in reversed-phase HPLC mode, aggregation of the CNTs during polymerisation was observed. Hence a further functionalisation method was developed which involved the covalent attachment of partially oxidised MWCNTs to the aminated surface of a GMA-*co*-EDMA monolith due to the interactions with the carboxylic acid functional groups present on the MWCNTs. High efficiencies up to 44,000 N/m were observed with small organic molecules in reversed-phase mode. The encapsulation of MWCNTs was also reported by Andre *et al.* [130] for the

preparation of an enzymatic reactor by immobilisation of arginase. A GMA-*co*-EDMA monolith was first prepared by thermal polymerisation with the addition of 0.10-0.30 wt% MWCNTs (5-10 nm i.d., 10-30 nm o.d. and 1-2 µm in length) to the monomers mixture. The monolith was then formed within a stainless steel housing (4.6 mm x 20 mm) and arginase was attached via linkage with glutaraldehyde, an amine-reactive crosslinker which was immobilised after the amination of the monolithic surface.

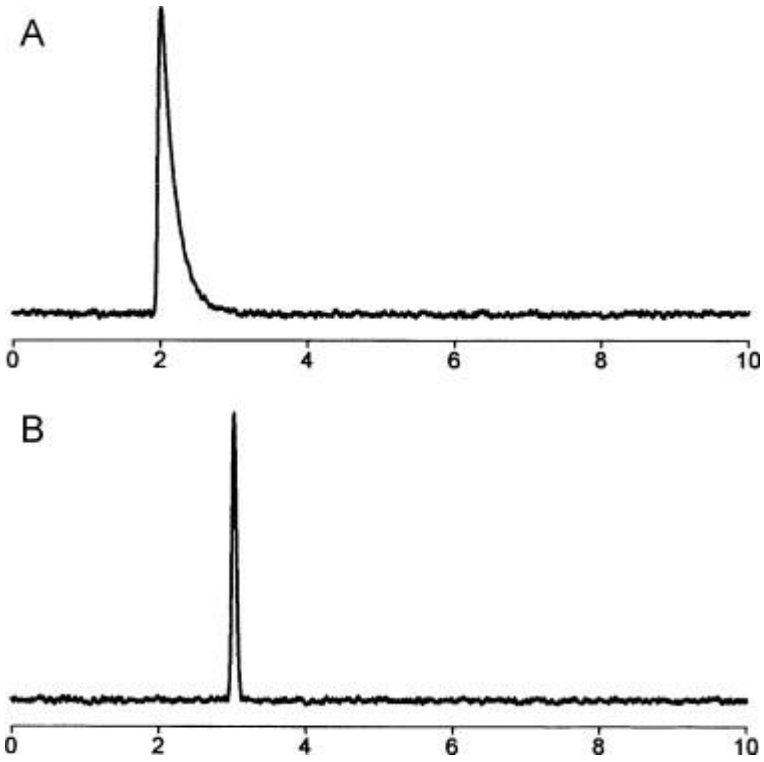

Figure 1.24*: Chromatograms showing the retention of m-nitroaniline on GMA-co-EDMA monoliths in (a) the absence and (b) the presence of 30 wt % MWCNTs Mobile phase: 0.1 mM Tris–HCl buffer pH 7.4, 10 mM $MnCl_2$. Flow rate: 0.4 mL/min. Column temperature: 25 °C. Detection wavelength: 372 nm [130].*

No changes in porous structure (1.70 µm) and surface area (39 m^2/g) were observed however, improved retention and efficiency of m-nitroaniline was verified as shown in Figure 1.24 due to π-π interactions between the aromatic group of the analyte with the CNTs.

Further work by Andrè *et al.* [131] involved an effective method for the immobilization of single wall carbon nano-tubes (SWCNTs) with an average diameter of 1 nm on silica monoliths.

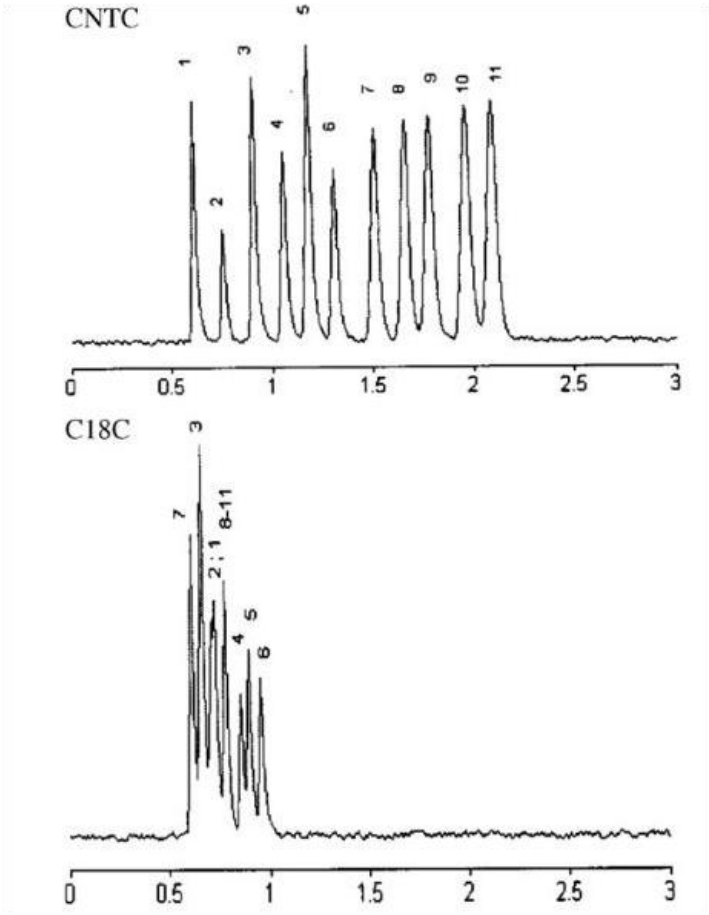

***Figure 1.25**: Chromatograms showing the separation of small molecules on (top) a carbon nano-tube modified silica monolith and on (bottom) a bare C_{18} Chromolith column. Analytes: (1) Phenol, (2) aniline, (3) cathecol, (4) 4-methoxy-phenol, (5) 4-ethoxy-phenol, (6) 4-propioxy-phenol, (7) 3-nitro-phenol, (8) 2,3-dihydroxynaphthalene, (9) 1,3-dihydroxynaphthalene, (10) 2,3-dinitronaphthalene and (11) 1,3 dinitronaphthalene. Mobile phase: ACN/H_2O (60/40)(v/v). Flow rate: 8.5 mL/min. Column temperature: 25 °C. UV detection at 254 nm [131].*

This involved coating the monolith with ultra short SWCNTs in a non-covalent way to preserve the sp^2 nano-tube structure and thus their physico–chemical properties. The aminated surface of the monolith was stabilised with 1-methyl-2-pyrrolidinone efficiently and allowed the adsorption of the SWCNTs onto the chromatographic support. The utility of this novel stationary phase was demonstrated by achieving a very fast HPLC isocratic separation of a series of small aromatic compounds (see Figure 1.25). The comparison with a commercial C_{18} monolithic column showed that the SWCNT-modified column presented the best efficiency under similar chromatographic conditions. For example the height equivalent to a theorical plate

for 4-ethoxy-phenol was 4 µm using the SWCNT-modified column at 1 µ*L*/min while a value of 10 µm was observed when using a commercial C_{18} monolithic column under identical conditions.

1.8.3 Hydroxyapatite nano-particles

Hydroxyapatite is a crystalline form of calcium phosphate which has been traditionally used for the purification and separation of proteins [132]. Krenkova *et al*. [133] described the preparation of hydroxyapatite nano-particle agglomerated polymer monoliths as shown in Figure 1.26.

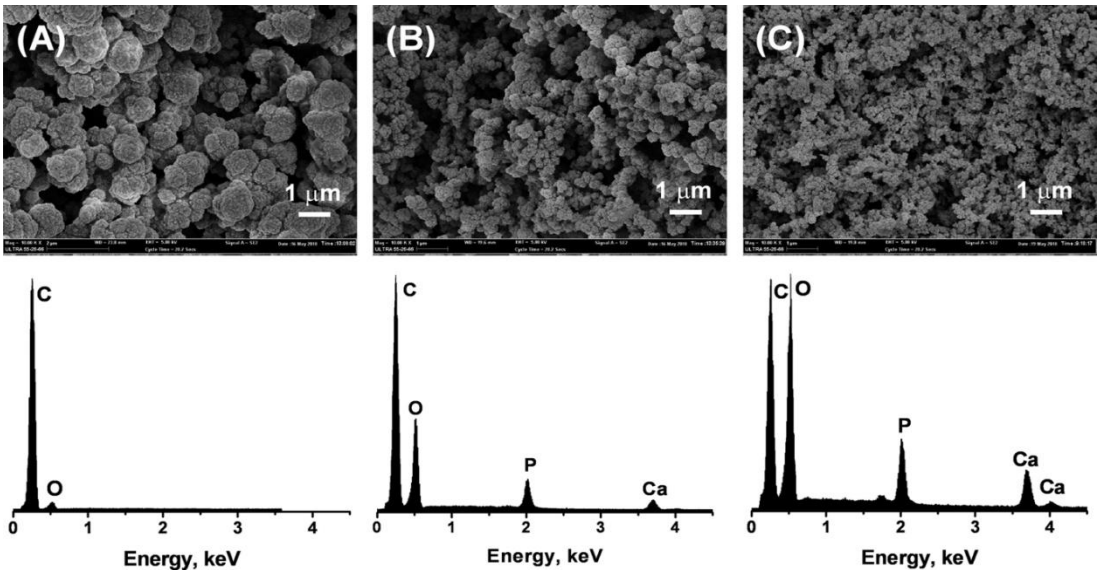

Figure 1.26*: SEM micrographs of monolithic columns containing hydroxyapatite nano-particles at a nano-particle/monomer ratio of (A) 0/50, (B)30/50, and (C) 60/50 (magnification 10,000x) and corresponding energy-dispersive X-ray spectroscopy (EDX) spectra [133].*

Rod shaped hydroxyapatite nano-particles (50 x 150 nm in dimensions) were either encapsulated within a 2-hydroxyethyl methacrylate and ethylene dimethacrylate monolith or immobilised as a further step after the monolith preparation. Although the latter method led to a higher surface coverage, it was demonstrated that column blocking could occur due to the electrostatic interaction between positively charged calcium ions and negatively charged phosphate groups on the surfaces of the nano-particles which led to agglomeration effects, hence the encapsulation route was preferred. An increase in nano-particle concentration

relative to the monomer, led to smaller flow paths and smaller micro-globules as shown in Figure 1.26.

The affinity of the nano-particle agglomerated monoliths towards phosphopeptides enabled their isolation from a tryptic digest of α/β-casein and ovalbumin prior to detection by MALDI-MS. Also a sample mixture of proteins was separated using the same stationary phases and a phosphate-acetonitrile eluent.

1.8.4 Metal nano-particles

Metal nano-particles exhibit different functionalities relative to their bulk scale counterparts, finding interesting applications in catalysis [118] sensors [119] and fuel cells [134]. Several reports describe the modification of polymer monoliths with gold nano-particles (AuNPs) [135-139] however, this topic will be discussed in detail in Chapter 4. The modification of silica monoliths with AuNPs has also been reported [140]. A silica matrix (see Figure 1.27) was prepared from 3-mercaptopropyltrimethoxysilane which provided thiol groups upon which AuNPs could be immobilised.

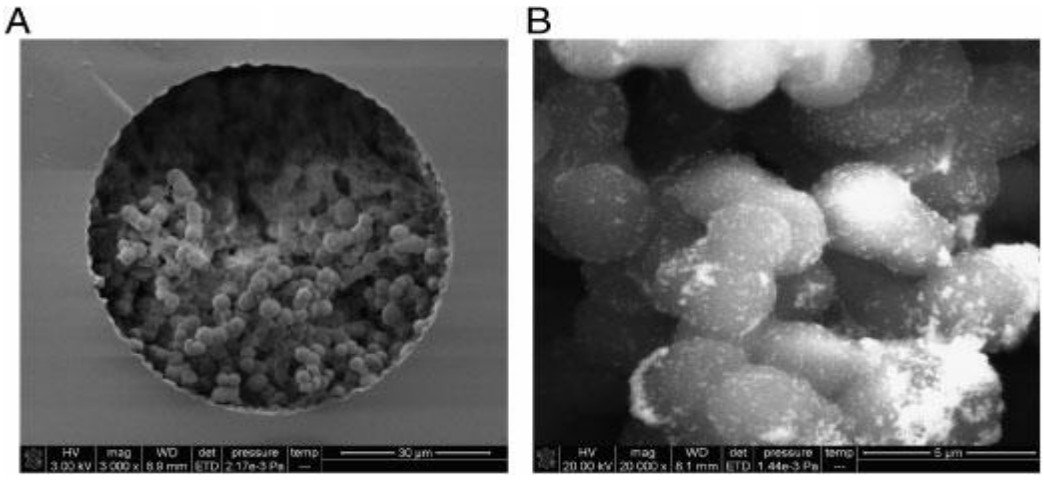

***Figure 1.27**: SEM images of a silica monolith modified with BSA-AuNPs [140].*

Palladium/platinum nano-particles have also been immobilised onto monolithic supports, especially for their catalytic activity towards coupling reactions such as the Suzuki-Miyaura and Heck reactions which will be discussed extensively in Section 1.10.

Bovine serum albumin (BSA) was used to further modify the surface of the immobilised Au NPs and to prove chiral selective properties, since these monoliths were applied for the enantioseparation of a number of phenylthiocarbamyl amino acids by CEC. Ten pairs of amino acids enantiomers were resolved within 18 minutes with resolution values between 1.5-2.1.

Nano-particles based on Ag (AgNPs) have also been successfully immobilised on monoliths for Surface Enhanced Raman Spectroscopy (SERS) applications as shown in Figure 1.28 [141]. The convective nature of the flow and the short diffusion lengths present with polymer monoliths led to considerable reductions in the time involved for the analytes to reach the SERS active sites relative to traditional detectors. Clogging was initially observed when a BuMA-*co*-EDMA monolith was used however, the use of GMA as the monomer with trivinyl cross-linkages (due to the presence of ethoxylated-trimethylolpropane-triacrylate) led instead to more favourable flow-through properties. Aggregates of AgNPs were formed from individual particles (approximately 50 nm in size) and trapped inside the monolith leading to a SERS detection limit of 220 fmol for Rhodamine 6G with excellent signal stability over a 24 hours period.

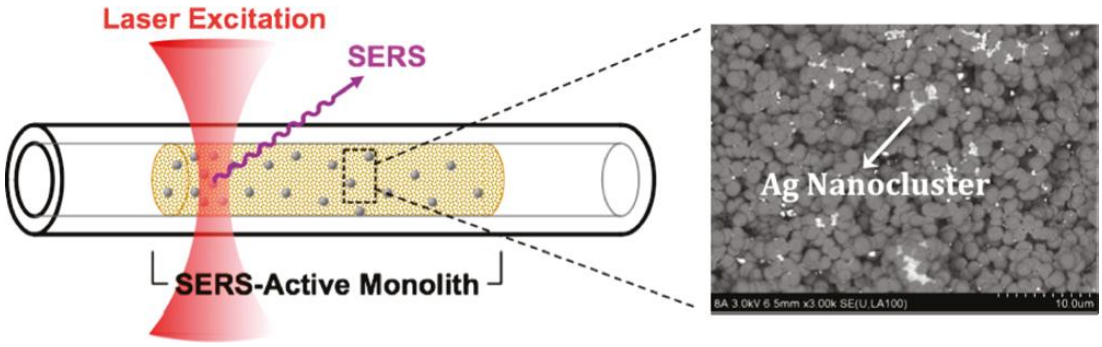

***Figure 1.28**: Image showing a polymer monolith functionalised with AgNPs for SERS applications [141].*

Furthermore, the capability of the SERS-active monolith for the detection of biomolecules was demonstrated by measurements of bradykinin and cyctochrome *c*, demonstrating the benefits of the improved mass-transfer effects present with polymer monoliths since higher signals were observed relative to AgNPs in colloidal form.

1.8.5 Metal oxide nano-particles

Metal oxides are well known for their affinity towards phosphate containing groups hence the main area of application lies in the enrichment of phosphopeptides. In 2006 Liang *et al*. [142] modified a EDMA monolith with 38 nm TiO_2 nano-particles for this purpose. The nano-particles were first silanised with methacryloxypropyltrimethoxysilane (MPTMS) and then photopolymerised in the presence of the cross-linker. Agglomeration allowed the retention of the NPs in the cartridges used, demonstrating a higher binding capacity towards phosphate groups relative to micron sized TiO_2 particles. Similar applications in polypropylene tip formats have also been reported [143]. EDMA monoliths were prepared in such format and TiO_2 nano-particles (10-20 nm) were dispersed within the monomer/porogen solution, leading to clusters of nano-particles appearing on the surface. A tryptic digest from α-casein and β-casein spiked into bovine serum albumin (BSA) nonphosphorylated peptides (molar ratio 1:1:10) was used to assess the selectivity of TiO_2 tips. The effect of 50 m*M* ammonium hydrogencarbonate (p*H* 8) in 50% acetonitrile, which was used as a wash buffer in the reduction of nonspecific bound peptides to the TiO_2 tip, was dramatic. Almost all non-phosphopeptides were not detected by MALDI-MS analysis. The lowest detectable amount of phosphopeptide was estimated at low femtomole level.

Rainer *et al*. [107] immobilised TiO_2 and ZrO_2 (both less than 100 nm in size) onto a series of highly porous DVB monoliths, shown in Figure 1.29, which demonstrated a high capacity and selectivity towards phosphopeptides.

The effect of the nano-particles was studied and compared with micro-scale TiO_2 and ZrO_2 powders. Eleven phosphopeptides from an α-casein digest were recovered with the micro-scale particles whereas nine additional phosphopeptides were retained with the nano-particle functionalised monoliths. Citrate stabilised Fe_3O_4 nano-particles, 20 nm in size, have also been recently immobilised on a GMA-*co*-EDMA monolith in capillary format modified with quaternary ammonium functionality which allowed the electrostatic bonding of the nano-particles [144].

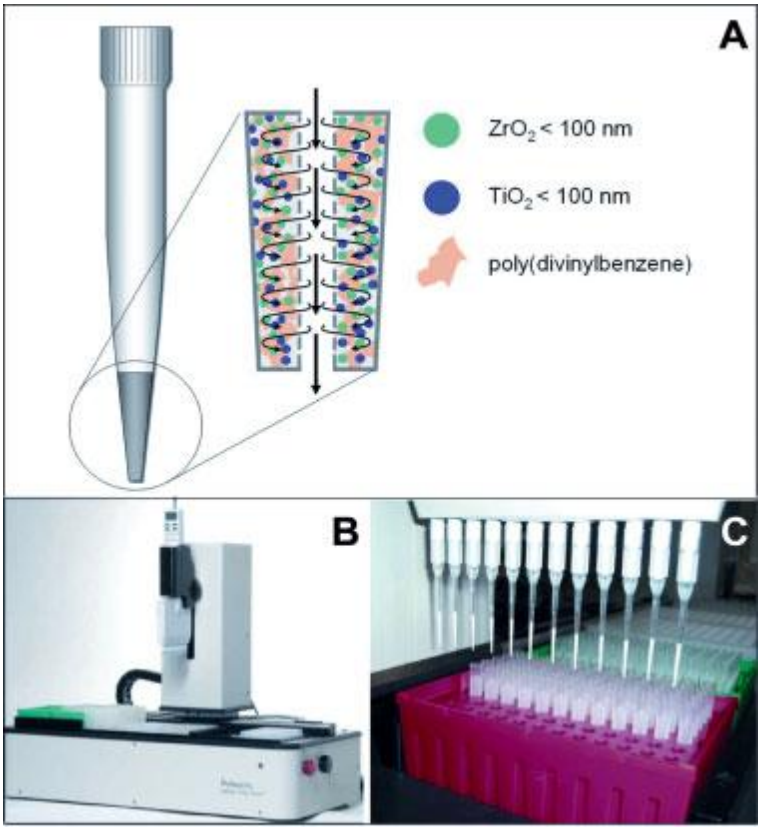

***Figure 1.29**: Image showing (a) a DVB monolith in tip format with immobilised TiO2/ZrO2 nano-particles, (b) and (c) the automated system developed for optimising the enrichment of phosphopeptides [107].*

A high dynamic binding capacity of 86 µmol/m*L* was measured with adenosine-5'-triphosphate. Performance of the monolithic column was demonstrated with the efficient and selective enrichment of phosphopeptides from peptide mixtures of α-casein and β-casein digests and their MALDI/MS characterization in off-line mode, showing an improved enrichment relative to commercially available MonoTip TiO pipette tips.

1.8.6 Silica nano-particles

The modification of polymer monolithic materials with silica nano-particles was originally dated in 1999 when Johnson *et al.* [145] described the preparation of DVB-*co*-EDMA monoliths in bulk format templated by 35 nm silica nano-particles The silica was removed using 48% aqueous HF and the resulting polymer structure featured pores with sizes ranging between 15 and 35 nm due to shrinkage of the polymer material once the silica had been removed. No application of these

templated monoliths was demonstrated by the authors. Thabano *et al.* [146] also reported the preparation of silica nano-particle templated polymer monoliths for on-line SPE-CE applications. The nano-particle suspension (80 nm in size) was added to the polymerisation mixture of a methacrylic acid-*co*-ethylene glycol dimethacrylate (MA-*co*-EGDMA) monolith. UV transparent fused silica capillaries (75 µm i.d.) were filled with the monomer solution, allowing the monolith to form in a 8 cm zone of a 36.5 cm long capillary. After polymerisation, the nano-particles were removed by flushing a sodium hydroxide solution leading to columns with a 33-fold increased ion-exchange capacity relative to untemplated columns. An increase in surface area was however, not observed (27.2 ± 0.5 and 28.4 ± 1.4 m^2/g for untemplated and templated monoliths respectively). It was anticipated that the hydrogen bonding occuring between the silica nano-particles and the methacrylic acid groups, leading to a re-orientation of more methacrylic acid groups after nano-particle removal, was responsible for the increased capacity. This allowed the injection time to be increased 10 times over that of an untemplated monolith, allowing 10 times more sample to be injected with no negative impact upon separation efficiencies. Efficiencies values for the test mixture of neurotransmitters dopamine, norepinephrine and metanephrine similar to capillary zone electrophoresis (100,000–260,000 plates) were also observed.

1.8.7 Nickel-cobalt nano-particles

Tobal *et al.* [147] described the encapsulation of Ni-Co nano-particles (10 nm in size) in polymer monoliths for the enrichment of β-casein tryptic peptides. A 10 wt% solution of nano-particles was added to the monomer mixture before polymerisation in capillaries of 75 µm i.d. and up to 1 m in length. A loading of 10 pmol of protein digest was reported on a 15 cm column, which was further eluted with a water-acetonitrile gradient and characterised by MALDI-MS.

1.9 Catalytic applications of nano-particle functionalised monoliths.

One of the most commonly used supports for catalysis is represented by 100 µm carbon powder which is micro-porous in structure hence providing a large surface area but the absence of macro-pores limits the diffusion of the substrate towards the immobilised catalyst [148]. Recent reports highlight the applications of polymeric

monolithic materials as supports in the area of heterogeneous catalysis [149-153]. Traditionally porous catalytic supports have shown an inferior catalytic activity compared to standard homogeneous catalysis [58, 149] In order to deliver efficient catalytic properties, all solid supports must possess certain features. Ideally they should be easy to prepare, they should prevent the leaching of the catalyst into the products [153] and they should have physical properties which allow sufficient contact between catalysts and substrates. Because of these reasons, monolithic columns represent ideal supports for catalytic applications.

1.9.1. Nano-particle functionalised silica monoliths for catalysis

Sato *et al.* [154, 155] have demonstrated that bimodal porus silica was more active than purely meso-porous structures since the presence of macro-pores facilitated the diffusion of substrate to the catalyst surface enabling faster kinetics hence reports illustrating the preparation of highly macro-porous silica monoliths have started to emerge recently for this purpose [156, 157]. Sasche *et al.* reported the immobilisation of palladium nano-particles (PdNPs) on silica monoliths for hydogenation reactions [157]. The synthetic method was adjusted to facilitate the formation of a large macro-porous structure (4 μm) with meso-pores of 11 nm. The immobilisation of $Pd(NH_3)_4^{2+}$ was performed via ion-exchange mechanism with the negatively charged surface of the silica. Subsequent washing of the monolith at p*H* 8-10 and further calcination led to PdO nano-particles forming which were further transformed into PdNPs after H_2 reduction at 280 °C. These were found to be between 6-7 nm in size which allowed their immobilisation inside the meso-pores of the monolith to maximise the catalytic efficiency. The formation of nano-particles was further confirmed by a change in colour of the monolith from yellow to brown as shown in Figure 1.30. The PdNP-functionalised silica monoliths were applied towards the hydrogenation of cyclo-octadiene where a conversion of 95 % and selectivity of 90 % was observed over a period of 70 hours.

The immobilisation of metal-oxide nano-particles on silica monoliths for catalytic applications was also reported by Yang *et al.* [158] using a one-step procedure. The nano-particles appeared to be rod-shaped with diameters of 5 nm and aspect ratios between 3-6 however, the shape could be controlled by altering the concentrations of the metal precursors.

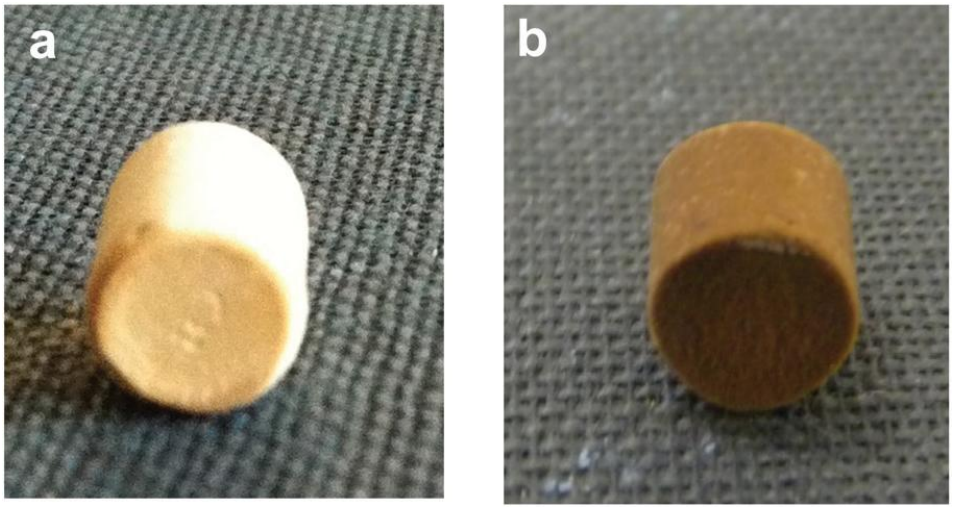

***Figure 1.30**: Silica monoliths (a) before and (b) after modification with PdNPs [157].*

Oxides of various metal salts such as iron, cobalt, copper, nickel and manganese were added at the sol-preparation step. The combustion of CH_4 in the presence of O_2 was selected as a model reaction to demonstrate the catalytic properties of immobilised Co_3O_4 nano-particles which represent an ideal alternative to the traditional Pd catalyst. A conversion of 44 % was reported at 500 °C which was found to be superior to the values reported in the literature for Co_3O_4 nano-particles immobilised on other solid supports.

1.9.2 Nano-particle functionalised polymer monoliths for catalysis

Polymer monoliths have been more widely used as supports because of their highly macro-porous structure leading to improved mass transfer effects. The immobilisation of nano-particles also aims to counteract the low surface area issues which always represented a limitation of these supports.

Kirschning originally realised the potential of polymer based monolithic materials as supports for heterogeneous catalysis when he developed a PASSflow (Polymer Assisted Solution-Phase Synthesis flow-through mode) system which allows solid-phase supported synthesis performed in a flow-through mode [159]. A monolith consisting of vinyl benzyl chloride cross-linked with divinylbenzene in the presence of AIBN was formed within a porous glass column, 110 mm x 5.3 mm in dimensions [160] as shown in Figure 1.31 below.

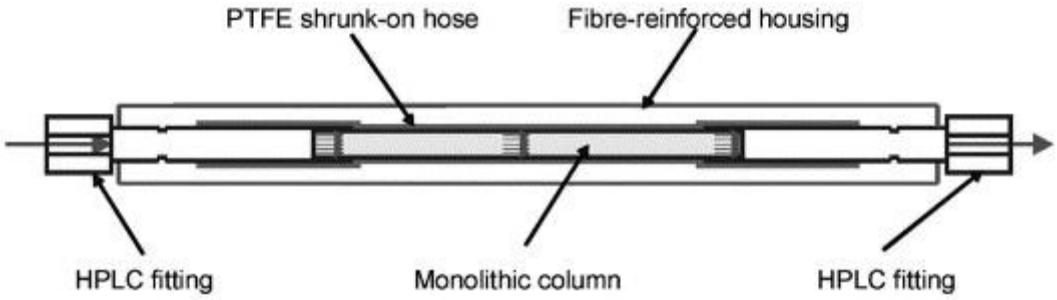

***Figure 1.31**: Schematic showing a PASSflow* (*Polymer Assisted Solution-Phase Synthesis flow-through mode) system [160]. A monolith is placed in a glass rod which can be integrated with a HPLC system.*

The result of the polymerisation process was an agglomeration of gel-like polymer particles with a diameter of 1–3 μm inside the void pore space of the carrier material. The particles were interconnected by polymer bridges, so that they could not be washed out of the glass rod even under forced flow hence demonstrating high stability. Triethyl amine was used to functionalise the surface of the monolith with quaternary ammonium groups, upon which PdNPs where immobilised by flushing a sodium tetrachloropalladate solution (0.5 mol %) in a first step and reducing Pd^{2+} ions to Pd^{0} in a second step by the addition of $NaBH_4$ as shown in Figure 1.32 [161]. The utility of the reactor formed was demonstrated by reacting *p*-iodoanisole with n-butylacrylate in the presence of triethylamine and 1-methyl-2-pyrrolidinone as solvent at 110 °C in 30 minutes, leading to complete transformation of the anisole reactant into an isobutyl ester [161].

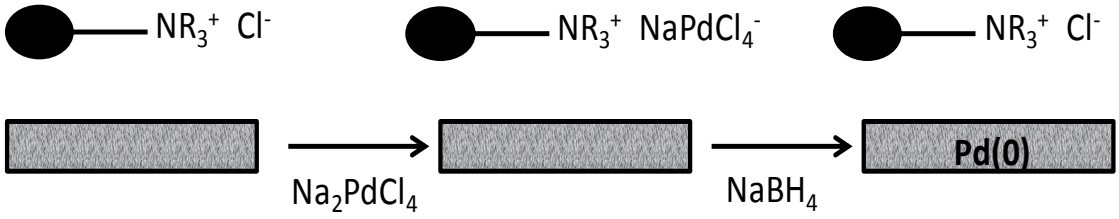

***Figure 1.32**: Schematic showing the immobilisation of PdNPs on a PASSflow (Polymer Assisted Solution-Phase Synthesis flow-through mode) system [161].*

Nikbin *et al.* [162] also prepared vinyl benzyl chloride-*co*-divinyl benzene (VBC-*co*-DVB) monoliths by thermal polymerisation in 70 mm x 6.6 mm glass columns, to perform Heck coupling reactions as part as an automated flow-through set-up. Quaternary ammonium functionalities were added by pumping triethylamine in toluene and PdNPs were immobilised by flushing sodium Na_2PdCl_4 in a first step

and $NaBH_4$ in a further step. Aryl iodides and alkenes were reacted using DMF as the solvent and triethylamine as the base at 130 °C, with 100 % conversions observed in each case and isolated yields in the 82-87 % range. Aryl chlorides were found to be unreactive under the same conditions.

Kirschning further developed PASSflow systems with the introduction of Raschig rings [163-165]. These are small tubes made of glass which were used as housings for the preparation of polymer monoliths, showing greater flexibility relative to the rod-type reactors since the rings can be removed and substituted easily with new rings (shown in Figure 1.33). Also this solution is highly cost-effective since rings can be produced in large quantities. Monoliths consisting of styrene, divinyl benzene and vinylbenzyl chloride were prepared and functionalised with PdNPs between 7-10 nm using the procedures previously described [162]. Initially applications with Suzuki coupling reactions between *p*-bromotoluene and phenyl boronic acid in DMF at 95 °C using CsF as the base led to 99% yields, in cyclic mode at a flow rate of 2 m*L*/min with a contact time of only 10 minutes.Excellent stability of the catalyst was observed even after the tenth run, with low leaching observed (0.7 ppm). Heck coupling reactions were also very succesful with complete conversions achieved for the reaction between *p*-iodoacetophenone and styrene under similar flow-through conditions.

Bandari *et al*. prepared Pd and Pt nano-particle functionalised polymer monoliths for Heck, Suzuki and Sonogashira-Hagihara cross-coupling reactions [53, 56, 166]. Glycidyl methacrylate monoliths were prepared using trimethylolpropan triacrylate (TMPTA) as the cross-linker in stainless steel columns of dimensions 100 x 4.6 mm by electron beam-triggered polymerisation [56].

Pore-size selective functionalisation was used to locate the nano-particles only in the small pores in order to extend the life span of the catalytic materials since Ostwald-ripening effects would be reduced. The epoxy groups present on the surface of the monolith were reacted with poly(styrene sulphonic acid) and norborn-5-en-2-ylmethylamine, followed by grafting by ring-opening methathesis polymerisation using a first generation Grubbs initiator of a series of norborn-2-ene-based dicarboxylic anhydride monomers, carboxylic amides and phosphonates.

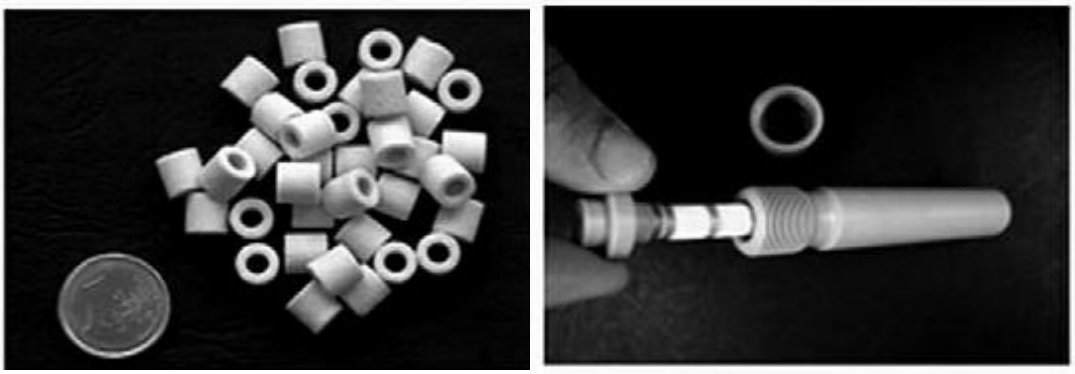

***Figure 1.33**: (left) Raschig rings and (right) a Raschig ring inserted in a PASSflow (Polymer Assisted Solution-Phase Synthesis flow-through mode) reactor [164].*

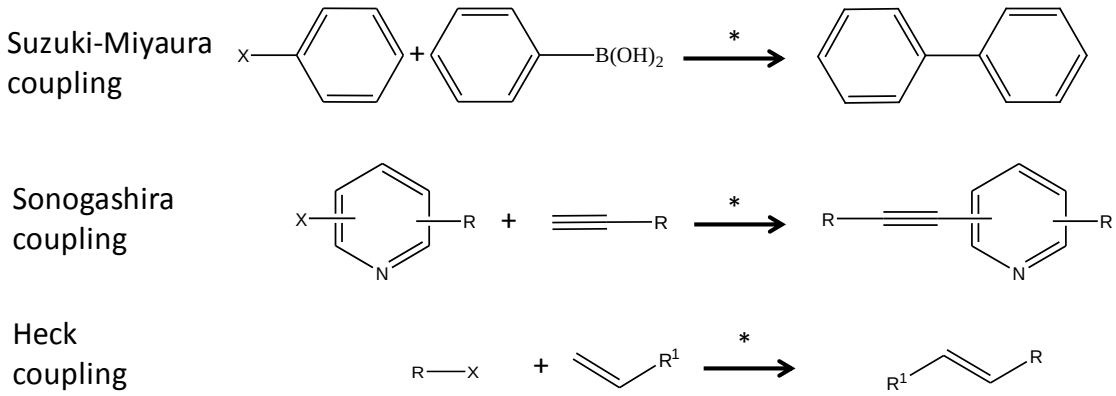

***Figure 1.34**: Schematic illustrating a series of coupling reactions. Suzuki-Miyaura reactions involve the reaction between an aryl-vinyl boronic acid with an aryl-vinyl halide. Sonogashira reactions involving terminal alkyne and aryl/vinyl halide. Heck coupling involve the reaction of a unsaturated halide with an alkene. * All reactions performed in the presence of a base, a Pd/Pt based calyst and at elevated temperatures.*

Finally the prepared monoliths were flushed with H_2PdCl_4 and $PtCl_4$ which were immobilised by coordination with di-2-pyridylamide ligands present on the surface, achieving loadings of 2.7 mg/g for Pd and 3.8 mg/g for Pt (see schematic shown in Figure 1.35).

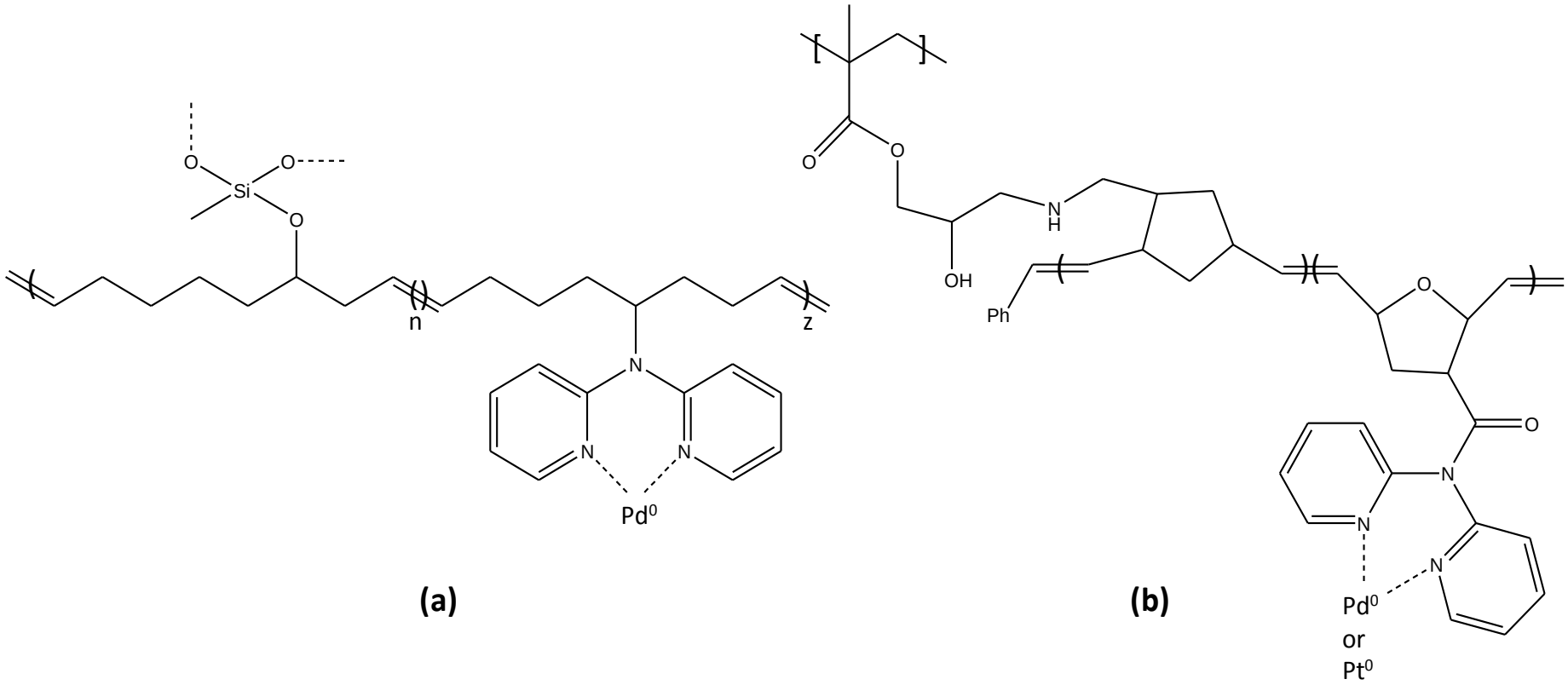

Figure 1.35*: Schematic showing the immobilisation of nano-particles on (a) a monolith prepared by ROMP polymerisation of (Z)-9 oxabicyclo[6.1.0]non-4-ene (OBN) and tris(cyclooct-4-en-1-yloxy)methylsilane [53] and (b) a glycidyl methacrylate monoliths cross-linked with trimethylolpropan triacrylate (TMPTA) prepared using electro beam-triggered polymerisation [56].*

By flushing $NaBH_4$, nano-particles of < 2 nm in size were formed as verified by TEM. Heck and Suzuki-type coupling reactions were performed with turnovers of 167,000 and 63,000 and product yields of up to 99% for the coupling of aryl bromides.

Subsequently, other polymer monoliths were prepared for Suzuki-type coupling reactions in glass discs, 20 x 10 mm i.d., as shown in Figure 1.36.

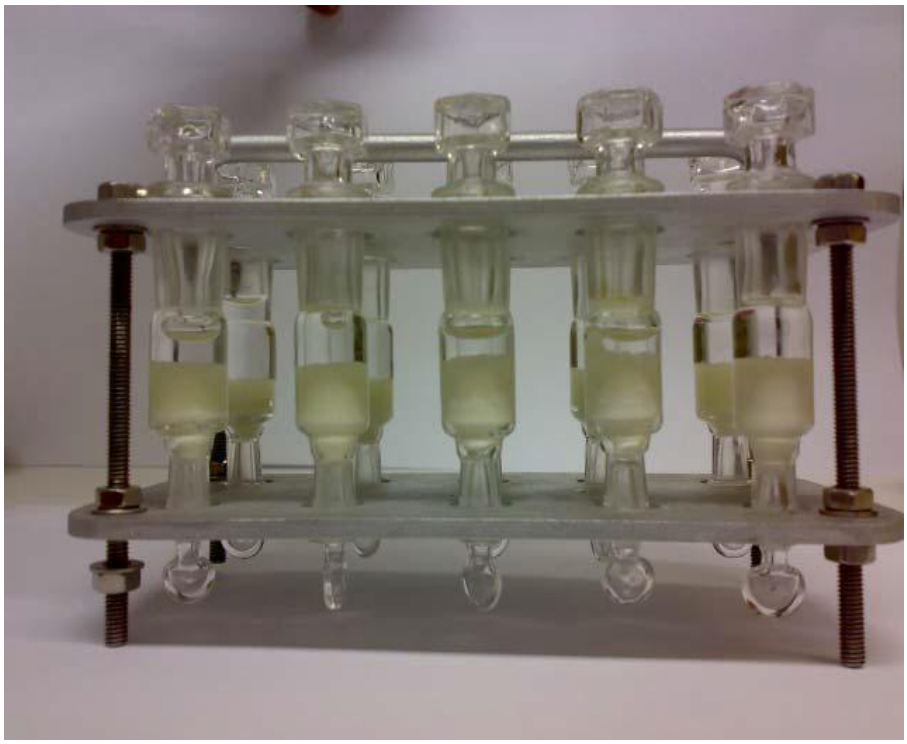

Figure 1.36*: Glass discs 20 x 10 mm i.d. used as housings for monoliths prepared by ROMP and subsequent loading with PdNPs [53]*.

These monoliths were prepared by ROMP from (Z)-9 oxabicyclonon-4-ene (OBN) and tris(cyclooct-4-en-1-yloxy)methylsilane monomers using 2^{nd} generation Grubbs catalysts [53]. Similarly as described for the methacrylate monoliths previously prepared [56], poly(styrene sulphonic acid) and N,N-dipyrid-2-ylamine were used for the hydrolysis of epoxy groups present in pores above and below 6 nm in size respectively. The formation of Pd (< 4 nm) was confirmed by SEM within the small pores of the monolith after the immobilisation and reduction of the metal salt precursor, [53] with metal loading values of 1 mg/g and low metal leaching observed (< 0.13%). Similar monoliths were also prepared for modification with Pt nano-particles (< 7 nm) achieving metal loadings of 1.7 mg/g [166]. The ideal catalytic

properties of these supports were demonstrated by performing the hydrosilylation of olefins under continuous conditions. Yields of 98 % were reported at a linear flow rate of 12 mm/min.

1.10 Characterisation methods of polymer monoliths

Several techniques are available to gain information on the structural and chemical properties of polymer monoliths. The most simple technique to characterise monolithic structures involves chromatographic evaluation for example observing efficiency and selectivity towards particular analytes [124]. The advantage of this method is its obvious simplicity and non-destructive features however, it does not provide any specific information on physical properties. Another non-destructive technique which has gained in popularity, especially concerning monoliths in capillary and micro-chip format, involves the use of scanning capacitively coupled contactless conductivity detection (sC^4D). This was originally aimed at the detection of ions in CE however, it was more recently applied in scanning mode to characterise the surface of monoliths depending on the distribution of charged functionalities across the surface [167]. Other techniques which have been used include Brunauer, Emmett, and Teller isotherm (BET) analysis for surface area determination, mercury porosimetry for determination of pore size distribution, scanning electron microscopy (SEM) and energy-dispersive X-ray spectroscopy (EDX) which are destructive techniques that allow to gain important information on the physical and chemical properties of the monoliths.

1.10.1 Scanning capacitively coupled contactless conductivity detection (sC^4D)

1.10.1.1 History and operating principles

The first reports of conductivity detectors based on a pair of capacitively coupled ring electrodes are dated back to 1998 where such detectors were used for detecting inorganic ions in CE [168, 169]. The concept of capacitance, which is the ability to store a charge in an electro-static field, is behind the operational basis of sC^4D. As shown in Figure 1.37, two ring-shaped metal electrodes are present, an actuator electrode and a pick-up electrode, based around a capillary which is generally of a

non-conductive material (such as teflon, fused silica, peek etc). These two electrodes form capacitors with the inside of the fused silica capillaries that they surround. A resistor is formed by the electrolyte solution inside the capillaries. When an oscillating frequency between 20-900 kHz is applied, the current passes from the actuator electrode through the capillary wall interacting with the liquid inside it. The signal then passes the detection gap between the two electrodes and it reaches the pick-up electrode, where the signal undergoes amplification and further processing. The two electrodes are placed within a solid insulated socket which ensures that the distance between them is always constant. Also in order to prevent stray capacitance, a metal foil is placed in between the two electrodes which has a shielding function.

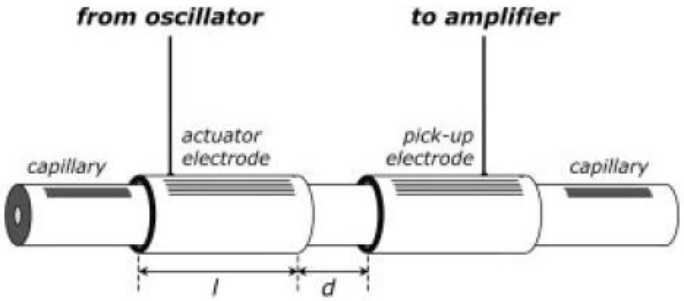

Figure 1.37*: Image showing the schematic of C^4D electrodes with l: electrode length and d: distance gap between electrodes [169].*

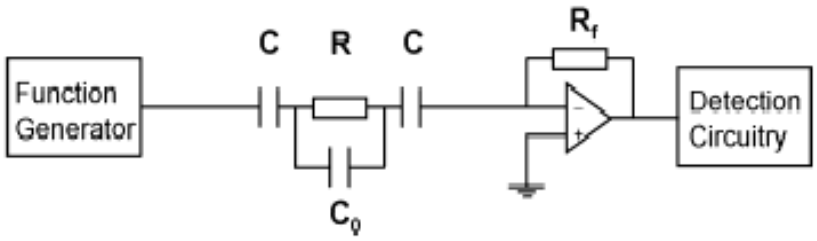

Figure 1.38: *Schematic showing the circuitry of a C^4D cell [170] where C: cell capacitance formed by the 2 electrodes, R: resistance from electrolyte inside capillary, C_0: stray capacitance, R_f: feedback resistor on the pick-up amplifier.*

Further shielding is also achieved by using a metal housing. For measurements, the cell is connected to a circuit consisting of a function generator and a detection circuitry as shown in Figure 1.38. If the AC voltage is kept constant, the passage of a charged species in the detection gap causes a decrease in resistance which increases the current as described by Ohm's law:

$$V = IR \qquad \text{(Equation 1.3)}$$

where V = Voltage, I = Current and R = Resistance.

The pick-up electrode is connected to an amplifier which converts the signal to voltage hence the readings from C^4D are expressed in m*V*. The increase in current leads to an increase in voltage due to the the relationship outlined below:

$$V_{out} = -IR_f \qquad \text{(Equation 1.4)}$$

Where V_{out} = output voltage, I = current, R_f = feedback resistor value on the pick-up amplifier (constant). Note: the minus sign for the current will revert the phase of the output voltage back to that of the input voltage.

Kubán *et al*. performed an evaluation of all the parameters that could affect a conductive response in sC^4D [170, 171]. A plot which relates the applied frequency to the output voltage (V_{out}) is known as a Bode plot and this allows the determination of the optimal operational frequency of a sC^4D cell which is within the plateau region of the curves as shown in Figure 1.39 below.

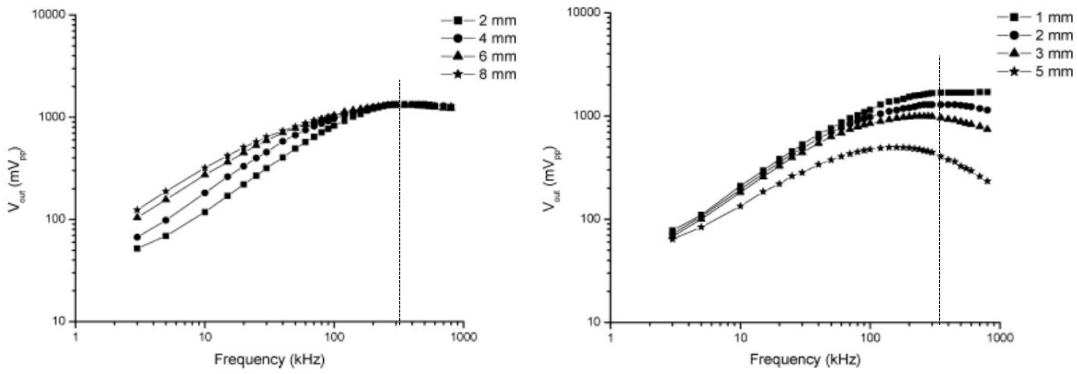

Figure 1.39: *(left) Bode plot illustrating the effect of electrode length (l) on operating frequency, (right) Bode plot illustrating the effect of detection gap (d) on operating frequency [170]. The dotted lines indicate the frequency settings at which a Tracedec operates.*

Initially the effect of electrode lengths, l, was studied. Electrodes of 4 different lengths (2, 4, 6 and 8 mm) were fitted in a C^4D cell, separated by a 2 mm gap (d) with a 50 µm i.d. capillary placed inside which was filled with a 10 m*M* Histidine solution (His) (p*H* 2.75). The effects of the output signal excitation frequencies

between 3-800 kHz were studied. All 4 electrodes showed a similar pattern with small differences at low frequencies (3-150 kHz), all reaching plateau at the same frequency range (260-280 kHz) with roughly the same output voltage (1.3 V) indicating that V_{out} is independent on electrode lengths at high frequencies.

Similarly the effect of increasing the gap, d, between the electrodes was studied. Two 4 mm long electrodes were separated by 1, 2, 3 and 5 mm gaps. The overall observed trend was that lower plateaus were present at higher gaps. Also for the larger gaps the plateau appeared to be shortened at high frequencies which is a behaviour that is not fully understood. In any case the unique pattern observed for each curve indicates that optimisation of the cell conditions is dependant on the gap size. Because of this reasons commercially available C^4D detectors manufactured by Tradedec operate at frequencies of approximately 300 kHz where plateau regions are observed as shown from the Bode plots in Figure 1.39.

1.10.1.2 Applications of sC^{4}D

The use of sC^4D as a detection tool for ions was reported in 2001 by Hilder *et al.* [172] who used this technique for the detection of a series of anions using a capillary column packed with quaternary ammonium functionalised particles. Improved sensitivity of this detection technique was observed relative to indirect UV detection. For example the LOD for chloride were found to be 5 µg/L using on-column C^4D detection relative to 11 µg/L using indirect UV detection. Mai *et al*. [173] also recently used on column C^4D to detect inorganic and organic cations in CEC mode, comparing a commercially available C_{18} functionalised silica monolith with monoliths prepared in-house and demonstrated that the amplitude of the conductive response was proportional to the porosity of the monolith. Several other applications as a detection tool in CEC and CE have been summarised in a recent review by Kuban *et al*. [174].

The ability to operate the cell in scanning mode also allowed its use as a characterisation tool of stationary phases with a spatial resolution of 1 mm. Some applications include the evaluation of the stability of surfactant coatings on silica monolithic capillary columns [175, 176], the determination of variations in column packings [167], the evaluation of stationary phase gradients [177, 178] and spatially

distributed photografted regions along the length of monoliths which were modified with charged monomers or proteins [82]. These applications will be discussed in detail in Chapter 2. The characterisation of micro-fluidic devices has also been documented by Walsh *et al*. [179] where by scanning the detector along the channels, a study of the conductive response permitted the evaluation of any variation in charge density present along the surface of the monolithic materials. Many reviews are present in the literature which outline the main development of sC^4D in the area of column characterisation [99, 167, 180]. The application of this technique has also been extended to columns of larger diameters as recently shown by Gillespie *et al.* who prepared a C^4D cell suitable for PEEK tubings with 1.6 mm o.d. [181].

1.10.2 Scanning electron microscopy (SEM)/ Energy-dispersive X-ray spectroscopy (EDX)

Scanning electron microscopy (SEM) has been used for the visualisation of monolithic stationary phases in both capillary and bulk formats, down to the micro-meter and even nano-meter scale depending on the type of instrument used. The energy source in SEM is characterised by tungsten filaments which are heated up by an electrical current. The resolution of SEM in the nano-scale is limited however, by the broadness of the beam. Field emission SEM (FE-SEM) counteracts this limitation since here the energy source is represented by a tungesten filament tip with a radius of ~ 100 nm. As shown in Figure 1.40, a focused electron beam scans the surface and once it interacts with the specimem, electrons are scattered. The penetration volume of the beam, which affects the type of electrons that are scattered, depends on the magnitude of the current, the accelerating voltage and the angle of incidence. The secondary electrons (SE) are the ones closest to the surface which lead to the production of an image. Back-scattered electrons (BSE) are used for distinguishing elements with high atomic numbers since these will back-scatter electrons more strongly relative to elements with low atomic numbers. For obtaining the best images possible, the surface observed must be flat, thermally stable and conductive [182]. Polymer monoliths do not possess any of these features and especially the thermal stability of the polymers limits the voltage that can be applied.

A layer of gold is often applied on the surface by sputtering onto the monolith's surface allowing it to be conductive. The main drawbacks of this technique are: (a) the inability to use wet samples hence not providing information of the monolith in its actual working state for liquid separations and (b) the destruction of the sample itself. Also the the beam used in SEM can provide information only from the 1-5 μm from the surface hence a large part of the inner structure remains uncharacterised.

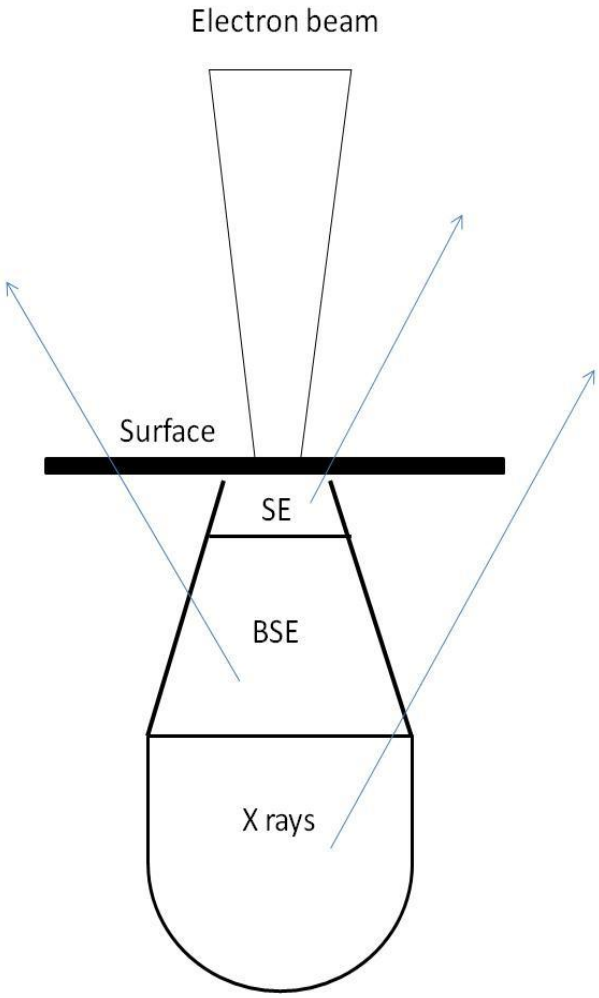

Figure 1.40*: Image showing the operating principles behind scanning electron microscopy (SEM) and energy-dispersive x-ray spectroscopy (EDX).*

Some SEM instruments can be equipped for energy dispersive x-ray spectroscopy (EDX), a technique used for the elemental analysis of samples. It relies on the principle that each element has a unique atomic structure which generates specific x-rays. In order to generate such x-rays, a high-energy beam of highly charged particles irradiates the sample zone which contains the desired elements. A detector

is used to convert the generated x-rays into a voltage which is sent to a pulse process and generates the data.

This technique has proven to be particularly useful for the determination of atomic % of metals immobilised onto monolithic surfaces. For example EDX was used to confirm the % loading of Au nano-particles onto polymer monoliths [135, 137].

1.10.3 BET isotherm technique and mercury porosimetry

While techniques such as SEM provide visual information on the physical morphology of a monolith, other techniques such as Brunauer, Emmett, and Teller isotherm (BET) technique and mercury porosimetry are used for obtaining more detailed information on the porous structure of monolithic stationary phases. The BET measurement technique involves the adsorption of an inert gas onto the surface. The degree of adsorption is not just dependant on the level of exposure but on temperature, gas pressure and strength of interaction between the solid and gas phases. Nitrogen is the most commonly used gas because it is highly pure and its coolant form, liquid nitrogen, is readily available. The isotherm obtained from the adsorption of nitrogen at 77 K allows the measurement of the surface area of a sample. Recent reports have been aimed at the modification of monolithic stationary phases with nano-particles in order to increase the surface area present and BET has often been used for evaluating any changes caused by such modifications [121, 146]. Another technique often used in conjunction with BET which gives information on pore size is the mercury porosimetry technique, as shown for example in Figure 1.41.

This technique involves forcing mercury under pressure into the pores of a solid material, allowing the determination of the pore size of a monolith by calculating the force needed to push the liquid into a pore against the opposing force of the liquid surface tension. Lubda *et al*. [183] availed of all these techniques to characterise the porous structure of two sets of silica monoliths which exhibited macro-pores and meso-pores of different sizes.

It is worth mentioning however, that these physical studies require sufficient mass of monolithic material in order to be performed and hence can not be applied to monoliths in capillary format which do not possess the required amount of mass.

Also other restrictions need to be considered depending on the applications. For example mercury is known to dissolve certain metals hence it can not be used with monolithic samples modified with metal nano-materials.

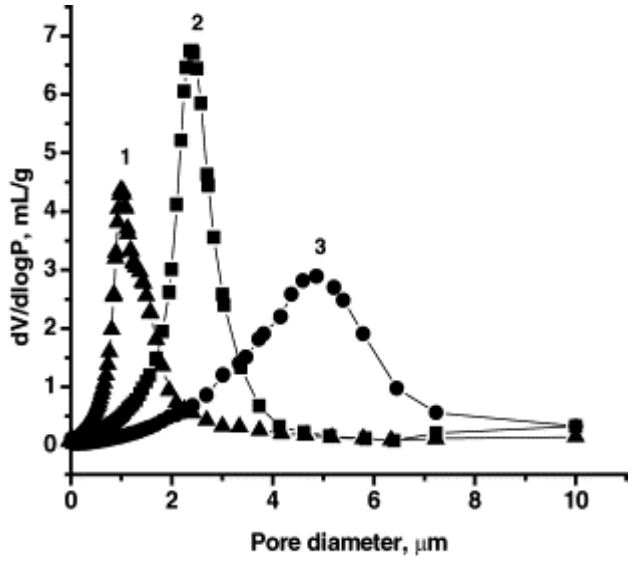

Figure 1.41: *Determination of pore size distribution by mercury porosimetry in three polymer monoliths. The average pore sizes were reported to be: (1) 0.97 μm, (2) 2.30 μm and (3) 4.07 μm [121].*

1.11 References

1. Guiochon, G. Monolithic columns in high-performance liquid chromatography. *Journal of Chromatography A* **2007,** *1168* (1-2), 101-168.

2. Mould, D. L.; Synge, R. L. M. Electrokinetic ultrafiltration analysis of polysaccharides - A new approach to the chromatography of large molecules. *Analyst* **1952,** *77* (921), 964-969.

3. Minakuchi, H.; Nakanishi, K.; Soga, N.; Ishizuka, N.; Tanaka, N. Effect of skeleton size on the performance of octadecylsilylated continuous porous silica columns in reversed-phase liquid chromatography. *Journal of Chromatography A* **1997,** *762* (1-2), 135-146.

4. Minakuchi, H.; Nakanishi, K.; Soga, N.; Ishizuka, N.; Tanaka, N. Octadecylsilylated porous silica rods as separation media for reversed-phase liquid chromatography. *Analytical Chemistry* **1996,** *68* (19), 3498-3501.

5. Minakuchi, H.; Nakanishi, K.; Soga, N.; Ishizuka, N.; Tanaka, N. Effect of domain size on the performance of octadecylsilylated continuous porous silica columns in reversed-phase liquid chromatography. *Journal of Chromatography A* **1998,** *797* (1-2), 121-131.

6. Nakanishi, K.; Minakuchi, H.; Soga, N.; Tanaka, N. Double pore silica gel monolith applied to liquid chromatography. *Journal of Sol-Gel Science and Technology* **1997,** *8* (1-3), 547-552.

7. Liao, J. L.; Zhang, R.; Hjerten, S. Continuous beds for standard and micro high-performance liquid-chromatography. *Journal of Chromatography* **1991,** *586* (1), 21-26.

8. Svec, F.; Frechet, J. M. J. Continuous rods of macroporous polymer as high-performance liquid-chromatography separation media. *Analytical Chemistry* **1992,** *64* (7), 820-822.

9. Wang, Q. C.; Svec, F.; Frechet, J. M. J. Macroporous polymeric stationary-phase rod as continuous separation medium for reversed-phase chromatography. *Analytical Chemistry* **1993,** *65* (17), 2243-2248.

10. Nguyen, D. T. T.; Guillarme, D.; Rudaz, S.; Veuthey, J. L. Fast analysis in liquid chromatography using small particle size and high pressure. *Journal of Separation Science* **2006,** *29* (12), 1836-1848.

11. Paull, B.; Nesterenko, P. N. New possibilities in ion chromatography using porous monolithic stationary-phase media. *Trac-Trends in Analytical Chemistry* **2005,** *24* (4), 295-303.

12. Brice, R. W.; Zhang, X.; Colon, L. A. Fused-core, sub-2 mu m packings, and monolithic HPLC columns: a comparative evaluation. *Journal of Separation Science* **2009,** *32* (15-16), 2723-2731.

13. Slater, M. D.; Frechet, J. M. J.; Svec, F. In-column preparation of a brush-type chiral stationary phase using click chemistry and a silica monolith. *Journal of Separation Science* **2009,** *32* (1), 21-28.

14. Miyamoto, K.; Hara, T.; Kobayashi, H.; Morisaka, H.; Tokuda, D.; Horie, K.; Koduki, K.; Makino, S.; Nunez, O.; Yang, C.; Kawabe, T.; Ikegami, T.; Takubo, H.; Ishihama, Y.; Tanaka, N. High-efficiency liquid chromatographic separation utilizing long monolithic silica capillary columns. *Analytical Chemistry* **2008,** *80* (22), 8741-8750.

15. Cabrera, K. Applications of silica-based monolithic HPLC columns. *Journal of Separation Science* **2004,** *27* (10-11), 843-852.

16. Hara, T.; Makino, S.; Watanabe, Y.; Ikegami, T.; Cabrera, K.; Smarsly, B.; Tanaka, N. The performance of hybrid monolithic silica capillary columns prepared by changing feed ratios of tetramethoxysilane and methyltrimethoxysilane. *Journal of Chromatography A* **2010,** *1217* (1), 89-98.

17. Nakanishi, K.; Minakuchi, H.; Soga, N.; Tanaka, N. Structure design of double-pore silica and its application to HPLC. *Journal of Sol-Gel Science and Technology* **1998,** *13* (1-3), 163-169.

18. Morisaka, H.; Kobayashi, K.; Kirino, A.; Furuno, M.; Minakuchi, H.; Nakanishi, K.; Ueda, M. Performance of wide-pore monolithic silica column in protein separation. *Journal of Separation Science* **2009,** *32* (15-16), 2747-2751.

19. Mallik, R.; Hage, D. S. Affinity monolith chromatography. *Journal of Separation Science* **2006,** *29* (12), 1686-1704.

20. Tanaka, N.; Kobayashi, H.; Ishizuka, N.; Minakuchi, H.; Nakanishi, K.; Hosoya, K.; Ikegami, T. Monolithic silica columns for high-efficiency chromatographic separations. *Journal of Chromatography A* **2002,** *965* (1-2), 35-49.

21. Ishizuka, N.; Minakuchi, H.; Nakanishi, K.; Soga, N.; Hosoya, K.; Tanaka, N. Chromatographic properties of miniaturized silica rod columns. *Hrc-Journal of High Resolution Chromatography* **1998,** *21* (8), 477-479.

22. Wu, Q. R.; Bienvenue, J. M.; Hassan, B. J.; Kwok, Y. C.; Giordano, B. C.; Norris, P. M.; Landers, J. P.; Ferrance, J. P. Microchip-based macroporous silica sol-gel monolith for efficient isolation of DNA from clinical samples. *Analytical Chemistry* **2006,** *78* (16), 5704-5710.

23. Kumazawa, T.; Hasegawa, C.; Lee, X. P.; Sato, K. New and unique methods of solid-phase extraction for use before instrumental analysis of xenobiotics in human specimens. *Forensic Toxicology* **2010,** *28* (2), 61-68.

24. Glenn, K. M.; Lucy, C. A.; Haddad, P. R. Ion chromatography on a latex-coated silica monolith column. *Journal of Chromatography A* **2007,** *1155* (1), 8-14.

25. Svec, F. Preparation and HPLC applications of rigid macroporous organic polymer monoliths. *Journal of Separation Science* **2004,** *27* (10-11), 747-766.

26. Svec, F.; Huber, C. G. Monolithic materials - Promises, challenges, achievements. *Analytical Chemistry* **2006,** *78* (7), 2100-2107.

27. Fan, L. Q.; Zhang, Y. P.; Chen, N.; Gong, W. J.; Qu, L. B.; Lee, K. P. Rapid preparation and characterization of methacrylate-based monoliths for chromatographic and electrophoretic separation. *Journal of Chromatographic Science* **2010,** *48* (5), 399-405.

28. Svec, F. Porous polymer monoliths: Amazingly wide variety of techniques enabling their preparation. *Journal of Chromatography A* **2010,** *1217* (6), 902-924.

29. Nischang, I.; Bruggemann, O. On the separation of small molecules by means of nano-liquid chromatography with methacrylate-based macroporous polymer monoliths. *Journal of Chromatography A* **2010,** *1217* (33), 5389-5397.

30. Urban, J.; Svec, F.; Frechet, J. M. J. Hypercrosslinking: New approach to porous polymer monolithic capillary columns with large surface area for the highly efficient separation of small molecules. *Journal of Chromatography A* **2010,** *1217* (52), 8212-8221.

31. Courtois, J.; Szumski, M.; Bystrom, E.; Iwasiewicz, A.; Shchukarev, A.; Irgum, K. A study of surface modification and anchoring techniques used in the preparation of monolithic microcolumns in fused silica capillaries (vol 29, pg 14, 2006). *Journal of Separation Science* **2006,** *29* (2), 325.

32. Zhang, Z. B.; Zhu, X. L.; Zhu, J.; Cheng, Z. P.; Zhu, S. P. Thermal-initiated reversible addition-fragmentation chain transfer polymerization of methyl methacrylate in the presence of oxygen. *Journal of Polymer Science Part A-Polymer Chemistry* **2006,** *44* (10), 3343-3354.

33. Peters, E. C.; Svec, F.; Frechet, J. M. J. Rigid macroporous polymer monoliths. *Advanced Materials* **1999,** *11* (14), 1169-1181.

34. Svec, F.; Frechet, J. M. J. Kinetic control of pore formation in macroporous polymers - formation of molded porous materials with high-flow characteristics for separations or catalysis. *Chemistry of Materials* **1995,** *7* (4), 707-715.

35. Viklund, C.; Ponten, E.; Glad, B.; Irgum, K.; Horstedt, P.; Svec, F. "Molded" macroporous poly(glycidyl methacrylate-co-trimethylolpropane trimethacrylate) materials with fine controlled porous properties: Preparation of monoliths using photoinitiated polymerization. *Chemistry of Materials* **1997,** *9* (2), 463-471.

36. Viklund, C.; Svec, F.; Frechet, J. M. J.; Irgum, K. Monolithic, "molded", porous materials with high flow characteristics for separations, catalysis, or solid-phase

chemistry: Control of porous properties during polymerization. *Chemistry of Materials* **1996,** *8* (3), 744-750.

37. Eeltink, S.; Geiser, L.; Svec, F.; Frechet, J. M. J. Optimization of the porous structure and polarity of polymethacrylate-based monolithic capillary columns for the LC-MS separation of enzymatic digests. *Journal of Separation Science* **2007,** *30* (17), 2814-2820.

38. Buchmeiser, M. R. Polymeric monolithic materials: Syntheses, properties, functionalization and applications. *Polymer* **2007,** *48* (8), 2187-2198.

39. Santora, B. P.; Gagne, M. R.; Moloy, K. G.; Radu, N. S. Porogen and cross-linking effects on the surface area, pore volume distribution, and morphology of macroporous polymers obtained by bulk polymerization. *Macromolecules* **2001,** *34* (3), 658-661.

40. Trojer, L.; Bisjak, C. P.; Wieder, W.; Bonn, G. K. High capacity organic monoliths for the simultaneous application to biopolymer chromatography and the separation of small molecules. *Journal of Chromatography A* **2009,** *1216* (35), 6303-6309.

41. Yu, C.; Xu, M. C.; Svec, F.; Frechet, J. M. J. Preparation of monolithic polymers with controlled porous properties for microfluidic chip applications using photoinitiated free-radical polymerization. *Journal of Polymer Science Part A-Polymer Chemistry* **2002,** *40* (6), 755-769.

42. Rohr, T.; Hilder, E. F.; Donovan, J. J.; Svec, F.; Frechet, J. M. J. Photografting and the control of surface chemistry in three-dimensional porous polymer monoliths. *Macromolecules* **2003,** *36* (5), 1677-1684.

43. Geiser, L.; Eeltink, S.; Svec, F.; Frechet, J. M. J. Stability and repeatability of capillary columns based on porous monoliths of poly(butyl methacrylate-co-ethylene dimethacrylate). *Journal of Chromatography A* **2007,** *1140* (1-2), 140-146.

44. Gu, B.; Li, Y.; Lee, M. L. Polymer monoliths with low hydrophobicity for strong cation-exchange capillary liquid chromatography of peptides and proteins. *Analytical Chemistry* **2007,** *79* (15), 5848-5855.

45. Walsh, Z.; Levkin, P. A.; Jain, V.; Paull, B.; Svec, F.; Macka, M. Visible light initiated polymerization of styrenic monolithic stationary phases using 470 nm light emitting diode arrays. *Journal of Separation Science* **2010,** *33* (1), 61-66.

46. Andrzejewska, E. Photopolymerization kinetics of multifunctional monomers. *Prog. Polym. Sci.* **2001,** *26* (4), 605-665.

47. Beiler, B.; Vincze, A.; Svec, F.; Safrany, A. Poly(2-hydroxyethyl acrylate-co-ethyleneglycol dimethaerylate) monoliths synthesized by radiation polymerization in a mold. *Polymer* **2007,** *48* (11), 3033-3040.

48. Vizioli, N. M.; Rusell, M. L.; Carbajal, M. L.; Carducci, C. N.; Grasselli, M. On-line affinity selection of histidine-containing peptides using a polymeric monolithic support for capillary electrophoresis. *Electrophoresis* **2005,** *26* (15), 2942-2948.

49. Chuda, K.; Jasik, J.; Carlier, J.; Tabourier, P.; Druon, C.; Coqueret, X. Characteristics and fluidic properties of porous monoliths prepared by radiation-induced polymerization for Lab-on-a-Chip applications. *Radiation Physics and Chemistry* **2006,** *75* (1), 26-33.

50. Georges, M. K.; Veregin, R. P. N.; Kazmaier, P. M.; Hamer, G. K. Narrow Molecular-Weight Resins by A Free-Radical Polymerization Process. *Macromolecules* **1993,** *26* (11), 2987-2988.

51. Yamago, S.; Lida, K.; Yoshida, J. Tailored synthesis of structurally defined polymers by organotellurium-mediated living radical polymerization (TERP): Synthesis of poly(meth)acrylate derivatives and their Di- and triblock copolymers. *Journal of the American Chemical Society* **2002,** *124* (46), 13666-13667.

52. Kanamori, K.; Hasegawa, J.; Nakanishi, K.; Hanada, T. Facile synthesis of macroporous cross-linked methacrylate gels by atom transfer radical polymerization. *Macromolecules* **2008,** *41* (19), 7186-7193.

53. Bandari, R.; Prager, A.; Hoche, T.; Buchmeiser, M. R. Formation of Pd-nanoparticles within the pores of ring opening metathesis polymerization-derived polymeric monoliths for use in organometallic catalysis. *Arkivoc* **2011,** 54-70.

54. Sinner, F.; Buchmeiser, M. R. A new class of continuous polymer supports prepared by ring-opening metathesis polymerization: A straightforward route to functionalized monoliths. *Macromolecules* **2000,** *33* (16), 5777-5786.

55. Sinner, F. M.; Buchmeiser, M. R. Ring-opening metathesis polymerization: Access to a new class of functionalized, monolithic stationary phases for liquid chromatography. *Angewandte Chemie-International Edition* **2000,** *39* (8), 1433-+.

56. Bandari, R.; Hoche, T.; Prager, A.; Dirnberger, K.; Buchmeiser, M. R. Ring-opening metathesis polymerization based pore-size-selective functionalization of glycidyl methacrylate based monolithic media: access to size-stable nanoparticles for ligand-free metal catalysis. *Chemistry-A European Journal* **2010,** *16* (15), 4650-4658.

57. Buchmeiser, M. R.; Sinner, F.; Mupa, M.; Wurst, K. Ring-opening metathesis polymerization for the preparation of surface-grafted polymer supports. *Macromolecules* **2000,** *33* (1), 32-39.

58. Xie, S. F.; Svec, F.; Frechet, J. M. J. Design of reactive porous polymer supports for high throughput bioreactors: Poly(2-vinyl-4,4-dimethylazlactone-co-acrylamide-co-ethyl dimethacrylate) monoliths. *Biotechnology and Bioengineering* **1999,** *62* (1), 30-35.

59. Chambers, S. D.; Holcombe, T. W.; Svec, F.; Frechet, J. M. J. Porous Polymer Monoliths Functionalized through Copolymerization of a C60 Fullerene-Containing

Methacrylate Monomer for Highly Efficient Separations of Small Molecules. *Analytical Chemistry* **2011,** *83* (24), 9478-9484.

60. Svec, F.; Frechet, J. M. J. Molded rods of macroporous polymer for preparative separations of biological products. *Biotechnology and Bioengineering* **1995,** *48* (5), 476-480.

61. Petro, M.; Svec, F.; Frechet, J. M. J. Immobilization of trypsin onto "molded" macroporous poly(glycidyl methacrylate-co-ethylene dimethacrylate) rods and use of the conjugates as bioreactors and for affinity chromatography. *Biotechnology and Bioengineering* **1996,** *49* (4), 355-363.

62. Ueki, Y.; Umemura, T.; Li, J. X.; Odake, T.; Tsunoda, K. Preparation and application of methacrylate-based cation-exchange monolithic columns for capillary ion chromatography. *Analytical Chemistry* **2004,** *76* (23), 7007-7012.

63. Gillespie, E.; Connolly, D.; Nesterenko, P. N.; Paull, B. Accurate non-invasive determination of pK(a) of surface functionalised ion exchange monoliths using capacitively coupled contactless conductivity detection. *Analyst* **2008,** *133* (7), 874-876.

64. Buck, M. E.; Lynn, D. M. Azlactone-functionalized polymers as reactive platforms for the design of advanced materials: Progress in the last ten years. *Polymer Chemistry* **2012,** *3* (1), 66-80.

65. Yang, W. T.; Ranby, B. Bulk surface photografting process and its applications .1. Reactions and kinetics. *Journal of Applied Polymer Science* **1996,** *62* (3), 533-543.

66. Yang, W. T.; Ranby, B. Bulk surface photografting process and its applications .2. Principal factors affecting surface photografting. *Journal of Applied Polymer Science* **1996,** *62* (3), 545-555.

67. Ulbricht, M.; Yang, H. Porous polypropylene membranes with different carboxyl polymer brush layers for reversible protein binding via surface-initiated graft copolymerization. *Chemistry of Materials* **2005,** *17* (10), 2622-2631.

68. Ranby, B. Surface modification of polymers by photoinitiated graft-polymerization. *Makromolekulare Chemie-Macromolecular Symposia* **1992,** *63*, 55-67.

69. Ma, H. M.; Davis, R. H.; Bowman, C. N. A novel sequential photoinduced living graft polymerization. *Macromolecules* **2000,** *33* (2), 331-335.

70. Edmondson, S.; Osborne, V. L.; Huck, W. T. S. Polymer brushes via surface-initiated polymerizations. *Chemical Society Reviews* **2004,** *33* (1), 14-22.

71. Kim, N. Y.; Jeon, N. L.; Choi, I. S.; Takami, S.; Harada, Y.; Finnie, K. R.; Girolami, G. S.; Nuzzo, R. G.; Whitesides, G. M.; Laibinis, P. E. Surface-initiated ring-opening metathesis polymerization on Si/SiO2. *Macromolecules* **2000,** *33* (8), 2793-2795.

72. Moon, J. H.; Swager, T. M. Poly(p-phenylene ethynylene) brushes. *Macromolecules* **2002,** *35* (16), 6086-6089.

73. Ejaz, M.; Yamamoto, S.; Ohno, K.; Tsujii, Y.; Fukuda, T. Controlled graft polymerization of methyl methacrylate on silicon substrate by the combined use of the Langmuir-Blodgett and atom transfer radical polymerization techniques. *Macromolecules* **1998,** *31* (17), 5934-5936.

74. Jones, D. M.; Huck, W. T. S. Controlled surface-initiated polymerizations in aqueous media. *Advanced Materials* **2001,** *13* (16), 1256-1259.

75. Tsubokawa, N.; Ichioka, H.; Satoh, T.; Hayashi, S.; Fujiki, K. Grafting of 'dendrimer-like' highly branched polymer onto ultrafine silica surface. *Reactive & Functional Polymers* **1998,** *37* (1-3), 75-82.

76. Guo, Z. X.; Yu, J. Grafting of dendritic polyethers onto nanometre silica surface. *Journal of Materials Chemistry* **2002,** *12* (3), 468-472.

77. Jackowska, M.; Bocian, S.; Buszewski, B. Dendrimer modified silica gel for anion exchange chromatography: synthesis, characterization and application. *Analyst* **2012,** *137* (19), 4610-4617.

78. Blokhina, S. V.; Usol'tseva, N. V.; Ol'khovich, M. V.; Sharapova, A. V. Liquid-crystalline polypropyleneimine dendrimer as a stationary phase for gas chromatography. *Journal of Analytical Chemistry* **2007,** *62* (6), 559-563.

79. Palmer, C. P.; McCarney, J. P. Developments in the use of soluble ionic polymers as pseudo-stationary phases for electrokinetic chromatography and stationary phases for electrochromatography. *Journal of Chromatography A* **2004,** *1044* (1-2), 159-176.

80. Castagnola, M.; Zuppi, C.; Rossetti, D. V.; Vincenzoni, F.; Lupi, A.; Vitali, A.; Meucci, E.; Messana, I. Characterization of dendrimer properties by capillary electrophoresis and their use as pseudostationary phases. *Electrophoresis* **2002,** *23* (12), 1769-1778.

81. Peterson, D. S.; Rohr, T.; Svec, F.; Frechet, J. M. J. Dual-function microanalytical device by in situ photolithographic grafting of porous polymer monolith: Integrating solid-phase extraction and enzymatic digestion for peptide mass mapping. *Analytical Chemistry* **2003,** *75* (20), 5328-5335.

82. Connolly, D.; O'Shea, V.; Clark, P.; O'Connor, B.; Paull, B. Evaluation of photografted charged sites within polymer monoliths in capillary columns using contactless conductivity detection. *Journal of Separation Science* **2007,** *30* (17), 3060-3068.

83. Hjerten, S.; Liao, J. L.; Zhang, R. High-performance liquid-chromatography on continuous polymer beds. *Journal of Chromatography* **1989,** *473* (1), 273-275.

84. Ericson, C.; Liao, J. L.; Nakazato, K.; Hjerten, S. Preparation of continuous beds for electrochromatography and reversed-phase liquid chromatography of low-molecular-mass compounds. *Journal of Chromatography A* **1997,** *767* (1-2), 33-41.

85. Byström, E. Porous polymeric materials for chromatography: synthesis, functionalisation and characterisation. PhD thesis 2009.

86. Svec, F.; Peters, E. C.; Sykora, D.; Frechet, J. M. J. Design of the monolithic polymers used in capillary electrochromatography columns. *Journal of Chromatography A* **2000,** *887* (1-2), 3-29.

87. Sondergeld, L. J.; Bush, M. E.; Bellinger, A.; Bushey, M. M. Butyl acrylate porous polymer monoliths in fused-silica capillaries for use in capillary electrochromatography. *Journal of Chromatography A* **2003,** *1004* (1-2), 155-165.

88. Peters, E. C.; Petro, M.; Svec, F.; Frechet, J. M. J. Molded rigid polymer monoliths as separation media for capillary electrochromatography. *Analytical Chemistry* **1997,** *69* (17), 3646-3649.

89. Peters, E. C.; Petro, M.; Svec, F.; Frechet, J. M. J. Molded rigid polymer monoliths as separation media for capillary electrochromatography. 2. Effect of chromatographic conditions on the separation. *Analytical Chemistry* **1998,** *70* (11), 2296-2302.

90. Moravcova, D.; Jandera, P.; Urban, J.; Planeta, J. Characterization of polymer monolithic stationary phases for capillary HPLC. *Journal of Separation Science* **2003,** *26* (11), 1005-1016.

91. Gu, B. H.; Chen, Z. Y.; Thulin, C. D.; Lee, M. L. Efficient polymer monolith for strong cation-exchange capillary liquid chromatography of peptides. *Analytical Chemistry* **2006,** *78* (11), 3509-3518.

92. Svec, F.; Frechet, J. M. J. Modified poly(glycidyl methacrylate-co-ethylene dimethacrylate) continuous rod columns for preparative-scale ion-exchange chromatography of proteins. *Journal of Chromatography A* **1995,** *702* (1-2), 89-95.

93. Bisjak, C. P.; Bakry, R.; Huck, C. W.; Bonn, G. K. Amino-functionalized monolithic poly(glycidyl methacrylate-codivinylbenzene) ion-exchange stationary phases for the separation of oligonucleoticles. *Chromatographia* **2005,** *62*, S31-S36.

94. Hutchinson, J. P.; Hilder, E. F.; Shellie, R. A.; Smith, J. A.; Haddad, P. R. Towards high capacity latex-coated porous polymer monoliths as ion-exchange stationary phases. *Analyst* **2006,** *131* (2), 215-221.

95. Svec, F. Less common applications of monoliths: Preconcentration and solid-phase extraction. *Journal of Chromatography B-Analytical Technologies in the Biomedical and Life Sciences* **2006,** *841* (1-2), 52-64.

96. Quirino, J. P.; Dulay, M. T.; Zare, R. N. On-line preconcentration in capillary electrochromatography using a porous monolith together with solvent gradient and sample stacking. *Analytical Chemistry* **2001,** *73* (22), 5557-5563.

97. Thabano, J. R. E.; Breadmore, M. C.; Hutchinson, J. P.; Johns, C.; Haddad, P. R. Capillary electrophoresis of neurotransmitters using in-line solid-phase extraction and preconcentration using a methacrylate-based weak cation-exchange monolithic stationary phase and a pH step gradient. *Journal of Chromatography A* **2007,** *1175* (1), 117-126.

98. Fan, Y.; Feng, Y. Q.; Da, S. L.; Shi, Z. G. Poly (methacrylic acid-ethylene glycol dimethacrylate) monolithic capillary for in-tube solid phase microextraction coupled to high performance liquid chromatography and its application to determination of basic drugs in human serum. *Analytica Chimica Acta* **2004,** *523* (2), 251-258.

99. Vazquez, M.; Paull, B. Review on recent and advanced applications of monoliths and related porous polymer gels in micro-fluidic devices. *Analytica Chimica Acta* **2010,** *668* (2), 100-113.

100. Nischang, I.; Brueggemann, O.; Svec, F. Advances in the preparation of porous polymer monoliths in capillaries and microfluidic chips with focus on morphological aspects. *Analytical and Bioanalytical Chemistry* **2010,** *397* (3), 953-960.

101. Augustin, V.; Proczek, G.; Dugay, J.; Descroix, S.; Hennion, M. C. Online preconcentration using monoliths in ellectrochromatography capillary format and microchips. *Journal of Separation Science* **2007,** *30* (17), 2858-2865.

102. Sauer-Budge, A. F.; Mirer, P.; Chatterjee, A.; Klapperich, C. M.; Chargin, D.; Sharon, A. Low cost and manufacturable complete microTAS for detecting bacteria. *Lab on A Chip* **2009,** *9* (19), 2803-2810.

103. He, M.; Zeng, Y.; Sun, X. J.; Harrison, D. J. Confinement effects on the morphology of photopatterned porous polymer monoliths for capillary and microchip electrophoresis of proteins. *Electrophoresis* **2008,** *29* (14), 2980-2986.

104. Rohr, T.; Ogletree, D. F.; Svec, F.; Frechet, J. M. J. Surface functionalization of thermoplastic polymers for the fabrication of microfluidic devices by photoinitiated grafting. *Advanced Functional Materials* **2003,** *13* (4), 264-270.

105. Liu, J. K.; Chen, C. F.; Tsao, C. W.; Chang, C. C.; Chu, C. C.; Devoe, D. L. Polymer microchips integrating solid-phase extraction and high-performance liquid chromatography using reversed-phase polymethacrylate monoliths. *Analytical Chemistry* **2009,** *81* (7), 2545-2554.

106. Yu, C.; Svec, F.; Frechet, J. M. J. Towards stationary phases for chromatography on a microchip: Molded porous polymer monoliths prepared in capillaries by photoinitiated in situ polymerization as separation media for electrochromatography. *Electrophoresis* **2000,** *21* (1), 120-127.

107. Rainer, M.; Sonderegger, H.; Bakry, R.; Huck, C. W.; Morandell, S.; Huber, L. A.; Gjerde, D. T.; Bonn, G. K. Analysis of protein phosphorylation by monolithic extraction columns based on poly(divinylbenzene) containing embedded titanium dioxide and zirconium dioxide nano-powders. *Proteomics* **2008,** *8* (21), 4593-4602.

108. Liang, S. S.; Chen, S. H. Monolithic microextraction tips by emulsion photopolymerization. *Journal of Chromatography A* **2009,** *1216* (12), 2282-2287.

109. Altun, Z.; Blomberg, L. G.; Abdel-Rehim, M. Increasing sample preparation throughput using monolithic methacrylate polymer as packing material for 96-tip robotic device. *Journal of Liquid Chromatography & Related Technologies* **2006,** *29* (10), 1477-1489.

110. Shah, V. P.; Midha, K. K.; Findlay, J. W.; Hill, H. M.; Hulse, J. D.; McGilveray, I. J.; Mckay, G.; Miller, K. J.; Patnaik, R. N.; Powell, M. L.; Tonelli, A.; Viswanathan, C. T.; Yacobi, A. Bioanalytical method validation--a revisit with a decade of progress. *Pharm. Res.* **2000,** *17* (12), 1551-1557.

111. www.biaseparations.com [accessed 30 january 2013]. 2013.
Ref Type: Online Source

112. www.dionex.com [accessed 30 january 2013]. 2013.
Ref Type: Online Source

113. www.bio-rad.com [accessed 30 january 2013]. 2013.
Ref Type: Online Source

114. Djakovitch, L.; Heise, W.; Kohler, K. Heck reactions between aryl halides and olefins catalysed by Pd-complexes entrapped into zeolites NaY. *Journal of Organometallic Chemistry* **1999,** *584* (1), 16-26.

115. Kwon, M. S.; Kim, N.; Park, C. M.; Lee, J. S.; Kang, K. Y.; Park, J. Palladium nanoparticles entrapped in aluminum hydroxide: Dual catalyst for alkene hydrogenation and aerobic alcohol oxidation. *Organic Letters* **2005,** *7* (6), 1077-1079.

116. Bedford, R. B.; Singh, U. G.; Walton, R. I.; Williams, R. T.; Davis, S. A. Nanoparticulate palladium supported by covalently modified silicas: Synthesis, characterization, and application as catalysts for the Suzuki coupling of aryl halides. *Chemistry of Materials* **2005,** *17* (4), 701-707.

117. Guo, Z. H.; Henry, L. L.; Palshin, V.; Podlaha, E. J. Synthesis of poly(methyl methacrylate) stabilized colloidal zero-valence metallic nanoparticles. *Journal of Materials Chemistry* **2006,** *16* (18), 1772-1777.

118. Haruta, M. Size- and support-dependency in the catalysis of gold. *Catalysis Today* **1997,** *36* (1), 153-166.

119. Luo, X.; Morrin, A.; Killard, A.; Smyth, M. Application of nanoparticles in electrochemical sensors and biosensors. *Electroanalysis* **2006,** *18* (4), 319-326.

120. Guihen, E.; Glennon, J. D. Nanoparticles in separation science - Recent developments. *Analytical Letters* **2003,** *36* (15), 3309-3336.

121. Hilder, E. F.; Svec, F.; Frechet, J. M. J. Latex-functionalized monolithic columns for the separation of carbohydrates by micro anion-exchange chromatography. *Journal of Chromatography A* **2004,** *1053* (1-2), 101-106.

122. Hutchinson, J. P.; Zakaria, P.; Bowiet, A. R.; Macka, M.; Avdalovic, N.; Haddad, P. R. Latex-coated polymeric monolithic ion-exchange stationary phases. 1. Anion-exchange capillary electrochromatography and in-line sample preconcentration in capillary electrophoresis. *Analytical Chemistry* **2005,** *77* (2), 407-416.

123. Zakaria, P.; Hutchinson, J. P.; Avdalovic, N.; Liu, Y.; Haddad, P. R. Latex-coated polymeric monolithic ion-exchange stationary phases. 2. Micro-ion chromatography. *Analytical Chemistry* **2005,** *77* (2), 417-423.

124. Hutchinson, J. P.; Hilder, E. F.; Macka, M.; Avdalovic, N.; Haddad, P. R. Preparation and characterisation of anion-exchange latex-coated silica monoliths for capillary electrochromatography. *Journal of Chromatography A* **2006,** *1109* (1), 10-18.

125. Ibrahim, M. E. A.; Lucy, C. A. Mixed mode HILIC/anion exchange separations on latex coated silica monoliths. *Talanta* **2012,** *100*, 313-319.

126. Ibrahim, M. E. A.; Zhou, T.; Lucy, C. A. Agglomerated silica monolithic column for hydrophilic interaction LC. *Journal of Separation Science* **2010,** *33* (6-7), 773-778.

127. Popov, V. N. Carbon nanotubes: properties and application. *Materials Science & Engineering R-Reports* **2004,** *43* (3), 61-102.

128. Li, Y.; Chen, Y.; Xiang, R.; Ciuparu, D.; Pfefferle, L. D.; Horwath, C.; Wilkins, J. A. Incorporation of single-wall carbon nanotubes into an organic polymer monolithic stationary phase for mu-HPLC and capillary electrochromatography. *Analytical Chemistry* **2005,** *77* (5), 1398-1406.

129. Chambers, S. D.; Svec, F.; Frechet, J. M. J. Incorporation of carbon nanotubes in porous polymer monolithic capillary columns to enhance the chromatographic separation of small molecules. *Journal of Chromatography A* **2011,** *1218* (18), 2546-2552.

130. Andre, C.; Agiovlasileti, D.; Guillaume, Y. C. Peculiarities of a novel bioenzymatic reactor using carbon nanotubes as enzyme activity enhancers: Application to arginase. *Talanta* **2011,** *85* (5), 2703-2706.

131. Andre, C.; Lenancker, G.; Guillaume, Y. C. Non-covalent functionalisation of monolithic silica for the development of carbon nanotube HPLC stationary phases. *Talanta* **2012,** *99*, 580-585.

132. Kawasaki, T. Hydroxyapatite as a liquid-chromatographic packing. *Journal of Chromatography* **1991,** *544* (1-2), 147-184.

133. Krenkova, J.; Lacher, N. A.; Svec, F. Control of selectivity via nanochemistry: monolithic capillary column containing hydroxyapatite nanoparticles for separation of proteins and enrichment of phosphopeptides. *Analytical Chemistry* **2010,** *82* (19), 8335-8341.

134. Chan, K. Y.; Ding, J.; Ren, J.; Cheng, S.; Tsang, K. Y. Supported mixed metal nanoparticles as electrocatalysts in low temperature fuel cells. *Journal of Materials Chemistry* **2004,** *14* (4), 505-516.

135. Cao, Q.; Xu, Y.; Liu, F.; Svec, F.; Frechet, J. M. J. Polymer monoliths with exchangeable chemistries: use of gold nanoparticles as intermediate ligands for capillary columns with varying surface functionalities. *Analytical Chemistry* **2010,** *82* (17), 7416-7421.

136. Xu, Y.; Cao, Q.; Svec, F.; Frechet, J. M. J. Porous polymer monolithic column with surface-bound gold nanoparticles for the capture and separation of cysteine-containing peptides. *Analytical Chemistry* **2010,** *82* (8), 3352-3358.

137. Connolly, D.; Twamley, B.; Paull, B. High-capacity gold nanoparticle functionalised polymer monoliths. *Chemical Communications* **2010,** *46* (12), 2109-2111.

138. Lv, Y. Q.; Alejandro, F. M.; Frechet, J. M. J.; Svec, F. Preparation of porous polymer monoliths featuring enhanced surface coverage with gold nanoparticles. *Journal of Chromatography A* **2012,** *1261*, 121-128.

139. Alwael, H.; Connolly, D.; Clarke, P.; Thompson, R.; Twamley, B.; O'Connor, B.; Paull, B. Pipette-tip selective extraction of glycoproteins with lectin modified gold nano-particles on a polymer monolithic phase. *Analyst* **2011,** *136* (12), 2619-2628.

140. Lu, J.; Ye, F.; Zhang, A.; Wei, Z.; Peng, Y.; Zhao, S. Preparation and characterization of silica monolith modified with bovine serum albumin-gold nanoparticles conjugates and its use as chiral stationary phases for capillary electrochromatography. *Journal of Separation Science* **2011,** *34* (16-17), 2329-2336.

141. Liu, J. K.; White, I.; Devoe, D. L. Nanoparticle-functionalized porous polymer monolith detection elements for Surface-Enhanced Raman Scattering. *Analytical Chemistry* **2011,** *83* (6), 2119-2124.

142. Liang, S. S.; Makamba, H.; Huang, S. Y.; Chen, S. H. Nano-titanium dioxide composites for the enrichment of phosphopeptides. *Journal of Chromatography A* **2006,** *1116* (1-2), 38-45.

143. Hsieh, H. C.; Sheu, C.; Shi, F. K.; Li, D. T. Development of a titanium dioxide nanoparticle pipette-tip for the selective enrichment of phosphorylated peptides. *Journal of Chromatography A* **2007,** *1165* (1-2), 128-135.

144. Krenkova, J.; Foret, F. Iron oxide nanoparticle coating of organic polymer-based monolithic columns for phosphopeptide enrichment. *Journal of Separation Science* **2011,** *34* (16-17), 2106-2112.

145. Johnson, S. A.; Ollivier, P. J.; Mallouk, T. E. Ordered mesoporous polymers of tunable pore size from colloidal silica templates. *Science* **1999,** *283* (5404), 963-965.

146. Thabano, J. R. E.; Breadmore, M. C.; Hutchinson, J. P.; Johns, C.; Haddad, P. R. Silica nanoparticle-templated methacrylic acid monoliths for in-line solid-phase extraction-capillary electrophoresis of basic analytes. *Journal of Chromatography A* **2009,** *1216* (25), 4933-4940.

147. Tobal, K.; Guerre, O.; Rolando, C.; Le Gac, S. Metal nanoparticle-based polymer a monolithic columns dedicated to the specific trapping of phosphopeptides. *Molecular & Cellular Proteomics* **2006,** *5* (10), S278.

148. Blaser, H. U.; Indolese, A.; Schnyder, A.; Steiner, H.; Studer, M. Supported palladium catalysts for fine chemicals synthesis. *J. Mol. Catal. A: Chem.* **2001,** *173* (1-2), 3-18.

149. Mayr, M.; Mayr, B.; Buchmeiser, M. R. Monolithic materials: new high-performance supports for permanently immobilized metathesis catalysts. *Angewandte Chemie-International Edition* **2001,** *40* (20), 3839-+.

150. Krause, J. O.; Lubbad, S. H.; Nuyken, O.; Buchmeiser, M. R. Heterogenization of a modified Grubbs-Hoveyda catalyst on a ROMP-derived monolithic support. *Macromolecular Rapid Communications* **2003,** *24* (15), 875-878.

151. Krause, J. O.; Lubbad, S.; Nuyken, O.; Buchmeiser, M. R. Monolith- and silica-supported carboxylate-based Grubbs-Herrmann-type metathesis catalysts. *Advanced Synthesis & Catalysis* **2003,** *345* (8), 996-1004.

152. Frost, C. G.; Mutton, L. Heterogeneous catalytic synthesis using microreactor technology. *Green Chemistry* **2010,** *12* (10), 1687-1703.

153. Anderson, E. B.; Buchmeiser, M. R. Catalysts immobilized on organic polymeric monolithic supports: from molecular heterogeneous catalysis to biocatalysis. *Chemcatchem* **2012,** *4* (1), 30-44.

154. Sato, S.; Takahashi, R.; Sodesawa, T.; Koubata, M. Bimodal porous Pd-silica for liquid-phase hydrogenation. *Applied Catalysis A-General* **2005,** *284* (1-2), 247-251.

155. Takahashi, R.; Sato, S.; Sodesawa, T.; Arai, K.; Yabuki, M. Effect of diffusion in catalytic dehydration of alcohol over silica-alumina with continuous macropores. *Journal of Catalysis* **2005,** *229* (1), 24-29.

156. Fletcher, P. D. I.; Haswell, S. J.; He, P.; Kelly, S. M.; Mansfield, A. Permeability of silica monoliths containing micro- and nano-pores. *Journal of Porous Materials* **2011,** *18* (4), 501-508.

157. Sachse, A.; Linares, N.; Barbaro, P.; Fajula, F.; Galarneau, A. Selective hydrogenation over Pd nanoparticles supported on a pore-flow-through silica monolith microreactor with hierarchical porosity. *Dalton transactions (Cambridge, England : 2003)* **2013,** *42* (5), 1378-1384.

158. Yang, H. F.; Lu, Q. Y.; Gao, F.; Shi, Q. H.; Yan, Y.; Zhang, F. Q.; Xie, S. H.; Tu, B.; Zhao, D. Y. One-step synthesis of highly ordered mesoporous silica monoliths with metal oxide nanocrystals in their channels. *Advanced Functional Materials* **2005,** *15* (8), 1377-1384.

159. Kirschning, A.; Altwicker, C.; Drager, G.; Harders, J.; Hoffmann, N.; Hoffmann, U.; Schonfeld, H.; Solodenko, W.; Kunz, U. PASSflow syntheses using

functionalized monolithic polymer/glass composites in flow-through microreactors. *Angewandte Chemie-International Edition* **2001,** *40* (21), 3995-+.

160. Kunz, U.; Schonfeld, H.; Kirschning, A.; Solodenko, W. Polymer/carrier composites as materials and reactors for organic synthesis. *Journal of Chromatography A* **2003,** *1006* (1-2), 241-249.

161. Solodenko, W.; Wen, H. L.; Leue, S.; Stuhlmann, F.; Sourkouni-Argirusi, G.; Jas, G.; Schonfeld, H.; Kunz, U.; Kirschning, A. Development of a continuous-flow system for catalysis with palladium(O) particles. *Eur. J. Org. Chem.* **2004,** (17), 3601-3610.

162. Nikbin, N.; Ladlow, M.; Ley, S. V. Continuous flow ligand-free Heck reactions using monolithic Pd [0] nanoparticles. *Organic Process Research & Development* **2007,** *11* (3), 458-462.

163. Mennecke, K.; Solodenko, W.; Kirschning, A. Carbon-carbon cross-coupling reactions under continuous flow conditions using poly(vinylpyridine) doped with palladium. *Synthesis-Stuttgart* **2008,** (10), 1589-1599.

164. Mennecke, K.; Cecilia, R.; Glasnov, T. N.; Gruhl, S.; Vogt, C.; Feldhoff, A.; Vargas, M. A. L.; Kappe, C. O.; Kunz, U.; Kirschning, A. Palladium(0) nanoparticles on glass-polymer composite materials as recyclable catalysts: A comparison study on their use in batch and continuous flow processes. *Advanced Synthesis & Catalysis* **2008,** *350* (5), 717-730.

165. Michrowska, A.; Mennecke, K.; Kunz, U.; Kirschning, A.; Grela, K. A new concept for the noncovalent binding of a ruthenium-based olefin metathesis catalyst to polymeric phases: Preparation of a catalyst on Raschig rings. *Journal of the American Chemical Society* **2006,** *128* (40), 13261-13267.

166. Bandari, R.; Buchmeiser, M. R. Polymeric monolith supported Pt-nanoparticles as ligand-free catalysts for olefin hydrosilylation under batch and continuous conditions. *Catalysis Science & Technology* **2012,** *2* (1), 220-226.

167. Connolly, D.; Floris, P.; Nesterenko, P. N.; Paull, B. Non-invasive characterization of stationary phases in capillary flow systems using scanning capacitively coupled contactless conductivity detection (sC(4)D). *Trac-Trends in Analytical Chemistry* **2010,** *29* (8), 870-884.

168. Zemann, A. J.; Schnell, E.; Volgger, D.; Bonn, G. K. Contactless conductivity detection for capillary electrophoresis. *Analytical Chemistry* **1998,** *70* (3), 563-567.

169. da Silva, J. A. F.; do Lago, C. L. An oscillometric detector for capillary electrophoresis. *Analytical Chemistry* **1998,** *70* (20), 4339-4343.

170. Kuban, P.; Hauser, P. C. Fundamental aspects of contactless conductivity detection for capillary electrophoresis. Part I: Frequency behavior and cell geometry. *Electrophoresis* **2004,** *25* (20), 3387-3397.

171. Kuban, P.; Hauser, P. C. Fundamental aspects of contactless conductivity detection for capillary electrophoresis. Part II: Signal-to-noise ratio and stray capacitance. *Electrophoresis* **2004,** *25* (20), 3398-3405.

172. Hilder, E. F.; Zemann, A. J.; Macka, M.; Haddad, P. R. Anion-exchange capillary electrochromatography with indirect UV and direct contactless conductivity detection. *Electrophoresis* **2001,** *22* (7), 1273-1281.

173. Mai, T. D.; Pham, H. V.; Hauser, P. C. Capillary electrochromatography with contactless conductivity detection for the determination of some inorganic and organic cations using monolithic octadecylsilica columns. *Analytica Chimica Acta* **2009,** *653* (2), 228-233.

174. Kuban, P.; Hauser, P. C. Contactless conductivity detection for analytical techniques: Developments from 2010 to 2012. *Electrophoresis* **2013,** *34* (1), 55-69.

175. Gillespie, E.; Macka, M.; Connolly, D.; Paull, B. Evaluation of capillary ion exchange stationary phase coating distribution and stability using radial capillary column contactless conductivity detection. *Analyst* **2006,** *131* (8), 886-888.

176. Riordain, O.; Gillespie, E.; Connolly, D.; Nesterenko, P. N.; Paull, B. Capillary ion chromatography of inorganic anions on octadecyl silica monolith modified with an amphoteric surfactant. *Journal of Chromatography A* **2007,** *1142* (2), 185-193.

177. Currivan, S.; Connolly, D.; Gillespie, E.; Paull, B. Fabrication and characterisation of capillary polymeric monoliths incorporating continuous stationary phase gradients. *Journal of Separation Science* **2010,** *33* (4-5), 484-492.

178. Currivan, S.; Connolly, D.; Paull, B. Production of novel polymer monolithic columns, with stationary phase gradients, using cyclic olefin co-polymer (COC) optical filters. *Analyst* **2012,** *137* (11), 2559-2566.

179. Walsh, Z.; Vazquez, M.; Benito-Lopez, F.; Paull, B.; Macka, M.; Svec, F.; Diamond, D. The use of scanning contactless conductivity detection for the characterisation of stationary phases in micro-fluidic chips. *Lab on A Chip* **2010,** *10* (14), 1777-1780.

180. Coltro, W. K. T.; Lima, R. S.; Segato, T. P.; Carrilho, E.; de Jesus, D. P.; do Lago, C. L.; da Silva, J. A. F. Capacitively coupled contactless conductivity detection on microfluidic systems-ten years of development. *Analytical Methods* **2012,** *4* (1), 25-33.

181. Gillespie, E.; Connolly, D.; Macka, M.; Hauser, P.; Paull, B. Development of a contactless conductivity detector cell for 1.6 mm OD (1/16th inch) HPLC tubing and micro-bore columns with on-column detection. *Analyst* **2008,** *133* (8), 1104-1110.

182. Cabral, J. L.; Bandilla, D.; Skinner, C. D. Pore size characterization of monolith for electrochromatography via atomic force microscopy studies in air and liquid phase. *Journal of Chromatography A* **2006,** *1108* (1), 83-89.

183. Lubda, D.; Lindner, W.; Quaglia, M.; von Hohenesche, C. D.; Unger, K. K. Comprehensive pore structure characterization of silica monoliths with controlled mesopore size and macropore size by nitrogen sorption, mercury porosimetry,

transmission electron microscopy and inverse size exclusion chromatography. *Journal of Chromatography A* **2005,** *1083* (1-2), 14-22.

Chapter 2: Characterisation of monolithic stationary phases and polyelectrolyte coatings in fused silica capillaries using scanning capacitively coupled contactless conductivity detection (sC^{4}D)

Abstract

In this Chapter scanning capacitively coupled contactless conductivity detection (sC^4D) was used as a non-destructive characterisation tool for monolithic stationary phases and fused silica capillaries. Polymer monoliths in capillary format, prepared by a colloborating group, whereby they were functionalised with 5-amino-1,10-phenanthroline or 1-methylimidazole and subsequently loaded with a palladium catalyst [as $PdCl_2(NCMe)_2$] for performing flow-through catalytic reactions. In order to prevent product contamination, metal leaching from micro-reactors should be kept to a minimum. Here for the first time sC^4D is used as an evaluation tool for determining the distribution and stability of a palladium catalyst along the surface of a polymer monolith. Conductivity measurements revealed that a non-homogeneous coverage of catalyst was present on the monoliths evaluated and that the catalyst could be easily removed after flushing an EDTA buffer. In a related study, fused silica capillaries were modified with a double-chained surfactant and several layers of polyelectrolytes. These procedures are well established in capillary electrophoresis in order to prevent issues like protein adsorption which can interact with the negatively charged silanol groups present on the surface of fused silica capillaries. Here sC^4D was used to confirm the modification of empty fused silica capillaries with several layers of polyelectrolytes and to monitor their removal after fixed washing periods. Finally another polymer monolith was photografted with a negatively charged monomer, sulphopropyl methacrylate, in a selected region of the monolith using photo-masks. The utility of sC^4D was again demonstrated since it allowed to precisely visualise the distribution of the charged species in the photografted region at mm increments.

Aims

The aim of this Chapter was to demonstrate the versatility of sC^4D as a characterisation tool for evaluating the presence of charged functionalities along the length of fused silica capillaries and polymer monoliths.

2.1 Introduction

In capillary electrophoresis, the non-specific adsorption of certain organic analytes on the inner walls of fused silica capillary represents an issue which must be prevented in order to maximise separation efficiency. For example a great number of reports have dealt with the issue of proteins adsorption [1, 2] which is caused by the interaction between the negative silanol groups on the surface of the capillaries, present above p*H* 2, and the ionisable amino acid residues present on the protein's surface which leads to zone broadening effects and unreproducible peak areas or migration times [3, 4]. Several attempts to resolve this issue have been reported such as the use of background electrolytes (BGE) at extreme p*H* values [5], the use of a high ionic strength BGE and the coating of the capillary surface in order to create a repulsive force between the capillary surface and the analytes [5]. Polyacrylamides are used for example to coat the inner capillary surface [1] but this is a time consuming process and often non-homogenous coverage is achieved. Other methodologies known for the modification of the inner surface of capillaries involve the electrostatic interactions of surfactants [6] or polymers coatings, which are less costly and more easy to perform.

These types of modifications can be static or dynamic. In the dynamic approach, the coating solution is added to the BGE which can lead to further complications such as protein denaturation due to its presence or issues with detection. When the modification is static however, the capillary is coated before the run and when high molecular weight polyelectolytes are used, quasi-stable and uniform coatings are obtained. Katayama *et al.* [7, 8] developed a Successive Multiple Ionic Layers (SMIL) approach where a cationic polyelectrolyte was positioned between an anionic polyelectrolyte and the negatively charged fused silica capillary as shown in Figure 2.1. Subsequently, Nehmé *et al.* [9] reported the formation of multilayers (5-11) of polydiallyldimethylammonium chloride [PDADMAC, $(C_8H_{16}ClN)_n$] and poly(sodium 4-styrenesulphonate) [PSS, $(C_8H_7NaO_3S)_n$] to prevent protein adsorption. The concentrations of polyelectrolytes had a critical effect on the stability of the coatings and the presence of salts in between the coating steps was reported to lead to increased performance. The repeatability of migration times (RSD < 0.33%) (n=15) obtained for peptides in these conditions was indicative of the high

stability of the coatings. The modification of monolithic stationary phases with surfactants has also been described for the preparation of stationary phases suitable for ion chromatography [10, 11].

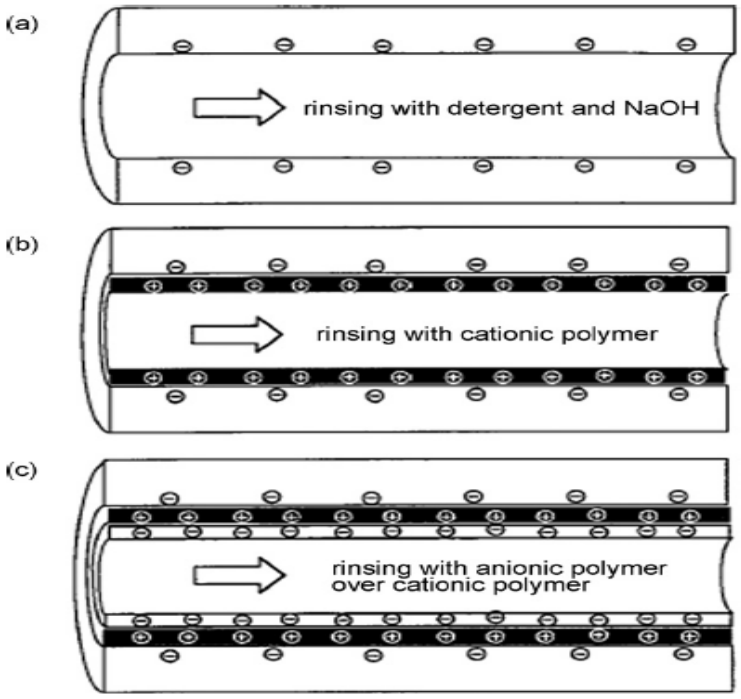

Figure 2.1: *Schematic showing the principles of Successive Multiple Ionic Layers (SMIL) inside capillaries [7].*

Recently, several publications have emerged describing the use of sC^4D for the characterisation of surfactant modified monolithic stationary phases [12, 13]. One significant aspect of sC^4D is that detection is indeed "contactless" (i.e. the conducting species in the fluidic system is not in direct contact with the cell electrodes). The signal is capacitively coupled through the walls of insulating tubing, which is passed through the bore of two ring electrodes placed a fixed distance apart, allowing the cell to be operated in 'scanning' mode leading to great versatility. Scanning C^4D involves passing a capillary through the bore of the electrode ring pair and measuring the conductive response at millimitre increments along the capillary length. The column/capillary is usually held stationary and the detector head is moved by hand using a ruler as a detector location guide. In this way, a ''sC^4D profile'' can be plotted as detector response (m*V*) versus detector location (mm), showing the axial distribution of charged density along the entire length of the column/capillary in a completely non-invasive manner.

In 2006 Gillespie *et al.* reported the first characterisation of a surfactant-modified silica monolith using sC^{4}D [12] (see Figure 2.2). Conductive measurements obtained at 30 minutes intervals for 240 minutes allowed the visualisation of the removed excess sodium dioctyl sulphosuccinate (DOSS). Furthermore, constant monitoring of the conductive responses allowed to confirm that a stable surfactant layer was present after 18 hours with conductive responses approximately 4 times higher relative to an unmodified column. The use of sC^{4}D allowed the monitoring of the surfactant coating by visualising a break-through curve upon flushing in the forward and reverse directions, allowing to establish the complete saturation of the column with surfactant molecules [13].

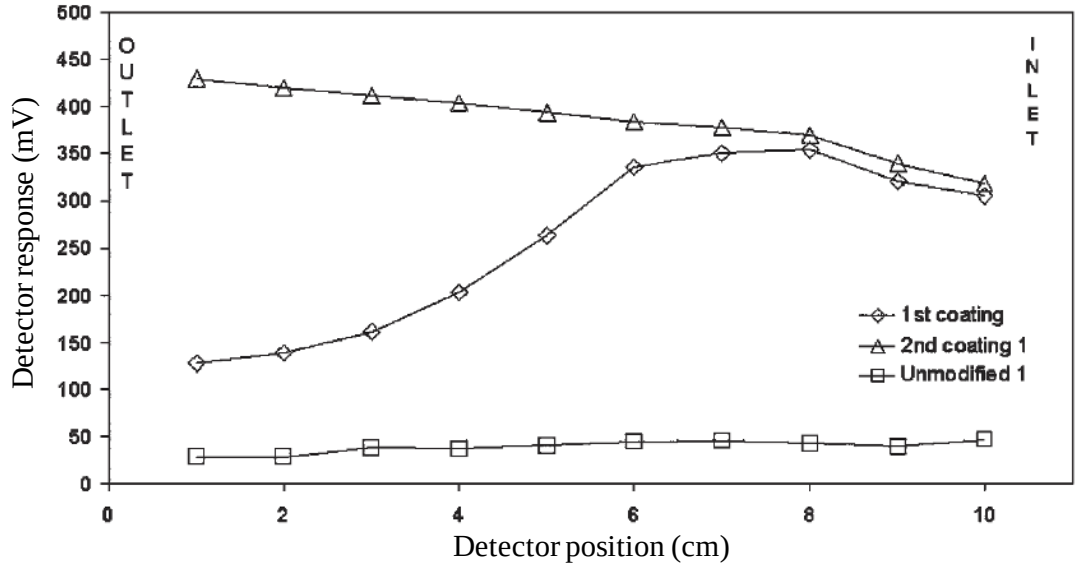

***Figure 2.2**: Plot showing the sC^{4}D profiles of a silica monolith after coating with sodium dioctyl sulphosuccinate (DOSS) initially from inlet to outlet and in a second step in the reverse direction [12].*

Connolly *et al.* used sC^{4}D for the characterisation of a capillary packed column, allowing the visualisation of voids in the packing material due to poor packing procedures [14]. It was demonstrated that the relationship between C^{4}D response and the density of the stationary phase are inversely proportional since an increase in signal was observed in void regions. The explanation for this phenomenon was attributed to the structure of the C^{4}D cell. According to Kuban [15] two 'virtual electrodes' are present in between the two real electrodes of the cell with a size dependant on the cross-sectional areas of the capillaries which depends on their i.d..

When a stationary phase is present inside the capillary, a smaller fluid volume is present between the two real electrodes which provides a smaller virtual electrode area leading to a lower response.

The characterisation of monolithic stationary phases which had been grafted in specific regions along their length with charged functionalities has also been documented using sC^4D. For example 2-acrylamido-2-methylpropane sulphonic acid (AMPS) was photografted in two 1 cm long regions along the length of a monolith (12 cm long) and the presence of sulphonate groups was readily identified by the observation of sharp boundaries which delimited the grafted regions and distinguished them from the surrounding ungrafted areas [16]. Similarly a fluorescent protein (GFP) was immobilised in three selected regions of a polymer monolith which had been photografted with vinyl azlactone and the presence of the immobilised proteins was visualised using sC^4D. All proteins carry a net charge at a given p*H* due to the presence of amino acids with ionisable R groups such as lysine, argine, glutamic acid and aspartic acid hence a response was obtained by scanning the cell along the length of the protein-modified regions as seen in Figure 2.3.

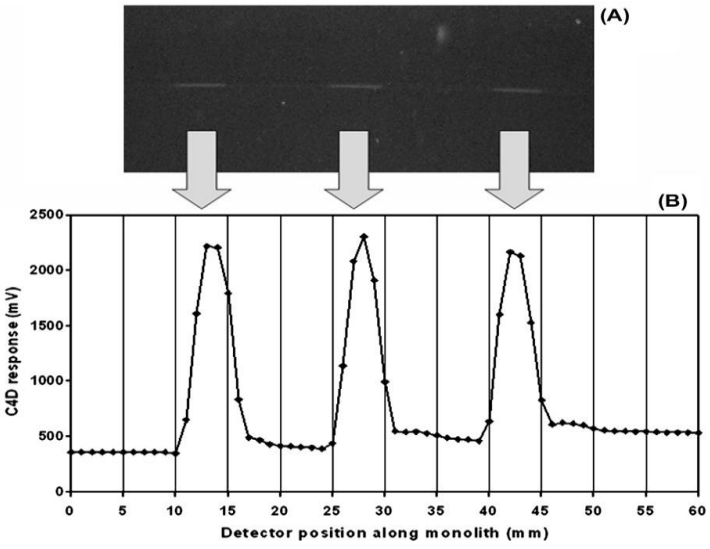

Figure 2.3: *Overlay showing (a) a digital image of a monolith modified with GFP in 3 zones and (b) the corresponding sC^4D profile illustrating an increased conductive response due to the presence of GFP.*

In this Chapter further applications of sC^4D are reported. The presence and stability of surfactant and polyelectrolyte coatings in fused silica capillary were initially evaluated. Similarly, the benefits of this characterisation technique were further

illustrated by visualising the presence of a charged monomer (sulphopropyl methacrylate) in a specific region along the length of a polymer monolith which had been photografted by using a masking technique. Other polymer monoliths which had been modified with Pd-ligand complexes for flow-through catalytic applications, where finally characterised with sC^4D and the removal of the catalyst was confirmed upon flushing with a EDTA solution.

2.2 Experimental

2.2.1 Instrumentation

Photopolymerisation and photografting were carried out using a Spectrolinker XL-1000 UV Crosslinker at 254 nm (Spectronics Corp., Westbury, NY, USA). The balance used was a Sartorius Extend (Sartorius, Goettingen, Germany). A KD Scientific syringe pump (KDS-100-CE, KD Scientific Inc, Holliston, MA, USA) was used for all washing and functionalisation of monoliths, while a Model K120 Knauer pump (Knauer, Berlin, Germany) was used for pumping eluents through the capillary columns while obtaining conductivity measurements. The conductivity detector used was a TraceDec capacitively coupled contactless conductivity detector (Innovative Sensor Technologies GmbH, Innsbruck, Austria).

2.2.2 Materials and reagents

3-(trimethoxysilyl) propyl methacrylate, 3-sulphopropylmethacrylate (SPM), benzophenone, 2,2-dimethoxy-2-phenylacetophenone (DAP), ethylene glycol dimethacrylate (EDMA), butyl methacrylate (BuMA), 1-decanol, sodium hydroxide, sodium benzoate, nitric acid, hydrochloric acid, dihexadecyldimethyl ammonium bromide (DHDAB), 2-(N-morpholino)ethanesulphonic acid (MES), L(-)-histidine (HIS), *tris*(hydroxymethyl)aminomethane (TRIS), hydrochloric acid (HCl), sodium hydroxide (NaOH), sodium chloride, phosphoric acid, ethylenediaminetetra acetic acid (EDTA), polydiallyldimethylammonium chloride (PDADMAC) $(C_8H_{16}ClN)_n$ and *poly(sodium 4-styrenesulphonate)* (PSS) $(C_8H_7NaO_3S)_n$ were all purchased from Sigma-Aldrich (Dublin, Ireland). Methanol and acetone were purchased from Fisher Scientific (Dublin, Ireland). All chemicals were used as received and without further purification. Teflon-coated fused silica capillary (100 μm i.d.) was supplied by

Composite Metal Services (Shipley, England, www.cmscientific.com). Deionised water was produced with a Millipore Direct-Q 5 (Millipore, Bedford, MA, USA).

2.2.3 Characterisation of Pd-ligand modified polymer monoliths using sC^{4}D

Polymer monoliths from chloromethylstyrene-*co*-divinylbenzene (CMS-*co*-DVB) in capillary format were prepared by a collaborating research group and they were functionalised by that group with 5-amino-1,10-phenanthroline or 1-methylimidazole for susbequent loading with palladium [as $PdCl_2(NCMe)_2$]. Details of the monoliths fabrication, functionalisation and loading of metals can be found in a report described by Goemann *et al*. [17]. This paper also describes the subsequent use of the monoliths for applications in micro-scale catalysis. These monoliths were characterised by sC^{4}D for evaluating the distribution of such complexes along the monoliths before and after flushing 10 m*M* EDTA (p*H* 8.0) for three hours prior to obtaining sC^{4}D measurements in water. As shown in Figure 2.4, water was pumped in the direction from inlet to outlet. The cell was moved along the length of the capillaries at 5 mm increments.

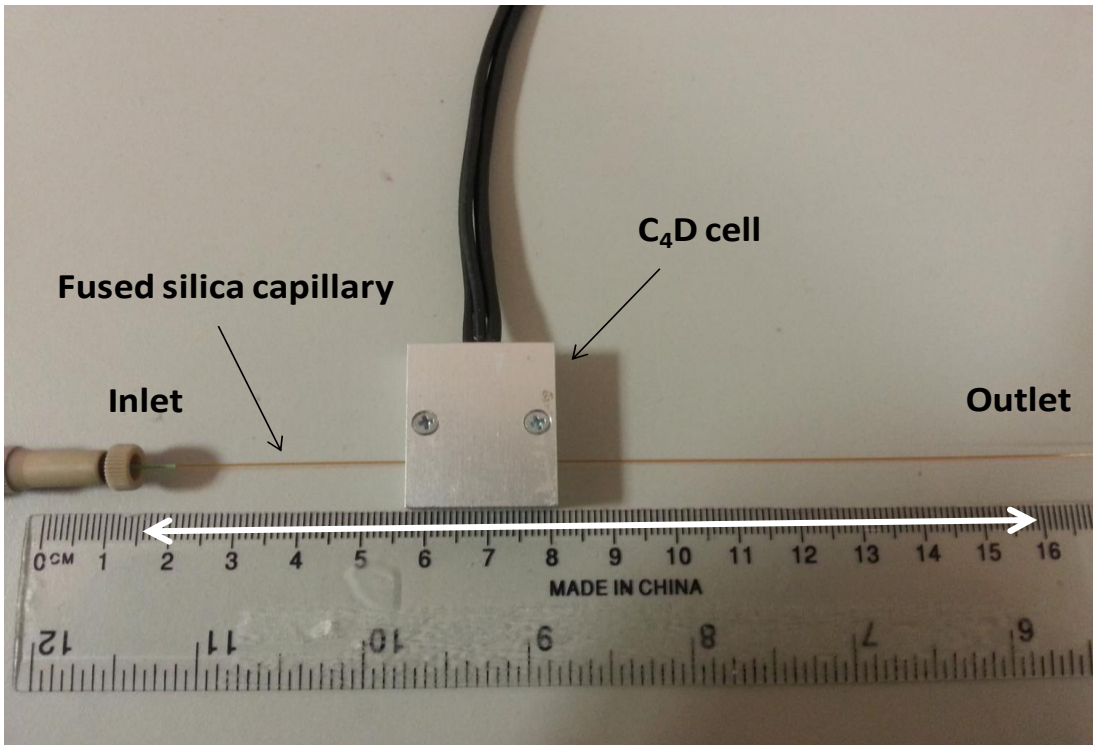

***Figure 2.4**: Image showing the experimental set up for the C^{4}D characterisation of monoliths and fused silica capillaries.*

2.2.4 Modification and characterisation of inner capillary surfaces with surfactant and polyelectrolyte coatings.

Fused silica capillary (50 µm i.d.) was modified initially by pumping NaOH (1 *M*) for 10 minutes, followed by a water rinse for 5 minutes and 0.1 m*M* surfactant, DHDAB, for 5 minutes. A BGE of MES/HIS (10 m*M*) in water was pumped for 2 minutes followed by a further water rinse and conductivity measurements were then obtained in water at 5 mm increments. Similarly, polyelectrolyte-modified capillaries were prepared according to the methods described by Nehme *et al*.[9]. Capillaries were initially rinsed in NaOH, followed by a water rinse. Subsequently, 0.2% w/vol PDADMAC in a 20 m*M* TRIS/1.5 *M* NaCl solution was pumped through for 10 minutes, followed by a 2 minute rinse with the BGE, (73 m*M* TRIS-100 m*M* H_3PO_4) and a 10 minutes rinse with 0.2 % w/vol PSS in a 20 m*M* TRIS/1.5 *M* NaCl solution. The process was repeated up to a total of five layers and conductivity measurements were obtained in deionised water at 10 mm increments.

2.2.5 Preparation of polymer monoliths in capillary format

Teflon coated UV transparent fused silica capillary (100 µm i.d.) was silanised using the following procedure. Initally the capillary was rinsed with acetone for 10 minutes and dried with N_2. Subsequently 0.2 *M* NaOH and 0.2 *M* HCl was pumped through for 30 and 5 minutes respectively with a 5 minute water rinse in between. Finally the capillary was rinsed in acetone and dried again with N_2. All pumping steps were performed at a flow rate of 1 µ*L*/min. A 50% v/v solution of 3-(trimethoxysilyl) propyl methacrylate in acetone was then pumped through the capillary, which was then sealed at both ends, immersed in a water bath at 60 ºC for 20 hours and finally rinsed with acetone.

A polymer monolith was made from a deoxygenated mixture containing BuMA 24 %, EDMA 16 %, decanol 60 % and 4 mg DAP. A capillary was filled by capillary force, end-capped with rubber septa and irradiated with 2 J/cm^2 of UV energy. Methanol was used to remove unreacted monomers by pumping for 3 hours at 1 µ*L*/min

2.2.6 Surface modification with sulphopropyl methacrylate and sC^{4}D characterisation

A solution of benzophenone (5% w/v) in methanol was prepared and deoxygenated with N_2 for 10 minutes. This was pumped through the BuMA-*co*-EDMA monolith at 1 µ*L*/min for 30 minutes. The monolith was sealed at both ends and two photomasks were applied leaving a 1 cm region of the monolith exposed. This was irradiated with 1 J/cm^2 of UV energy followed by a methanol wash for 30 minutes at 1 µ*L*/min. An aqueous solution of 3-sulphopropylmethacrylate (2% w/v) was prepared and similarly degassed. This solution was pumped for 30 minutes through the same monolith and the monolith was irradiated with 0.25 J/cm^2 of UV energy by using photomasks as described above followed by a water rinse. Sodium benzoate (2 m*M*) was pumped through overnight to remove ungrafted monomers and conductivity measurements were obtained at 1 mm increments at a flow rate of 1 µ*L*/min.

2.3 Results and discussion

2.3.1 Characterisation of the distribution and stability of Pd-ligand complexes along the axial length of monolithic columns

The use of flow-through micro-reactors for catalysis/organic synthesis has received increasing attention due to the benefits of rapid heat and mass transfer, reduction of unwanted side reactions and reduced solvent consumption. Recently, a collaborating research group based in the University of Tasmania donated chloromethylstyrene-*co*-divinylbenzene (CMS-*co*-DVB) polymer monoliths which were functionalised with 5-amino-1,10-phenantroline or 1-methylimidazole, and subsequently loaded with palladium [as $PdCl_2(NCMe)_2$] to facilitate both Pd-catalyzed Suzuki–Miyaura and Sonogashira reactions in a flow-through system [17-20] (see Figure 2.5).

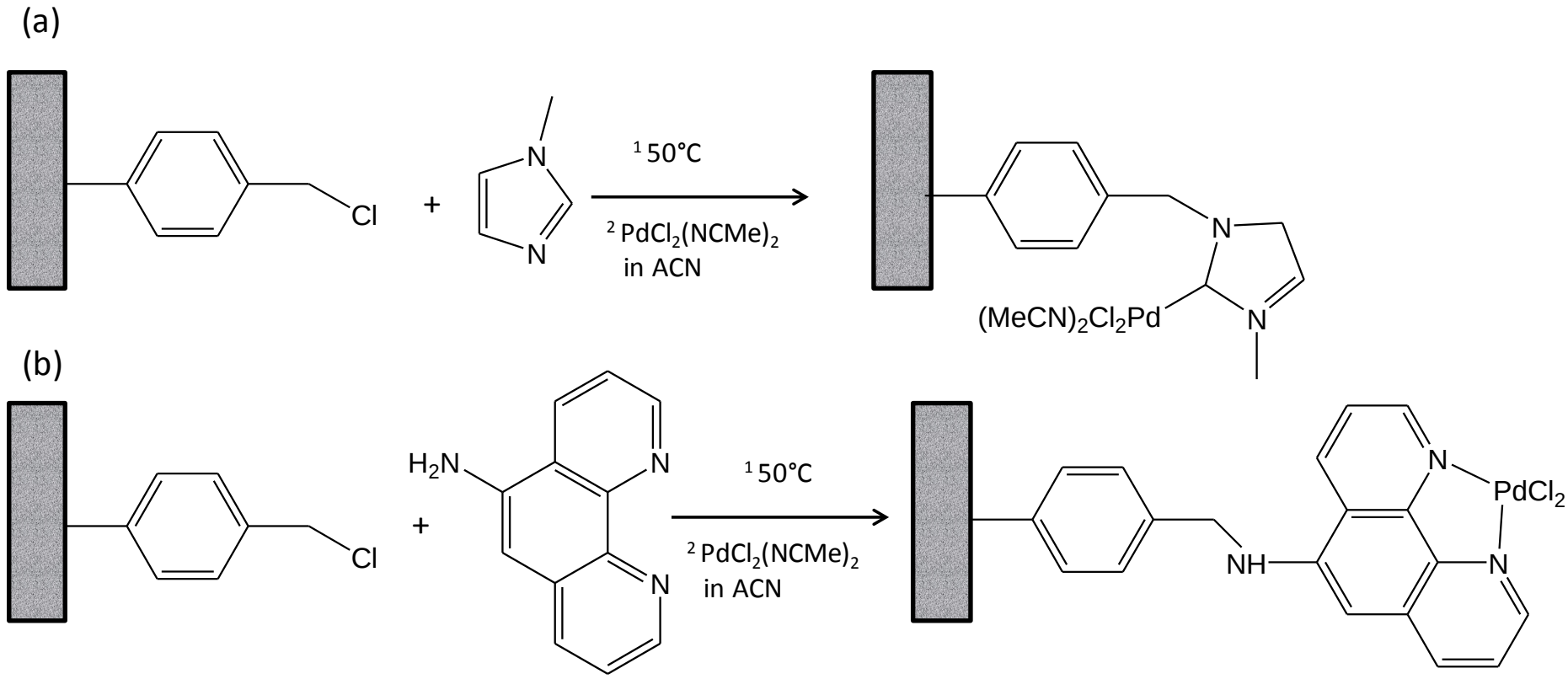

Figure 2.5*: Schematic representations of the immobilisation of Pd on CMS-co-DVB monoliths modified with (a) 1-methylimidazole (Monolith A) and (b) 5-amino-1,10-phenanthroline (monoliths B and C).*

Four monolithic micro-reactors were donated, the first being a monolith prepared in a capillary of 250 μm i.d. modified with 1-methylimidazole and loaded with the palladium complex (Monolith A), the second being a monolith prepared in a 100 μm i.d. fused silica capillary, modified with 5-amino-1,10-phenanthroline and loaded with the Pd complex (Monolith B), the third one being indentical to Monolith B but prepared in a fused silica capillary of different i.d., 250 μm, (Monolith C). The fourth column was a blank monolith, identical to Monolith C in terms of porous structure but it was not modified with any Pd functionality (Monolith D).

The efficiency and the long-term stability of the monolithic-based catalytic reactor is a function of the capillary dimensions, the distribution of catalyst and metal leaching which was reported by Gomann *et al.* as being 4 % [19]. The stability of the coating was verified using sC^4D in the work presented herein. Following equilibration in water, conductivity measurements at 5 mm intervals were obtained using sC^4D for the non-invasive determination of the metal loading and the distribution of such metal-ligand complexes along the axial length of the columns.

Each of the three micro-reactors did not show a homogeneous coverage of palladium. For Monolith A, the surface density of the palladium catalyst increased almost linearly along the monolith length as shown in Figure 2.6 (a). This gradient profile (a) is clearly a function of catalyst distribution rather than other factors (such as poor axial homogeneity of monolith density). This was verified since a comparatively straight sC^4D profile (b) (with a lower signal amplitude, as expected) was obtained after removal of the palladium catalyst with EDTA. Some variations in detector response were observed over a 5 cm region at the front of the column (see Figure 2.6 b) after the removal of the metal possibly due to small variations in porous structure of the monolith. It can be therefore hypothesised that the column had been loaded with Pd in the reversed direction, by pumping from the outlet to the inlet.

A similar scenario was present with Monolith B (see Figure 2.7) where the loading of the catalyst was localised closer to the inlet rather than the outlet. As revealed by the sC^4D scan (a), an increased distribution of metal was especially observed in the region from 10 mm to 80 mm.

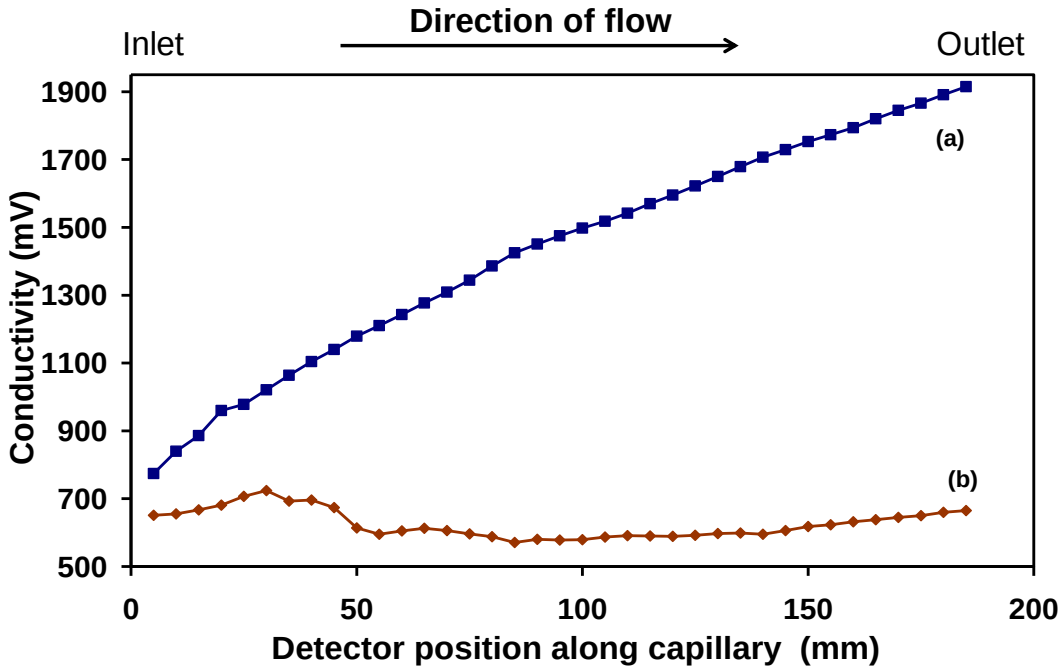

Figure 2.6: *sC^{4}D profile of a 1-methylimidazole/palladium modified polymer monolith (Monolith A) in a 250 µm i.d. fused silica capillary (a) before and (b) after metal removal by flushing with EDTA. Settings: frequency medium, -12dB, gain 50%.*

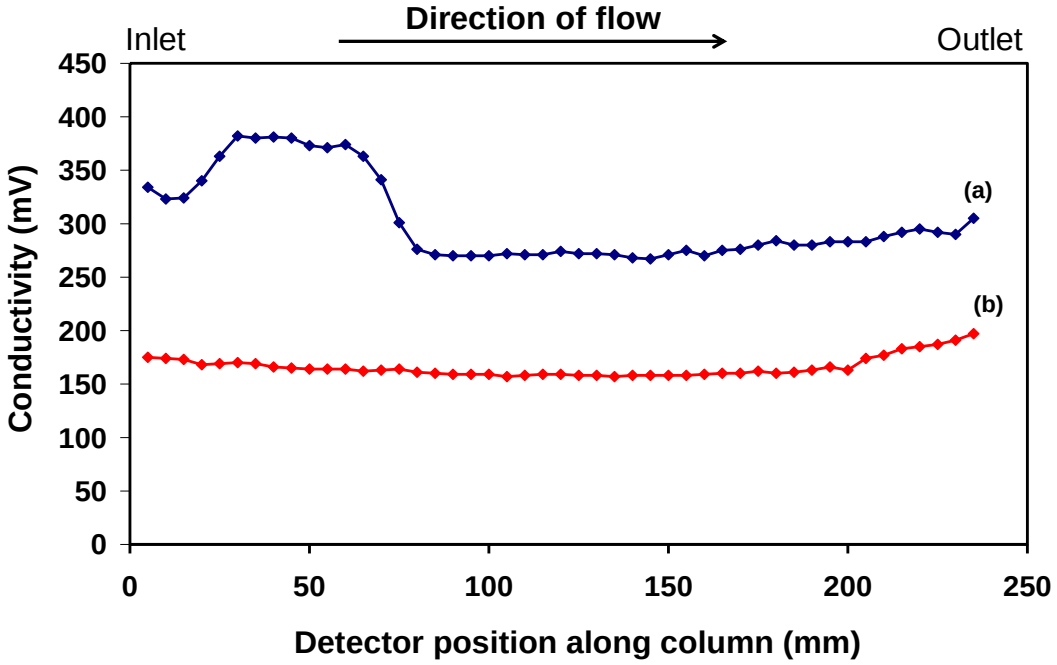

Figure 2.7: *sC^{4}D profile of a 5-amino-1,10-phenanthroline/palladium modified polymer monolith (Monolith B) prepared in 100 µm i.d. fused silica capillary (a) before and (b) after metal removal by flushing with EDTA. Settings: frequency 2x high, 0dB, gain 50%.*

Again after flushing EDTA, a further scan (b) revealed a decreased conductive response which indicated that the monolith density is axially homogeneous and that the previously observed increased conductive response could only be due to a localised increase in catalyst loading.

Finally Monolith C showed a higher presence of the metal complex at the extremities of the column rather than in the centre due to pre-concentration effects occurring during the loading of the catalyst as shown in Figure 2.8. The sC^4D profile of Monolith C after the removal of Pd was found to be similar to Monolith D which had a similar porosity but was not modified previously with any catalyst. The observed increase in conductive response was proportional to the metal loadings present in Monolith C, which were calculated to be 89% relative to the blank Monolith D.

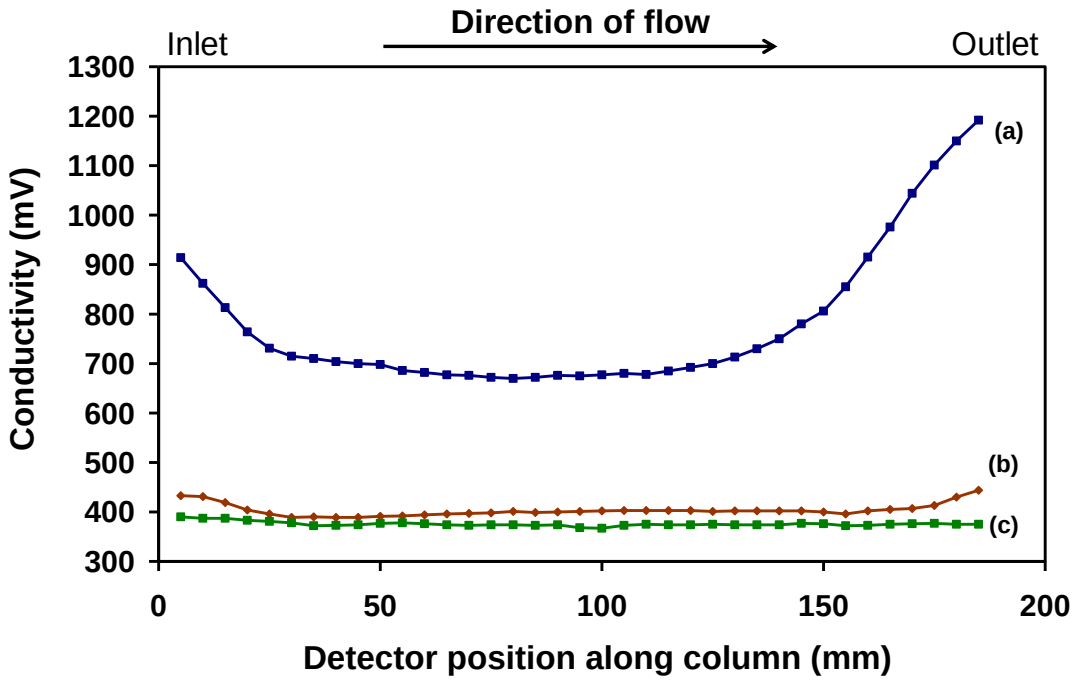

Figure 2.8: *sC^4D profile of a 5-amino-1,10-phenanthroline/palladium modified polymer monolith (Monolith C) prepared in 250 µm i.d. fused silica capillary (a) before, (b) after metal removal by rinsing with EDTA and (c) a blank unmodified monolith (Monolith D) of similar porosity. Settings: frequency 2x high, -6 dB, gain 50%.*

Optimisation of the Tracedec conditions was required in each scenario since the conductive response is dependent on the i.d. of the columns used. As described by

Kuban [15] an increase in capacitance occurs as the internal diameter of the capillary increases based on the relationship:

$$C = (2\pi\varepsilon_0\varepsilon_r l) / (\ln D - \ln r) \qquad \text{(Equation 2.1)}$$

where C = the cell capacitance in F, ε_0 = the relative permittivity of vacuum, ε_r = the relative permittivity of the silica capillary wall, l = the length of the electrodes in meters, D = the outer radius of the capillary in meters, and r = the internal radius of the capillary in meters.

An increase in capacitance would lead to a reduced resistance due to the following equation:

$$R = 1 / 2\pi fC \qquad \text{(Equation 2.2)}$$

Where f = cell frequency in Hz, C = capacitance in F and R = cell resistance in Ω

Ultimately the decreased resistance results in an increased voltage output (detector response) due to the inversely proportional relationship between V_{out} and R:

$$V_{out} = (V_{in} \times R_f) / R \qquad \text{(Equation 2.3)}$$

Where V_{out} = output voltage in V, V_{in} = excitation voltage in V, R_f = resistor value from pick up amplifier in Ω and R = cell resistance in Ω.

Monolith B was prepared in a 100 µm i.d. capillary and the amplitude of the signal was maximised by operating at 0 dB in order to characterise the column as accurately as possible. The same conditions could not be used with Monolith A and C which were prepared in a 250 µm i.d. capillary, since signal overflow would be obtained, hence the intensity of the signal was reduced by switching to -12 dB and -6 dB for monoliths A and C respectively.

In summary sC^4D proved to be a valuable tool for determining the distribution of a Pd catalyst along the axial length of polymer monoliths. The main benefits of this technique include the ability to precisely characterise the surface at mm increments which clearly revealed that the distribution of catalyst was not homogeneous. This can be done in a non-invasive manner without the need to cut the monolith into cross-sections for analysis.

2.3.2 Evaluation of surfactant and polyelectrolyte capillary coatings, stability and distribution

Reversed-phase stationary phases can be coated with both charged and neutral surfactants for a variety of chromatographic applications however, researchers have generally assumed that a homogeneous distribution of surfactant exists after coating along the entire column length. In the work here described, fused silica capillaries were initially modified with the surfactant DHDAB (shown in Figure 2.9), rinsed with a BGE and a C^4D profile in water was obtained.

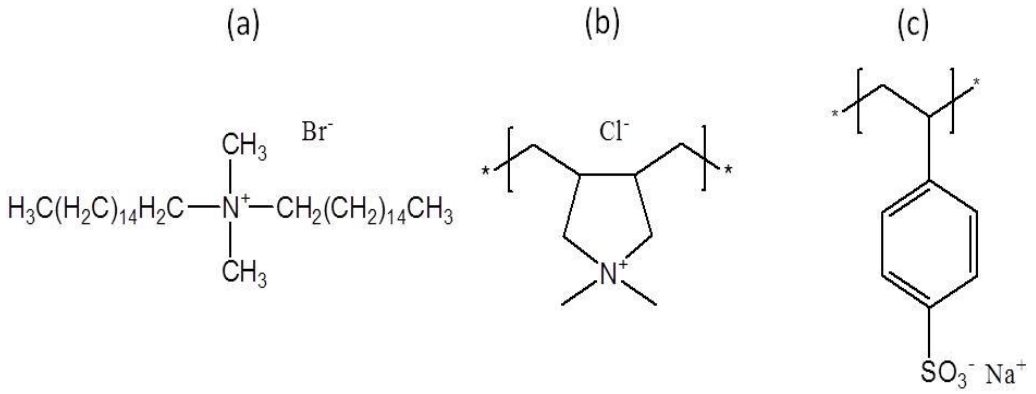

Figure 2.9: *Chemical structures of (a) the surfactant dihexadecyldimethyl ammonium bromide (DHDAB), (b) polydiallyldimethylammonium chloride (PDADMAC) and (c) poly(sodium 4-styrenesulphonate) (PSS).*

Surfactants bearing two alkyl chain substituents such as DHDAB were selected as they are known to lead to more stable coatings relative to single-chained surfactants due the formation of bi-layer configurations [21] as illustrated in Figure 2.10.

A C^4D scan in water after the modification with the surfactant, as shown in Figure 2.11, revealed that the column was not coated homogeneously along its length since a higher conductivity was observed closer to the inlet relative to the outlet. This confirmed the previously reported observation from Gillespie *et al*. [12] who demonstrated that by coating the column in one direction only (i.e. from column inlet to outlet) a higher loading of surfactant at the column head (inlet) would be observed.

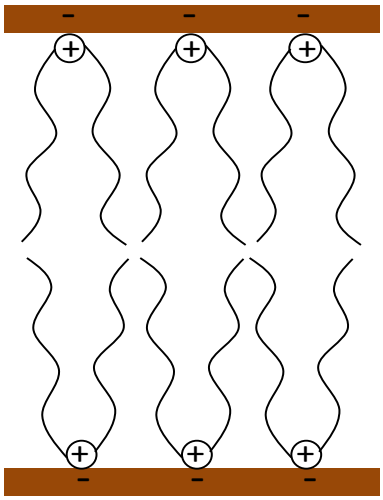

Figure 2.10: *Schematic showing a typical bi-layer configuration of positively charged surfactants bearing two alkyl chain substituents within a negatively charged fused silica capillary.*

The removal of the surfactant chains from the surface of the capillary was monitored using sC^{4}D (Figure 2.11 b-d) however, since this is a dynamic process, a degree of error is present with each measurement hence scans were performed in triplicate (*n*=3). Standard deviation values are included on the plot for illustrative purposes although it is acknowledged that use of error bars ought be used to visually evaluate the magnitude of *random* error; clearly the source of error in this work was systematic due to the manner in which replicate C^{4}D scans were made. After rinsing the capillary with water for 30 minutes, no further decrease in conductive response was observed (Figure 2.11 e) leading to the assumption that a stable surfactant coating was formed on the inner surface of the capillary.

The effects caused by the modification of fused silica capillary with polyelectrolytes were then evaluated. Charged polyelectrolytes are commonly used in CZE both to reverse the electro-osmotic flow (EOF) direction and to reduce or to eliminate non-specific adsorption of proteins to the capillary surface during bio-separations [8, 22]. For example, a cationic polyelectrolyte such as poly(diallyldimethylammonium) chloride (PDADMAC) can be adsorbed onto the capillary wall via electrostatic interactions with negatively charged silanol groups. An anionic polyelectrolyte such as poly(sodium 4-styrenesulphonate) (PSS) can then

be adsorbed onto the underlying cationic layer and thus multiple layers can be built up by repeating the procedure prior to the separation step.

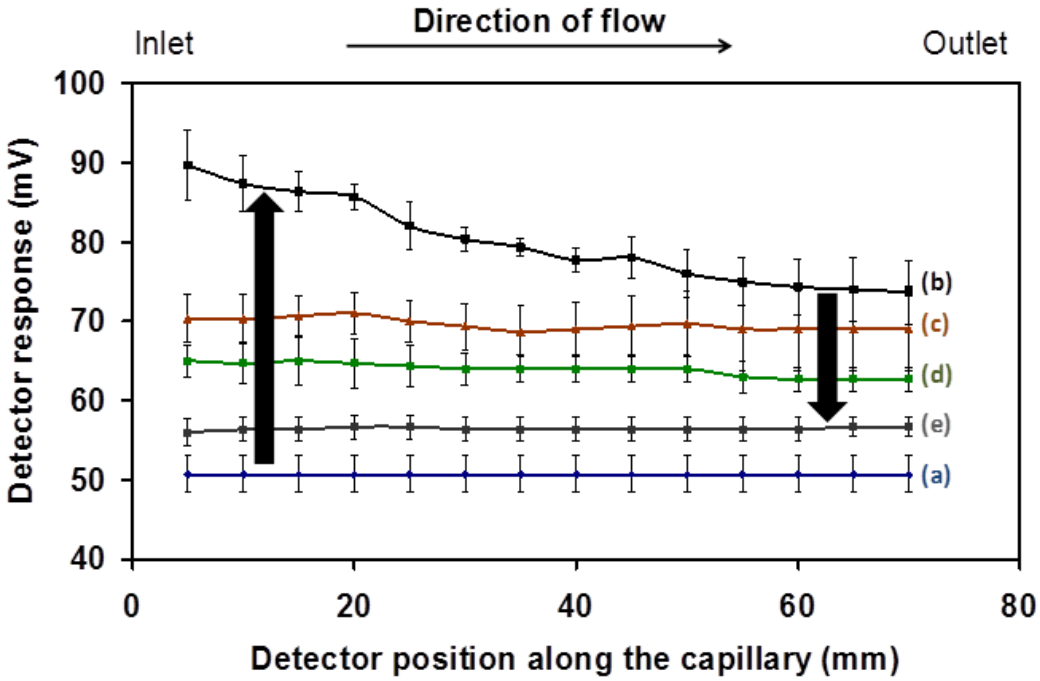

Figure 2.11: *sC^{4}D profile for a surfactant coated fused silica capillary (a) after modification with NaOH, (b) immediately after modification with DHDAB, (c) after pumping water for 10 minutes, (d) 20 minutes and (e) 30 minutes. Detector settings: 2x high, 0dB, gain 50%, offset 0, n=3.*

When used in CZE, the successful establishment of a polyelectrolyte multilayer and its subsequent stability are typically evaluated by measuring EOF magnitude and repeatability [9, 23]. However, sC^{4}D can also find a role in providing greater understanding of the surface properties of capillaries after the modification with polyelectrolytes. Using a capillary-coating procedure described by Nehmè *et al.* [9], a 50 µm i.d. fused silica capillary was flushed alternately with buffered solutions of 0.2 % w/v PDADMAC and 0.2 % w/v PSS, with 1.5 *M* NaCl present in each coating solution. Five layers were deposited, followed immediately by sC^{4}D evaluation while flushing the capillary with water. The obtained sC^{4}D data for this experiment is shown in Figure 2.12, where scans of the modified capillary were performed upon pumping water over a 50 minutes period.

The average conductive response increased significantly upon modification with polyelectrolytes and stabilised after a 50 minutes rinse with water. Figure 2.13 also

shows that the rate of decrease of conductive response slows significantly after the first 10 min.

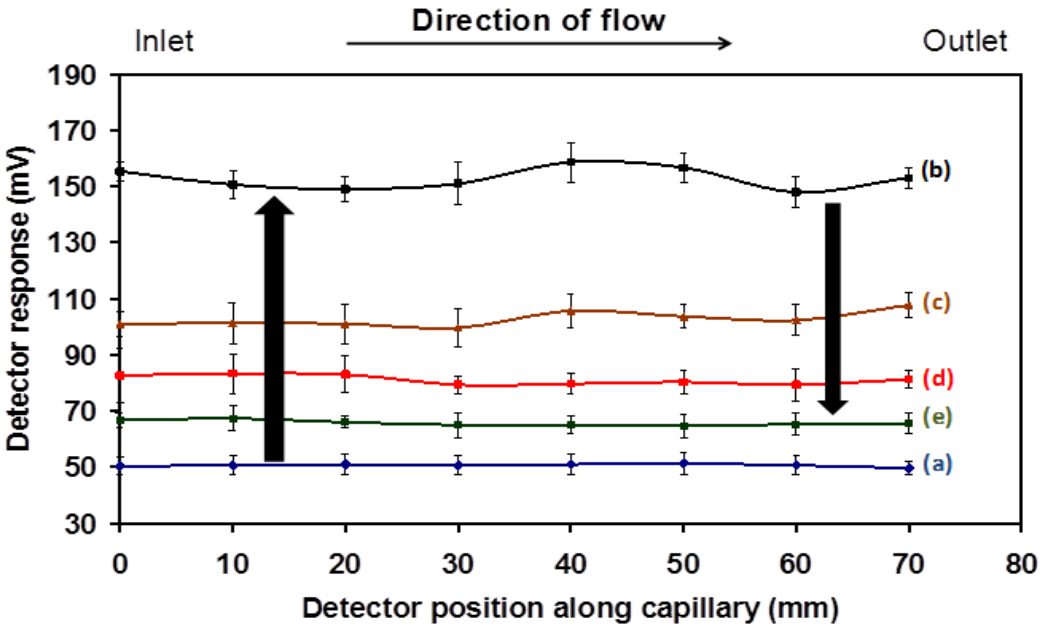

Figure 2.12: *sC^{4}D profile overlay showing the decrease in conductivity along the length of a capillary: (a) before modification with a polyelectrolyte solution, (b) immediately after coating, (c) after a 10 minutes water wash, (d) after 20 minutes and (e) after 50 minutes. Detector settings: 2x high, 0dB, gain 50%, offset 0.*

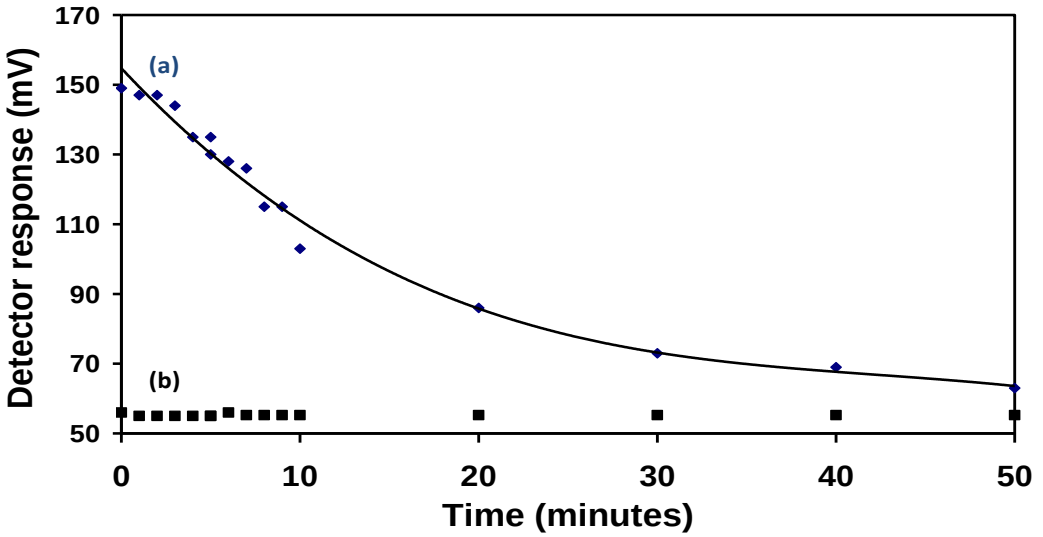

Figure 2.13: *sC^{4}D profile showing the decrease in conductivity at a fixed point along the length of the capillary (a) after the polyelectrolyte modification step and (b) conductivity of a capillary which was not modified with polyelectrolytes. Detector settings: 2x high, 0dB, gain 50%, offset 0.*

It was established that the thickness of the polyelectrolyte multilayer was significantly enhanced by the presence of salt during the coating step [8, 21] due to the coiled configuration of the polyelectrolyte chains. Schlenoff *et al.* demonstrated that the thickness of 5 layers of PDADMAC/PSS on a silicon wafer increases from 0.8 nm to 10 nm when 1 *M* NaCl is present during coating [24], which, in relation to the work here, suggests that sC^4D measurements can provide detailed information on wall coatings of thickness well below 10 nm. Indeed, this observation was recently supported by Takeuchi *et al.*, who investigated a similar application of a home-built, low-cost, capacitance-measurement device in scanning mode to study the distribution of ionic liquid coatings within capillary gas chromatography columns [25].

2.3.3 Characterisation of BuMA-co-EDMA monoliths photografted with sulphopropyl methacrylate.

Sulphonate groups are often used on monolithic stationary phases to achieve strong cation-exchange functionalities [26]. In the work here described, sulphopropyl methacrylate (SPM) chains was photografted on a selected region of a BuMA-co-EDMA monolith by applying photo-masks as shown in Figure 2.15 leading to the visualisation of negatively charged functionalities on the surface of the monolith. The grafting procedure was performed using a two-step method originally developed by Ma *et al*. [27] which is known to improve grafting efficiency relative to single-step processes. An initiator (benzophenone) was covalently attached to the surface by applying 1 J/cm^2 of UV energy followed by the grafting of the charged monomer using photomasks in a successive step. A UV energy dose of 0.25 J/cm^2 was applied in this last step based on previous work by Connolly *et al.* [28].

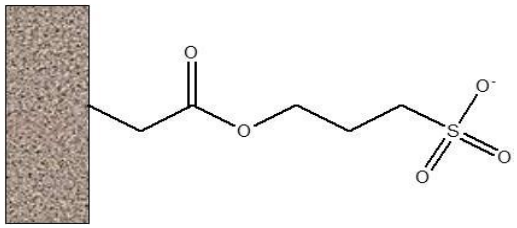

***Figure 2.14**: Structure of a polymer monolith grafted with sulphopropyl methacrylate (SPM) chains, leading to negatively charged sulphonate groups on the surface.*

Immediately after the monolith was photografted and adequately washed, sC^4D profiles were collected and overlaid using a low conductivity electrolyte, (sodium benzoate), for determining variations in charge distribution. As reported in Figure 2.16, a steep increase and decrease was observed on the edges of a 1 cm grafted zone. The intensity of the grafting is dependant on the intensity of the UV energy applied and the concentration of the monomer. The photografted region of the monolith showed an homogeneous conductive response, confirming that the photografting procedure occurred uniformly in this area. This was verified by moving the detector cell along the axial length of the column using the highest sensitivity settings. The surface was characterised as precisely as possible at 1 mm increments however, the spatial resolution of this technique can be improved by attaching the cell onto a motorised arm as recently reported in the literature [28].

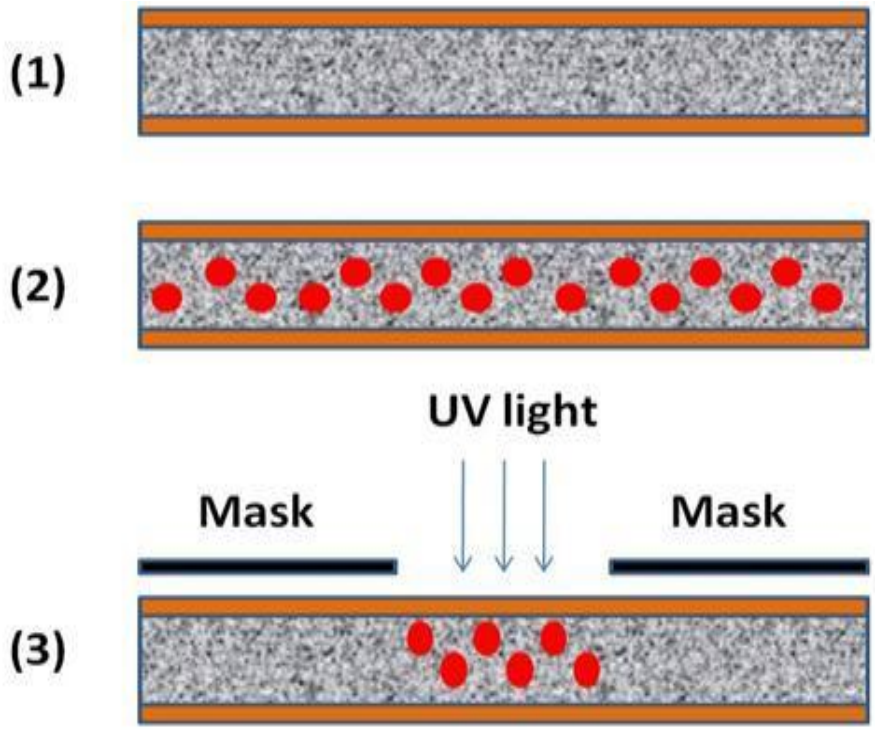

***Figure 2.15**: Image describing the the grafting process using photo-masking. (1) A monolith is prepared in UV transparent housing, (2) the monolith is filled with a solution containing the desired monomer and (3) masks are applied (such as black vinyl paper) to prevent the passage of UV light in undesired regions of the monolith. Extensive branching of polymer chains forms in the regions were UV light was allowed through.*

These results confirmed previously reported observations by Gillespie *et al.* [29] and Connolly *et al.* [16] who grafted 2-acrylamido-2-methylpropane sulphonic acid AMPS in different zones of a monolith and sC^4D was used to establish the linear relationship between conductive response and the UV energy applied for each of those zones.

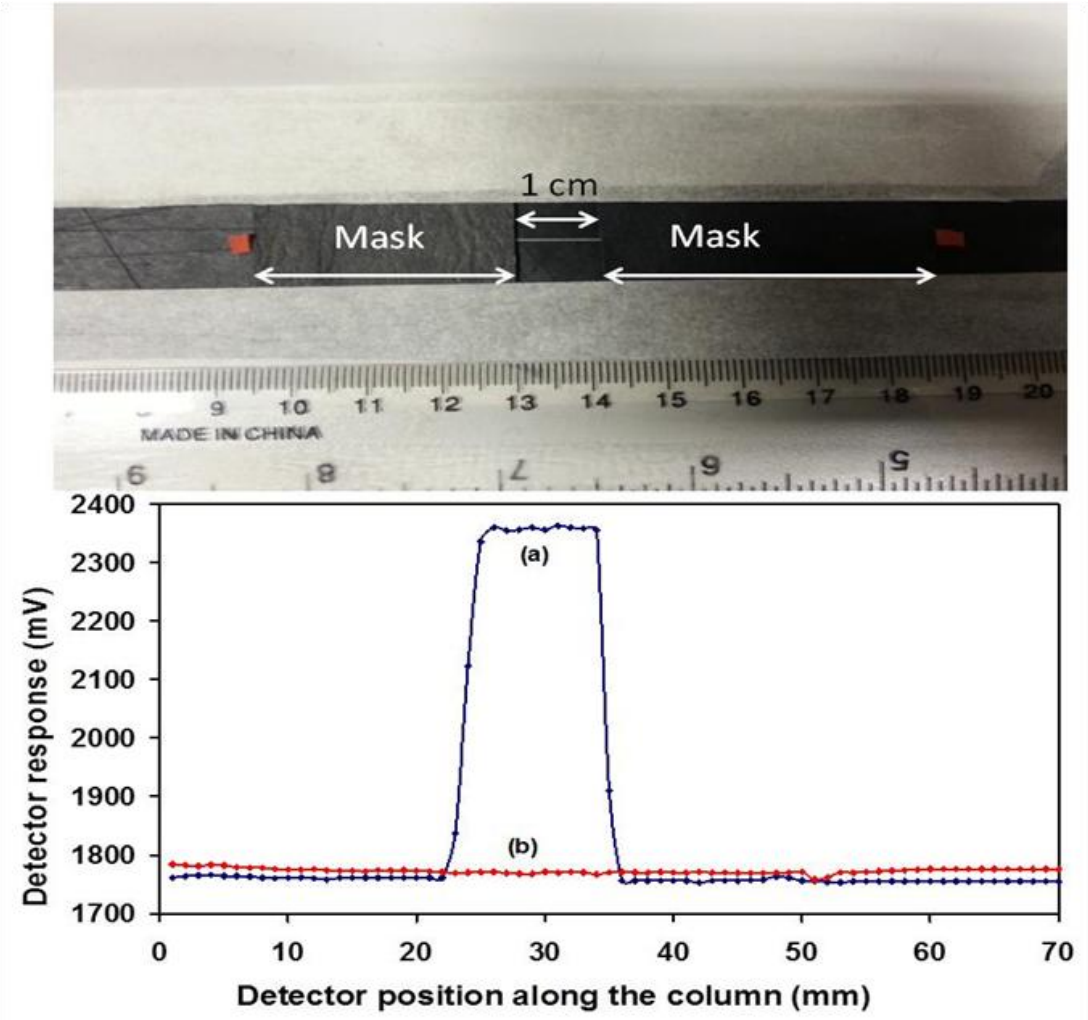

Figure 2.16: *(top) Image showing the applications of photomasks on a monolith prior to performing the grafting procedure and (bottom) conductivity profile of a BuMA-co-EDMA monolith grafted with SPM using a photo-masking technique: (a) a 1 cm region of the monolith exposed to 0.25 J/cm^2 UV irradiation and (b) a similar monolith which was not exposed to UV irradiation. Settings: 2x high, 0dB, gain 50%, offset 0. All readings obtained using 2mM sodium benzoate.*

2.4 Conclusion

In this Chapter sC^{4}D proved to be a useful tool for the characterisation of the physico-chemical properties of both monoliths and empty fused silica capillaries, modified with highly charged species. The non-invasive determination of metal catalyst distribution along the surface was verified and its removal upon complexation of the metal with a EDTA ligand was also confirmed. The presence of sulphonate groups in a specific region along the axial length of a column was verified using sC^{4}D and this allowed to gain a better understanding of the advantages present when availing of photomasking techniques since the distribution of the desired functional groups can be indirectly visualised with high precision. The same concept applies for capillaries coated with surfactants or polyelectrolytes, a procedure traditionally applied to reverse the EOF or prevent the absorption of target analytes onto the surface. It is generally assumed that the presence of coatings is homogeneous along the entire length of capillaries however, sC^{4}D can allow a more precise evaluation of the distribution of such species. The presence of coatings along the axial length of capillaries was verified as well as any variations in the coating distribution after extended washing periods.

2.5 References

1. Hjerten, S. High-performance electrophoresis - elimination of electroendosmosis and solute adsorption. *Journal of Chromatography* **1985,** *347* (2), 191-198.

2. Kaupp, S.; Watzig, H. Characterization of inner surface phenomena in capillary electrophoresis capillaries by electron microscopy, atomic force microscopy and secondary ion mass spectroscopy. *Journal of Chromatography A* **1997,** *781* (1-2), 55-65.

3. Ghosal, S. Fluid mechanics of electroosmotic flow and its effect on band broadening in capillary electrophoresis. *Electrophoresis* **2004,** *25* (2), 214-228.

4. Bushey, M. M.; Jorgenson, J. W. Capillary electrophoresis of proteins in buffers containing high-concentrations of zwitterionic salts. *Journal of Chromatography* **1989,** *480*, 301-310.

5. Lauer, H. H.; Mcmanigill, D. Capillary zone electrophoresis of proteins in untreated fused-silica tubing. *Analytical Chemistry* **1986,** *58* (1), 166-170.

6. Castelletti, L.; Verzola, B.; Gelfi, C.; Stoyanov, A.; Righetti, P. G. Quantitative studies on the adsorption of proteins to the bare silica wall in capillary electrophoresis III: Effects of adsorbed surfactants on quenching the interaction. *Journal of Chromatography A* **2000,** *894* (1-2), 281-289.

7. Katayama, H.; Ishihama, Y.; Asakawa, N. Stable capillary coating with successive multiple ionic polymer layers. *Analytical Chemistry* **1998,** *70* (11), 2254-2260.

8. Katayama, H.; Ishihama, Y.; Asakawa, N. Stable cationic capillary coating with successive multiple ionic polymer layers for capillary electrophoresis. *Analytical Chemistry* **1998,** *70* (24), 5272-5277.

9. Nehme, R.; Perrin, C.; Cottet, H.; Blanchin, M. D.; Fabre, H. Influence of polyelectrolyte coating conditions on capillary coating stability and separation efficiency in capillary electrophoresis. *Electrophoresis* **2008,** *29* (14), 3013-3023.

10. Riordain, O.; Gillespie, E.; Connolly, D.; Nesterenko, P. N.; Paull, B. Capillary ion chromatography of inorganic anions on octadecyl silica monolith modified with an amphoteric surfactant. *Journal of Chromatography A* **2007,** *1142* (2), 185-193.

11. Nesterenko, E. P.; Guivarc'h, C.; Duffy, C.; Paull, B. Separation of nucleic acid precursors on an amphoteric surfactant modified monolith using combined eluent flow, pH and concentration gradient. *Journal of Separation Science* **2007,** *30* (17), 2910-2916.

12. Gillespie, E.; Macka, M.; Connolly, D.; Paull, B. Evaluation of capillary ion exchange stationary phase coating distribution and stability using radial capillary column contactless conductivity detection. *Analyst* **2006,** *131* (8), 886-888.

13. Gillespie, E.; Connolly, D.; Macka, M.; Nesterenko, P. N.; Paull, B. Use of contactless conductivity detection for non-invasive characterisation of monolithic

stationary-phase coatings for application in capillary ion chromatography. *Analyst* **2007,** *132* (12), 1238-1245.

14. Connolly, D.; Barron, L. P.; Gillespie, E.; Paull, B. The use of contactless conductivity for the on-column characterisation and visualisation of packing homogeneity and band broadening in capillary LC. *Chromatographia* **2009,** *70* (5-6), 915-920.

15. Kuban, P.; Hauser, P. C. Fundamental aspects of contactless conductivity detection for capillary electrophoresis. Part I: Frequency behavior and cell geometry. *Electrophoresis* **2004,** *25* (20), 3387-3397.

16. Connolly, D.; O'Shea, V.; Clark, P.; O'Connor, B.; Paull, B. Evaluation of photografted charged sites within polymer monoliths in capillary columns using contactless conductivity detection. *Journal of Separation Science* **2007,** *30* (17), 3060-3068.

17. Goemann, A.; Deverell, J. A.; Munting, K. F.; Jones, R. C.; Rodemann, T.; Canty, A. J.; Smith, J. A.; Guijt, R. M. Palladium-mediated organic synthesis using porous polymer monolith formed in situ as a continuous catalyst support structure for application in microfluidic devices. *Tetrahedron* **2009,** *65* (7), 1450-1454.

18. Bolton, K. F.; Canty, A. J.; Deverell, J. A.; Guijt, R. M.; Hilder, E. F.; Rodemann, T.; Smith, J. A. Macroporous monolith supports for continuous flow capillary microreactors. *Tetrahedron Letters* **2006,** *47* (52), 9321-9324.

19. Canty, A. J.; Deverell, J. A.; Gomann, A.; Guijt, R. M.; Rodemann, T.; Smith, J. A. Microfluidic devices for flow-through supported palladium catalysis on porous organic monolith. *Australian Journal of Chemistry* **2008,** *61* (8), 630-633.

20. Jones, R. C.; Canty, A. J.; Deverell, J. A.; Gardiner, M. G.; Guijt, R. M.; Rodemann, T.; Smith, J. A.; Tolhurst, V. A. Supported palladium catalysis using a heteroleptic 2-methylthiomethylpyridine-N,S-donor motif for Mizoroki-Heck and

Suzuki-Miyaura coupling, including continuous organic monolith in capillary microscale flow-through mode. *Tetrahedron* **2009,** *65* (36), 7474-7481.

21. Melanson, J. E.; Baryla, N. E.; Lucy, C. A. Double-chained surfactants far semipermanent wall coatings in capillary electrophoresis. *Analytical Chemistry* **2000,** *72* (17), 4110-4114.

22. Graul, T. W.; Schlenoff, J. B. Capillaries modified by polyelectrolyte multilayers for electrophoretic separations. *Analytical Chemistry* **1999,** *71* (18), 4007-4013.

23. Nehme, R.; Perrin, C.; Cottet, H.; Blanchin, M. D.; Fabre, H. Influence of polyelectrolyte capillary coating conditions on protein analysis in CE. *Electrophoresis* **2009,** *30* (11), 1888-1898.

24. Schlenoff, J. B.; Dubas, S. T. Mechanism of polyelectrolyte multilayer growth: Charge overcompensation and distribution. *Macromolecules* **2001,** *34* (3), 592-598.

25. Takeuchi, M.; Li, Q. Y.; Yang, B. C.; Dasgupta, P. K.; Wilde, V. E. Use of a capacitance measurement device for surrogate noncontact conductance measurement. *Talanta* **2008,** *76* (3), 617-620.

26. Chen, X.; Tolley, H. D.; Lee, M. L. Polymeric strong cation-exchange monolithic column for capillary liquid chromatography of peptides and proteins. *Journal of Separation Science* **2009,** *32* (15-16), 2565-2573.

27. Ma, H. M.; Davis, R. H.; Bowman, C. N. A novel sequential photoinduced living graft polymerization. *Macromolecules* **2000,** *33* (2), 331-335.

28. Connolly, D.; Floris, P.; Nesterenko, P. N.; Paull, B. Non-invasive characterization of stationary phases in capillary flow systems using scanning capacitively coupled contactless conductivity detection (sC(4)D). *Trac-Trends in Analytical Chemistry* **2010,** *29* (8), 870-884.

29. Gillespie, E.; Connolly, D.; Paull, B. Using scanning contactless conductivity to optimise photografting procedures and capacity in the production of polymer ion-exchange monoliths. *Analyst* **2009,** *134* (7), 1314-1321.

Chapter 3: Agglomerated polymer monoliths with bimetallic nano-particles as flow-through micro-reactors

Abstract

In this Chapter polymer monoliths in capillary formats were modified for the first time with Pd/Pt nano-flowers and selected reactions in flow-through mode were performed to demonstrate the catalytic properties of these materials. The facile synthesis of these materials involved the initial production of polyvinylpyrrolidone-stabilised palladium nano-crystals, followed by the subsequent growth of platinum nano-flowers which emanate from the Pd core. These nano-flowers can be readily immobilised upon any aminated surface and in this Chapter we describe their immobilisation upon an aminated porous polymer monolith. These materials represent an ideal support for flow-through catalysis due to their porous structure and interconnected flow-paths (pore diameter ~ 1-2 µm), thereby eliminating the need for centrifugation/filtration steps after the catalytic reaction is complete. Therefore, a methacrylate monolith was fabricated within the confines of a 100 µm i.d. fused silica capillary, and subsequently modified with grafted polymer chains of vinyl azlactone or glycidyl methacrylate followed by amination with ethylenediamine. Palladium/platinum nano-flowers with a narrow size distribution (particle size ~ 20 nm) were flushed through the aminated monolith to facilitate their immobilisation. Field emission scanning electron microscopy (FE-SEM) was used to confirm a very dense coverage of bimetallic nano-flowers on the polymer surface. Surface area measurements were also obtained after modifying a monolithic CIM disk of similar porosity with nano-flowers. Finally, selected redox reactions like the oxidation of NADH and the reduction of ferrocyanide (III) were carried out in flow-through mode in order to evaluate the catalytic properties of the nano-flowers.

Aims

The aim of this Chapter was to perform flow-through catalytic reactions using Pd/Pt nano-flower agglomerated polymer monoliths in capillary format and to evaluate variations in surface chemistry upon the functionalisation of monolithic surfaces with these nano-materials.

3.1 Introduction

Micro-reactors have gained the attention of researchers over the last decade for their applicability to traditional chemical reactions involving much smaller volumes of reagents and eluents, hence proving to be simultaneously more economical and environmentally sustainable. Metal nano-particles (NPs) have been widely used in micro-reactors [1, 2] due to their higher surface to volume ratio. The ability to generate nano-structures of various morphologies is of fundamental importance in order to fully exploit the catalytic capabilities of such materials. Branched shaped nano-particles have proven to be particularly interesting [3-5] as their surface roughness and tendency to exhibit highly active facets makes them attractive materials for catalysis [6]. Several synthetic routes have been developed over recent years to generate highly branched nanostructures, including kinetic controlled overgrowth, aggregation based growth, heterogeneous seeded growth, selective etching and template-directed methods [7]. Because of the need to relate catalytic activity and particle structure, bimetallic nano-materials have gained in popularity, since these types of materials can increase catalytic activity and offer alternative selectivity relative to their monometallic counterparts [8-10].

Metallic nano-materials are used either in a colloidal form or attached onto a solid support, the latter strategy having several advantages, such as easy recovery of the catalyst by filtration in an industrial application. The most commonly used support materials are various organic polymers [11], silica [12], carbonaceous materials [13] and metal oxides [14]. Among the various support options, monolithic porous supports have gained importance over recent years [15]. Organo polymer monoliths exhibit several advantages as support phases, as they can be readily generated in various moulds in-situ, and by controlling the monomer to porogen ratio, pores of desired size can be obtained. These properties make polymer monoliths attractive for flow-through catalytic applications, as firstly the necessity of a filtration/centrifugation step required in heterogeneous catalysis is removed, and secondly, they can be easily incorporated into micro-reactors (without the need of retaining frits). Recently, reports which describe the utility of nano-particle agglomerated monoliths in the area of separation science and for the enrichment of biomolecules have appeared in the literature [16]. However, very few reports

describe their application in the area of catalysis [15]. Generally metal NPs can be immobilised by in-situ reduction from metal ions or by pumping a colloid through a monolith modified with either amino, cyano or thiol functional groups [17]. Nikbin *et al.* [18] described the synthesis of a styrenic monolith bearing quaternary amine groups through which a solution of palladium salt was flushed, followed by reduction to Pd^0 using $NaBH_4$. Heck coupling reactions were performed with high yields, although a serious drawback was identified with the heavy leaching of Pd into the product, which then required the use of a second column for Pd trapping. Alternatively, Bandari *et al.* [19] described the preparation of a polymethacrylate based monolith via electron beam polymerisation, within the confinements of a 2 cm × 30 cm stainless steel column. The surface was functionalised with N,N-dipyrid-2-ylmethacryl amide groups and palladium nano-particles (PdNPs), synthesised in-situ from Pd^{2+} ions, and was successively used for Heck coupling reactions under a continuous flow procedure, with only a limited leaching of Pd observed at 4.2 %. Also Mennecke *et al.* [20] reported the use of an aminated co-polymer of DVB, styrene and vinylbenzyl chloride inside glass as a surface to immobilise PdNPs by a process of ion exchange. These functionalised Raschig-rings were placed inside a housing with a dead-volume of 1–2 m*L* and Suzuki-Miyaura coupling reactions were performed in a cyclic mode, since single pass experiments did not result in any product yield. Other flow-through catalytic applications involving monoliths in capillary format have been reported, however in these examples the monoliths have not been functionalised with metal NPs, but metal-ligand complexes instead [21-23].

In this Chapter bimetallic nano-flowers consisting of a Pd core and Pt branches were immobilised covalently on the aminated surface of polymer monoliths. The catalytic properties of the immobilised nano-flowers were demonstrated using selected redox reactions.

3.2 Experimental

3.2.1 Instrumentation

The instrumentation used was as described in Section 2.2.1 with the following additions. Field emission scanning electron microscopy (SEM) and energy dispersive X-ray spectroscopy (EDX) was performed using a Hitachi S-5500

instrument (Hitachi, Maidenhead, UK) equipped with an Oxford Instruments PentaFETx3 detector with the INCA Microanalysis Suite (Oxford Instruments, Oxfordshire, UK). UV spectra were obtained using a Lambda 900 UV–Vis spectrophotometer (Perkin Elmer, USA, www.perkinelmer.com), while for measurements in flow-through mode a UV detector with a 3 n*L* flow cell was used (Dionex Ultimate LC system, Sunnyvale, CA, USA). A Varian ICP-AES was used for determination of metal concentrations in nano-agglomerated CIM disc monoliths (Varian, CA, USA). A capillary ICS-5000 system (Dionex, Sunnyvale, CA, USA) was used for the characterisation of ion-exchange properties of nano-agglomerated monoliths equipped with Chromeleon 6.8 software. Surface area measurements were obtained using a Micrometrics ASAP 2400 BET Surface Area Analyser (Norcross, GA, USA). A Zetasizer Nano ZS particle analyser (Malvern Instruments, Westborough, MA, USA) was used for obtaining particle size and zeta potential data of the colloidal suspensions. A Quorum Emitech K575x (Quorum, Kent, UK) sputter coater was used to apply a 45 nm layer of chromium prior to EDX analysis. A GFL water bath (MSC Medical Supply, Dublin, Ireland) was used for the amination of the polymer monoliths.

3.2.2 Materials and reagents

The materials used were as described in Section 2.2.2 with the following additions. Glycidyl methacrylate (GMA), propanol, 1,4-butanediol, ethylenediamine, poly(vinyl pyrrolidone) (PVP), ascorbic acid, citric acid, sodium borohydride, sodium tetrachloropalladate, potassium tetrachloroplatinate, phthalic acid, potassium perchlorate, potassium hexacyanoferrate (III) were all purchased from Sigma-Aldrich (Dublin, Ireland, www.sigmaaldrich.com). 4,4-Dimethyl-2-vinyl-2-oxazolin-5-one (VAL) was purchased from TCI Europe (Zwijndrecht, Belgium, www.tcichemicals.com/en/eu). NADH was purchased from Merck KGaA (Darmstadt, Germany, www.merckmillipore.com). All chemicals were used as received and without further purification.

3.2.3 Preparation of Pd/Pt nano-flowers

Bimetallic nano-flowers (NFs) consisting of a Pd core and Pt branches emanating from the core were prepared as described in a procedure by Lim *et al.* [24] as shown

in Figure 3.1. Briefly poly(vinyl pyrrolidone) (105 mg, MW 40,000 g/mol), ascorbic acid (60 mg) and citric acid (60 mg) were added to 8 m*L* of deionised water and heated to boiling during constant stirring. Sodium tetrachloropalladate (II) (57 mg in 3 mL H_2O) was injected rapidly into the solution, which was left under reflux for 3 hours. Subsequently, 1 mL of the resulting Pd nano-particles (PdNPs) was combined with 35 mg PVP, 60 mg ascorbic acid and 6 m*L* of H_2O and the mixture held at 90 °C with constant stirring. Potassium tetrachloroplatinate (II) (27 mg in 3 m*L* H_2O) was injected rapidly into the solution which was left under reflux for 3 hours. The resulting aqueous suspension of PVP-stabilised Pd/Pt nano-flowers (NFs) had a deep black colour and was stable at room temperature.

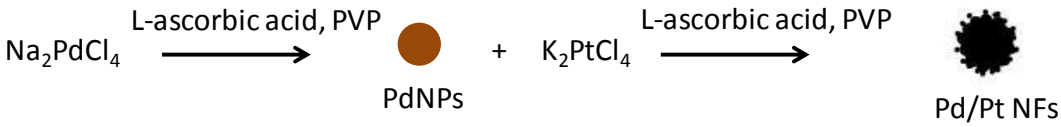

Figure 3.1*: Image showing the two-step synthesis for the formation of Pd/Pt nano-flowers.*

3.2.4 Preparation of polymer monoliths

A series of polymer monoliths were prepared as summarised in Table 3.1. Fused silica capillary was silanised as described in Section 2.2.4. Nitrogen was bubbled into each monomer mixture for 10 minutes for deoxygenation and fused silica capillaries were subsequently filled by capillary action. These were sealed with rubber septa, irradiated with 2 $J.cm^{-2}$ of energy (254 nm) and finally rinsed with methanol at 3 µ*L*$.min^{-1}$ for 30 minutes. Monolith GMA-1 incorporated encapsulated nano-flowers and was not subjected to further treatment. Monoliths GMA-2%, GMA-6%, GMA-12% and GMA-24% were functionalised in order to allow the attachment of nano-flowers on the surface. These were aminated by filling the pore volume with 1 *M* ethylenediamine and incubating in a water bath at 70 ºC for 24 hours followed by a water rinse. Monoliths BuMA-1 and BuMA-2 were photografted with GMA and vinyl azlactone respectively. In a first step, a deoxygenated solution of 5% benzophenone in methanol was pumped through for 30 minutes, followed by irradiation with 1 $J.cm^{-2}$ of UV energy (254 nm) and a methanol rinse for another 30 minutes. BuMA-1 was then flushed with deoxygenated 15 % GMA in methanol, irradiated again with 1 $J.cm^{-2}$ of UV energy

and washed with methanol. Similarly this procedure was repeated for BuMA-2, with the only exception of using VAL instead of GMA. Amination of the BuMA-1 monolith was performed as described above for monoliths GMA 2%-24%, while for BuMA-2, ethylenediamine (1 *M*) was pumped for 3 hours at room temperature and then rinsed with H_2O. All monoliths were prepared in capillary formats. Amination of monolithic GMA-*co*-EDMA discs (Convective Interactive Media (CIM) Discs) was performed by flushing a 1 *M* ethylenediamine solution for 6 hours at room temperature, in order to functionalise the surface with free NH_2 functional groups, followed by a final rinse with water.

3.2.5 Immobilisation of nano-flowers

The solution containing Pd/Pt nano-flowers was diluted 1 in 10 with deionised water, filled into a PEEK loop and flushed through the functionalised monoliths using a Knauer pump at flow rates between 1-10 $\mu L.min^{-1}$. Clear droplets from the column end confirmed that the nano-flowers were being retained and a gradual increase in colour of the monolith from white to black confirmed the covalent immobilisation of the Pd/Pt nano-flowers. When the column turned completely black, it was reversed and again the nano-flowers suspension was flushed through to allow the complete saturation of the monolith. Similarly with the monolithic CIM discs, a diluted suspension of Pd/Pt nano-flowers was flushed at 500 $\mu L.min^{-1}$ for 72 hours in both directions to maximise coverage of the monolith. Images of the nano-flower modified monoliths are shown in Figure 3.2.

3.2.6 Surface area and ICP measurements

Surface area measurements were obtained using BET methods for both blank CIM discs and discs which had been modified with Pd/Pt nano-flowers. The concentration of metals present on a CIM disc sample was determined by ICP-AES. The modified monolith was placed in aqua regia to allow dissolution of the metals. Prior to analysis, this sample was diluted 1 in 50 for Pt and 1 in 9 for Pd analysis with 0.1 *M* HNO_3.

Table 3.1: *Summary of polymer monoliths prepared for modification with Pd/Pt nano-flowers.*

Monolith[a]	GMA (wt%)	BuMA (wt%)	EDMA (wt%)	Decanol (wt%)	Propanol (wt%)	1,4-Butanediol (wt%)	H_2O[b] (wt%)	Grafted GMA (wt%)	Grafted VAL (wt%)
GMA-1	22.5	-	7.5	-	35	28	7	-	-
GMA-2%	2	22	16	60	-	-	-	-	-
GMA-6%	6	18	16	60	-	-	-	-	-
GMA-12%	12	12	16	60	-	-	-	-	-
GMA-24%	24	0	16	60	-	-	-	-	-
BuMA-1	-	24	16	60	-	-	-	15	-
BuMA-2	-	24	16	60	-	-	-	-	15

[a] All monoliths contained DAP as the initiator, 1% w.r.t. monomer

[b] Aqueous suspension of Pd/Pt nano-flowers included in the monomer mixture

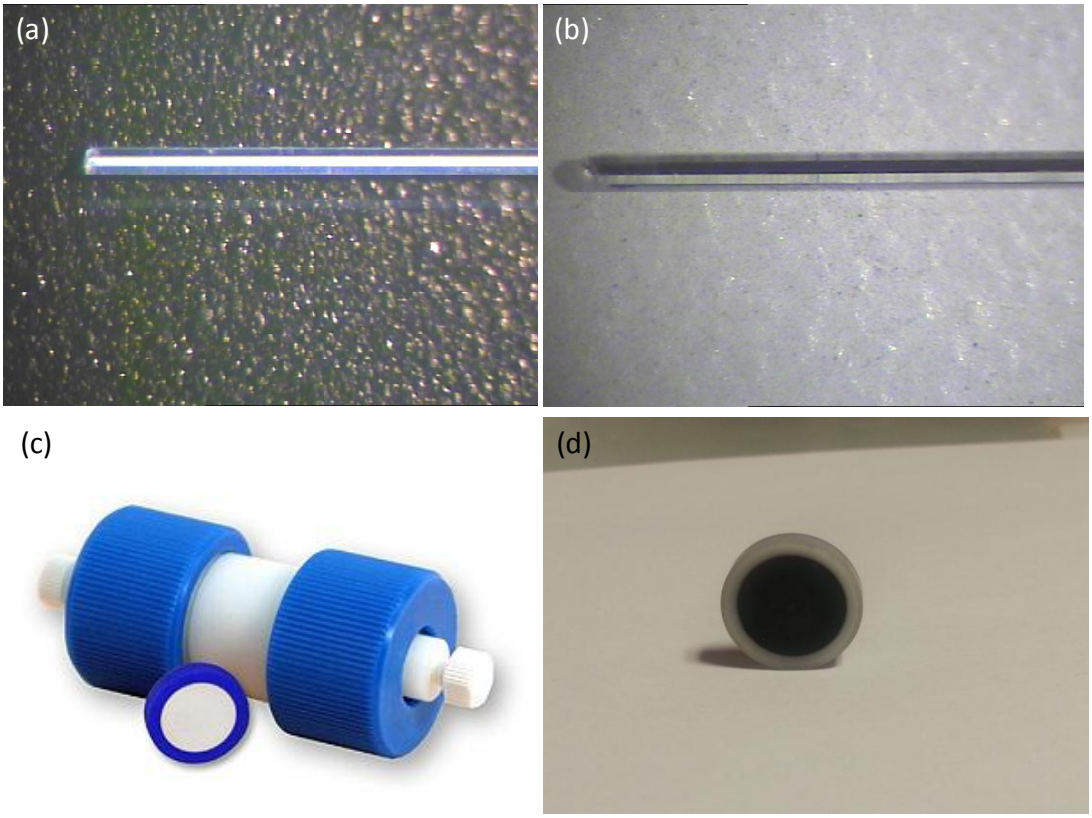

Figure 3.2*: Images showing (a) a blank BuMA-2 monolith in capillary format, (b) a similar monolith functionalised with Pd/Pt nano-flowers, (c) a blank GMA-co-EDMA CIM disc [25] and (d) a similar CIM disc modified functionalised with Pd/Pt nano-flowers.*

3.2.7 Investigation of nano-flower attachment mechanism via ion-exchange chromatography

The presence of Pd/Pt nano-flowers on the surface of the monoliths was confirmed using ion chromatography. A BuMA-2 monolith was functionalised with Pd/Pt nano-flowers and compared with a similar monolith which had been modified with ethylenediamine. The free NH_2 groups on the surface were protonated by using a phthalic acid eluent (p*H* 4.5) followed by injections of perchlorate (100 ppm).

3.2.8 Catalytic oxidation of NADH to NAD^+ using Pd/Pt nano-flowers as a colloidal suspension

A calibration plot relating absorbance versus NADH concentration at 340 nm was prepared in a 0-0.6 m*M* range. Two NADH solutions of different concentrations (0.1

and 0.5 m*M*) were prepared and 2 m*L* aliquots of each solution were added to separate quartz cuvettes followed by the addition of 100 µ*L* of the nano-flowers suspension. UV-Vis spectra were obtained at various time intervals to verify the conversion to NAD^+.

3.2.9 Catalytic oxidation of NADH to NAD^+ via flow-through monolithic micro-reactors

Aqueous solutions of NADH (0.1 m*M*, 0.25 m*M*, 0.5 m*M*) were placed in a PEEK loop and pumped through a monolithic micro-reactor in capillary format with immobilised Pd/Pt nano-flowers (BuMA-2) at 10 µ*L*/min using a Knauer pump as shown in Figure 3.3.

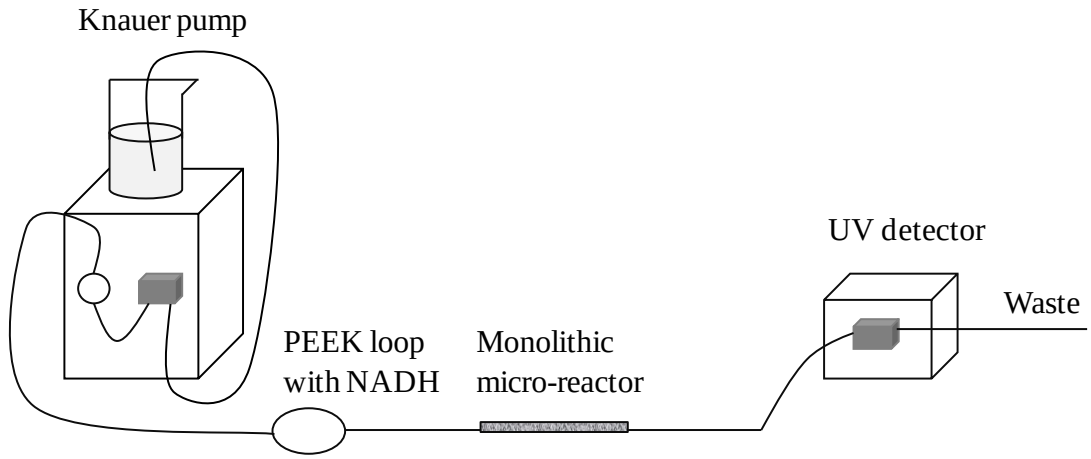

Figure 3.3: *Schematic showing the experimental set up for the flow-through catalytic oxidation of NADH to NAD^+ via the Pd/Pt nano-flower functionalised monolithic micro-reactor*.

The flow was stopped for selected time intervals to allow sufficient contact time between the Pd/Pt nano-flowers and NADH. The flow was then re-started to allow the movement of the reaction product out of the micro-reactor through a UV-Vis detector with a 3 n*L* flow cell. The formation of NAD^+ was observed by monitoring the decrease in absorbance at 340 nm, in this way establishing the optimal contact time required for each concentration.

3.2.10 Catalytic reduction of Fe (III) to Fe (II) via flow-through monolithic micro-reactors

Another redox reaction was used to evaluate the catalytic properties of the immobilised Pd/Pt nano-flowers using a set-up as shown in Figure 3.3. A mixture of $K_3[Fe(CN)_6]$ (8 m*M*) and $NaBH_4$ (0.6 m*M*) was prepared in a p*H* 11.5 aqueous solution, adjusting the ionic strength to 0.085 *M* with NaCl and filled into a 500 µ*L* loop. This solution was pumped through a monolith functionalised with Pd/Pt nano-flowers (monolith BuMA-2) at different flow-rates (10, 15 and 20 $\mu L.min^{-1}$). The reaction products were collected in a micro-cuvette and UV–Vis analysis was used to confirm the complete reduction of ferrocyanide(III) due to the elimination of the absorbance peak at 420 nm.

3.3 Results and discussion

3.3.1 Synthesis of Pd/Pt nano-flowers

For any practical application, the processing conditions involved in the synthesis of nano-particles need to be controlled in such a way that resulting materials have the following characteristics: (1) uniform size distribution, (2) identical shape or morphology, (3) identical chemical composition and crystal structure (core and surface composition must be the same), and (4) individually dispersed materials with no signs of agglomeration. In the work here described, bimetallic nano-flowers consisting of a palladium core and platinum grown upon the cores were initially synthesised. In order to understand how nano-materials with such morphological properties are prepared, it is necessary to illustrate the theory behind the formation of nano-particles using a thermodynamic equilibrium approach. The main steps present in this approach are: (1) the formation of a supersaturated solution, (2) nucleation and (3) subsequent growth. A supersaturated solution has a high Gibbs free energy. A decrease in the overall energy of the system occurs as the solute segregates from the solution leading to the formation of a new phase. As shown in Figure 3.4, a reduction of the overall Gibbs free energy of a supersaturated solution occurs as a new solid phase forms. This reduction of Gibbs free energy is the driving force for both nucleation and growth.

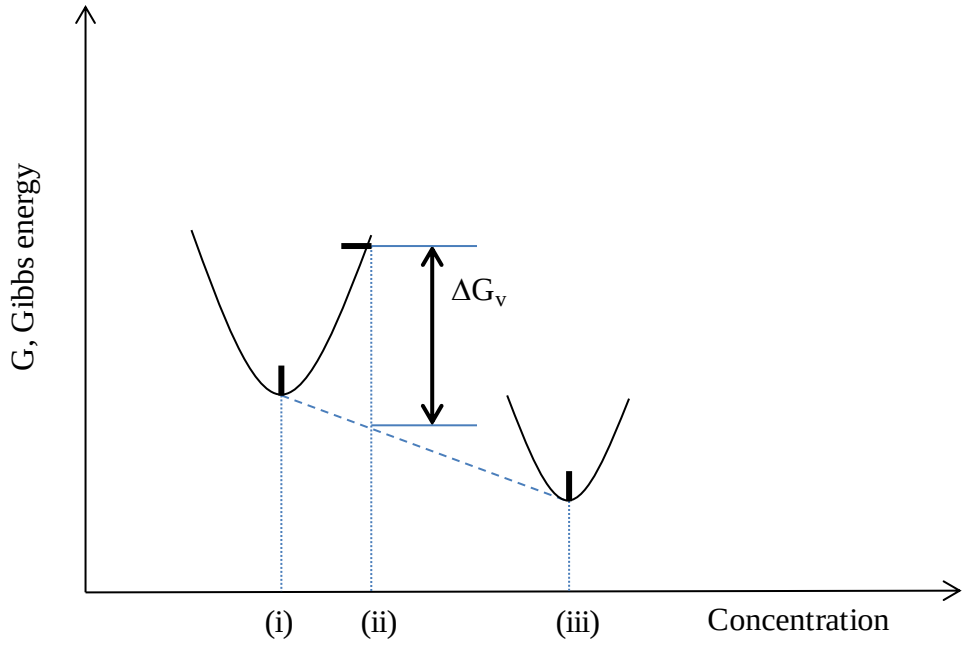

***Figure 3.4**: Schematic showing the reduction in Gibbs energy of a supersaturated solution as a solid phase forms. (i): concentration at equilibrium in solution, (ii): concentration of a supersaturated solution and (iii): concentration of a formed solid phase (adapted from [26]).*

The change of Gibbs free energy per unit volume of the solid phase, ΔG_v, is dependent on the concentration of the solute and can be defined as:

$$\Delta G_v = - kT \ln(C_s-C_0)/\Omega \qquad \text{(Equation 3.1)}$$

Where k = Boltzmann constant, T = temperature, Ω = atomic volume, C_s = concentration of the solute, C_0 = concentration at equilibrium.

Nucleation can occur only when the concentration of solute reaches a certain value above its solubility and it is interrupted as the concentration decreases over time. The radius of the nuclei, r, illustrated as a crude circle in Figure 3.5, must be at least equal to a critical r_c value, otherwise they will dissolve again in solution. At this stage no more nuclei would form and growth can occur on the nuclei already formed until an equilibrium concentration is reached which corresponds to the solubility of the species.

In practice it is preferred to form all the nuclei simultaneously since in this case they would be all similar to each other and a narrow size distribution can be

achieved. The desired size distribution can then be achieved by controlling the subsequent growth step.

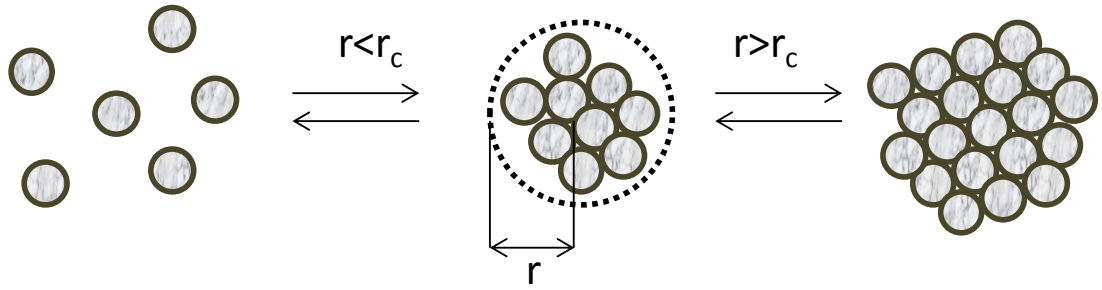

Figure 3.5: *Image showing the nucleation process. A stable nucleus forms when a minimum size of r is present. If the nucleus size is below the critical size r_c, it will dissolve back into solution while if it is larger, it will continue to grow.*

Factors such as the choice of the reducing agents and the type of stabilisers can affect the growth step and they can have a significant impact on the size and morphology of the nano-particles formed. A strong reducing agent (such as $NaBH_4$) promotes a fast reaction rate and favours the formation of smaller nano-particles while a weak reducing agent (such as L-ascorbic acid) induces a slow reaction rate and favours relatively larger particles. Also polymers have often been used as stabilisers for colloidal suspensions of nano-particles and can also affect the growth step. For example if a polymer strongly adsorbs on the surface of the growth sites, the growth rate of nano-particles will be significantly reduced.

The preparation of the Pd/Pt nano-flowers here described is based on a seeded growth method. In seeding growth methods, small metal particles are prepared first and later used as seeds (nucleation centers) for the preparation of larger size particles. By providing a controlled number of preformed seeds (as nucleation centers) and a growth condition that inhibits any secondary nucleation, the particle size can be controlled simply by varying the ratio of seed to metal salt. In general, these conditions include using a reducing agent too weak to reduce the metal salt (in the growth stage) without the presence of seeds. In some instances, the presence of seeds often induce further nucleation rather than growth when the ratio of seed to metal salt is relatively small, resulting in a broad size distribution [27].

To avoid additional nucleation, a step by step particle enlargement method is more useful, allowing a large seed to metal salt ratio to be maintained throughout

successive growth steps. Initially PVP-stabilised palladium seeds were synthesised under heated reflux. Platinum branches were then grown upon the Pd cores after further heating under reflux, using ascorbic acid as the reducing agent. The weak reducing strength of ascorbic acid were found to be the key for the formation of the branch-shaped structure as previously reported [4, 28]. The use of a polymer such as PVP as stabiliser also serves as a diffusion barrier, which promotes the diffusion-limited growth, favouring a narrow size distribution.

3.3.2 Evaluation of Pd and Pd/Pt nano-flowers physical properties

Particle size measurements of the nano-materials here prepared were obtained in triplicate for each nano-particle suspension (n=3). Palladium cores with dimensions of 11.6 ± 0.9 nm were initially synthesised. The subsequent modification with platinum led to nano-structures of 26.3 ± 0.6 nm. The standard deviation is indicative of a narrow size distribution obtained, probably caused by PVP which acts as a diffusion barrier. Further characterisation by FE-SEM allowed the visualisation of the branched morphology of the Pd/Pt nano-flowers as shown in Figure 3.6.

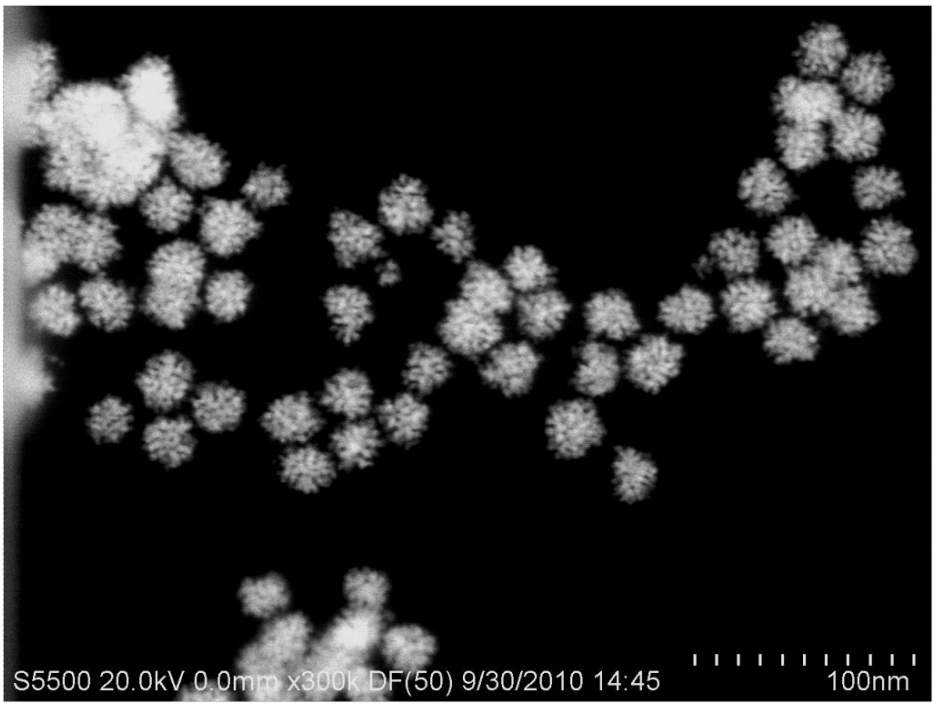

Figure 3.6: *FE-SEM image of Pd/Pt NFs (~ 26 nm) (magnification 300,000x).*

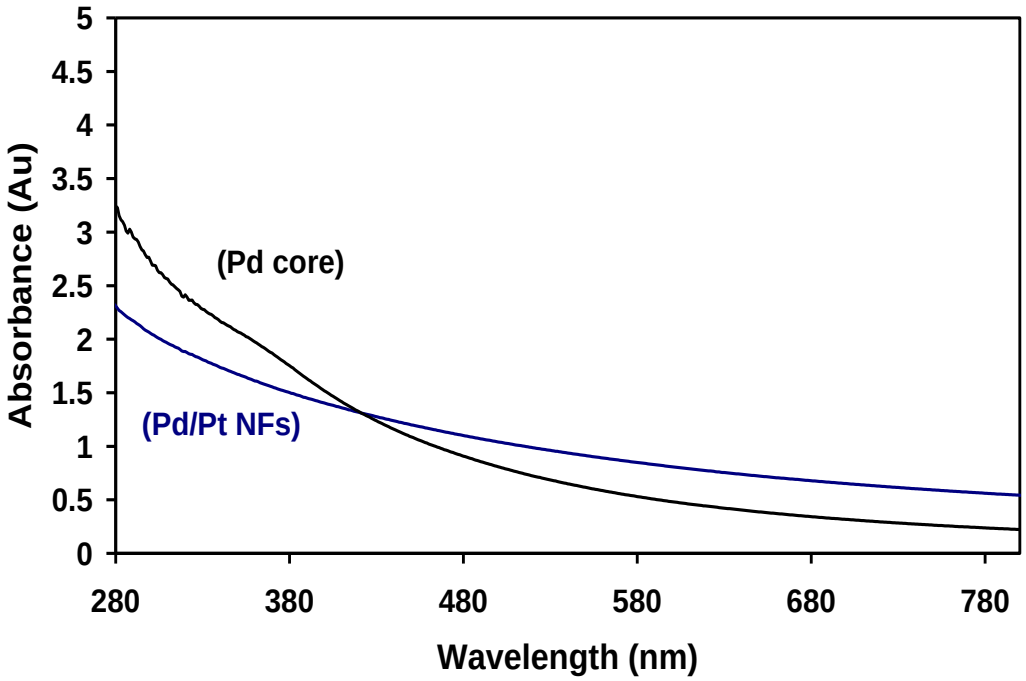

Figure 3.7: *UV-Vis spectra of PVP capped Pd seeds and Pd/Pt nano-flowers*

Negative zeta potential values were also observed. Since the capping agent PVP is not charged, a negative surface net charge could only be due to the presence of residual citrate ions (used during the synthesis) on the surface of the nano-materials. The preparation of Pd/Pt nano-flowers from the Pd cores involved further additions of citrate, hence more negative zeta potential values were visualised with values of -3.3±0.5 m*V* for the Pd cores and -16.8±1.2 m*V* for the Pd/Pt NFs.

Absorption spectroscopy was also used to characterise both materials as illustrated in Figure 3.7, which revealed the presence of exponential decays with no characteristic λ_{max}, confirming previous reports present in the literature [29, 30].

Table 3.2: *Characterisation data for Pd seeds and Pd/Pt nano-flowers (NFs).*

	Size (nm) (*n*=3)	**Zeta potential (γ) (m*V*)**	**λ_{max}**
Pd core	11.6±0.9	-3.3±0.5	n/a
Pd/Pt NFs	26.3±0.6	-16.8±1.2	n/a

3.3.3 Encapsulation of nano-flowers in polymer monoliths

The attachment of metallic nano-particles upon aminated surfaces has been reported before [31, 32], however, an optimal methodology for controlling the level of coverage of such materials is not clearly described in the literature. In the work here described, various types of monoliths were prepared, which were then used to evaluate the impact of several parameters upon the final level of coverage. These included the effect of encapsulation of nano-particles into the monomer mixture, the effects of varying the amount of epoxy groups on the monolith's surface, and the impact of grafting amine reactive polymer chains onto the surface of a pre-formed monolith. Synthetic parameters known to affect monolith morphology (pore size and surface area) such as porogen composition [33] and polymerisation conditions were held constant; therefore variations in the nano-particle coverage ultimately observed could attributed to tailored monolith surface chemistry.

In a first step, flower shaped nano-materials consisting of a palladium core and platinum branches of approximately 20 nm in size were synthesised according to the procedure described by Lim *et al.* [24]. An obvious strategy to incorporate nano-materials in a polymer monolith is to embed or "encapsulate" them within the bulk polymer globules during polymerisation, as has been reported previously by Thabano *et al.* [34] and more recently by Krenkova *et al.* [35]. Typically the monomer mixture is designed in such a way that the nano-particles form a stable suspension within the monomer/porogen mixture prior to polymerisation and their concentration can be controlled across a reasonably broad range. However, the independent control of monolith morphology and nano-particle loading is difficult to achieve using this approach. For example, in this case water needed to be included as one of the porogens within a ternary porogen mixture as previously described by Peters *et al.* [36] so that an aqueous nano-flower suspension could be added to a monomer mixture.

In the initial stages of the work presented herein, a monomer mixture (GMA-1) was prepared as described in Table 3.1, which was gray in colour but transparent, which was a good indicator of colloidal stability prior to UV initiated polymerisation. However, FE-SEM images of a cross-section of the resulting monolith GMA-1 shown in Figure 3.8 (a) show that no nano-particles were

presented at the monolith surface (which otherwise would have appeared as white dots). Further attempts to increase the nano-particle concentration in further monomer mixtures led to either cloudy monomer mixtures, or gross precipitation of aggregated nano-particles. Although the porogen composition (1-propanol/1,4-butanediol/water) could have been optimised to include more water, this strategy was also not pursued since higher levels of water in this well-studied ternary porogen mixture is known to result in unfavourable monolith morphology [36]. Hence, all further optimisation of nano-particle coverage involved tailored control of the monolith surface chemistry as described in the following sections based upon the known affinity of platinum nanoparticles for aminated surfaces [37] as described in the following sections.

3.3.4 Modification of monolith surface chemistry via co-polymerisation

The epoxy groups present in GMA are well known for their ability to react with amines [17], so ethylenediamine was reacted with a number of BuMA-*co*-GMA-*co*-EDMA monoliths, in which the concentration of GMA was varied systematically from 2 % to 24 %, while holding the total functional monomer concentration (BuMA+GMA) and the total crosslinker concentration (EDMA) constant, as shown in Table 3.1. The lone pair of electrons present on the primary amine groups introduced by reaction with surface epoxy groups is responsible for forming covalent linkages with the bimetallic nano-flowers since these electrons interact with the vacant orbitals of Pt [38]. The controlled increase in the distribution of amine-reactive epoxy groups presented at the monolith surface can be indirectly visualised by inspection of the relative coverage of nano-flowers in Figure 3.8 (b-e). Relatively sparse nano-flower coverage was obtained with the GMA-2 % monolith (19 nano-flowers/500 nm^2) whereas a considerable increase in coverage is obtained for the GMA-6 % monolith (98 nano-flowers/500 nm^2). Coverage was found to plateau between monoliths GMA-12 % (135 nano-flowers/500 nm^2) and GMA-24 %.

The nano-flower coverage was reasonably dense and homogeneous on monoliths incorporating 12 % and 24% GMA in the co-polymer (Figure 3.8 d, e), nevertheless large gaps are evident on the monolith surface between adjacent nano-particles. Clearly the use of co-polymerisation techniques is rather limiting in that not all

amine-reactive epoxy groups will be presented at the monolith surface as documented by Hilder *et al.* [39].

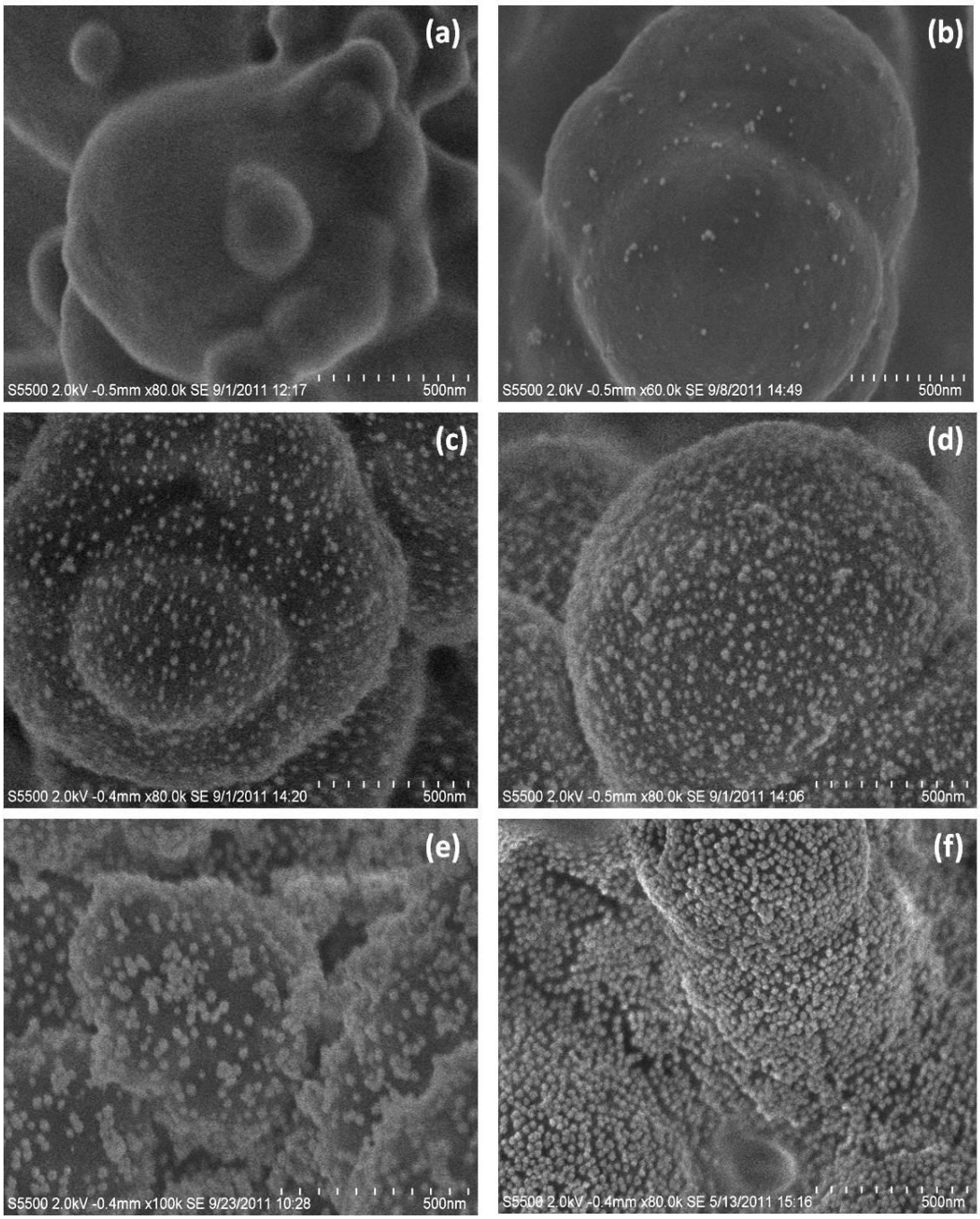

***Figure 3.8**: FE-SEM images of (a) monolith GMA-1 (magnification 80,000x), (b) monolith GMA (2 %) (magnification 60,000x), (c) monolith GMA (6 %) (80,000x), (d) monolith GMA (12 %) (magnification 80,000x), (e) monolith GMA (24 %) (magnification 100,000x) and (f) monolith BuMA-2 (magnification 80,000x).*

In addition, to obtain monoliths with the desired porosity to maintain low

backpressure under flowing conditions, the maximum concentration of GMA present in monoliths had to be limited in this study to 24 %. Furthermore, it is known that unwanted changes in the physical morphology (average pore size and surface area) of polymer monoliths can also occur due to relatively small variation in monomer ratios. This effect was indeed observed, with an increase in operating backpressure from 6 bar.cm^{-1} for GMA-2 % to 49 bar.cm^{-1} for GMA-24 % at a nominal flow rate of 5 μL.min^{-1}.

Preliminary EDX analysis was performed at operational settings that allowed a penetration volume of 10 µm in both depth and width. The data summarised in Table 3.3 approximately corresponds to the visual image shown in Figure 3.8 since there is a rise in the amount in wt % of Pd/Pt going from a mean of 0.03: 1.1 in the GMA- 2 % monolith to 1.3: 39.6 in the GMA-24 % monolith. Although the limited sensitivity of EDX does not allow the quantitative determination of Pd and Pt present, it can nevertheless be used to confirm the higher presence of Pt relative to Pd.

Table 3.3: *Summary of EDX data obtained from GMA monoliths.*

	Pd (weight %)	Pt (weight %)	Ratio Pt/Pd
GMA-2%	0.03±0.01	1.10±0.14	37
GMA-6%	0.06±0.02	0.60±0.01	9
GMA-12%	0.12±0.04	1.40±0.40	12
GMA-24%	1.30±0.28	39.6±2.27	30

3.3.5 Modification of monolith surface chemistry via photografting

The use of photografting methods [40, 41] to increase the number of nano-flower attachment sites on the monolith surface relative to the earlier described co-polymerised monoliths was investigated. Initial grafting efforts involved the grafting of GMA to a BuMA-*co*-EDMA monolith (BuMA-1; Table 3.1) as shown in Figure 3.9 (b).

Although the graft density can be increased by control of both the incident UV energy [42] and the grafting monomer concentration [43], a relatively low concentration of 15 % GMA was chosen to minimise the possibility of UV self-

screening effect. When GMA was grafted on monolith BuMA-1 followed by amination and modification with nano-flowers, there was no observed visible increase in nano-flower coverage relative to the un-grafted GMA-24 % monolith shown in Figure 3.8 (e). Rather than exhaustively optimise GMA graft density on the monoliths, another amine-reactive monomer, vinyl azlactone (VAL) was selected as an alternative grafting monomer for monolith BuMA-2 as shown in Figure 3.9 (a).

The results obtained with the VAL-grafted monolith BuMA-2 are shown in Figure 3.8 (f). The coverage density was increased and uniform coverage of nano-flowers was observed. This dense coverage may be due in part to a higher grafting efficiency of VAL relative to GMA. Previously Yang *et al.* [40, 41] illustrated that a higher grafting efficiency is achieved with acrylates relative to methacrylates due to the absence of tertiary hydrogens on the polymer formed.

3.3.6 Surface area measurements

The most widely used isotherm dealing with multilayer adsorption was derived by Stephen Brunauer, Paul Emmett and Edward Teller and is known as the BET isotherm. This technique involves the measuring of an adsorbed inert gas (generally N_2 at 77 K) on a surface at various pressures and at a constant temperature. The BET equation is expressed as:

$$\frac{1}{W[(P_0-P)-1]} = \frac{C-1}{(Wm.C)}\left(\frac{P}{P_0}\right) + \frac{1}{(Wm.C)} \qquad \text{(Equation 3.2)}$$

Where W= weight of gas adsorbed, P/P_0=relative pressure, W*m*= weight of adsorbate as monolayer, C=BET constant.

A linear plot of $\frac{1}{W[(P_0-P)-1]}$ versus $\left(\frac{P}{P_0}\right)$ would be linear with slope (s) $\frac{C-1}{(Wm.C)}$ and intercept (i) $\frac{1}{(Wm.C)}$. Hence from this data it is possible to determine the weight of a monolayer (W*m*) from the following relationship:

$$Wm = 1/ (s + i) \qquad \text{(Equation 3.3)}$$

The total surface area (S*t*) can then be defined as:

$$St = (Wm\ N\ A_{cs}/\ M) \qquad \text{(Equation 3.4)}$$

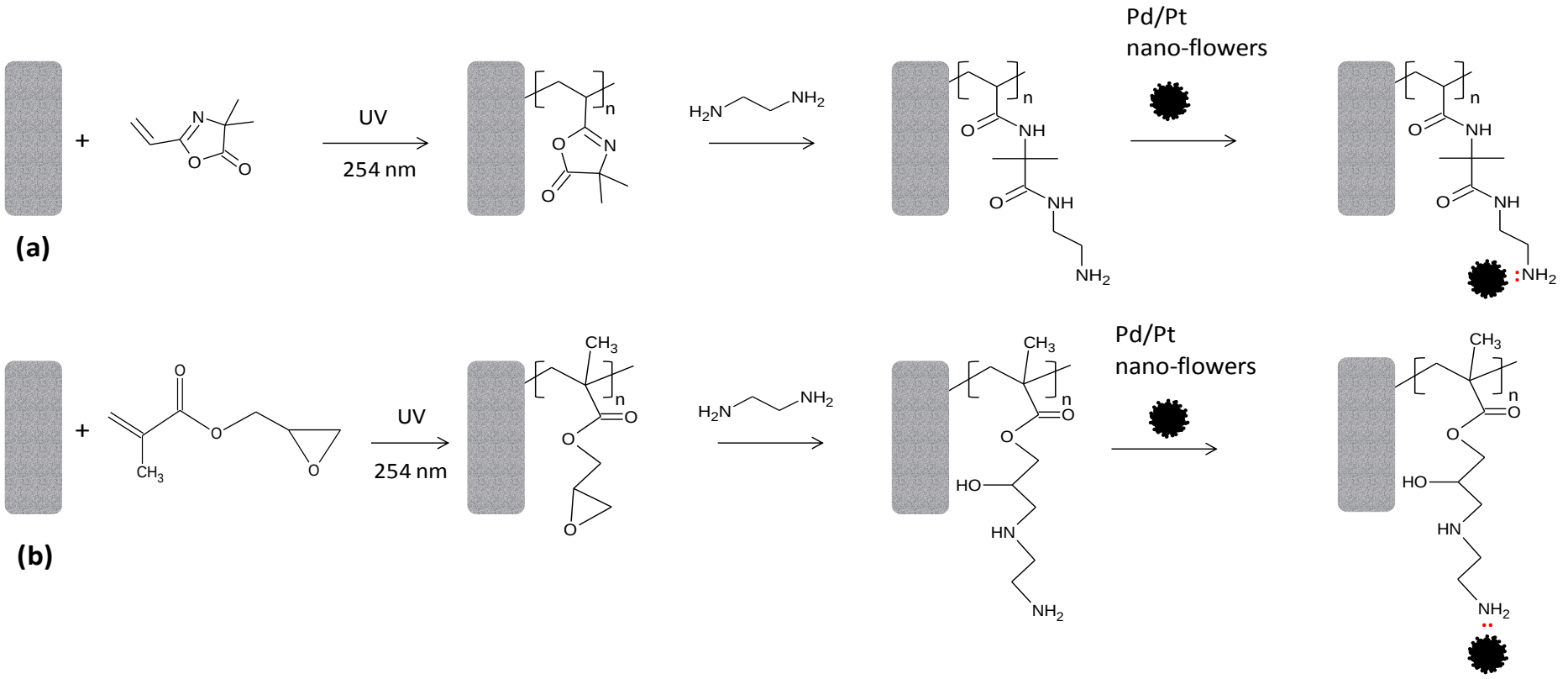

***Figure 3.9**: Schematic showing the covalent immobilisation of Pd/Pt nano-flowers via lone-pair interactions with primary NH_2 groups on (a) BuMA-2 monoliths photografted with VAL and (b) BuMA-1 monoliths photografted with GMA.*

Where N = Avogadro's number, A_{cs} = adsorbate cross-sectional area (16.2 $Å^2$ for nitrogen) and M = molecular weight of adsorbate.

Finally the specific surface area (S) can be defined as the total surface area (S*t*) per unit of mass (m) as illustrated in Equation 3.5 below:

$$S = St/m \qquad \text{(Equation 3.5)}$$

The determination of accurate surface area data for polymer monoliths formed within fused silica capillaries is not possible due to the very low mass of monolith present. Therefore, a commercially available monolith in disc format (an epoxy CIM disc; representing a total dry mass of monolith of 159 mg) was aminated and modified with nano-flowers as shown in Figure 3.10. Using BET measurements, changes in surface area before and after modification with Pd/Pt nano-flowers could readily be determined with results shown in Table 3.4.

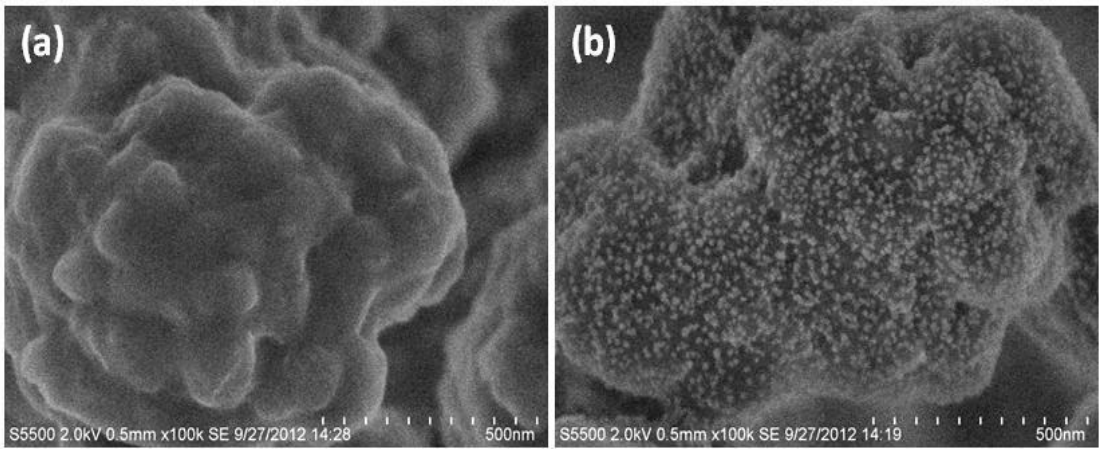

Figure 3.10*: FE-SEM images of (a) a blank GMA-co-EDMA CIM disc and (b) a similar disc modified with Pd/Pt nano-flowers.*

Immobilisation of nano-flowers resulted in an unexpected 71 % decrease in surface area, with each nano-flower possibly causing partial blockage of meso-pores present, which are pores between 2 nm to 50 nm in size. Specifically, the calculated surface area of an unmodified monolith was in close agreement (within 5 %) with the manufacturer specification of 40 $m^2.g^{-1}$, while the surface area of a nano-flower modified monolith fell to 12 $m^2.g^{-1}$. This was determined by taking into account the increased mass of the sample due to the presence of the nano-flowers which was

determined by ICP-AES. The combined mass of Pd and Pt present on a 21.4 mg CIM disc sample was found to be 4.1 mg (19.2 % by weight).

Table 3.4: *ICP and BET data of nano-agglomerated CIM disc analysis.*

	BET surface area ($m^2.g^{-1}$)	**Pd determined by ICP (wt %)**	**Pt determined by ICP (wt %)**
Manufacturers specification	40	-	-
Unmodified CIM disc	42	-	-
CIM disc with Pd/Pt nano-flowers	12	0.7	18.5

The BET surface area measurements under liquid nitrogen are affected by the amount of meso-pores present. Manufacturer specifications of the unmodified CIM disc describe an average macro-pore size of 1.5 μm with pores down to 15 nm also present [25]. Since the nano-flowers used in this study are approximately 20 nm in size, substantial blocking of such pores could be occurring with each nano-flower sitting neatly inside each pore. It is possible to relate this finding back to the polymer phases formed within capillaries, as the monolith chemistry and pore structures are very similar. Nevertheless, nano-flowers were still presented directly at the surface of the monolith and sufficiently strongly attached to be used as immobilised catalysts as shall be shown later.

3.3.7 Investigation of nano-flower attachment mechanism via ion-exchange chromatography

The use of monolith BuMA-2 as an ion-exchanger before and after attachment of nano-flowers confirmed that the nano-flowers were immobilised via their interaction with the surface amine groups on the monolith.

The extent of nano-flower coverage (and the nature of their surface attachment) on monolith BuMA-2 (shown in Figure 3.8 f) was investigated by using the monolith

as a weak anion exchange column. Several reports have appeared in the literature involving the use of monoliths modified with ethylenediamine for the anion-exchange separation of selected anions [44, 45]. Such weak base ion-exchangers require an acidic p*H* for protonation of the surface amine groups to facilitate retention and so phthalic acid (p*H* 4.5) was used as an eluent. The relatively low equivalent ionic conductance of phthalate also allowed non-suppressed conductivity to be used.

As illustrated in Figure 3.11 (b), the retention of a selected anion (perchlorate, positive peak at 5 minutes) on monolith BuMA-2 before nano-flower attachment contrasted sharply with the complete loss of retention for monolith BuMA-2 after nano-flower attachment shown in Figure 3.11 (a).

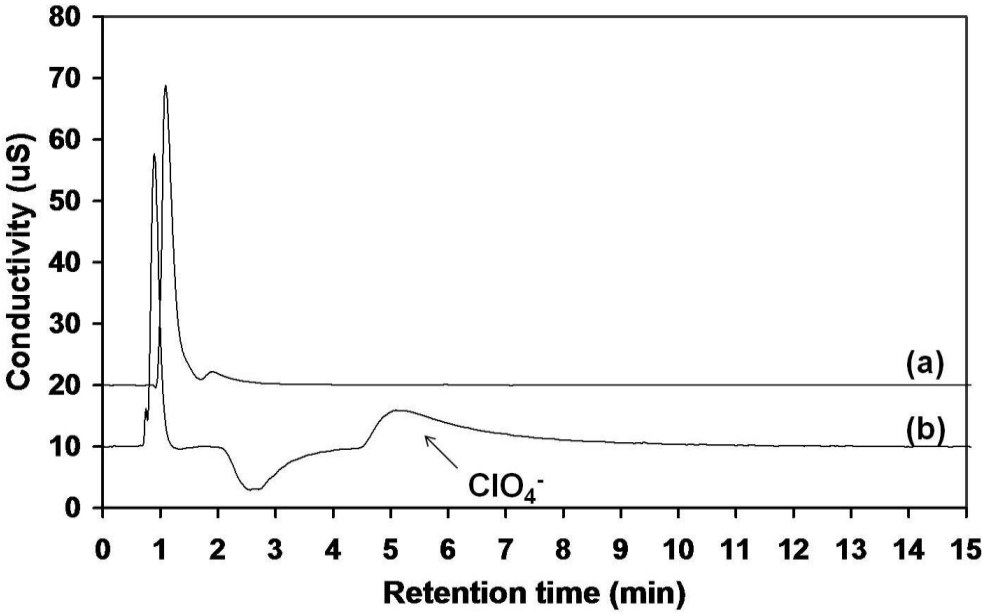

Figure 3.11: *Retention of perchlorate ions (100 ppm) on (b) a BuMA-2 monolith before nano-flower attachment. No retention was observed on (a) which was a BuMA-2 monolith functionalised with Pd/Pt nano-flowers. Conditions: 0.5 mM phthalic acid pH 4.5, injection volume 0.4 µL, non-suppressed conductivity detection. Flow rate: 3 µL.min^{-1}, length of column (a): 14 cm, length of column (b): 12 cm.*

Clearly the attachment of the nano-flowers via their interaction with the lone pair of electrons on multiple surface amine groups significantly reduced the remaining free

amine moieties available as ion-exchange sites, leading to a significant loss of ion-exchange capacity. This observation is significant, as unreacted surface chemistry could negatively impact upon subsequent flow through reactions.

3.3.8 Catalytic oxidation of NADH to NAD^+ using Pd/Pt nano-flowers as a colloidal suspension

For any given reaction, a certain activation energy (E_a) must be present in order to convert reactants to products as shown in Figure 3.12. If the activation energy of a reaction is high, a large input of energy is required in order to maximise the number of molecular interactions. In order to facilitate the formation of products a catalyst can be used which provides an alternative path that avoids the slow rate-determining step of the uncatalysed reaction and improves the reaction rate, hence requiring a lower activation energy (E_a) for the formation of products. A lower E_a will lead to a faster reaction rate based on the Arrhenius equation shown below:

$$k = Ae^{-Ea/RT} \qquad \text{(Equation 3.6)}$$

Where k=rate constant, A=pre-exponential factor, E_a=activation energy, R=gas constant and T=temperature in K.

The high surface area of nano-particles presents a surface upon which reactant molecules can adsorb; the catalyst material itself is not consumed in the reaction.. As a reaction proceeds, reactants come into contact, distort and begin to exchange atoms. The potential energy rises to a maximum and the group of atoms that are present in the region close to the maxium is called the ‘activated complex’. The climax of the reaction is at the peak of the potential energy where two reactant molecules reach a degree of interaction which leads to the formation of a reaction intermediate and any small further distortions will send them in the direction of products. This interaction state is known as the ‘transition state’.

Here the oxidation of NADH to NAD^+ was investigated in the presence of the bimetallic Pd/Pt nano-flowers. NADH has 2 absorption bands, one at 340 nm due to the n-π^* transition in the dihydronicotinamide moiety and the other at 260 nm due to the π-π^* transition in the adenine ring [46].

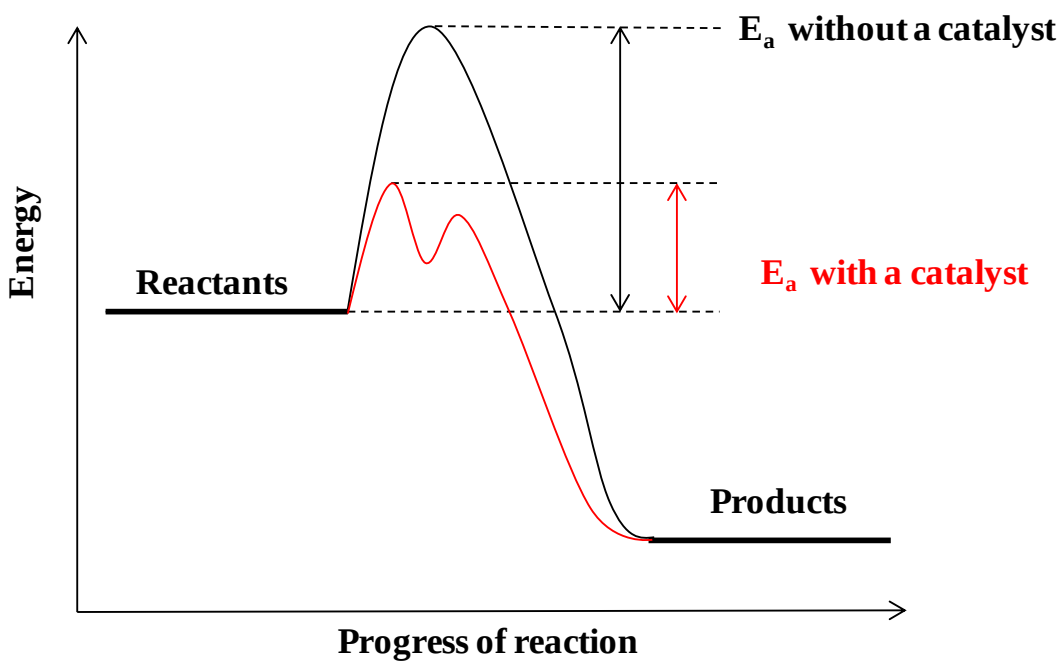

***Figure 3.12**: Image showing the effects of a catalyst on the activation energy (E_a) of a reaction.*

Conversely, NAD^+ has a higher extinction coefficient at 260 nm (18×10^{-3} $L.mol^{-1}.cm^{-1}$) than that of NADH (14.4×10^{-3} $L.mol^{-1}.cm^{-1}$) due to the contribution from oxidised nicotinamide and no absorption band at 340 nm, which is due to a twisted conformation between the oxidised nicotinamide and carboxamide. The mechanism by which metallic nano-particles facilitate the oxidation has been previously described in the literature and involves the deposition of oxygen on the surface of the nano-particle which becomes activated and acts as the oxidant of NADH [46]. This has been demonstrated by running the oxidation reaction both under N_2 and under aerobic conditions, demonstrating that under N_2 the reaction proceeds much slower.

The rate of reaction was previously found to be dependant on the concentration of catalyst [46] however, in the experiment here described a fixed amount of nano-flower colloidal suspension was used (100 µ*L*) hence variations in kinetics could only be due to other parameters such as NADH concentration. Indeed the reaction order was found to depend on the initial concentration of NADH. By far the greatest variation in absorbance between the $NADH/NAD^+$ species is observed at 340 nm hence the progress of the reaction was monitored at this wavelength.

Initially a calibration plot for NADH was obtained in the range between 0-0.6 m*M* as shown in Figure 3.13. The catalytic oxidation of NADH was then performed in the presence of bimetallic nano-flowers as a colloidal suspension at two different concentrations of NADH, 0.11 and 0.56 m*M*, and integrated rate laws were used for determining the order of reaction in both cases.

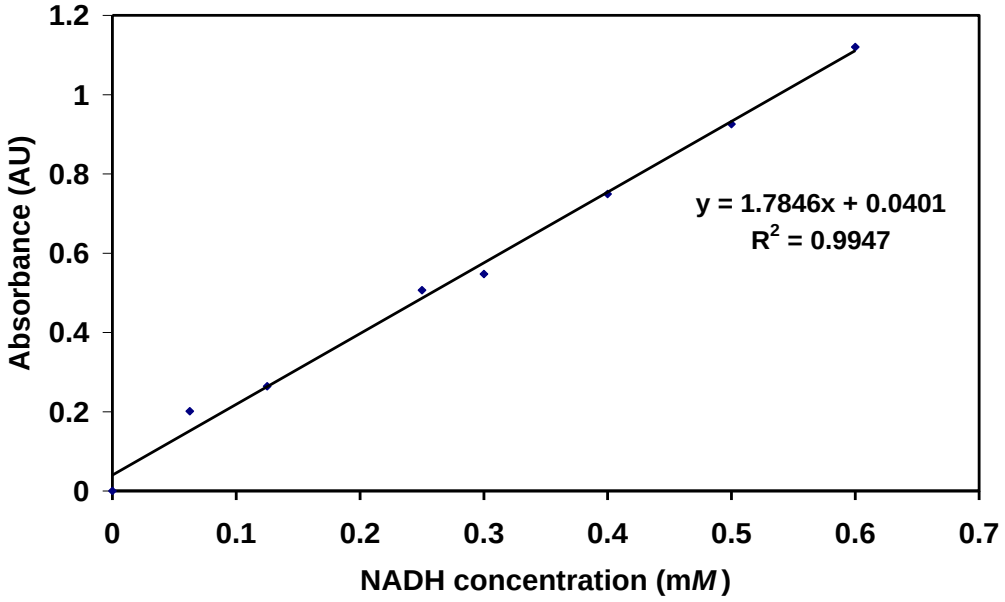

Figure 3.13: *Calibration plot relating absorbance (at 340 nm) versus concentration of NADH in the range 0-0.6 mM.*

A plot showing the variation of concentration with time was used to reveal preliminary information on the reaction kinetics. For zero order reaction a straight line would be observed however, in this case an exponential decay is present as shown in Figure 3.14, hence the reaction could only be of first or second order. From the line equations, an estimation of the rate constants (k) can be obtained. For example at a NADH concentration of 0.56 mM, k was found to be 0.01 min^{-1} while at a concentration of NADH of 0.11, k was found to be 0.03 min^{-1}. In order to obtain further information on the reaction orders, integrated rate laws were used.

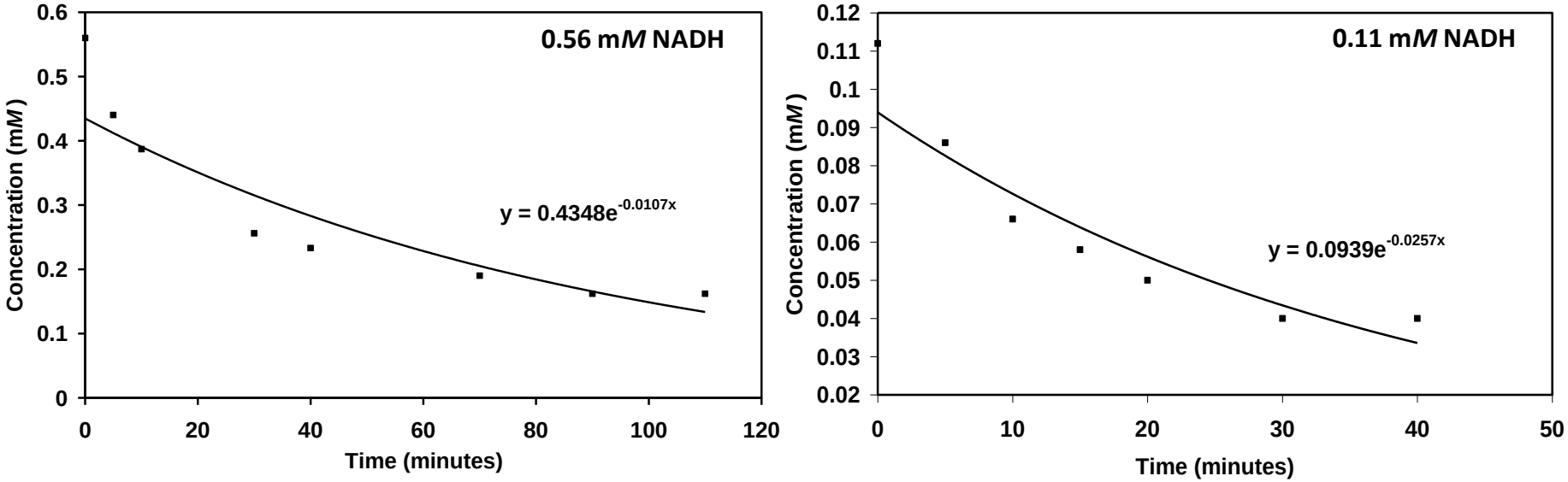

***Figure 3.14**: Plot of concentration versus time for the oxidation of NADH to NAD^+ catalysed in the presence of Pd/Pt nano-flowers (100 µL) as a colloidal suspension.*

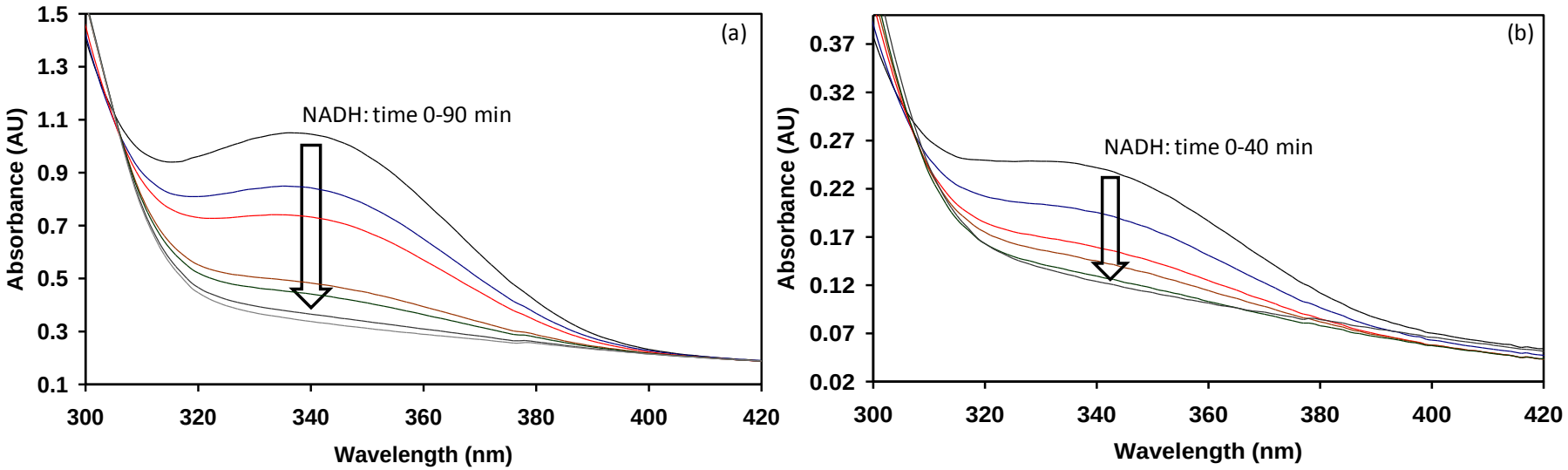

Figure 3.15: *(a) UV spectra showing the catalytic oxidation of NADH to NAD^+ in the presence of (100 µL) Pd/Pt nano-flowers as a colloidal suspension using an initial 0.56 mM concentration. Time intervals: (—) 0, (—) 5, (—)10 , (—) 40, (—) 50, (—) 70, (—) 90 minutes. (b) The same reaction when using 0.11 mM initial NADH concentration and the same amount of Pd/Pt nano-flowers. Time intervals: (—) 0, (—) 5, (—)10 , (—) 15, (—) 20, (—) 40 minutes.*

The integrated rate law for 1st order reactions is illustrated below in Equation 3.7:

$$\ln[C] = -kt + \ln[C_0] \qquad \text{(Equation 3.7)}$$

where C = concentration of product, k = rate constant, t = time and C_0 = concentration at time 0.

In this case a plot of ln[C] vs t would be linear with slope *–k*. For second order reactions the integrated law is expressed by the Equation 3.8 shown below instead:

$$1/[C] = kt + 1/[C_0] \qquad \text{(Equation 3.8)}$$

Here a linear relationship would be obtained by plotting of 1/[C] versus t. As summarised in Table 3.5, the reaction order at the lower concentration of NADH (0.11 m*M*) could not be determined due to the similar R^2 values obtained from both plots. Previous reports however have suggested that this is a first order reaction at similar concentrations. At higher NADH concentrations (0.56 m*M*), it is more likely to be a second order reaction since in this case the highest linearity is clearly for that model. The reaction also proceeded faster at higher NADH concentration. The calculated rate of reaction increased from 0.002 m*M*.min^{-1} to 0.004 m*M*.min^{-1}.

Table 3.5*: Summary of kinetic data for the oxidation of NADH to NAD^+ in the presence of Pd/Pt nano-flowers as a colloidal suspension.*

	0.56 m*M* NADH		0.11 m*M* NADH	
	Line equation	R^2 value	Line equation	R^2 value
C vs time for zero order	y = -0.0031x + 0.437	0.7672	y = -0.0015x + 0.1489	0.7345
Ln[C] vs time for 1st order	y = -0.0107x – 0.8329	0.877	y = -0.0337x - 2.2875	0.9583
1/[C] vs time for 2nd order	y = 0.0409x + 2.2432	0.9516	y = 0.428x + 10.227	0.9409
Rate of reaction (m*M*.min^{-1})	0.004		0.002	
Rate contant	0.04 mM^{-1}.min^{-1}		0.03 min^{-1}	

Previous reports in the literature have indicated that the reaction obeyed first order kinetics below 0.4 m*M* and pseudo-first order kinetics above 0.4 m*M* NADH [47]. Pseudo-first order reactions are second order reactions in which a reactant is present at a very high concentration which is considered to stay constant as the reaction proceeds. Below a critical concentration this is not the case and the reaction is considered to be second order.

3.3.9 Catalytic oxidation of NADH to NAD^+ via flow-through monolithic micro-reactors

The oxidation of NADH to NAD^+ was also carried out using the monolithic micro-reactor in capillary format using a "stopped flow" configuration in order to control contact time as explained in Section 3.2.9. As shown before, UV–Vis spectroscopy was used to monitor the reaction progress. In the present work, aqueous NADH solutions were pumped through monolith BuMA-2 to ensure that the entire pore volume was filled. The UV detector (equipped with a 3 n*L* flow-cell) connected in series monitored the high absorbance of NADH at 340 nm. The flow was then interrupted and the reaction allowed to proceed within the micro-reactor for controlled periods of time. Turning the external pump back on then allowed the reaction product (NAD^+) to be pumped out of the reactor resulting in a negative peak due to the low extinction coefficient of NAD^+ at 340 nm.

Figure 3.16 (b) illustrates the effect of contact time (ranging from 5 min to 90 min) on the magnitude of the negative peak caused by a decrease in NADH concentration. Using a 0.5 m*M* NADH solution, the production of NAD^+ appears to plateau after at a contact time of 60 minutes, a behaviour which is quite similar to experiments performed in colloidal format shown in Figure 3.15, where plateau was reached just after 70 minutes with a 0.56 m*M* NADH solution. To demonstrate that the negative peak was due to the catalytic activity of the nano-flowers, similar experiments were performed using a blank BuMA-2 (that is, an aminated monolith not bearing immobilised nano-flowers). The baseline disturbances in Figure 3.16 (a) align with those in Figure 3.16 (b) but did not increase with time. These disturbances were due to flow disruption in the UV flow cell when the flow-rate is re-established. The effect of NADH concentration upon contact time was examined over the range 0.1 m*M* to 0.5 m*M* NADH.

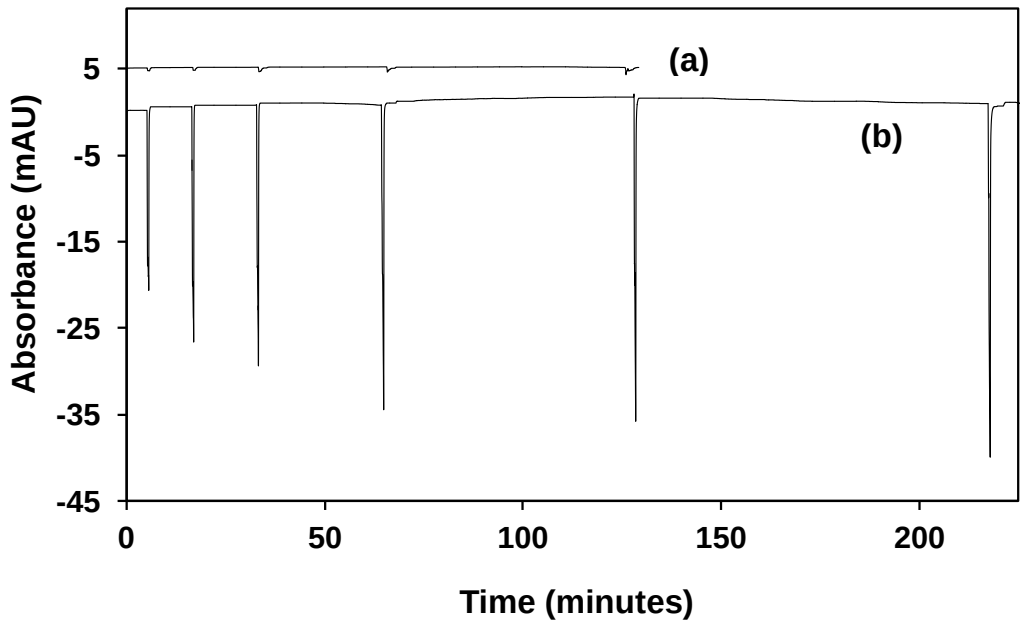

Figure 3.16: *UV profile at 340 nm of a 0.5mM NADH solution pumped through (a) a blank BuMA-2 monolith, (b) a BuMA-2 monolith modified with Pd/Pt nano-flowers demonstrating the effects of contact time on the catalytic reaction. The flow was stopped at various time intervals such as 5, 10, 15, 30, 60, 90 minutes and the height of the negative peak observed was proportional to the amount of* NAD^+ *formed.*

Higher concentrations of NADH required longer contact times in order to achieve a more complete oxidation as illustrated in Figure 3.17, which is a similar behaviour as shown previously for experiments in colloidal solution (see Figure 3.14). In this case it was observed that when 0.1 m*M* NADH was flushed through the micro-reactor, the NAD^+ peak height plateaus after 10 minutes relative to 60 minutes when 0.5 m*M* NADH was used. The values for the rate constants were also determined (k=0.01 min^{-1}) from the equations of the exponential curves.

As shown previously in Table 3.5 for experiments in colloidal format, a higher rate of reaction is present at higher NADH concentrations hence the reaction proceeded faster at 0.5 m*M* NADH rather than at a 0.1 m*M* concentration. From Figure 3.18, the catalytic efficiency of the monolithic micro-reactor was demonstrated to be highly repeatable.

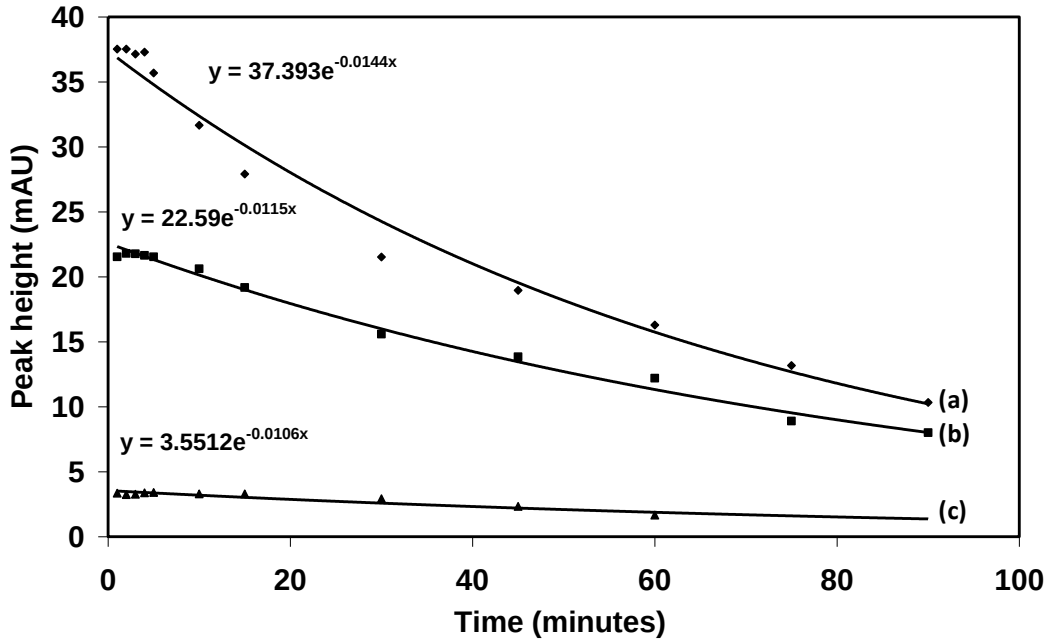

Figure 3.17: *Plot illustrating the effects of contact time on peak height between the NADH and Pd/Pt nano-flowers at (a) 0.5 mM, (b) 0.25 mM (c) 0.1 mM NADH concentrations.*

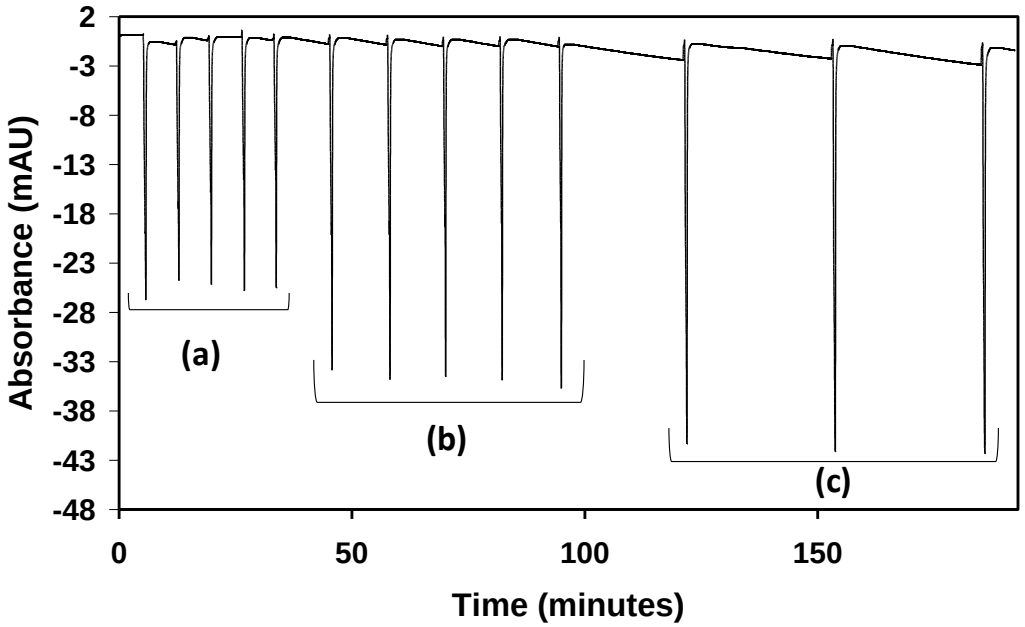

Figure 3.18: *Plot demonstrating the repeatability of the catalytic oxidation of NADH. Experiments were carried out using a 0.5mM NADH solution by performing (a) 5 replicates with a 5 minute contact time, (b) 5 replicates with a 10 minute contact time, (c) 3 replicates with a 30 minutes contact time.*

The low % RSD values summarised in Table 3.6 for triplicate catalytic conversions at 3 different contact time intervals revealed that the poorest % RSD (3.2 %) was observed for a 5 minutes contact time while the best was 1.1 % for 30 minutes (1.9 % was observed for 10 minutes). Presumably poorer precision was achieved at the shorter contact time due to the reaction not having gone to completion within the micro-reactor.

Table 3.6: *Summary of data from repeatability studies for the oxidation of 0.5 mM NADH to NAD^+ using flow-through nano-flower functionalised monolithic micro-reactors.*

Contact time (minutes)	**% RSD**
5	3.2 (*n*=5)
10	1.9 (*n*=5)
30	1.1 (*n*=3)

3.3.10 Catalytic reduction of Fe (III) to Fe (II) via flow-through micro-reactors

In order to further evaluate the catalytic activity of Pd/Pt nano-flowers immobilised upon a polymer monolith in flow-through mode, the well known reduction of Fe(III) to Fe(II) was selected for demonstrative purposes. The strong reducing agent sodium borohydride was used as shown in the reaction scheme below, with the p*H* of the system adjusted to 11.5 to prevent decomposition of borohydride [48].

$$BH_4^- + 8[Fe(CN)_6]^{3-} + 3H_2O \longrightarrow H_2BO_3^- + 8[Fe(CN)_6]^{4-} + 8H^+ \quad \text{(Equation 3.9)}$$

The role of the reducing agent is to act as a reservoir of electrons which are donated to the immobilised nano-catalyst and are "stored" on its surface as demonstrated by Henglein *et al*. [49, 50]. As the ferrocyanate(III) complex comes in contact with the nano-catalyst, the electrons present are readily available to convert $8[Fe(CN)_6]^{3-}$ to $8[Fe(CN)_6]^{4-}$. The reaction between ferrocyanate and borohydride ions in the absence of a catalyst has been reported to have a half life of 5,000 seconds [51], while in the presence of a catalytically active material this value drastically decreases

to less than 10 seconds. The reaction progress could be readily studied before and after passage through the nano-flower-modified reactor since the starting material ferrocyanate(III) absorbs strongly at 420 nm, whereas the ferrocyanate (II) product is colourless. As shown in Figure 3.19, UV spectrum (a) was collected immediately after preparation of the ferrocyanate(III) and borohydride solution, but before passage through the micro-reactor. UV spectrum (b) was collected at a nominal time of 60 min later, showing that some modest conversion to ferrocyanate (II) has occurred in the absence of catalyst. In contrast, UV spectra (c,d,e) were collected without delay after the reaction mixture had been pumped through the micro-reactor at flow rates ranging from 10 $\mu L.min^{-1}$ to 20 $\mu L.min^{-1}$. In all cases, complete reduction has occurred despite the extremely short contact time through the micro-reactor. At a volumetric flow rate of 20 $\mu L.min^{-1}$ the linear velocity was 50 $mm.sec^{-1}$ such that the contact time through a 100 mm micro-reactor was approximately 2 seconds.

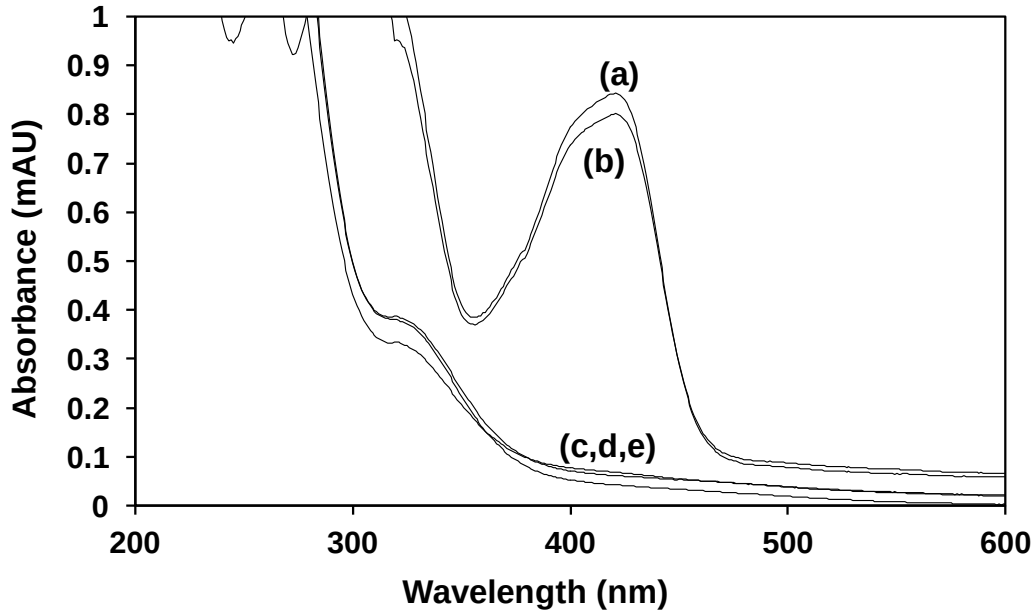

Figure 3.19: *UV spectra showing the reduction of (a) a ferrocyanate(III) solution with $NaBH_4$, (b) same solution after 60 minutes and (c,d,e) the solution after being pumped through the Pd/Pt modified micro-reactor at 10, 15 and 20 µL/min respectively.*

3.4 Conclusion

Bimetallic nano-flowers consisting of platinum branches grown upon a palladium core have been successfully immobilised on methacrylate monoliths via covalent bonds with free primary amine groups present on the surface of the monoliths. FE-SEM was used to verify that a highly dense coverage was obtained when branches of vinyl azlactone were grafted onto the monolith's surface. These monoliths were used to carry out catalytic redox reactions availing of the catalytic properties of the nano-flowers and the ideal flow through properties of the monolithic structure. A final confirmation of the comprehensive coverage of nano-flowers was assessed by using the monoliths prepared with amine functionality as weak anion exchangers. The coverage of nano-flowers was also demonstrated by the lack of retention of perchlorate which was retained when using an identically prepared monolith which only differentiated in the absence of nano-flowers. The micro-reactors here prepared demonstrate potential applications towards more complex catalytic reactions such as Suzuki and Heck-type coupling reactions.

3.5 References

1. Basheer, C.; Shahitha, F.; Hussain, J.; Lee, H. K.; Valiyaveettil, S. Design of a capillary-microreactor for efficient Suzuki coupling reactions. *Tetrahedron Letters* **2004,** *45* (39), 7297-7300.

2. Ahmed-Omer, B.; Brandt, J. C.; Wirth, T. Advanced organic synthesis using microreactor technology. *Organic & Biomolecular Chemistry* **2007,** *5* (5), 733-740.

3. Grzelczak, M.; Perez-Juste, J.; Mulvaney, P.; Liz-Marzan, L. M. Shape control in gold nanoparticle synthesis. *Chemical Society Reviews* **2008,** *37* (9), 1783-1791.

4. Xia, Y. N.; Xiong, Y. J.; Lim, B.; Skrabalak, S. E. Shape-Controlled Synthesis of Metal Nanocrystals: Simple Chemistry Meets Complex Physics? *Angewandte Chemie-International Edition* **2009,** *48* (1), 60-103.

5. Gong, X.; Yang, Y.; Zhang, L.; Zou, C.; Cai, P.; Chen, G.; Huang, S. Controlled synthesis of Pt nanoparticles via seeding growth and their shape-dependent catalytic activity. *Journal of Colloid and Interface Science* **2010,** *352* (2), 379-385.

6. Wang, J.; Thomas, D. F.; Chen, A. Direct growth of novel alloyed PtAu nanodendrites. *Chemical Communications* **2008,** *0* (40), 5010-5012.

7. Lim, B.; Xia, Y. N. Metal Nanocrystals with Highly Branched Morphologies. *Angewandte Chemie-International Edition* **2011,** *50* (1), 76-85.

8. Peng, X. H.; Pan, Q. M.; Rempel, G. L. Bimetallic dendrimer-encapsulated nanoparticles as catalysts: a review of the research advances. *Chemical Society Reviews* **2008,** *37* (8), 1619-1628.

9. Toshima, N.; Yonezawa, T. Bimetallic nanoparticles - novel materials for chemical and physical applications. *New Journal of Chemistry* **1998,** *22* (11), 1179-1201.

10. Chung, Y. M.; Rhee, H. K. Partial hydrogenation of 1,3-cyclooctadiene using dendrimer-encapsulated Pd-Rh bimetallic nanoparticles. *Journal of Molecular Catalysis A-Chemical* **2003,** *206* (1-2), 291-298.

11. Burguete, M. I.; Garcia-Verdugo, E.; Luis, S. V.; Restrepo, J. A. Preparation of polymer-supported gold nanoparticles based on resins containing ionic liquid-like fragments: easy control of size and stability. *Physical Chemistry Chemical Physics* **2011,** *13* (33), 14831-14838.

12. Budnyk, A. P.; Damin, A.; Agostini, G.; Zecchina, A. Gold nanoparticle aggregates immobilized on high surface area silica substrate for efficient and clean SERS applications. *Journal of Physical Chemistry C* **2010,** *114* (9), 3857-3862.

13. Reetz, M. T.; Winter, M.; Tesche, B. Self-assembly of tetraalkylammonium salt-stabilized giant palladium clusters on surfaces. *Chemical Communications* **1997,** (2), 147-148.

14. Zheng, N. F.; Stucky, G. D. A general synthetic strategy for oxide-supported metal nanoparticle catalysts. *Journal of the American Chemical Society* **2006,** *128* (44), 14278-14280.

15. Sachse, A.; Galarneau, A.; Coq, B.; Fajula, F. Monolithic flow microreactors improve fine chemicals synthesis. *New Journal of Chemistry* **2011,** *35* (2), 259-264.

16. Connolly, D.; Currivan, S.; Paull, B. Polymeric monolithic materials modified with nanoparticles for separation and detection of biomolecules: A review. *Proteomics* **2012,** *12* (19-20), 2904-2917.

17. Cao, Q.; Xu, Y.; Liu, F.; Svec, F.; Frechet, J. M. J. Polymer monoliths with exchangeable chemistries: use of gold nanoparticles as intermediate ligands for capillary columns with varying surface functionalities. *Analytical Chemistry* **2010,** *82* (17), 7416-7421.

18. Nikbin, N.; Ladlow, M.; Ley, S. V. Continuous flow ligand-free Heck reactions using monolithic Pd [0] nanoparticles. *Organic Process Research & Development* **2007,** *11* (3), 458-462.

19. Bandari, R.; Knolle, W.; Prager-Duschke, A.; Glasel, H. R.; Buchmeiser, M. R. Monolithic media prepared via electron beam curing for proteins separation and flow-through catalysis. *Macromolecular Chemistry and Physics* **2007,** *208* (13), 1428-1436.

20. Mennecke, K.; Kirschning, A. Polyionic polymers - heterogeneous media for metal nanoparticles as catalyst in Suzuki-Miyaura and Heck-Mizoroki reactions under flow conditions. *Beilstein Journal of Organic Chemistry* **2009,** *5*.

21. Bolton, K. F.; Canty, A. J.; Deverell, J. A.; Guijt, R. M.; Hilder, E. F.; Rodemann, T.; Smith, J. A. Macroporous monolith supports for continuous flow capillary microreactors. *Tetrahedron Letters* **2006,** *47* (52), 9321-9324.

22. Gomann, A.; Deverell, J. A.; Munting, K. F.; Jones, R. C.; Rodemann, T.; Canty, A. J.; Smith, J. A.; Guijt, R. M. Palladium-mediated organic synthesis using porous

polymer monolith formed in situ as a continuous catalyst support structure for application in microfluidic devices. *Tetrahedron* **2009,** *65* (7), 1450-1454.

23. Jones, R. C.; Canty, A. J.; Deverell, J. A.; Gardiner, M. G.; Guijt, R. M.; Rodemann, T.; Smith, J. A.; Tolhurst, V. A. Supported palladium catalysis using a heteroleptic 2-methylthiomethylpyridine-N,S-donor motif for Mizoroki-Heck and Suzuki-Miyaura coupling, including continuous organic monolith in capillary microscale flow-through mode. *Tetrahedron* **2009,** *65* (36), 7474-7481.

24. Lim, B.; Jiang, M. J.; Camargo, P. H. C.; Cho, E. C.; Tao, J.; Lu, X. M.; Zhu, Y. M.; Xia, Y. N. Pd-Pt Bimetallic Nanodendrites with High Activity for Oxygen Reduction. *Science* **2009,** *324* (5932), 1302-1305.

25. http://www.biaseparations.com. 24-2-2013. 24-2-2013.
Ref Type: Online Source

26. Cao G.Z. *Nanostructures & nanomaterials: synthesis, properties and applications.;* Imperial College press, London: 2004.

27. Jana, N. R.; Gearheart, L.; Murphy, C. J. Seeding growth for size control of 5-40 nm diameter gold nanoparticles. *Langmuir* **2001,** *17* (22), 6782-6786.

28. Kuo, C. H.; Huang, M. H. Synthesis of branched gold nanocrystals by a seeding growth approach. *Langmuir* **2005,** *21* (5), 2012-2016.

29. Hikosaka, K.; Kim, J.; Kajita, M.; Kanayama, A.; Miyamoto, Y. Platinum nanoparticles have an activity similar to mitochondrial NADH : ubiquinone oxidoreductase. *Colloids and Surfaces B-Biointerfaces* **2008,** *66* (2), 195-200.

30. Papp, S.; Dekany, I. Nucleation and growth of palladium nanoparticles stabilized by polymers and layer silicates. *Colloid and Polymer Science* **2006,** *284* (9), 1049-1056.

31. Connolly, D.; Twamley, B.; Paull, B. High-capacity gold nanoparticle functionalised polymer monoliths. *Chemical Communications* **2010,** *46* (12), 2109-2111.

32. Grabar, K. C.; Freeman, R. G.; Hommer, M. B.; Natan, M. J. Preparation and characterization of Au colloid monolayers. *Analytical Chemistry* **1995,** *67* (4), 735-743.

33. Svec, F.; Frechet, J. M. J. New designs of macroporous polymers and supports: From separation to biocatalysis. *Science* **1996,** *273* (5272), 205-211.

34. Thabano, J. R. E.; Breadmore, M. C.; Hutchinson, J. P.; Johns, C.; Haddad, P. R. Silica nanoparticle-templated methacrylic acid monoliths for in-line solid-phase extraction-capillary electrophoresis of basic analytes. *Journal of Chromatography A* **2009,** *1216* (25), 4933-4940.

35. Krenkova, J.; Lacher, N. A.; Svec, F. Control of Selectivity via Nanochemistry: Monolithic Capillary Column Containing Hydroxyapatite Nanoparticles for Separation of Proteins and Enrichment of Phosphopeptides. *Analytical Chemistry* **2010,** *82* (19), 8335-8341.

36. Peters, E. C.; Petro, M.; Svec, F.; Frechet, J. M. J. Molded rigid polymer monoliths as separation media for capillary electrochromatography. *Analytical Chemistry* **1997,** *69* (17), 3646-3649.

37. Yang, M. H.; Yang, Y. H.; Liu, Y. L.; Shen, G. L.; Yu, R. Q. Platinum nanoparticles-doped sol-gel/carbon nanotubes composite electrochemical sensors and biosensors. *Biosensors & Bioelectronics* **2006,** *21* (7), 1125-1131.

38. Ryu, J. H.; Han, S. S.; Kim, D. H.; Henkelman, G.; Lee, H. M. Ligand-Induced Structural Evolution of Pt55 Nanoparticles: Amine versus Thiol. *ACS Nano* **2011,** *5* (11), 8515-8522.

39. Hilder, E. F.; Svec, F.; Frechet, J. M. J. Latex-functionalized monolithic columns for the separation of carbohydrates by micro anion-exchange chromatography. *Journal of Chromatography A* **2004,** *1053* (1-2), 101-106.

40. Yang, W. T.; Ranby, B. Bulk surface photografting process and its applications .1. Reactions and kinetics. *Journal of Applied Polymer Science* **1996,** *62* (3), 533-543.

41. Yang, W. T.; Ranby, B. Bulk surface photografting process and its applications .2. Principal factors affecting surface photografting. *Journal of Applied Polymer Science* **1996,** *62* (3), 545-555.

42. Stachowiak, T. B.; Svec, F.; Frechet, J. M. J. Patternable protein resistant surfaces for multifunctional microfluidic devices via surface hydrophilization of porous polymer monoliths using photografting. *Chemistry of Materials* **2006,** *18* (25), 5950-5957.

43. Gillespie, E.; Connolly, D.; Paull, B. Using scanning contactless conductivity to optimise photografting procedures and capacity in the production of polymer ion-exchange monoliths. *Analyst* **2009,** *134* (7), 1314-1321.

44. Li, Y.; Gu, B. H.; Tolley, H. D.; Lee, M. L. Preparation of polymeric monoliths by copolymerization of acrylate monomers with amine functionalities for anion-exchange capillary liquid chromatography of proteins. *Journal of Chromatography A* **2009,** *1216* (29), 5525-5532.

45. Yang, G. L.; Feng, S.; Liu, H. Y.; Yin, J. F.; Zhang, L.; Cai, L. P. On-line clean-up and screening of oxacillin and cloxacillin in human urine and plasma with a weak ion exchange monolithic column. *Journal of Chromatography B-Analytical Technologies in the Biomedical and Life Sciences* **2007,** *854* (1-2), 85-90.

46. Huang, X. H.; El-Sayed, I. H.; Yi, X. B.; El-Sayed, M. A. Gold nanoparticles: Catalyst for the oxidation of NADH to NAD(+). *Journal of Photochemistry and Photobiology B-Biology* **2005,** *81* (2), 76-83.

47. Gopalan, A.; Ragupathy, D.; Kim, H. T.; Manesh, K. M.; Lee, K. P. Pd (core)-Au (shell) nanoparticles catalyzed conversion of NADH to NAD(+) by UV-vis spectroscopy-A kinetic analysis. *Spectrochimica Acta Part A-Molecular and Biomolecular Spectroscopy* **2009,** *74* (3), 678-684.

48. Chatenet, M.; Micoud, F.; Roche, I.; Chainet, E. Kinetics of sodium borohydride direct oxidation and oxygen reduction in sodium hydroxide electrolyte - Part I. BH_4^- electro-oxidation on Au and Ag catalysts. *Electrochimica Acta* **2006,** *51* (25), 5459-5467.

49. Henglein, A.; Lilie, J. Radiation Electrochemistry of the Colloidal Cadmium Microelectrode - Catalysis of Hydrogen Formation by Organic Free-Radicals. *Journal of Physical Chemistry* **1981,** *85* (9), 1246-1251.

50. Henglein, A.; Lilie, J. Storage of electrons in aqueous-solution - the rates of chemical charging and discharging the colloidal silver microelectrode. *Journal of the American Chemical Society* **1981,** *103* (5), 1059-1066.

51. Freund, T. Kinetics of the reduction of inorganic ions by borohydride .1. ferricyanide. *Journal of Inorganic & Nuclear Chemistry* **1959,** *9* (3-4), 246-251.

Chapter 4: Gold nano-particle agglomerated monoliths for flow-through catalytic reactions

Abstract

Polymer monoliths in capillary and polypropylene pipette tip formats were modified with gold nano-particles and subsequently used for flow-through catalytic reactions. Specifically, methacrylate monoliths were modified with acrylates and methacrylates using a two-step photografting method and then reacted with ethylenediamine to provide amine attachment sites for the subsequent immobilisation of gold nano-particles (AuNPs). This was achieved by flushing colloidal suspensions of gold nano-particles through each aminated polymer monolith which resulted in a multi-point covalent attachment of gold via the lone pair of electrons on the nitrogen of the free amine groups. Field emission scanning electron microscopy and scanning capacitively coupled conductivity detection was used to characterise the surface coverage of AuNP on the monoliths. The catalytic activity of AuNP immobilised on the polymer monoliths in both pipette tip and capillary formats was then demonstrated using selected redox reactions such as the reduction of Fe(III) to Fe(II) by sodium borohydride and it was found to be dependent on the size of the immobilised nano-particles. The elimination of the absorption band at 420 nm which was indicative of the hexacyanoferrate (III) complex indicated the reduction of Fe(III) to Fe(II). Almost complete reductions (95%) were observed when using monoliths agglomerated with 7 nm AuNPs.

Aims

The aims of this Chapter were to demonstrate the catalytic properties of AuNP-agglomerated polymer monoliths and to evaluate the effect of nano-particle size on catalytic efficiency.

4.1 Introduction

Considerable interest has surrounded metal nano-particles over recent years due to their interesting catalytic [1], optical [2] and electrical properties [3]. The use of gold nano-particles (AuNPs) in particular as a catalyst in electron transfer reactions has been well documented [4-6] however, as mentioned in Chapter 3, one of the main disadvantages of common catalytic reactions is that the catalyst (in this case AuNP) is often difficult to isolate from the product(s) after the completion of the reaction. Recently, the functionalisation of polymers [7], silica [8, 9] and carbon based surfaces [10] with AuNPs has been reported. Focusing on catalytic applications, these nano-particles have also been attached on a vast range of metal oxides based especially on titania, silica and alumina with demonstrated applications towards hydrogenation and oxidation reactions [11-13]. Supported nano-particles have proven to be particularly advantageous since they can be recovered after each catalytic reaction and they can be re-used several times without affecting their catalytic activity [14, 15].

Monolithic materials, generally based on polymer or silica, have seen application as stationary phases in liquid chromatography due to the ability to operate at a higher linear velocity relative to particulate packed columns without large reductions in efficiency and considerable increases in backpressure. Among the various types of monolithic stationary phases, polymer monoliths in particular have gained in popularity because of their high p*H* compatibility and facile fabrication methods. Their main limitation however, is their relatively low surface area which traditionally varied between 5-25 m^2/g [16] and limited their applications in separation science to mainly large molecules. Recently, several reports have emerged describing the modification of polymer monoliths with metal nano-particles as an effort to solve this problem, based on the high surface to volume ratio of these materials. Current methodologies involve the encapsulation of nano-particles prior to the polymerisation [17] or their subsequent attachment upon an activated monolithic surface [18-22]. While the former method leads to the majority of nano-particles located deep within the bulk polymer, the latter is preferred since a higher surface coverage is achieved. Very few reports however, describe applications of polymer monoliths functionalised with nano-catalysts for flow-through catalytic reactions,

and the vast majority published to date are based on Pd or Pt nano-materials as described in Section 3.1

The immobilisation of AuNPs on polymer monoliths has also been reported. Svec's group originally prepared GMA-*co*-EDMA monoliths which were modified with either cysteamine or sodium hydrogen sulphide, allowing the formation of thiol functional groups on the surface which allowed the subsequent covalent attachment of AuNPs [21, 22]. The gold agglomerated monoliths were applied for the removal of cysteine-containing peptides from a complex mixture. These were then further eluted with a solution of mercaptoethanol and separated on a packed capillary C_{18} column. Similarly, such columns have demonstrated reversed-phase and ion-exchange applications for the separation of proteins after modification with 1-octadecanethiol and 2-mercaptoethanesulphonate, respectively. These applications will be discussed in detail in Section 5.1. Further developments were more recently reported indicating high loadings of AuNPs as shown in Figure 4.1, up to 60 wt%, after liberating the desired thiol groups of the cysteamine-functionalised monolith by reaction with tris(2-carboxyethyl) phosphine which allowed the cleavage of its disulphide bonds [19].

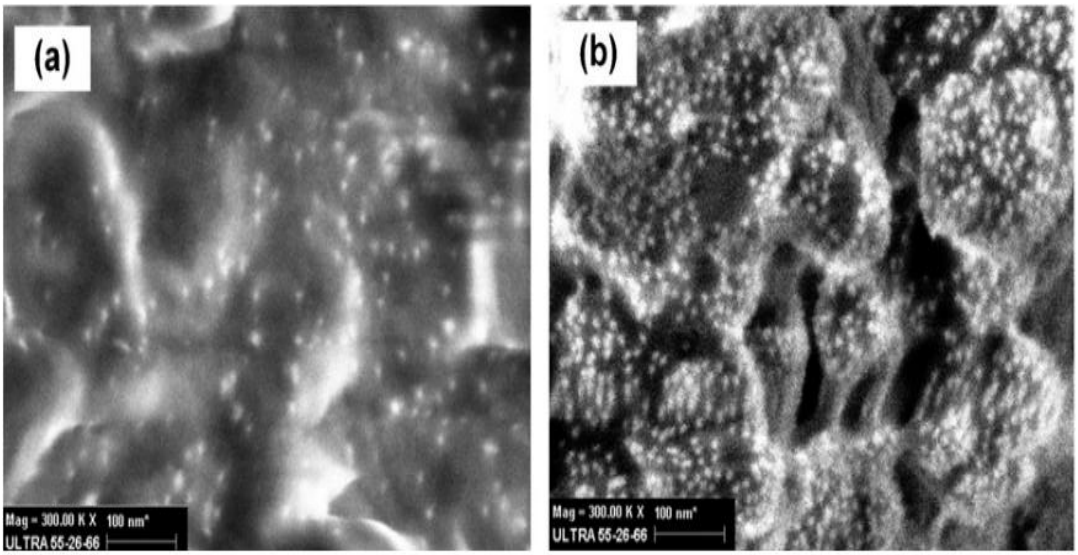

Figure 4.1: *Scanning electron micrographs of a GMA-co-EDMA monolith modified with (a) 5 nm and (b) 10 nm AuNPs [19].*

Connolly *et al.* [20] evaluated the effects of photografting on the coverage of AuNPs on polymer monoliths. A BuMA-*co*-EDMA monolith was photografted with vinyl azlactone and modified with ethylenediamine. The NH_2 moieties present on the

surface allowed the covalent attachment of citrate stabilised AuNPs. The effects of grafting led to a highly cross-linked network of azlactone groups, which ultimately led to a high presence of NH_2 functional groups on the surface and highly dense AuNP coverage, as confirmed by FE-SEM. Similar monoliths in polypropylene pipette-tip formats were also prepared and AuNPs were used as anchoring sites for the immobilisation of a lectin via a bi-functional linker (DTSP) for the extraction of selected proteins [18].

This Chapter explores a new application area of AuNP-agglomerated polymer monoliths, demonstrating the preservation of catalytic properties of such nano-materials even after immobilisation upon a monolithic surface. The flow-through reduction of hexacyanoferrate (III) was selected for this purpose using monoliths fabricated both in pipette-tip and capillary (100 μm i.d.) formats demonstrating applications in either off-line or on-line modes.

4.2 Experimental

4.2.1 Instrumentation

The instrumentation used was as described in Sections 2.2.1 and 3.2.1 with the following additions. On-line catalytic experiments in flow-through mode were performed using a Dionex Ultimate 3000 system equipped with a 3 n*L* flow cell (Dionex Ultimate LC system, Sunnyvale, CA, USA). A Mistral Column Oven 880 (Spark Holland, The Netherlands) was used for the modification of monoliths with ethylenediamine in continuous flow mode.

4.2.2 Materials and reagents

The materials used were as described in Sections 2.2.2 and 3.2.2 with the following additions. Lauryl methacrylate (LMA), gold (III) chloride, sodium citrate, tetrakis(hydroxymethyl) phosphonium chloride (THPC), dimethylformamide (DMF) were all purchased from Sigma-Aldrich (Dublin, Ireland). N-succinimidyl acrylate (NSA) was purchased from TCI Europe (Zwijndrecht, Belgium). Ethanol was purchased from Fisher Scientific (Dublin, Ireland). All chemicals were used as received without further purification.

4.2.3 Preparation of methacrylate monoliths within pipette-tip housings

Monoliths in tip format were prepared as described by Alwael *et al*. [18]. In order to allow stable anchoring of the stationary phase to the inner walls of the polypropylene tip, the inner surface was modified with grafted chains of EDMA. Firstly, the tip was washed with 10 µ*L* of ethanol (10 times) and 10 µ*L* acetone (10 times) and dried using nitrogen to remove any impurities on the surface of the polypropylene. The tip was filled with 10 µ*L* of deoxygenated 5% benzophenone in methanol and irradiated with 1 J/cm^2 of UV energy at 254 nm, followed by a methanol rinse. The tip was then filled with deoxygenated 15% EDMA in methanol and irradiated under the same conditions. A final wash in methanol was performed and the tip was dried under nitrogen. A polymerisation mixture consisting of EDMA (40 wt%), 1-decanol (60 wt%) and DAP (1 wt%, w.r.t. monomer) was prepared and deoxygenated with a nitrogen flow for 10 minutes. In order to ensure a constant and repeatable bed volume for each monolith, a guide ring of polypropylene (2 mm i.d.) was placed on the outside of the modified tip, which was subsequently filled by capillary action until the meniscus reached the bottom of the guide ring. The filled tip was placed upright in a coned centrifuge tube (polypropylene) and irradiated with 3 J/cm^2 of UV energy at 254 nm. The resulting monolith was washed with methanol at flow rate of 100 µ*L*/hr to remove the porogen and any unreacted monomers.

4.2.4 Amination of methacrylate monoliths within pipette-tip housings

The monolith was surface grafted with poly(vinyl azlactone) (VAL) as described by Connolly *et al*. [20]. Initially it was first conditioned with 50 m*L* of methanol followed by flushing the monolith with a deoxygenated solution of 5% benzophenone in MeOH for 30 minutes. The monolith was then irradiated with 3 J/cm^2 of UV energy at 254 nm followed by washing with methanol for 30 minutes. The monolith was then flushed with a deoxygenated solution of 15% VAL in methanol for 30 minutes and irradiated as in the previous step. A wash in methanol was then performed, followed by a wash with water for 30 minutes prior to flushing a 1 *M* ethylenediamine solution for 3 hours. The monolith was again washed with water until a neutral p*H* was observed to remove excess ethylenediamine.

4.2.5 Preparation of methacrylate monoliths in capillary formats

Fused silica capillary was silanised as described in Section 2.2.4. Monoliths consisting of 24 % LMA, 16 % EDMA, 45.5 % 1-propanol, 14.5 % 1,4-butanediol and 1 % DAP (w.r.t. monomers) were prepared in-situ by irradiation with 2 J/cm^2 of UV energy followed by a methanol rinse to remove unreacted materials.

4.2.6 Amination of methacrylate monoliths in capillary format

Previously prepared LMA-*co*-EDMA monoliths were initially conditioned with a 30 minutes methanol wash. A benzophenone solution (50 mg in 1 m*L* of methanol) was degassed for 10 minutes and pumped through the monoliths for 30 minutes. The columns were then sealed and irradiated with 1 J/cm^2 of UV energy followed by a methanol rinse. Different monomers were then grafted as illustrated in Table 4.1. Monoliths LMA-GMA were prepared by photografting a 15 % GMA solution in methanol, which was degassed for 10 minutes and pumped through for 30 minutes, followed by another dose of UV energy (1 J/cm^2). Monoliths LMA-NSA were photografted with a 15% NSA solution in DMF, which was degassed for 10 minutes and pumped through for 30 minutes. The same dose of UV energy as mentioned previously was applied followed by a final methanol rinse. Amination of the LMA-GMA monoliths was performed following two different protocols. In the first, a 1 *M* aqueous ethylenediamine solution was pumped through the monoliths for 1 hour at 1 μ*L*/min which were then end-capped and placed in a water bath at 70 °C for 24 hours followed by an extensive water rinse until neutral p*H* was observed. The second methodology required the constant pumping of the same ethylenediamine solution over 24 hours in a column oven at 70 °C followed by a final water rinse. Monolith LMA-NSA amination was also performed in constant flow mode over 24 hours at room temperature.

4.2.7 Synthesis of colloidal AuNP suspensions.

Three different colloidal suspensions of AuNPs were prepared. Citrate stabilised AuNPs were initially prepared according to the procedure outlined by Frens [23] with an anticipated size of 20 nm approximately.

Table 4.1: *Summary of polymer monoliths prepared for modification with AuNPs.*

Monolith[a]	**LMA (wt%)**	**EDMA (wt%)**	**Decanol (wt%)**	**1-Propanol (wt%)**	**1,4-Butanediol (wt%)**	**Grafted VAL (wt%)**	**Grafted GMA (wt%)**	**Grafted NSA (wt%)**
EDMA-Tip[b]	-	40	60	-	-	15	-	-
LMA-GMA[c]	24	16	-	45.5	14.5	-	15	-
LMA-NSA[c]	24	16	-	45.5	14.5	-	-	15

[a] All monoliths contain DAP as initiator, 1% w.r.t. monomer

[b] Monolith in pipette-tip format

[c] Monolith in capillary format

All glassware was acid-washed with aqua regia prior to use followed by rinsing with deionised water. Gold chloride (50 m*L*, 5 m*M*) was added to a stirred 425 m*L* volume of boiling deionised water. While the solution was boiling, 25 m*L* of 30 m*M* sodium citrate was rapidly added during vigorous stirring. After the evolution of a deep red wine colour, boiling and stirring were continued for 5 minutes, followed by stirring for an additional 30 minutes without the use of a hotplate. Finally upon cooling, the solution was made up to 500 m*L* with water and stored at 4 ^{o}C until use.

Another citrate stabilised colloidal suspension of AuNPs, with an anticipated nano-particle size of approximately 2 nm, was prepared as described by He *et al.* [24] . A 20 m*L* aqueous solution containing 2.5 x 10^{-4} *M* gold chloride (2 mg) and 2.5 x 10^{-4} *M* tri-sodium citrate (1.5 mg) was prepared in a conical flask. Then a 0.1 *M* ice-cold and freshly prepared $NaBH_4$ solution (0.6 m*L*, 2.3 mg) was added into the solution under stirring. The solution turned pink immediately after the addition of $NaBH_4$, indicating particle formation and it was kept stirring for 30 minutes after which it was stored at 4 ^{o}C until use.

Finally, THPC stabilised AuNPs with an anticipated size of 2 nm were also prepared following a procedure reported by Duff *et al.* [25],. A 25 m*M* gold chloride solution was prepared by dissolving 20 mg of gold chloride in 2 m*L* and this was left aging for 15 minutes. After this time interval, the gold chloride solution was added under fast stirring to another solution containing 1.5 m*L* of NaOH (0.2 *M*), 1 m*L* of a THPC solution (prepared by diluting 1.2 ml of a 80 % solution to 100 m*L*) and 45.5 m*L* of deionised water. The solution turned into a dark brown colour instantly indicating the formation of gold nano-particles and was left stirring for 30 mins. It was finally stored at 4 ^{o}C until use.

4.2.8 Modification of monolithic surfaces with AuNPs

Polymer monoliths in tip and capillary format were functionalised with AuNPs as summarised in Table 4.2 below, where the numbering is indicative of the actual AuNP sizes. Monoliths EDMA-Tip-16 were modified with 16 nm AuNPs by pumping the colloidal solution with a syringe pump at a flow rate of 0.25 m*L*.hr^{-1} until the monolith turned a deep burgundy colour throughout followed by a water rinse. The LMA-GMA and LMA-NSA monoliths in capillary formats were

connected to a 300 µ*L* PEEK loop, filled with the AuNP colloidal solutions, and flushed until the monoliths turned into a pink/burgundy colour, followed by a final water rinse.

Table 4.2: *Summary of nano-particle modified polymer monoliths.*

Monolith	16 nm citrate AuNPs	7 nm citrate AuNPs	4 nm THPC AuNPs
EDMA-Tip-16	X	-	-
LMA-GMA-16	X	-	-
LMA-GMA-7	-	X	-
LMA-GMA-4	-	-	X
LMA-NSA-16	X	-	-

4.2.9 Flow-through catalytic reduction of hexacyanoferrate(III)

Standard redox chemistry was used to evaluate the catalytic properties of the immobilised AuNPs in either an off-line or on-line set up. A mixture of K_3[] (4 m*M*) and $NaBH_4$ (0.6 m*M*) was prepared in a p*H* 11.5 aqueous solution, adjusting the ionic strength to 0.085 *M* with NaCl. This solution was pumped at 0.25 m*L*.hr^{-1} for 1 hour through the EDMA-Tip-16 and a blank EDMA-Tip for comparative purposes. UV-Vis analysis of the collected product was used to confirm the complete reduction of ferrocyanide (III) to (II), due to the elimination of the absorbance peak at 420 nm. Similarly, the experiment was performed on-line by injecting 100 n*L* amounts of the same mixture on AuNP functionalised monoliths LMA-GMA-16, LMA-GMA-7 and LMA-GMA-4, evaluating the progress of the reaction relative to a blank LMA-GMA monolith which did not contain any nano-particles.

4.3 Results and discussion

4.3.1 Synthesis of AuNP colloidal suspensions

In this Chapter, colloidal suspensions of gold nano-particles were prepared using citrate ions and phosphonium ions (from THPC) as capping agents, which are negatively and positively charged respectively.

Charged ligands are often used in the preparation of metal nano-particle colloidal suspensions in order to generate an electrostatic repulsive force and prevent aggregation. The presence of an electrostatic force between the surface and the surrounding charged species leads to a high distribution of counter-ions around the surface, which decreases as the distance from the surfaces increases, as shown in Figure 4.2. This non-homogeneous distribution of ions causes the formation of two layers around the surface of nano-particles which are known as the Stern layer and the Gouy layer, and these are separated by the Helmholtz plane. Within the Gouy layer, a slip plane exists which separates the liquid layer tightly bound to the nano-particle from the remaining liquid point, and the electric potential at this point (known as zeta potential, γ) is often measured to indicate the stability of a colloidal suspension.

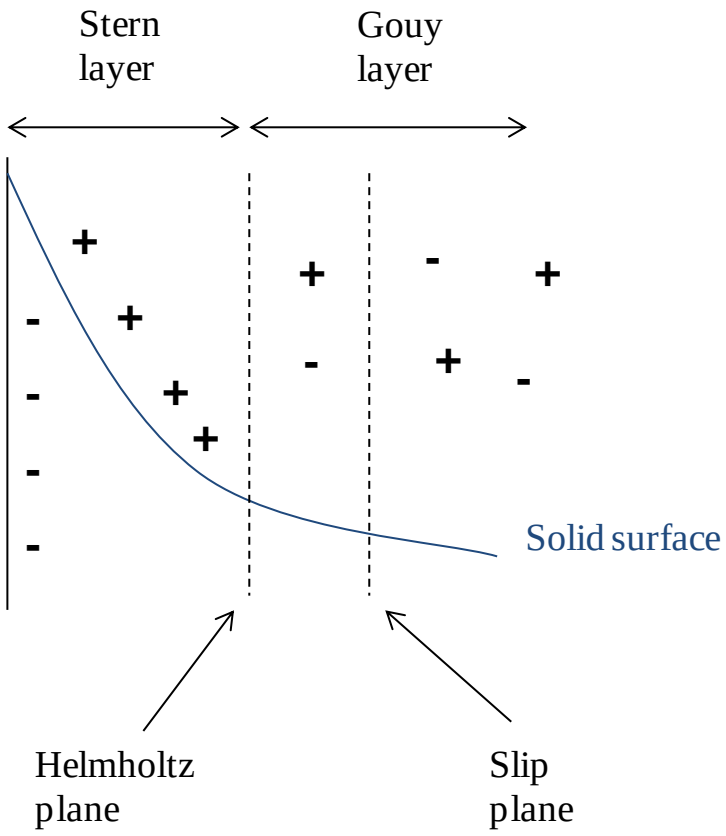

***Figure 4.2**: Schematic illustrating the electrical double layer structure and the electric potential near the surface of a nano-particle, with both Stern and Gouy layer indicated. Surface charge is assumed to be negative.*

A zeta potential value of ± 25 m*V* (for positively and negatively charged particles respectively) is considered to be indicative of a stable colloidal system [26]. A

constant collision between nano-particles in solution occurs due to Brownian motion effects. Also Van der Waals forces, caused by dipole-dipole interactions, are present at small inter-particle distances. When two particles in solution are distant and there is no overlap of the double layers, no interaction will be present and no repulsion will occur. However, when two particles move closer and the electrical double layers overlap, repulsion will occur.

4.3.2 Characterisation of AuNP colloidal suspensions

Citrate stabilised AuNPs prepared according to the Frens method [23] led to particles of approximately 16 nm in size with a zeta potential of -21.7 ± 6.6 m*V* (*n*=3) which seems to be in accordance with previous reports described in the literature [27], indicating that the particles form a stable colloidal suspension due to a permanent negative charge present on the surface.

Table 4.3: *Size and zeta potential data of AuNP colloidal suspensions.*

Capping agent	Particle size (*n*=3)	Zeta potential, γ, (mV) (*n*=3)	λ_{max} (nm)	Abs (AU)	$\varepsilon(M^{-1}cm^{-1})$	Concentration (*M*)
Citrate	16.0±0.1	-21.7±6.6	518	0.79	$1.0x10^{9}$	$1.6x10^{-9}$
Citrate	7.0±0.1	-22.7±7.3	508	0.48	$8.6x10^{6}$	$5.6x10^{-8}$
THPC	4.4±0.1	-0.6±2.8	489	1.06	$4.9x10^{6}$	$4.4x10^{-7}$

The use of $NaBH_4$ as a strong reducing agent instead of citrate led to a faster nucleation rate and, as mentioned previously in Section 3.3.1, to particles of smaller size (7 nm) which showed similar stability with a zeta potential of -22.7 ± 7.3 m*V* (*n*=3). However, the use of THPC as the capping agent led to poorly stable nano-particles (zeta potential -0.6 ± 2.8 m*V*, *n*=3) of 4 nm in size. The poor stability led to a visible change in colour of the colloidal suspension (from black to red) over time which is indicative of nano-particle aggregation.

Characterisation by UV-Vis spectroscopy, shown in Figure 4.3, also confirmed as expected an increase in λ_{max} as particle size increased [28], with values increasing from 489 nm for 4 nm AuNPs to 518 nm for 16 nm AuNPs, as summarised in Table 4.3.

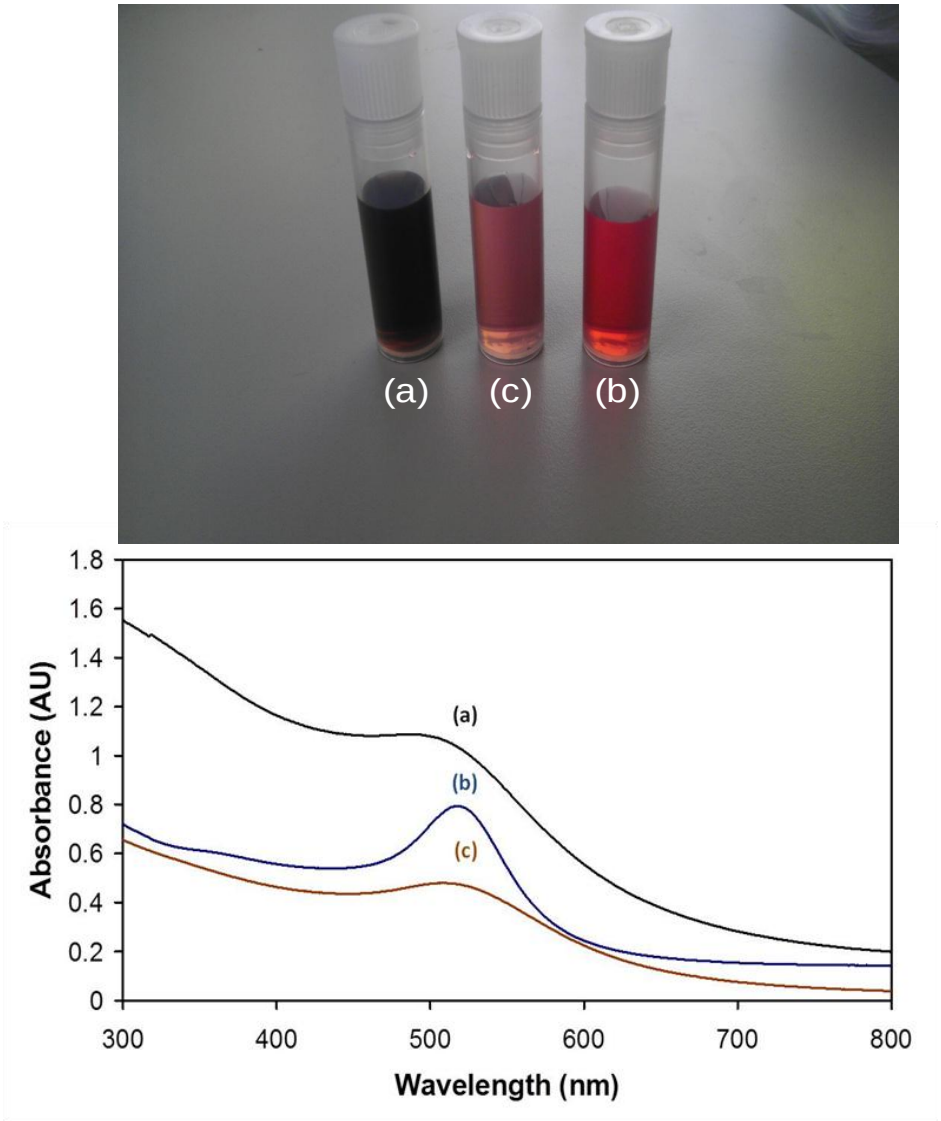

Figure 4.3: *(Top) image showing different colloidal suspensions of AuNPs. From left to right: 4 nm THPC stabilised AuNPs, 7 nm and 16 nm citrate stabilised AuNPs. (Bottom) UV-Vis spectra of (a) THPC stablised AuNPs with an average size of 4 nm (diluted 1 in 2), (b) 16 nm citrate stabilised AuNPs (diluted 1 in 2) and (c) 7 nm citrate stabilised AuNPs.*

The concentration of the colloidal suspensions was determined using methods described by Liu *et al.* [28] who reported the presence of a linear relationship

between molar extinction coefficient (ε) and nano-particle size (D) of AuNPs as illustrated in Equation 4.1 below:

$$\ln \varepsilon = k \ln D + a \qquad \text{(Equation 4.1)}$$

This relationship was used to calculate the extinction coefficient ε for the AuNPs here prepared.

By plotting ln(ε) vs ln(D) Liu *et al*. reported that k = 3.32111 and a = 10.80505. Hence by inserting in Equation 4.1 our values for D, it was possible to find ε. The concentration of the colloidal suspensions, c, can then be determined by rearranging Beer-Lambert law shown in Equation 4.2:

$$A = \varepsilon.c.l \qquad \text{(Equation 4.2)}$$

where A = absorbance (AU), c = concentration (M) and l = path length (cm).

4.3.3 Preparation of polymer monoliths

The catalytic reactivity of AuNPs has been well documented in the literature, however here for the first time an evaluation of the catalytic properties of these materials upon immobilisation on monolithic surfaces is described. Polymer monoliths were used as solid supports because of their ideal porous structure which makes them suitable for flow-through applications, customisable chemical properties and facile *in situ* photoinitiated fabrication methods. Polypropylene pipette tips and teflon coated fused silica capillary were considered to be suitable housings for hosting the monoliths due to their UV transparency, required for all photoinitiated steps, and compatibility with all the solvents used in our experiments. Both housings demonstrate distinctive advantages. Monoliths in capillary formats can be integrated with capillary LC systems leading to their operation in on-line mode and overall reduced analysis times, while monoliths in pipette tips can be used off-line for automating sample preparation when directly connected for example to 96-well plate robotic systems [29]. An initial pre-treatment of the inner walls of both housings was necessary in order to allow the successful bonding with the stationary phase as shown in Figure 4.4.

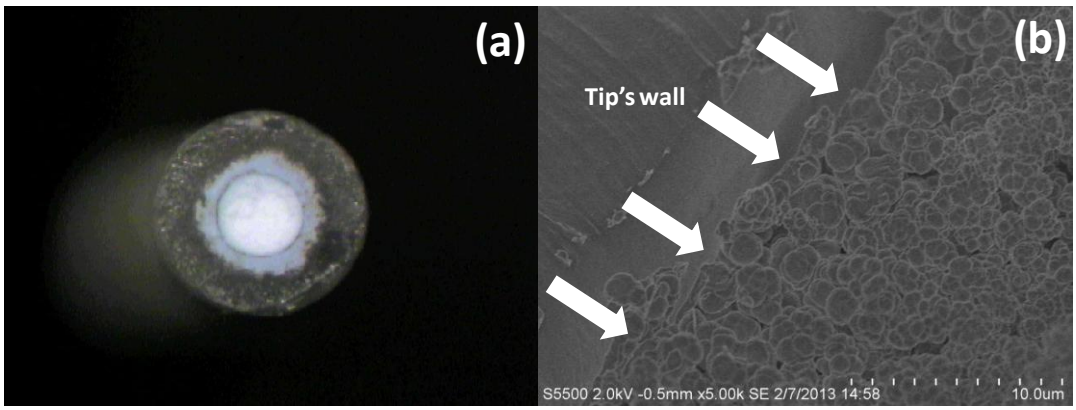

Figure 4.4: *Images of (a) a blank EDMA-tip visualised from the bottom of the tip and (b) FE-SEM image showing the attachment (as indicated by the pointed arrows) of the EDMA monolith onto the inner walls of the pipette tip (magnification 5,000x).*

This was performed in order to eliminate the presence of voids since issues such as sample loss and possible detachments of the solid support could develop which, in relation to catalysis, would result in the contamination of the reaction products. Capillaries were initially treated using well established chemistry involving a silane primer reagent [30], while pipette tips were photografted with EDMA polymer chains on the inner surface of the polypropylene tip which led to a properly bound monolithic structure capable of withstanding the high pressures of a nitrogen gas stream [18]. A 40/60 monomer to porogen ratio was kept constant in all cases here described which led to a desirable macro-porous structure suitable for flow-through applications [31].

4.3.4 Modification of surface chemistry for AuNP attachment

The functionalisation of the monoliths with AuNPs was performed following previously reported procedures [18, 20, 32]. These required the modification of the surface chemistry of the monolith via photografting of an amine-reactive monomer, either vinyl azlactone (VAL), glycidyl methacrylate (GMA) or N-succinimidyl acrylate (NSA), followed by the amination of the reactive functionalities present and the final flushing of a colloidal suspension of nano-particles which led to their covalent immobilisation due to interactions with the primary-amine lone pair electrons as shown in Figure 4.5. Other methodologies known for the preparation of nano-particle agglomerated monolithic stationary phases involve the encapsulation

of the nano-materials within the monolith by the addition of a nano-particle suspension to the monomer mixture, which would lead to poor nano-particle coverage on the surface, or the subsequent flushing upon a monolith prepared by direct co-polymerisation of the monomers containing the reactive moieties [17]. In this case some of the required functionalities would be embedded deep within the surface of the monolith therefore preventing an optimised surface coverage of nano-particles. It was anticipated however, that by availing of photografting techniques, a very high ligand density of reactive functionalities would be achieved on the surface of the monolith leading ultimately to an increased presence of nano-particles as discussed in Chapter 3.

In the work here described, EDMA monoliths were initially prepared in pipette-tip, followed by the photografting of VAL. A 15 % solution was selected in order to prevent any self-screening effects that could potentially arise during the grafting step in the presence of an excessively high monomer concentration.

Alternatively LMA-*co*-EDMA monoliths in capillary format were prepared using GMA instead as the amine reactive monomer (monoliths LMA-GMA). The ring-opening reaction of the epoxy groups with ethylenediamine was performed using two different procedures. In the first procedure, the columns were end-capped after flushing the amine solution for 1 hour and placed in a water bath at 70°C for 24 hours. The second methodology required the constant flushing of the same ethylenediamine solution in a column oven at 70°C for 24 hours. Both methodologies led to free primary amines available on the surface which served as point of attachment for the AuNPs. Another acrylate monomer, NSA, was alternatively photografted on similar monoliths LMA-NSA in order to evaluate if any variations in grafting efficiency relative to methacrylate monomers were present since it is known that the process of hydrogen abstraction, which determines the efficiency of the photografting process, is facilitated in the presence of acrylates [33].

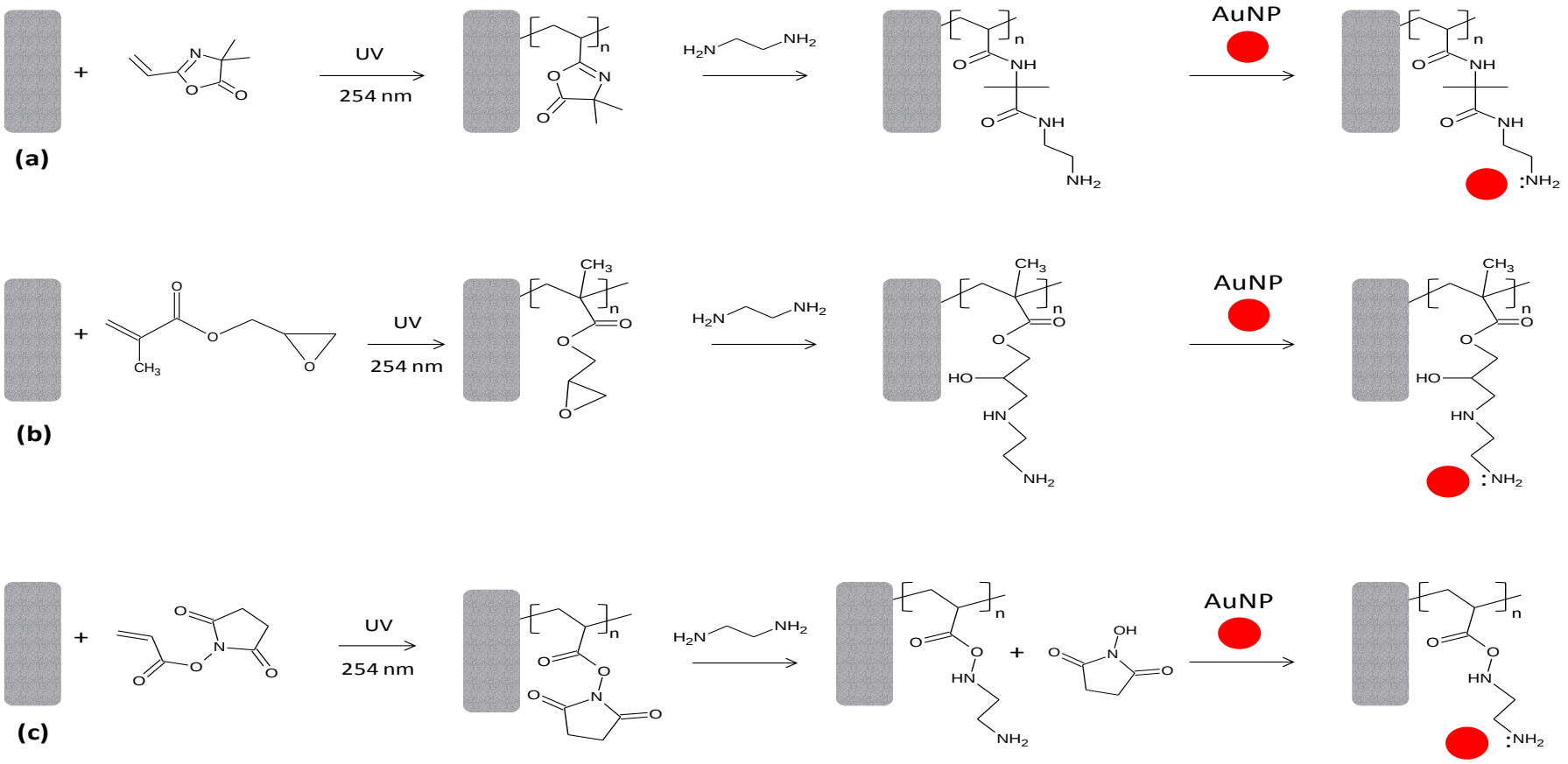

Figure 4.5: *Schematic showing the modification steps for the functionalisation of polymer monoliths with AuNPs for (a) monoliths EDMA-Tip-16 grafted with vinyl azlactone, (b) LMA-GMA monoliths grafted with glycidyl methacrylate and (c) LMA-NSA monoliths grafted with N-succinimidyl acrylate.*

4.3.5 Characterisation of AuNP coverage on monoliths in pipette-tip format

After the modification of the monolith with ethylenediamine, a colloidal suspension of AuNPs (16 nm) was initially pumped through the monoliths in the pipette tip, leading to the monolith turning completely into a dark burgundy colour after several hours of flushing, as shown in Figure 4.6 (a) .

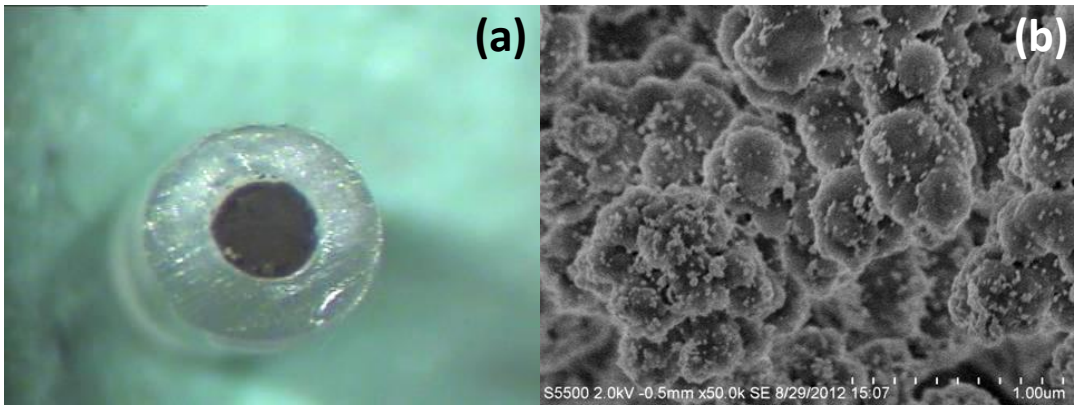

Figure 4.6: *Images of (a) a EDMA-Tip-16 monolith visualised from the bottom of the tip and (b) FE-SEM image showing the presence of 16 nm AuNPs on the surface of a EDMA-Tip-16 monolith (magnification 5,000x).*

Clear droplets were observed from the outlet of the tip since the nano-particles were retained by the stationary phase. The presence of gold nano-particles on the polymer monoliths was also confirmed by FE-SEM analysis, where each AuNP appeared as a white dot on the surface of the monolith, which would otherwise be completely smooth. The EDMA-Tip-16 shown in Figure 4.6 (b), which was grafted with 15% VAL, revealed a sparse coverage of 16 nm AuNPs with some unexpected signs of nano-particle aggregation.

Energy-dispersive X-ray spectroscopy (EDX) was also used to confirm qualitatively the presence of gold on the monolithic tip. The use of this technique for verifying the presence of gold on polymer monoliths was previously described by Xu *et al.* [22] who reported an average value of 15 ± 2 atom % Au on a GMA-*co*-EDMA monolith in capillary format which had been modified with a 50 nm AuNP colloidal suspension. As shown in Figure 4.7, signals for Au are present on the EDX

spectrum for monolith EDMA-Tip-16 which could only be due to the immobilised 16 nm AuNPs, as no signals for gold were visible on a blank EDMA-Tip monolith, as shown in Figure 4.7 (a). The amount of gold present on EDMA-Tip-16 (Figure 4.7 b) was found to be 8 ± 2 atom % Au. Both tips required coating with a 45 nm layer of chromium to reduce charging issues hence signals for Cr were also visible. Peaks for Fe and Cl were also observed on monolith EDMA-Tip-16, as a solution of hexacyanoferrate (III) in NaCl had been previously flushed through the same tip to demonstrate the catalytic properties of the immobilised nano-particles, as will be shown in Section 4.3.8.

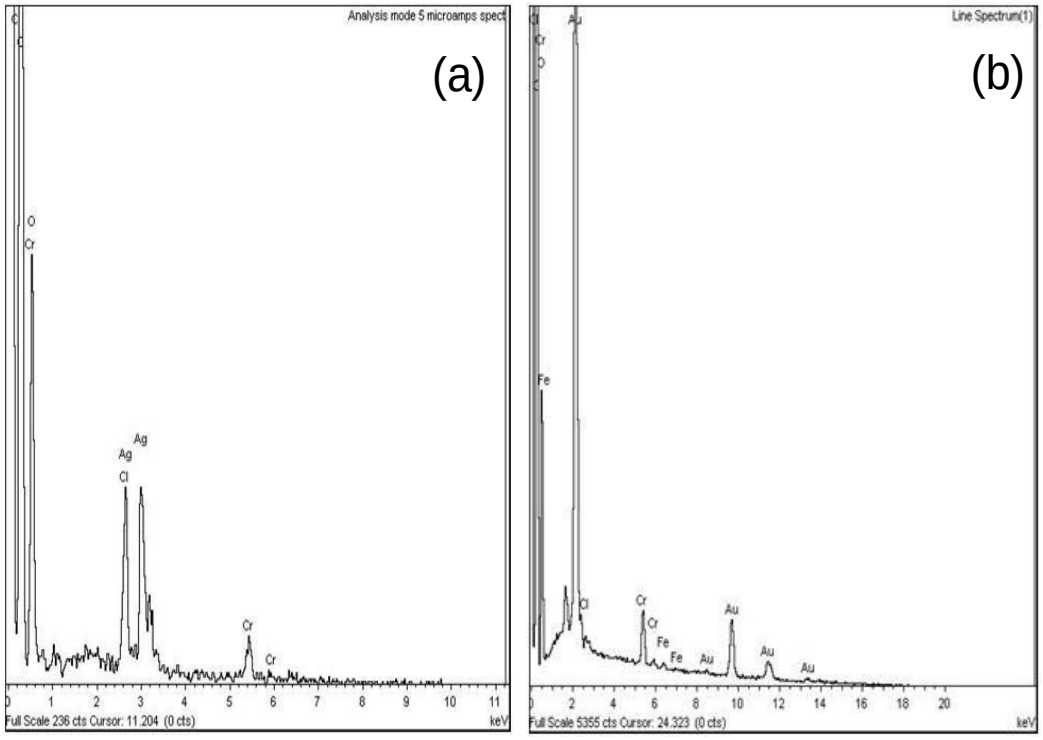

***Figure 4.7**: EDX spectra of (a) a blank EDMA-Tip and (b) a EDMA-Tip-16 modified with 16 nm AuNPs.*

Signals for Ag were also observed on the blank EDMA-Tip, as silver ions had been previously used to coat the sample in order to minimise charging issues prior to obtaining FE-SEM images.

4.3.6 FE-SEM characterisation of AuNP coverage on monoliths in capillary format

As described for the EDMA-Tips, the subsequent immobilisation of 16 nm AuNPs

on monoliths LMA-GMA in capillary format was carried out. A more homogeneous and dense coverage of AuNPs, relative to the pipette-tip monolith shown in Figure 4.6, was observed with monoliths LMA-GMA-16, which were grafted with 15% GMA as the reactive monomer (Figure 4.8 a-d). Several hours were required to modify a 13 cm long monolith (LMA-GMA-16) entirely with a 16 nm citrate stabilised AuNP suspension. This was initially confirmed by an increase in operating backpressure due to partial filling of the pores to 220 bar from 177 bar (24% increase) observed on a blank LMA-GMA monolith at a nominal flow rate of 3 μ*L*/min.

The amination procedure of the monoliths was also found to have a great impact on the level of coverage. This was verified by determining the number of nano-particles present in a random 500 nm x 500 nm region on the surfaces of two LMA-GMA-16 monoliths, using a procedure as described by Currivan *et al.* [32], which only differed in the protocol followed for amination. Figure 4.8 (a,b) and Figure 4.8 (c,d) represent the LMA-GMA-16 monolith which had been aminated using the ‘‘stopped flow’’ and the ‘‘continuous flow’’ methods respectively. The stopped flow method resulted in comparatively sparse coverage of AuNP (115/500 nm^2) with obvious signs of nano-particle aggregation (dimers, trimers and larger clusters) whereas the continuous flow method resulted in a clear increase in AuNP coverage (96%) to 225/500 nm^2. Aggregation was noticeably lower and adjacent nano-particles were more evenly spaced due to the expected electrostatic repulsive effects. Although nano-particle aggregation is usually strenuously avoided when working with colloidal suspensions, in this work the catalytic activity was not expected to be adversely affected by close-packing of AuNP on the surface and so efforts were made to further improve their surface density. Yang *et al.* [33] reported that acrylate monomers have higher photografting reactivities relative to methacrylate monomers due to the presence of allylic hydrogen atoms in the monomer and no tertiary hydrogens on the resulting polymer formed. Therefore the use of NSA was investigated as an alternative grafting monomer to glycidyl methacrylate, using a ‘‘continuous flow’’ amination at ambient temperature in the subsequent modification step. Figure 4.8 (e,f) shows that grafting an acrylate monomer resulted in a further increase in coverage to 272/500 nm^2, representing a 21% increase over the GMA-grafted monolith in Figure 4.8 (c,d) presumably due to improved grafting efficiency

relative to GMA.

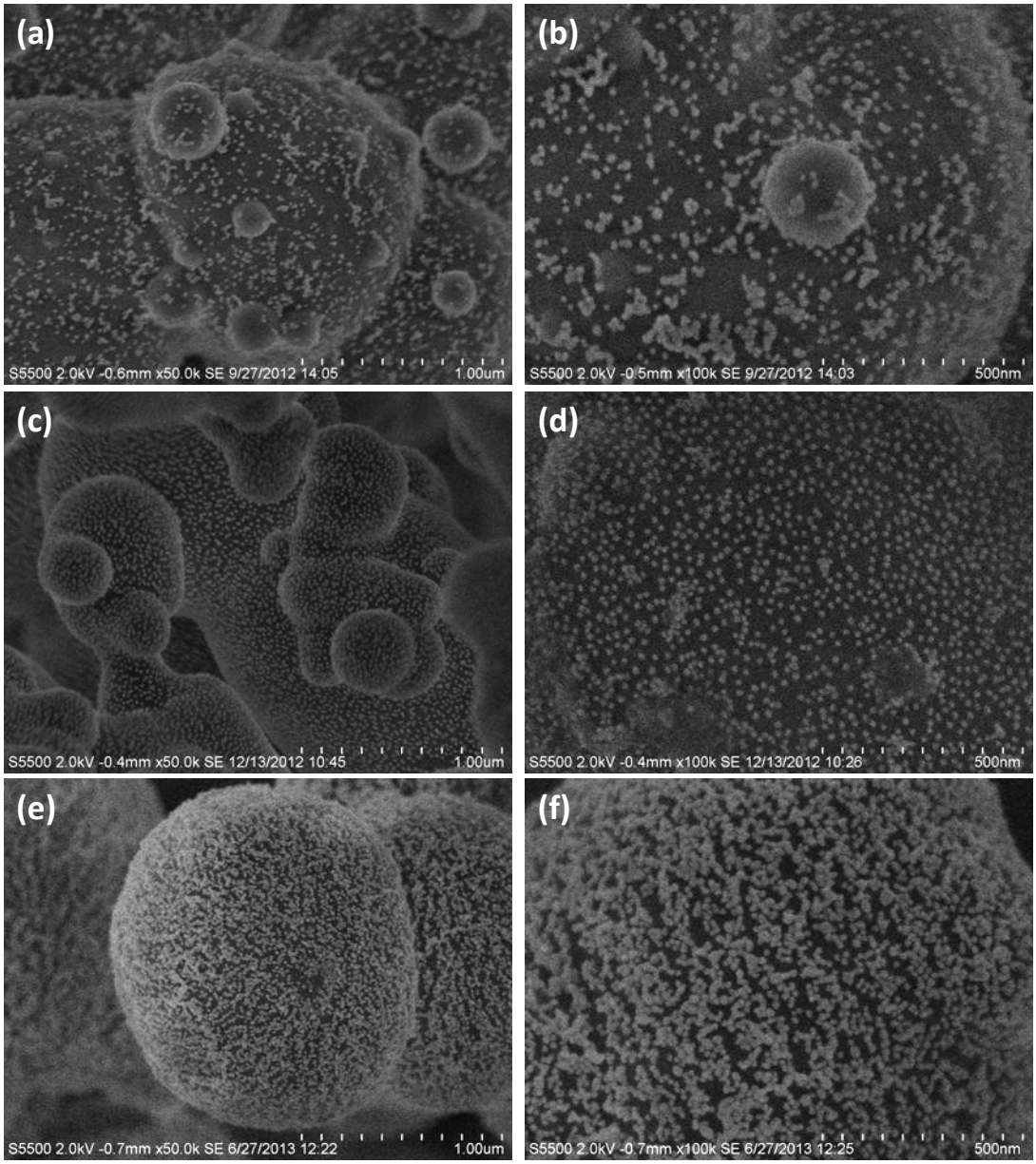

Figure 4.8: *FE-SEM images of (a and b) monolith LMA-GMA-16 which had been aminated by flushing ethylenediamine for 1 hour and placing the column in a water bath for 24 hours at 70 °C (magnification 50,000x and 100,000x), (c and d) monolith LMA-GMA-16 which had been aminated by constantly pumping ethylenediamine for 24 hours in a column oven at 70 °C (magnification 50,000x and 100,000x), (e and f) monolith LMA-NSA-16 which had been photografted with 15% NSA and aminated in constant flow mode over 24 hours at room temperature.*

Although the AuNP surface coverage was maximised with the use of NSA,

nevertheless for further studies GMA chemistry was adopted since pendant NHS esters (after grafting of NSA) are known to be subject to unwanted hydrolysis [34-36] (half-life of 1 hour at pH 8.0 and 25 °C) potentially leading to lower repeatability of AuNP coverage in this work relative to the more robust epoxy chemistry of GMA-grafted monoliths.

Some differences were observed when using colloidal suspensions of different particle size. The use of a 7 nm citrate stabilised suspension led to complete saturation within a matter of minutes, which was confirmed by the monolith LMA-GMA-7 turning into a light pink colour (different from the burgundy colour observed on monoliths LMA-GMA-16), indicating a different affinity of the two nano-particle suspensions towards the aminated surface. A 7% increase in backpressure were also observed (190 bar) using identical conditions as described previously for monoliths LMA-GMA-16.

Similarly the functionalisation with 4 nm THPC stabilised AuNPs (monolith LMA-GMA-4) turned the monolith into a dark brown colour within a matter of minutes, with backpressures of 210 bar (18% increase) for a column of the same length.

The use of FE-SEM is however, not ideal for visualising particles below 10 nm [37], and because of its invasive nature, it requires the sample to be sacrificed, representing a serious drawback of this technique. Monoliths LMA-GMA-7, which had been functionalised with 7 nm citrate stabilised AuNPs, were indeed quite difficult to image (Figure 4.9 a) and only the use of backscattered electrons allowed the visualisation of some nano-particles on the surface. A similar scenario was observed with monoliths LMA-GMA-4 (Figure 4.9 b), modified with 4 nm THPC stabilised AuNPs, where some signs of nano-particle aggregation were present on the surface, likely due to the instability of the nano-particles in the colloidal solution, as mentioned previously from the zeta potential studies which presumably led to Oswald ripening effects. This thermodynamically driven process occurs because larger particles are more energetically stable than smaller particles, hence the growth of larger particles is favoured at the expense of smaller ones.

The successful attachment of the THPC stabilised AuNPs on the aminated surface confirmed the covalent nature of the amine-gold interaction, which would otherwise be unfavourable in this case if it was only based on electrostatic forces, since the THPC capped AuNPs hold a very weak positive charge on their surface and they would be repelled by the partially positively charged surface present on the primary amine groups on the surface.

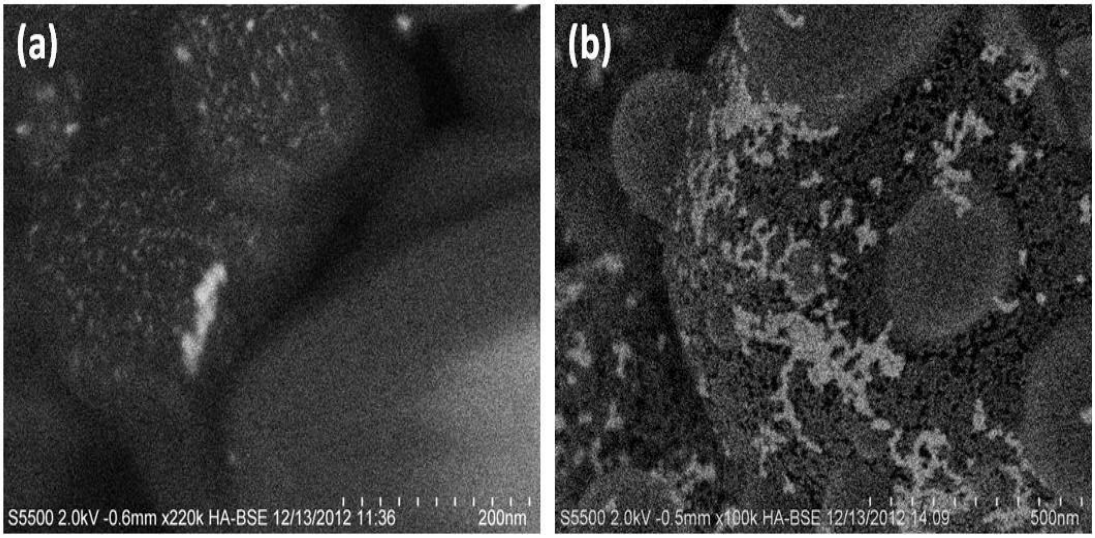

Figure 4.9: *FE-SEM images of (a) monoliths LMA-GMA-7 functionalised with 7 nm citrate stabilised AuNPs (magnification 220,000x) and (b) monoliths LMA-GMA-4 functionalised with 4 nm THPC capped AuNPs (magnification 100,000x).*

4.3.7 Characterisation of AuNP coverage on monoliths in capillary format using scanning capacitively coupled contactless conductivity detection (sC^{4}D)

Recently scanning capacitively coupled contactless conductivity detection (sC^{4}D), has emerged as a potential non-invasive characterisation tool for confirming the presence of nano-particles on monoliths in capillary formats [32]. For this purpose, sC^{4}D profiles of monoliths LMA-GMA-16 and LMA-GMA-7, modified with 16 and 7 nm nano-particles respectively, were obtained and using this technique it was possible to monitor the movement of the nano-particle plug as it progressed along the monolith during the nano-particle coating step. This was performed by determining the conductive response at 5 mm intervals for a total length of 7 cm (n=3) as shown in Figure 4.10.

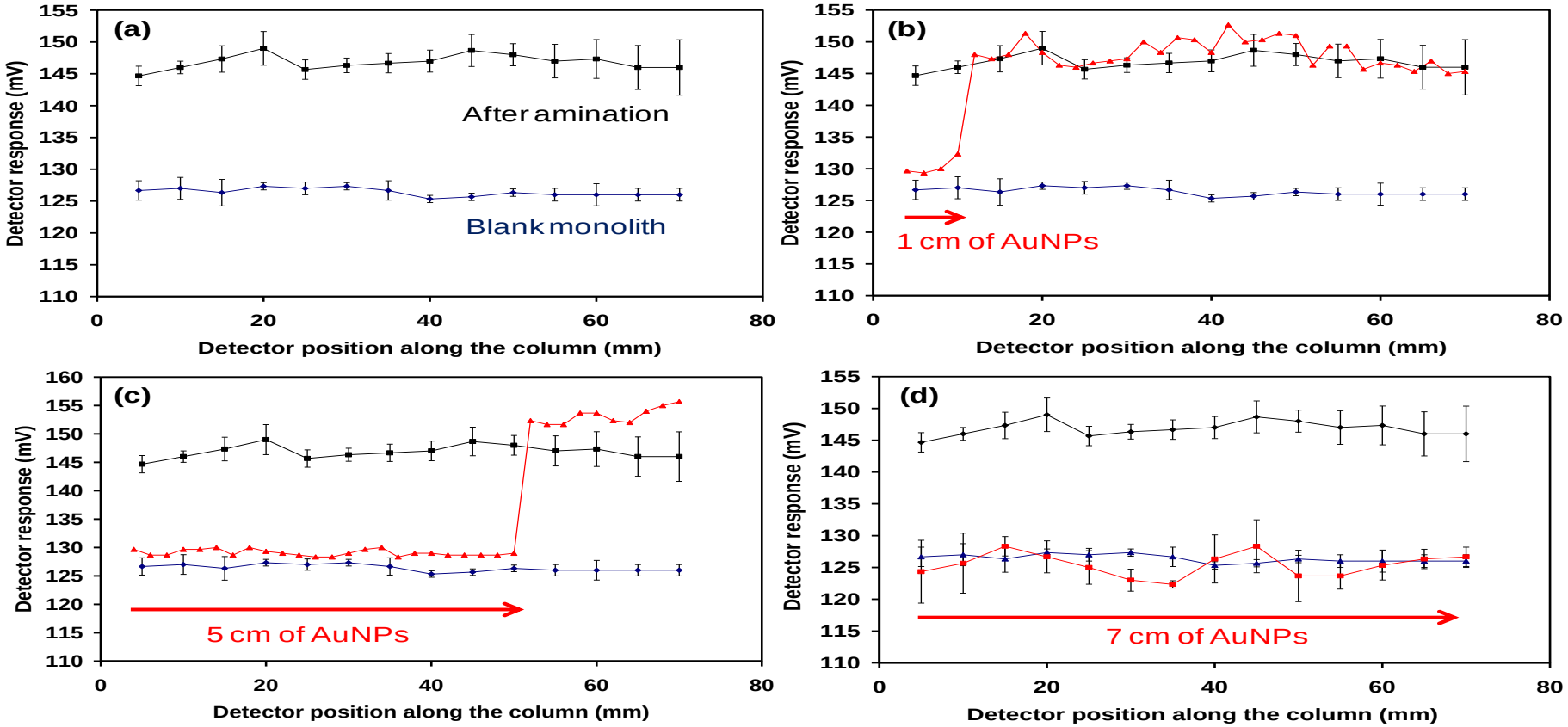

Figure 4.10: *Scanning capacitively coupled contactless conductivity (sC^4D) profiles of (a) a blank LMA-GMA monolith, (b, c and d) after modification with 1, 5, and 7 cm of 16 nm AuNPs for the preparation of monoliths LMA-GMA-16. sC^4D settings: frequency 2x high, voltage 0dB. All measurements were obtained in water.*

An increase in conductive response of 20-30% was observed after the amination of the LMA-GMA monoliths relative to the original sC^4D profiles as shown in Figure 4.10 (a) as described previously by Currivan *et al.* [32] who reported a 33 % increase in conductive response after the amination of similarly prepared monoliths. A straight conductive response was indicative of the homogenous presence of amine groups along the length of the monolith. Since the ionic strength of the colloidal suspension (due to the presence of citrate salts used during the nano-particle synthesis) led to erratic conductive responses, extensive water washing periods were required prior to obtaining stable measurements after the modification with AuNPs. The slow rate of immobilisation of the 16 nm colloidal suspension, allowed the monitoring of the nano-particle plug at several spatial intervals (1, 5 and 7 cm) as shown in Figure 4.10 (b, c and d). This was not possible when using a 7 nm colloidal suspension since the rate of immobilisation of nano-particles was much faster and complete saturation of the column was achieved within a few minutes rather than hours. Nevertheless a sC^4D profile was obtained after the immobilisation of a 7 nm AuNP suspension (Figure 4.11).

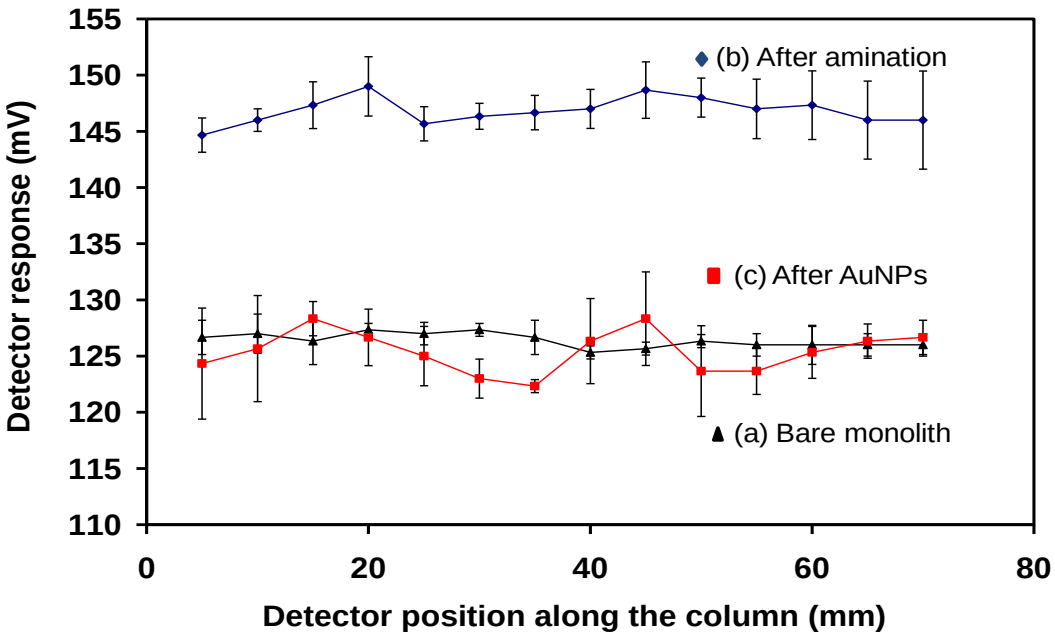

***Figure 4.11**: Scanning capacitively coupled contactless conductivity (sC^4D) profiles of (a) a blank LMA-GMA monolith, (b) same monolith after amination and (c) after modification with 7 nm AuNPs for the preparation of monoliths LMA-GMA-7. sC^4D settings: frequency 2x high, voltage 0dB. All measurements were obtained in water.*

Here a similar decrease in conductivity was observed which returned to the original values prior to amination, indicating an homogeneous presence of nano-particles along the axial length of the monolith. These results indicated the successful interaction of AuNPs with the free amine groups on the surface and demonstrated the usefulness of sC^4D as a non-invasive characterisation tool for confirming the presence of nano-particles irrespective of their size.

4.3.8 Off-line catalytic reduction of Fe(III) to Fe(II) via AuNP agglomerated monolithic tip

The catalytic reduction of ferrocyanide(III) was selected as a model reaction for demonstrating the catalytic properties of the AuNP agglomerated monoliths. Hexacyanoferrate(III) absorbs strongly in the visible spectrum at 420 nm, but when it is reduced to the Fe(II) state, a decrease in absorbance at this wavelength is observed. Initially $NaBH_4$ can inject electrons onto the AuNPs surfaces which can now act as a reservoir. In a second step, ferrocyanide molecules diffuse in and out of the NPs surfaces, gaining electrons and hence being reduced from Fe(III) to Fe(II). As shown in Figure 4.12, a hexacyanoferrate(III) solution in $NaBH_4$ was flushed for 1 hour through monolith EDMA-Tip-16 at a flow rate of 0.25 m*L*/hr. A blank EDMA-Tip monolith, which was not functionalised with AuNPs, was also used for comparative purposes.

Due to the experimental set up it was not possible to determine the operating backpressures at this flow rate. However, no degradation of the monolithic structure and no leakage of nano-particles into the collection vial was observed, indicating that the monolith was well bound to the inner walls of the pipette tip and represented a stable support for the catalyst. The solutions pumped through both monoliths were then collected in micro-cuvettes and UV-Vis spectra were thus obtained and shown in Figure 4.13.

Partial reduction of Fe(III) occurred after 1 hour even with the monolith which did not contain AuNPs due to the reducing activity of borohydrate. However, in the presence of AuNPs the reaction proceeded much faster, supporting the information present in the literature which indicates that the catalysed reaction occurs 4×10^4 times faster than in the absence of a catalyst [38].

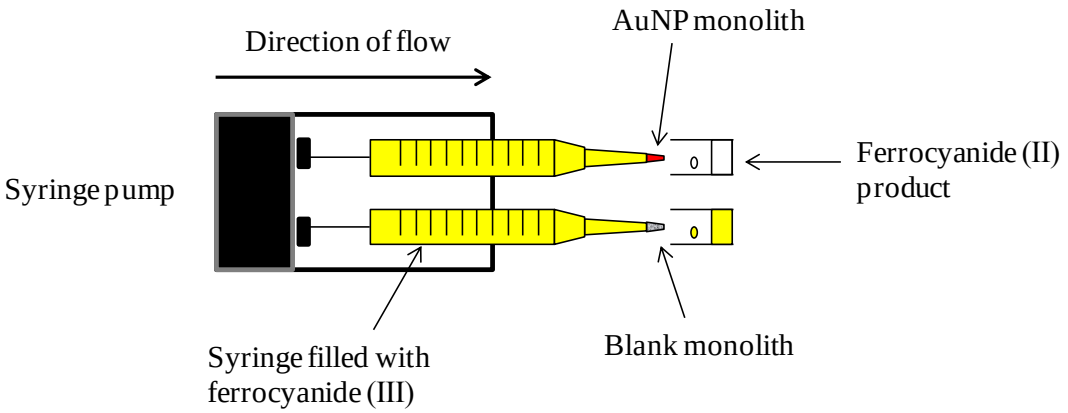

Figure 4.12: *Schematic showing the reduction of ferrocyanate from Fe(III) to Fe(II) on a monolith in a pipette tip modified with 16 nm AuNPs (shown in red on top). A blank monolith which did not contain AuNPs (bottom) is shown for comparative purposes. The colourless product obtained from flushing the ferrocyanide (III) solution (in yellow) through the AuNP-modified monolith was indicative of the successfull catalytic reduction of Fe(III) to Fe(II).*

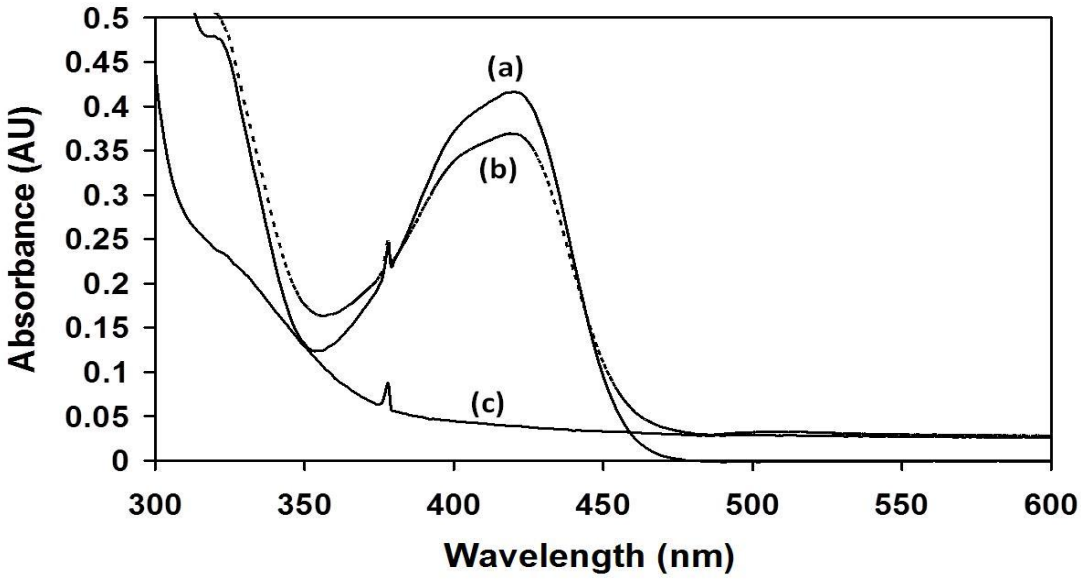

Figure 4.13: *UV spectra showing the reduction of ferrocyanide(III) to ferrocyanide(II) performed on monoliths in pipette-tip format by monitoring the absorbance at 420 nm of (a) an original ferrocyanide(III) with sodium borohydride solution at time 0, (b) the same solution flushed through a blank EDMA-Tip and (c) the solution collected from pumping through monolith EDMA-Tip-16.*

This was also verified by a visual inspection of the product collected since the

ferrocyanate(III) complex was yellow in colour, while the reduced complex was colourless as shown in Figure 4.12. Finally the absence of a peak at 518 nm in Figure 4.13, which is the λ_{max} for a 16 nm AuNP colloidal suspension, indicated that no gold nano-particles were present in the collected product, demonstrating their stability on the surface of the monolith.

4.3.9 On-line catalytic reduction of Fe(III) to Fe(II) via AuNP agglomerated capillary monoliths

The reduction of Fe(III) to Fe(II) was also performed on LMA-GMA monoliths in capillary format which were directly connected to a LC system. The effects of contact time between the analyte and the immobilised catalyst were also evaluated by performing the reaction at 2 different flow rates, 3 and 1 µ*L*/min as shown in Figure 4.14. A calibration plot between 0-17.5 m*M* (see Figure 4.14) was performed at both flow-rates in order to monitor the progress of the reaction quantitatively. Since peak tailing was observed at the lowest flow-rate, peak heights were used to determine the concentrations of Fe(III). It was estimated that by operating at a linear velocity of 15 mm/s (which corresponds to 3 µ*L*/min), the residence time (t) of the analyte inside the nano-particle functionalised monolith would only be limited to 25 seconds. By switching to a linear velocity of 5 mm/s, the residence time (t) was increased by a factor of 3 to 75 seconds. The decrease in ferrocyanide (III) concentration was determined and divided by the residence time which allowed to calculate linearised rates of turnover.

As highlighted in Table 4.4, variations in residence time did not affect reaction yields, since the % of Fe(III) reduced to Fe(II) was calculated to be the same with any of the AuNP functionalised LMA-GMA monoliths, with the exception of monolith LMA-GMA-4 where a slightly higher yield was observed at the highest linear velocity (90% relative to 87%). The linearised rates of turnover suggest that the reduction mechanism proceeds much faster by operating at the higher flow rate. For example with monolith LMA-GMA-7 the rate of reaction increases from 0.06 to 0.19 m$M.s^{-1}$.

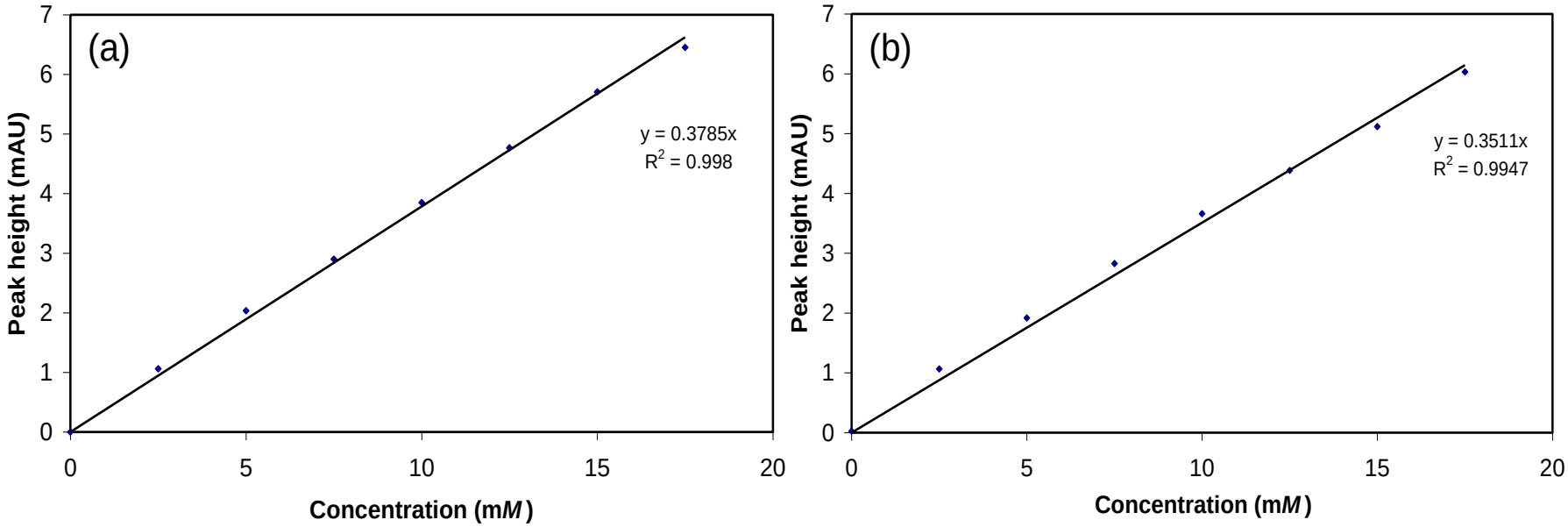

Figure 4.14: *Calibration plots at (a) 1 µL/min and (b) 3 µL/min relating peak height versus concentration for ferrocyanide(III) at 420 nm (0-17.5 mM).*

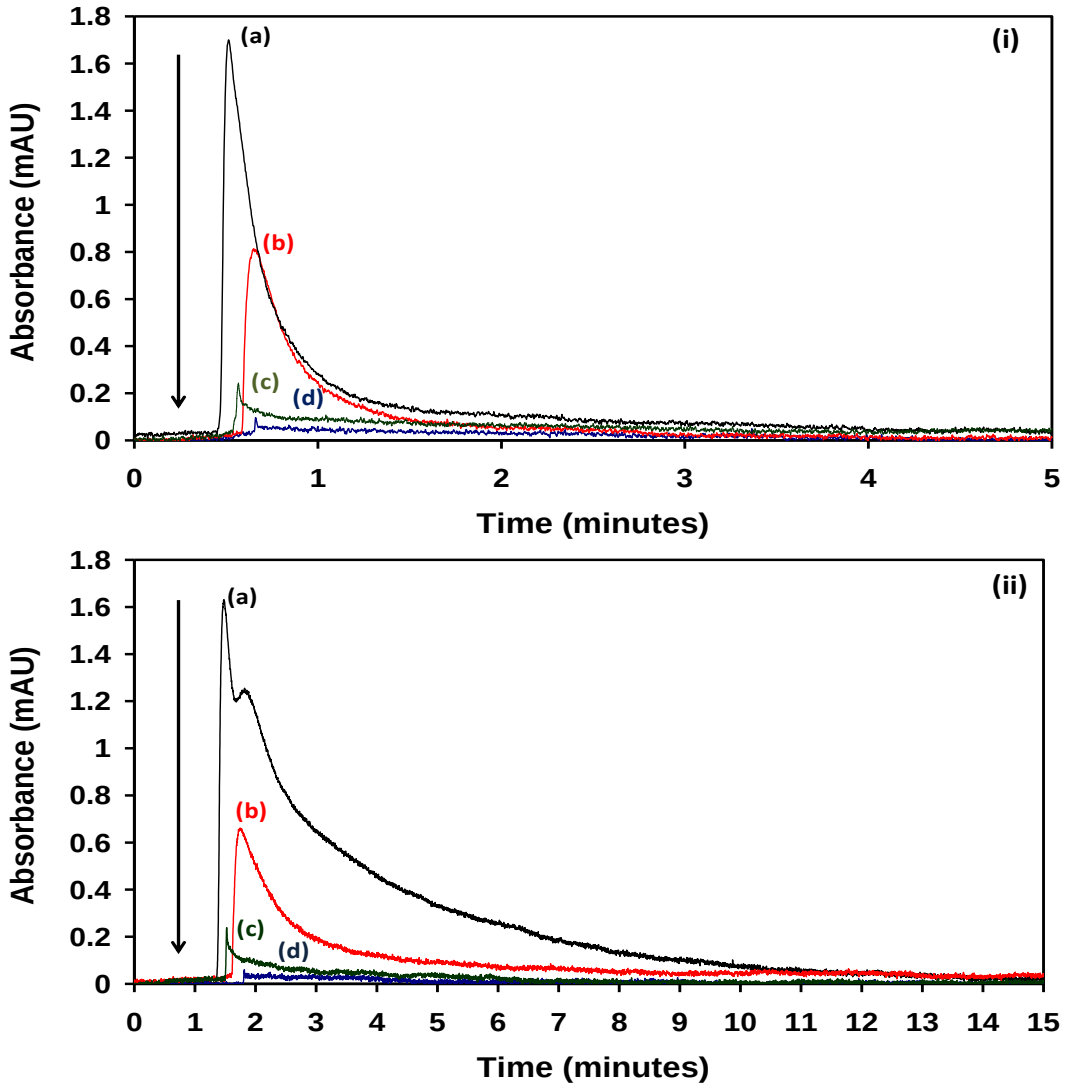

Figure 4.15: *Reduction of ferrocyanide(III) to (II) performed by injecting 100 nL amounts of a ferrocyanide/borohydride mixture at (i) 3 µL/min and (ii) 1 µL/min on (a) a blank LMA-GMA monolith, (b) a LMA-GMA-16 monolith functionalised with 16 nm citrate capped AuNPs, (c) LMA-GMA-4 monolith which contained 4 nm THPC capped AuNPs and (d) LMA-GMA-7 monolith which was functionalised with 7 nm citrate capped AuNPs. UV-Vis detection at 420 nm. Column lengths: 13 cm. Eluent: water.*

In both cases the highest catalytic activity was observed with monoliths LMA-GMA-7, which were functionalised with 7 nm citrate-stabilised AuNPs, followed by monoliths LMA-GMA-4 and LMA-GMA-16. This confirms previous reports in the literature which demonstrated that particles of smaller size can be catalytically more efficient to due their higher surface area [39]. Against this trend however, monoliths

LMA-GMA-4, which were modified with 4 nm THPC-stabilised AuNPs, were found to operate slightly less efficiently than monoliths LMA-GMA-7. The concentration of catalyst present and the different ligand used as the nano-particle capping agent could be possible causes of this phenomenon.

Table 4.4: *Experimental data for the flow-through reduction of hexacyanoferrate(III) on AuNP agglomerated LMA-GMA monoliths.*

	Concentration (m*M*)(*n*=3)	% Fe(III) reduced to Fe(II)	Linearised rate of turnover (m*M*.s^{-1}) $-(M-M_0)/(t-t_0)$
15 mm/s			
LMA-GMA	4.86 ± 0.09	-	
LMA-GMA-16	2.07 ± 0.26	57 %	0.11
LMA-GMA-4	0.49 ± 0.13	90 %	0.17
LMA-GMA-7	0.23 ± 0.05	95 %	0.19
5 mm/s			
LMA-GMA	4.41 ± 0.04	-	
LMA-GMA-16	1.89 ± 0.09	57%	0.03
LMA-GMA-4	0.59 ± 0.00	87%	0.05
LMA-GMA-7	0.23 ± 0.06	95%	0.06

The reduction of ferrocyanide in the presence of AuNPs was found to be dependent on the concentration of catalyst [38], so it is possible that the concentration of 7 nm AuNPs immobilised on the surface of monoliths LMA-GMA-7 is higher than the concentration of 4 nm THPC stabilised AuNPs in monoliths LMA-GMA-4.

Also the catalytic activity of AuNPs can be affected by the type of ligand present on the surface of the nano-particles [40], hence it can be hypothesised that the catalytic activity of AuNPs is enhanced when citrate is used as a capping agent

relative to THPC. The main reason for their inferior catalytic activity however, is more than likely to be related to the tendency of the 4 nm AuNPs here used to aggregate due to their weak repulsive force. This would results in the formation of larger particles which would lead to decreased catalytic properties.

4.4 Conclusions

In this Chapter gold nano-particle agglomerated polymer monoliths were prepared in capillary and polypropylene pipette tip formats. The photografting of reactive monomers upon the surface and the subsequent amination of the moieties present allowed the covalent attachment of AuNPs due to the interaction with the available free amine groups present. The successful modification of the stationary phase with 16 nm AuNPs was confirmed using FE-SEM and EDX techniques. However, these techniques require the destruction of the sample. Alternatively scanning capacitively coupled contactless conductivity detection (sC^4D) proved to be a valuable tool for confirming non-invasively the covalent attachment of nano-particle suspensions independently of their size on polymer monoliths in capillary format. Catalytic applications in flow-through mode using the nano-agglomerated monoliths were performed either off-line in pipette tip format or on-line when connected to a capillary LC system. The catalytic properties of the immobilised AuNPs led to almost complete conversions of Fe(III) to Fe(II) (up to 95% with monolith LMA-GMA-7). The use of monolithic supports in capillary format allowed the processing of n*L* amounts of materials and led to considerable shortened analysis times indicating that this AuNP-modified monolith could have potential application in liquid chromatography for pre- or post-column reactions if positioned upstream or downstream of an analytical column.

4.5 References

1. Cao, A.; Lu, R.; Veser, G. Stabilizing metal nanoparticles for heterogeneous catalysis. *Physical Chemistry Chemical Physics* **2010,** *12* (41), 13499-13510.

2. Kelly, K. L.; Coronado, E.; Zhao, L. L.; Schatz, G. C. The optical properties of metal nanoparticles: The influence of size, shape, and dielectric environment. *Journal of Physical Chemistry B* **2003,** *107* (3), 668-677.

3. Chatterjee, A.; Chakravorty, D. Electrical-conductivity of sol-gel derived metal nanoparticles. *Journal of Materials Science* **1992,** *27* (15), 4115-4119.

4. Corma, A.; Garcia, H. Supported gold nanoparticles as catalysts for organic reactions. *Chemical Society Reviews* **2008,** *37* (9), 2096-2126.

5. Thompson, D. T. Using gold nanoparticles for catalysis. *Nano Today* **2007,** *2* (4), 40-43.

6. Ishida, T.; Haruta, M. Gold catalysts: towards sustainable chemistry. *Angewandte Chemie-International Edition* **2007,** *46* (38), 7154-7156.

7. Shi, F.; Zhang, Q. H.; Ma, Y. B.; He, Y. D.; Deng, Y. Q. From CO oxidation to CO2 activation: an unexpected catalytic activity of polymer-supported nanogold. *Journal of the American Chemical Society* **2005,** *127* (12), 4182-4183.

8. Wu, P. P.; Xiong, Z. G.; Loh, K. P.; Zhao, X. S. Selective oxidation of cyclohexane over gold nanoparticles supported on mesoporous silica prepared in the presence of thioether functionality. *Catalysis Science & Technology* **2011,** *1* (2), 285-294.

9. Li, L.; Ji, W. J.; Au, C. T. Gold nanoparticles supported on mesoporous silica and their catalytic application. *Progress in Chemistry* **2009,** *21* (9), 1742-1749.

10. Downard, A. J.; Tan, E. S. Q.; Yu, S. S. C. Controlled assembly of gold nanoparticles on carbon surfaces. *New Journal of Chemistry* **2006,** *30* (9), 1283-1288.

11. Haruta, M. Catalysis of gold nanoparticles deposited on metal oxides. *Cattech* **2002,** *6* (3), 102-115.

12. Lin, S. D.; Bollinger, M.; Vannice, M. A. Low-temperature co oxidation over Au/Tio2 and Au/Sio2 catalysts. *Catalysis Letters* **1993,** *17* (3-4), 245-262.

13. Caballero, C.; Valencia, J.; Barrera, M.; Gil, A. Selective hydrogenation of citral over gold nanoparticles on alumina. *Powder Technology* **2010,** *203* (2), 412-414.

14. Ho, C. M.; Yu, W. Y.; Che, C. M. Ruthenium nanoparticles supported on

hydroxyapatite as an efficient and recyclable catalyst for cis-dihydroxylation and oxidative cleavage of alkenes. *Angewandte Chemie-International Edition* **2004,** *43* (25), 3303-3307.

15. Zhang, J.; Han, D.; Zhang, H.; Chaker, M.; Zhao, Y.; Ma, D. In situ recyclable gold nanoparticles using CO2-switchable polymers for catalytic reduction of 4-nitrophenol. *Chemical Communications* **2012,** *48* (94), 11510-11512.

16. Liapis, A. I.; Grimes, B. A. The effect of the pore structure and zeta potential of porous polymer monoliths on separation performance in ion-exchange mode. *Journal of Separation Science* **2007,** *30* (5), 648-657.

17. Krenkova, J.; Lacher, N. A.; Svec, F. Control of selectivity via nanochemistry: monolithic capillary column containing hydroxyapatite nanoparticles for separation of proteins and enrichment of phosphopeptides. *Analytical Chemistry* **2010,** *82* (19), 8335-8341.

18. Alwael, H.; Connolly, D.; Clarke, P.; Thompson, R.; Twamley, B.; O'Connor, B.; Paull, B. Pipette-tip selective extraction of glycoproteins with lectin modified gold nano-particles on a polymer monolithic phase. *Analyst* **2011,** *136* (12), 2619-2628.

19. Lv, Y. Q.; Alejandro, F. M.; Frechet, J. M. J.; Svec, F. Preparation of porous polymer monoliths featuring enhanced surface coverage with gold nanoparticles. *Journal of Chromatography A* **2012,** *1261*, 121-128.

20. Connolly, D.; Twamley, B.; Paull, B. High-capacity gold nanoparticle functionalised polymer monoliths. *Chemical Communications* **2010,** *46* (12), 2109-2111.

21. Cao, Q.; Xu, Y.; Liu, F.; Svec, F.; Frechet, J. M. J. Polymer monoliths with exchangeable chemistries: use of gold nanoparticles as intermediate ligands for capillary columns with varying surface functionalities. *Analytical Chemistry* **2010,** *82* (17), 7416-7421.

22. Xu, Y.; Cao, Q.; Svec, F.; Frechet, J. M. J. Porous polymer monolithic column with surface-bound gold nanoparticles for the capture and separation of cysteine-containing peptides. *Analytical Chemistry* **2010,** *82* (8), 3352-3358.

23. Frens, G. Controlled nucleation for regulation of particle-size in monodisperse gold suspensions. *Nature-Physical Science* **1973,** *241* (105), 20-22.

24. He, P.; Zhu, X. Phospholipid-assisted synthesis of size-controlled gold nanoparticles. *Materials Research Bulletin* **2007,** *42* (7), 1310-1315.

25. Duff, D. G.; Baiker, A.; Edwards, P. P. A new hydrosol of gold clusters .1. formation and particle-size variation. *Langmuir* **1993,** *9* (9), 2301-2309.

26. Riddick, T. M.; Ravina, L. A. Correspondence - Electrophoresis. *Industrial & Engineering Chemistry* **1970,** *62* (7), 70-73.

27. Gibson, M. I.; Danial, M.; Klok, H. A. Sequentially modified, polymer-stabilized gold nanoparticle libraries: convergent synthesis and aggregation behavior. *Acs Combinatorial Science* **2011,** *13* (3), 286-297.

28. Liu, X. O.; Atwater, M.; Wang, J. H.; Huo, Q. Extinction coefficient of gold nanoparticles with different sizes and different capping ligands. *Colloids and Surfaces B-Biointerfaces* **2007,** *58* (1), 3-7.

29. Altun, Z.; Skoglund, C.; Abdel-Rehim, M. Monolithic methacrylate packed 96-tips for high throughput bioanalysis. *Journal of Chromatography A* **2010,** *1217* (16), 2581-2588.

30. Stachowiak, T. B.; Rohr, T.; Hilder, E. F.; Peterson, D. S.; Yi, M. Q.; Svec, F.; Frechet, J. M. J. Fabrication of porous polymer monoliths covalently attached to the walls of channels in plastic microdevices. *Electrophoresis* **2003,** *24* (21), 3689-3693.

31. Urban, J.; Eeltink, S.; Jandera, P.; Schoenmakers, P. J. Characterization of polymer-based monolithic capillary columns by inverse size-exclusion chromatography and mercury-intrusion porosimetry. *Journal of Chromatography A* **2008,** *1182* (2), 161-168.

32. Currivan, S. a.; Connolly, D.; Paull, B. Production of polymer monolithic capillary columns with integrated gold nano-particle modified segments for on-capillary extraction. *Microchemical Journal* **2013,** *111* (0), 32-39.

33. Yang, W. T.; Ranby, B. Bulk surface photografting process and its applications

.2. Principal factors affecting surface photografting. *Journal of Applied Polymer Science* **1996,** *62* (3), 545-555.

34. Cuatreca, P.; Parikh, I. Adsorbents for Affinity Chromatography - Use of N-Hydroxysuccinimide Esters of Agarose. *Biochemistry* **1972,** *11* (12), 2291-2299.

35. Lomant, A. J.; Fairbanks, G. Chemical Probes of Extended Biological Structures - Synthesis and Properties of Cleavable Protein Cross-Linking Reagent [Dithiobis(Succinimidyl-S-35 Propionate). *Journal of Molecular Biology* **1976,** *104* (1), 243-261.

36. Staros, J. V. N-Hydroxysulfosuccinimide Active Esters - Bis(N-Hydroxysulfosuccinimide) Esters of 2 Dicarboxylic-Acids Are Hydrophilic, Membrane-Impermeant, Protein Cross-Linkers. *Biochemistry* **1982,** *21* (17), 3950-3955.

37. Elwazri, A. M.; Varano, R.; Siciliano, F.; Gauvin, R.; Yue, S. Microanalysis of very fine precipitates by FE-SEM. *Microscopy and Microanalysis* **2005,** *11* (Supplement S02), 1298-1299.

38. Carregal-Romero, S.; Perez-Juste, J.; Herves, P.; Liz-Marzan, L. M.; Mulvaney, P. Colloidal gold-catalyzed reduction of ferrocyanate (III) by borohydride ions: a model system for redox catalysis. *Langmuir* **2010,** *26* (2), 1271-1277.

39. Zhou, X. C.; Xu, W. L.; Liu, G. K.; Panda, D.; Chen, P. Size-dependent catalytic activity and dynamics of gold nanoparticles at the single-molecule level. *Journal of the American Chemical Society* **2010,** *132* (1), 138-146.

40. Biswas, M.; Dinda, E.; Rashid, M. H.; Mandal, T. K. Correlation between catalytic activity and surface ligands of monolayer protected gold nanoparticles. *Journal of Colloid and Interface Science* **2012,** *368*, 77-85.

Chapter 5: Nano-agglomerated polymer monoliths as stationary phases in liquid chromatography

Abstract

Agglomerated polymer monoliths functionalised with 16 nm gold nano-particles (AuNPs) were prepared as described in Chapter 4 and applied for capillary LC applications. Selected alkylamines or alkanethiols were used for the modification of AuNP-functionalised monoliths and a reversed-phase separation of alkylbenzenes was used to evaluate the properties of the stationary phases. Poor chromatographic efficiency was observed after modification with AuNPs due to reduced hydrophobicity. For example the retention factor of pentylbenzene decreased from 8.8 to 3.5. Partial modification with alkylamine chains led to small improvements in hydrophobicity as confirmed by the increase in retention factor for pentylbenzene to 3.7. Similar monoliths were modified with sodium-2-mercaptoethanesulphonate in order to be applied to cation-exchange separations. A higher ion-exchange capacity was observed after the modification with sulphonate groups (from 1.1 to 4.2 nequiv/column) which led to the retention of Ca^{2+}. Finally, novel silica-polymer nano-composites comprising a 100 nm silica core and grafted poly(acrylic acid) brushes bearing weak acid functional groups were electrostatically attached to a quaternary ammonium functionalised polymer monolith. The successful attachment of the nano-particles was confirmed by the loss of retention for a previously separated mixture of Cl^- and $H_2PO_4^-$, and demonstrated retention of Mg^{2+} and Ca^{2+} using an ethylenediamine/phthalic acid eluent (with efficiencies of up to 7,800 N/m for Mg^{2+}). Scanning capacitively coupled contactless conductivity detection (sC^4D) was also used to confirm non-invasively the successful functionalisation of the stationary phase by monitoring the movement of the nano-particle plug as it progressed along the column at 2, 6 and 10 cm intervals.

Aims

The aim of this Chapter was to illustrate the chromatographic properties of nano-agglomerated stationary phases in reversed-phase and ion-exchange chromatography for the separation of small molecules.

5.1 Introduction

The use of nano-particles, and specifically metallic nano-particles, in spectroscopy, electrochemistry and sensors is an area which has received considerable attention over the past decade and more [1-5]. In LC methods, less utility of metallic nano-particles has been demonstrated, although as the following studies show, metal nano-particles also exhibit unique properties and selectivity, which are gaining the attention of the chromatographic community.

Few reports illustrate the modification of particular and monolithic stationary phases with metal nano-particles [6]. Most of those which do are focused in particular on the use of gold nano-particles (AuNPs). Some of the earliest work in this area was carried out by Ortiz *et al.* [7] who investigated the covalent attachment of 1-mercaptoundec-11-yl diethylene glycol chains to a AuNP modified silica stationary phase, forming what can be described as a 'self-assembled monolayer' (SAM) type stationary phase. This idea was extended several years later with a more comprehensive examination of selectivity differences between similar SAM type stationary phases and conventional ODS stationary phases carried out by Kobayashi *et al*. [8]. In this instance, the authors used a stationary phase based upon commercially available gold-coated 5 µm polystyrene (PS) particles, however, the preparation procedure for this supporting material was proprietary information and thus not revealed. After modification with *n*-octadecanethiol, thiophenol or 2-phenylethanethiol in ethanol, the resulting SAM stationary phases were packed within 150 µm i.d. fused silica capillaries. Using water/MeOH or water/ACN mobile phases, the retention of different aromatic compounds was studied in comparison with a 5 µm Develosil ODS-5 column of the same dimensions. A unique selectivity was noted when thiol-modified AuNP-coated PS particles was used as the stationary phase. In particular a higher affinity for anthracene and phenanthrene over smaller aromatic molecules relative to a traditional ODS column was observed, with a distinguishable increase in shape selectivity for the two analytes using an *n*-octadecanethiol-AuNP column, which the authors proposed was due to the high density of *n*-octadecanethiol on the gold surface. Asymmetric peak shapes were however, observed with this column as shown in Figure 5.1, indicating a possible adsorption of analytes on the hydrophobic suface of the PS particles. No retention of anthracene and phenanthrene was observed on a capillary column packed with

unmodified PS-AuNP particles. Lower retention of the *n*-octadecanethiol-AuNP column relative to the silica-based ODS-5 column was attributed to the lower surface area of the underlying polystyrene particle.

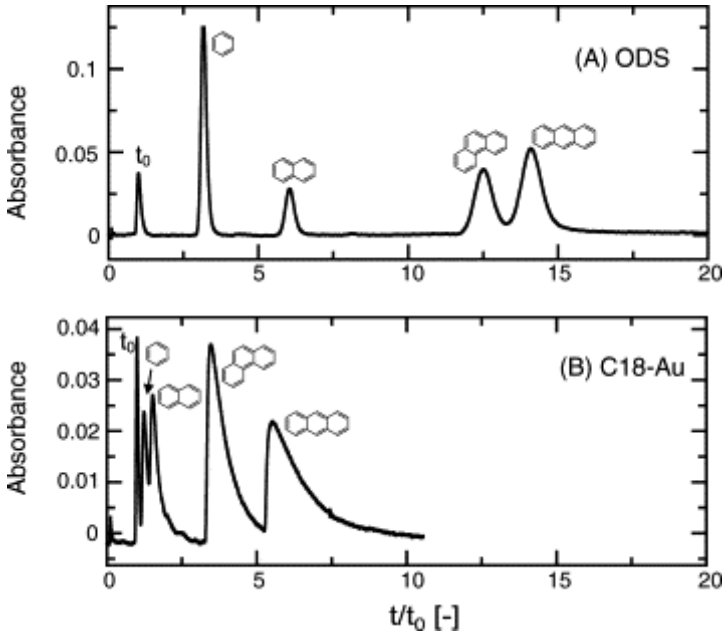

Figure 5.1*: Separation of aromatic compounds using (A) ODS and (B) C18-Au columns. Samples: uracil* (t_0)*, benzene, naphthalene, phenanthrene, and anthracene. ODS column: i.d. 0.15 mm, length 100 mm; C18-Au column: i.d. 0.15 mm, length 130 mm. Eluent: acetonitrile/water (50:50, v/v). UV detection at 254 nm [8].*

More recently, Qu *et al.* [9] used 4-12 nm AuNPs to modify non-porous ~ 1 µm silica particles. The AuNPs were immobilised following amination of the silica particles using 3-aminopropyltrimethoxysilane, and were subsequently further functionalised with *n*-octadecanethiol. The modified particles were packed within capillary columns and evaluated for chromatographic performance and selectivity using both capillary RP-HPLC and CEC. Reasonable peak efficiencies for the RP-HPLC separations were shown, with for example up to 61,000 N/m for benzene, although the system was not optimised for pressure and flow, indicating that greater efficiencies were possible, as might be expected for such sub-2 µm phases.

As described previously in Chapter 4, polymer monoliths have also been modified with AuNPs and applications in SPE [10-12] and capillary HPLC have been reported. Recently Cao *et al.* [13] applied AuNP-modified monoliths for the separation of three selected proteins, as shown in Figure 5.2, which were practically

unretained upon both the bare and gold modified monoliths. However, the further modification of the AuNP monolith with 1-octadecanetihol resulted in a significant increase in retention and a reasonably efficient separation of the three proteins in under 6 minutes using an acetonitrile gradient.

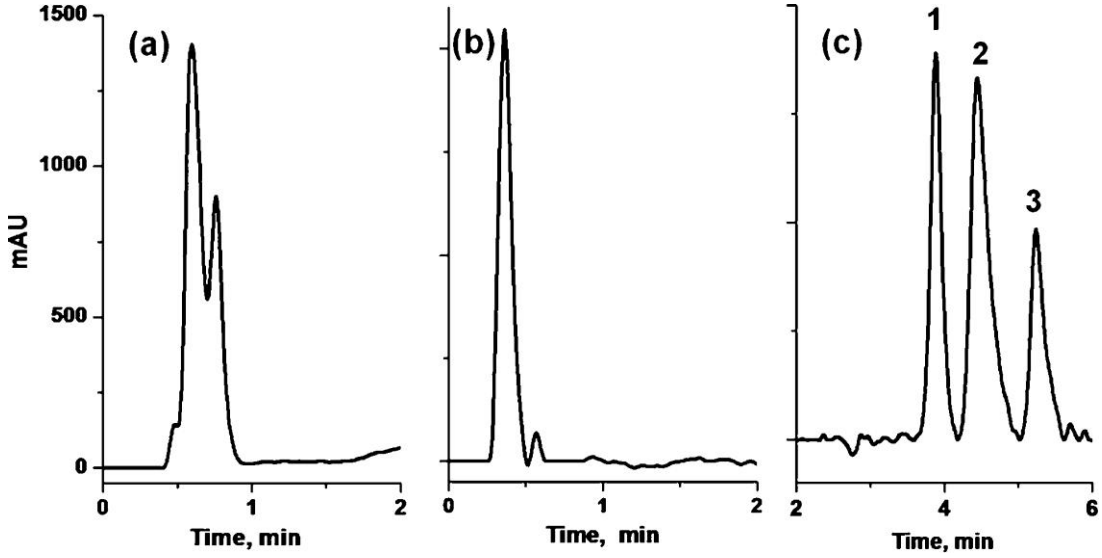

***Figure 5.2**: Reversed-phase separation of proteins using generic monolithic poly(glycidyl methacrylate-co-ethylene dimethacrylate) column (a), poly(glycidyl methacrylate-co-ethylene dimethacrylate) column with attached gold nanoparticles (b), and the latter modified with 1-octadecanethiol (c). Conditions: column 10 cm × 100 µm i.d., mobile phase A 0.1% aqueous formic acid, mobile phase B 0.1% formic acid in acetonitrile, gradient from 0 to 35% B in A in 5.2 min, flow-rate 2.5 µL/min, injection volume 100 nL, UV detection at 210 nm. Peaks: ribonuclease A (1), cytochrome c (2), myoglobin (3) [13].*

The versatility of this gold/thiol chemistry was further demonstrated by the authors via flushing a second AuNP modified monolith with 2-mercaptoethanesulphonate, this time producing an ion-exchange surface, which allowed the separation of the same three proteins using a NaCl gradient showing a totally different retention selectivity.

In a later study from the same group, Lv *et al*. [14], have reported applications of AuNP-agglomerated monoliths in hydrophilic interaction liquid chromatography (HILIC) mode to the separation of a number of nucleosides upon functionalisation of AuNPs with cysteine. However, the retention and separation of nucleosides was

improved substantially through the use of a polyethyleneimine (PEI) layer laid down upon the first AuNP layer, in place of cysteine. The resulting AuNP modified polymer monolith exhibited excellent performance, with the HILIC based separation of 8 peptides in under 10 minutes, using an ACN gradient. Most recently, Lv *et al.* [15] also reported the functionalisation of GMA-*co*-EDMA monoliths with AuNPs of different sizes (between 5 and 40 nm) and applied these for the separation of proteins in reversed-phase mode after modification of AuNPs with either 1-octanethiol or 1-octadecanthiol. The best separation were obtained using monoliths modified with 15, 20 and 30 nm AuNPs, since these sizes produced the most dense coverage of AuNPs.

Published material which focuses on the application of silica nano-particles (SiNPs) in LC is not available to the same extent as metallic nano-particles mainly due to issues related to hydrolytic and structural stability but also possibly due to the huge success of superficially porous micro-particle silica (core-shell silica gels). Some reports however, have recently emerged describing the formation of silica 'nano-templated' monoliths designed for in-line SPE-CZE of basic analytes [16] which have been previously discussed in Section 1.8.6.

In the work described herein, polymer monoliths in capillary format were modified with AuNPs and poly(acrylic acid)-grafted SiNPs (PAA-SiNPs) for chromatographic applications in reversed-phase and ion-exchange modes. Bare AuNPs are not suitable for applications in chromatography hence further functionalisation of their surface was performed with alkyl chains such as octadecanthiol to increase their hydrophobicity or with charged functionalities such as sulphonate groups to allow ion-exchange applications. Similarly, PAA-SiNPs demonstrated cation-exchange properties due to the presence of carboxyate functionalities. Chromatographic performance of the monolithic stationary phases was evaluated before and after the modification with the nano-materials mentioned above. The characterisation of the stationary phases by sC^4D also allowed the visualisation of the immobilised nano-particles on the surface.

5.2 Experimental

5.2.1 Instrumentation

The instrumentation used was as described in Sections 2.2.1, 3.2.1 and 4.2.1.

5.2.2 Materials and reagents

The materials used were as described in Sections 2.2.2, 3.2.2 and 4.2.2 with the following additions. Uracil. ethylbezene, propylbenzene, butylbenzene, pentylbenzene, 2-mercaptoethane sulphonate, 1-octadecanethiol, octadecylamine, copper (II) sulphate pentahydrate, calcium chloride, magnesium perchlorate, disodium hydrogen phosphate, iodoethane, nitromethane and diethylamine were purchased from Sigma-Aldrich (Dublin, Ireland, www.sigmaaldrich.com). Chloroform was purchased from Labscan (Gliwice, Poland). All mobile phases were filtered and degassed prior to use.

5.2.3 Preparation of AuNP-agglomerated polymer monoliths

Fused silica capillary was silanised as described in Chapter 2, Section 2.2.4. Monoliths LMA-*co*-EDMA were prepared as described in Chapter 4, Section 4.2.5. A 15% GMA solution in methanol was photografted using a two-step process using benzophenone as initiator and aminated with ethylenediamine by constant pumping over 24 hours at 70 °C as described in Section 4.2.6. Modification with 16 nm citrate stabilised AuNPs, which were prepared using the Frens method as described in Section 4.2.7, was performed as described in Section 4.2.8.

5.2.4 Separation of alkylbenzenes

A test mixture of alkylbenzenes was used to evaluate the chromatographic properties of the monolithic columns. Individual stock solutions of 1000 ppm uracil (unretained marker), ethylbenzene, propylbenzene and pentylbenzene were prepared in methanol. These were diluted to 100 ppm using 50/50 ACN/H_2O as diluent. van Deemter curves were plotted by injecting 100 nL amounts at flow-rates between 0.05-3.6 µL/min, using UV detection at 220 nm.

5.2.5 Phase-transfer of citrate-stabilised AuNPs to organic media in solution

The phase transfer of citrate-stabilised AuNPs from aqueous media to organic media was performed as reported by Karg *et al*. [17]. In two separate 5 m*L* glass vials, 2 m*L* aliquots of the colloidal suspension of 16 nm AuNPs (prepared as described in Section 4.2.7) were mixed with either a 2 m*L* aliquot of 0.75 m*M* octadecylamine solution in chloroform or a 0.75 m*M* 1-octadecanethiol solution in chloroform. Both solutions were mixed vigorously for 1 minute and allowed to stand for 30 seconds.

5.2.6 Modification of AuNP-agglomerated monoliths with alkyl chains for reversed-phase LC applications

Monoliths, prepared as described in Section 5.2.3, were initially rinsed with IPA for 30 minutes at 1 µ*L*/min. A 1 m*M* 1-octadecanethiol solution in chloroform was prepared and flushed through the AuNP agglomerated polymer monoliths in both directions for 18 hours at 1 µL/min, followed by a final chloroform rinse. The alkylbenzenes test mixture prepared in Section 5.2.4 was used to evaluate the chromatographic properties of the octadecanethiol-modified monolith. Subsequently, the modification with a 1 m*M* octadecylamine in chloroform was performed under identical conditions as mentioned above. The chromatographic properties were evaluated using the previously prepared test mixture of alkylbenzenes.

5.2.7 Modification of AuNP agglomerated monoliths for ion-exchange applications

Similar AuNP-agglomerated monoliths prepared as described in Section 5.2.3 were modified with a 50 m*M* sodium 2-mercaptoethanesulphonate solution in water for a 18 hour period at 1µ*L*/min in both directions followed by a final water rinse.

5.2.7.1 Determination of ion-exchange capacity of AuNP-agglomerated monoliths

The ion-exchange capacity of AuNP agglomerated monoliths was determined before and after modification with negatively charged sulphonate groups using calcium adsorption/desorption. The columns were loaded with 100 ppm Ca^{2+} until saturation.

The columns were then washed with water to remove interstitial Ca^{2+} and the bound calcium was eluted using a 0.5 m*M* $CuSO_4$ eluent and determined by UV absorbance at 210 nm due to the absorbance of Cu^{2+} at that wavelength.

5.2.8 Ion-exchange applications of AuNP-agglomerated monoliths

The presence of negatively charged sulphonate groups on the surface allowed cation-exchange applications which were demonstrated by injection 100 n*L* amounts of a 100 ppm Mg^{2+} and Ca^{2+} solution using a $CuSO_4$ eluent at various concentrations (0.5-5 m*M*) with UV detection at 210 nm.

5.2.9 Synthesis of poly(acrylic acid) grafted silica nano-particles (PAA-SiNPs)

Bare silica nano-particles were initially prepared[a] by a modified Stöber method [18] by controlled hydrolysis and condensation of tetraethyl *ortho*-silicate (TEOS) in a ethanol/water mixture under alkaline conditions. The silanol groups (Si-OH) on the surface of the Si-NPs were treated with a newly synthesised molecule, a silane coupling agent (SCA), shown in red in Figure 5.3, by a click chemistry approach. The SCA is able to link chemically on the SiNPs surface an initiator for radical polymerisations. The initiator-decorated SiNPs are so processed by Activators Re-Generated by Electron Transfer-Atom Transfer Radical Polymerization (ARGET-ATRP). Using the catalyst Cu(I)/*N,N,N′,N′,N′′*-pentamethyldiethylenetriamine (PMDETA) and *t*-BMA as a monomer in toluene and in oxygen free conditions at 45 °C, it was possible to synthesise the poly(*tert*-butyl acrylate) (p-tBA) brush-decorated SiNPs. An acidic treatment removes the *tert*-butyl protecting groups resulting in free poly(acrylic acid) linear chains on the Si-NPs surface (SiNPs/PAA).

[a]*Prepared by Marcello Iacono, a collaborator from the ISSC.*

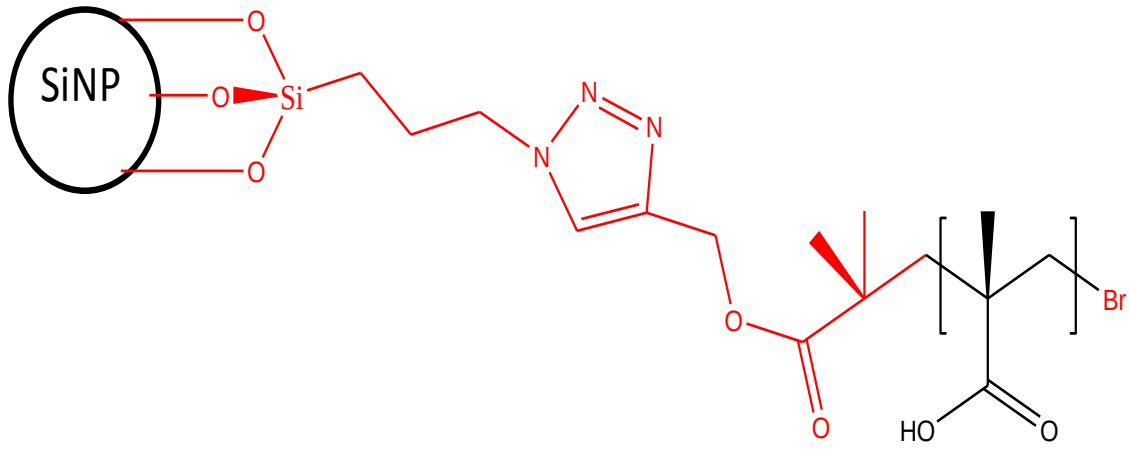

***Figure** 5.3: Structure of PAA-grafted SiNPs.*

5.2.10 Preparation of SiNP-agglomerated polymer monoliths

Monoliths LMA-*co*-EDMA were prepared as described in Section 4.2.5. GMA was photografted using a two-step process using benzophenone as initiator as described in Section 4.2.6. Functionalisation with quaternary ammonium groups (NR_4^+) was performed according to a two-step procedure described by Krenkova and Foret [19]. An aqueous 1 *M* diethylamine solution was pumped through for 1 hour after which the monolith was sealed and placed in a water bath at 70 °C for 7 hours. The column was then washed with water for 1 hour and a 1:1 (v/v) mixture of iodoethane:nitromethane was pumped through for 1 hour after which the monolith was sealed and placed in a water bath at 80 °C for 5 hours. A final wash in ethanol (for 2 hours) and water (overnight) was performed at 1 µ*L*/min.

A 200 µL amount of the SiNP suspension prepared in Section 5.2.9 was filled in a PEEK loop which was connected to a Knauer HPLC pump and pumped through the quaternary ammonium functionalised polymer monoliths at 1 µL/min.

5.2.11 Ion-exchange applications of SiNP-agglomerated polymer monoliths

The ion-exchange properties of the SiNP agglomerated polymer monoliths were evaluated before and after the attachment of the SiNPs. Quaternary ammonium functionalised (NR_4^+) monoliths were initially used as anion-exchangers. A mixture of Cl^- and $H_2PO_4^-$ (10 ppm) was separated using a 0.25 m*M* phthalic acid eluent at 1 µ*L*/min titrated to p*H* 6.5 with 0.25 m*M* ethylenediamine (100 n*L* injections). Non-

suppressed C^4D detection was used with an effective column length of 12 cm. After the modification with PAA-SiNPs, retention of cations Mg^{2+} (10 ppm) and Ca^{2+} (100 ppm) (100 n*L* injections) was observed using a 0.5 m*M* ethylenediamine eluent titrated to p*H* 6.5 with 0.5 m*M* phthalic acid at a flow-rate of 1 µ*L*/min.

5.3 Results and discussion

5.3.1 Chromatographic evaluation of AuNP-agglomerated polymer monoliths

5.3.1.1 Reserved-phase applications of AuNP-agglomerated polymer monoliths

Traditionally the application of polymer monoliths in liquid chromatography has been restricted mainly to large molecules due to the limited surface area present. More recently, the modification of monolithic stationary phases with nano-particles has been reported as an alternative route to increase the surface area which would led to improved mass transfer effects and theoretically more efficient columns. Reversed-phase applications of AuNP-modified stationary phases have recently appeared in the literature, generally involving the functionalisation of the AuNPs with long alkyl chains such as octadecanethiol or octadecylamine by availing of the affinity of gold for amino/thiol functionalities. Such modifications have also been reported on AuNP-functionalised polymer monoliths for the separation of proteins [13] however, in this Chapter, the chromatographic behaviour of similar monolithic stationary phases is evaluated in the presence of small molecules.

In Chapter 4, the fabrication of AuNP-modified LMA-*co*-EDMA monoliths was optimised and a very dense coverage of 16 nm AuNPs was achieved. Herein, these monoliths were selected for further modification with octadecanethiol and octadecylamine, by availing of the affinity of gold for amino and thiol functionalities, in order to increase the hydrophobicity of the stationary phase for applications in reversed-phase chromatography.

The choice of stabilising ligand used in the preparation of nano-particles is an important parameter that must be selected depending on the desired application of these materials. Citrate-stabilised AuNPs are characterised by a negative charge

around the surface, as demonstrated by zeta potential studies in Section 4.3.2, hence they are hydrophilic in nature. In order to convert these materials from hydrophilic to hydrophobic, it is necessary to introduce hydrophobic functionalities on the surface of the AuNPs by replacing the negatively charged citrate ions with long hydrophobic alkyl chains which would stabilise the AuNPs in the new organic solvent (such as chloroform) and prevent particle aggregation.

The initial tests were carried out in aqueous solutions in order to establish wether a phase transfer would occur under the same conditions in the gold-coated monoliths. The phase transfer of 16 nm citrate-stabilised AuNPs to organic media was performed as described by a procedure from Karg *et al*. [17], using solutions of octadecanethiol and octadecylamine in chloroform. Surprisingly, the phase transfer with octadecanethiol did not proceed at all despite the well known affinity of gold for thiol moieties [20].

It is widely accepted that the formation of Au-S bonds is dependant on two types of interactions. The first type requires the initial deprotonation of the SH functionalities leading to the formation of the thiyl radical which can form strong covalent bonds with gold. Since the p*H* of the aqueous AuNP suspension was found to be 9.5, the deprotonation of the thiol groups at the interface of the aqueous/organic layer was not favourable (pK_a values of alkylthiols are between 10-11). The second type of Au-S interactions involves weaker coordination-type bonds between the protonated SH groups and gold through the sulphur lone-pair electrons. In this case however, the SH groups of octadecanethiol are known to have insufficient polarity to be compressed at the aqueous/chloroform interface [21] hence no interaction can occur with the AuNPs in the aqueous phase.

A different scenario was observed when amine-functionalised alkyl chains were used instead. The amphiphilic character of octadecylamine [17] reduced the surface energy of the aqueous/organic solvent interface and allowed NH_2-Au interactions via the nitrogen lone-pair electrons. A partial phase transfer, as shown in Figure 5.4, was observed since the organic layer at the bottom of the vial turned into a faint pink colour after vigorous shaking, which facilitated the citrate-octadecylamine ligand exchange process on the surface of the AuNPs.

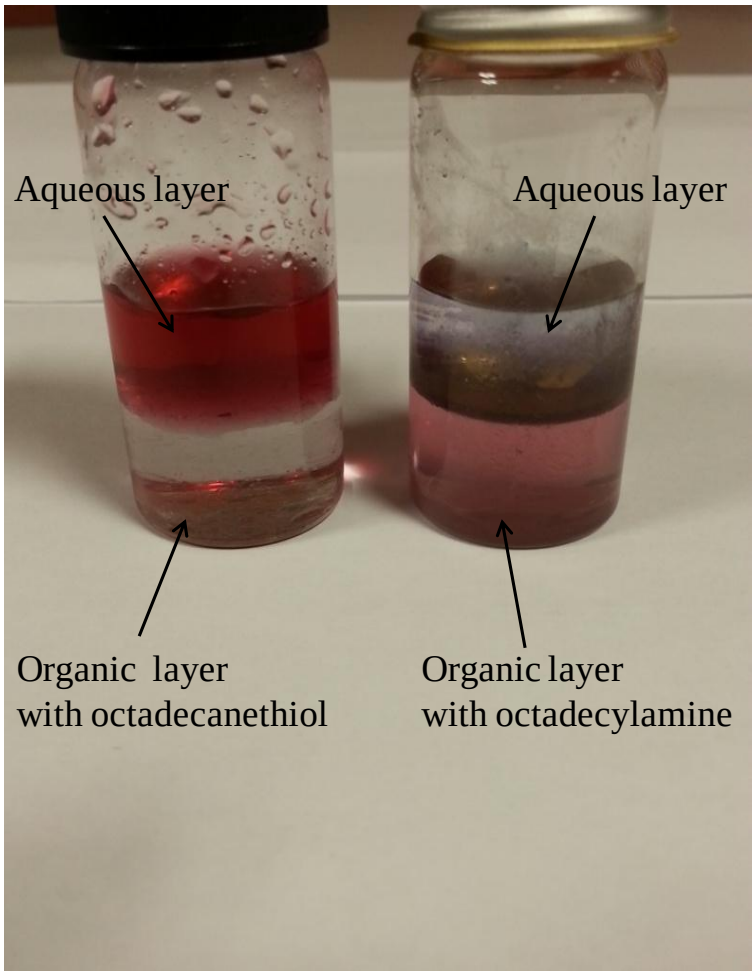

Figure 5.4: *Image showing the phase transfer of citrate-stabilised AuNP (present in the top aqueous layer) to an organic layer (at the bottom) via ligand exchange with octadecanethiol (on the left) and octadecylamine (on the right).*

5.3.1.2 Separation of alkylbenzenes on AuNP-agglomerated polymer monoliths

A test mixture of a series of alkylbenzenes was used to demonstrate the chromatographic efficiency of the AuNP-agglomerated columns which were prepared as described in Section 5.2.3. Initially this mixture was separated on a bare LMA-*co*-EDMA monolith (before attachment of citrate stabilised AuNPs) using an acetonitrile/water mobile phase. The hydrophobic nature of the stationary phase used allowed to achieve a complete separation of the alkylbenzenes mixture within 13 minutes at a flow-rate of 2 µL/min with well resolved and sharp peaks as shown in Figure 5.5.

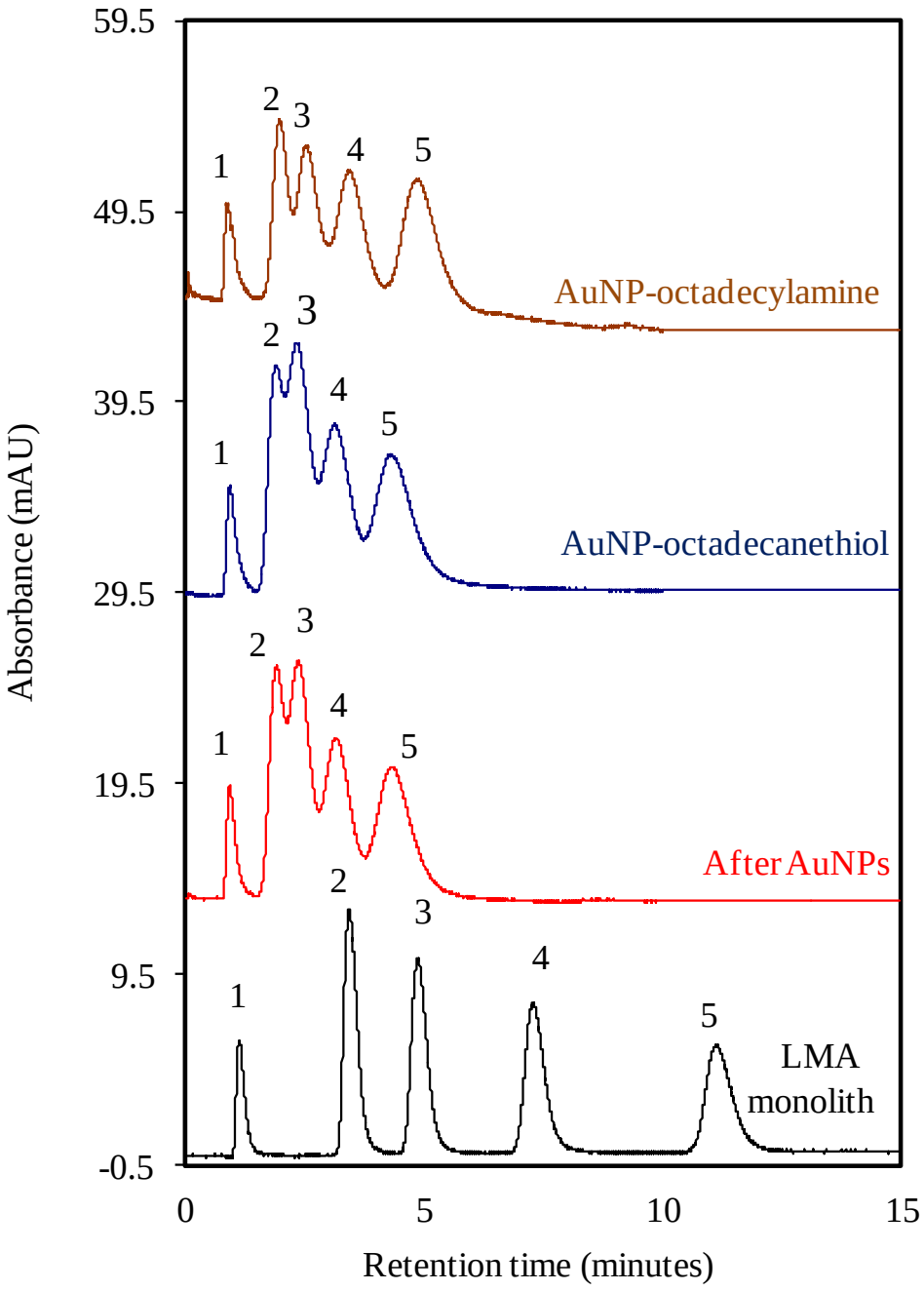

Figure 5.5: *Separation of alkylbenzenes on AuNP-agglomerated polymer monoliths before and after modification with alkyl chains (column length: 12 cm). Mobile phase: 50/50 ACN:H_2O at a flow-rate of 2µL/min (3.4 mm/sec). Injection volume: 100 nL. UV detection at 220 nm. Analytes: 100 ppm (1) uracil (unretained marker), (2) ethylbenzene, (3) propylbenzene, (4) butylbenzene and (5) pentylbenzene.*

The chromatographic efficiency of the column was studied by plotting van Deemter curves between linear velocities of 0.05-6.3 mm/s in order to determine the optimal value at which the highest efficiency was achieved (V_{opt}) as shown in Figure 5.6. Efficiencies of up to 14,000 N/m were observed for example with pentylbenzene at V_{opt} of 0.7 mm/sec which are in agreement with previously reported values of 13,000 N/m for the isocratic separation of three alkylbenzenes on polymer monoliths of similar composition [22].

Since a 60 minute run time was observed at $V(_{opt})$, it was not practical to perform a comparative study after each modification step of the stationary phase under these conditions, hence a comparison in column performance was determined by observing variations in retention factors (k') at a nominal linear velocity of 3.4 mm/sec instead (2 µL/min). The retention factor is a very useful constant for any analyte and chromatographic system because it does not vary with column length or flow-rate.

In the next step of this study, the separation of the same mixture of alkylbenzenes was performed on AuNP-modified monoliths using identical conditions as described above with bare LMA monoliths. The modification with AuNPs required the grafting of a reactive monomer, GMA, which causes a decrease in hydrophobicity of the monolith leading ultimately to reduced retention factor values (k') as summarised in Table 5.1 and shown in Figure 5.5. The retention factor for pentylbenzene for example decreased from 8.8 to 3.5 representing a decrease of 60%. This new retention factor value for pentylbenzene is close to that exhibited by propylbenzene *before modification* despite the difference in hydrophobicity of the two molecules.

Further modification of the AuNP-agglomerated monoliths with octadecanethiol and octadecylamine was performed as described in Section 5.2.6 and the chromatographic properties were evaluated by separating the same alkylbenzene mixture under indentical conditions as previously described. Upon modification with octadecanethiol, similar k' and efficiency values were observed relative to a blank AuNP-modified column which confirmed that no exchange of ligands occurred on the surface of AuNPs, as expected from the observations previously reported in solution.

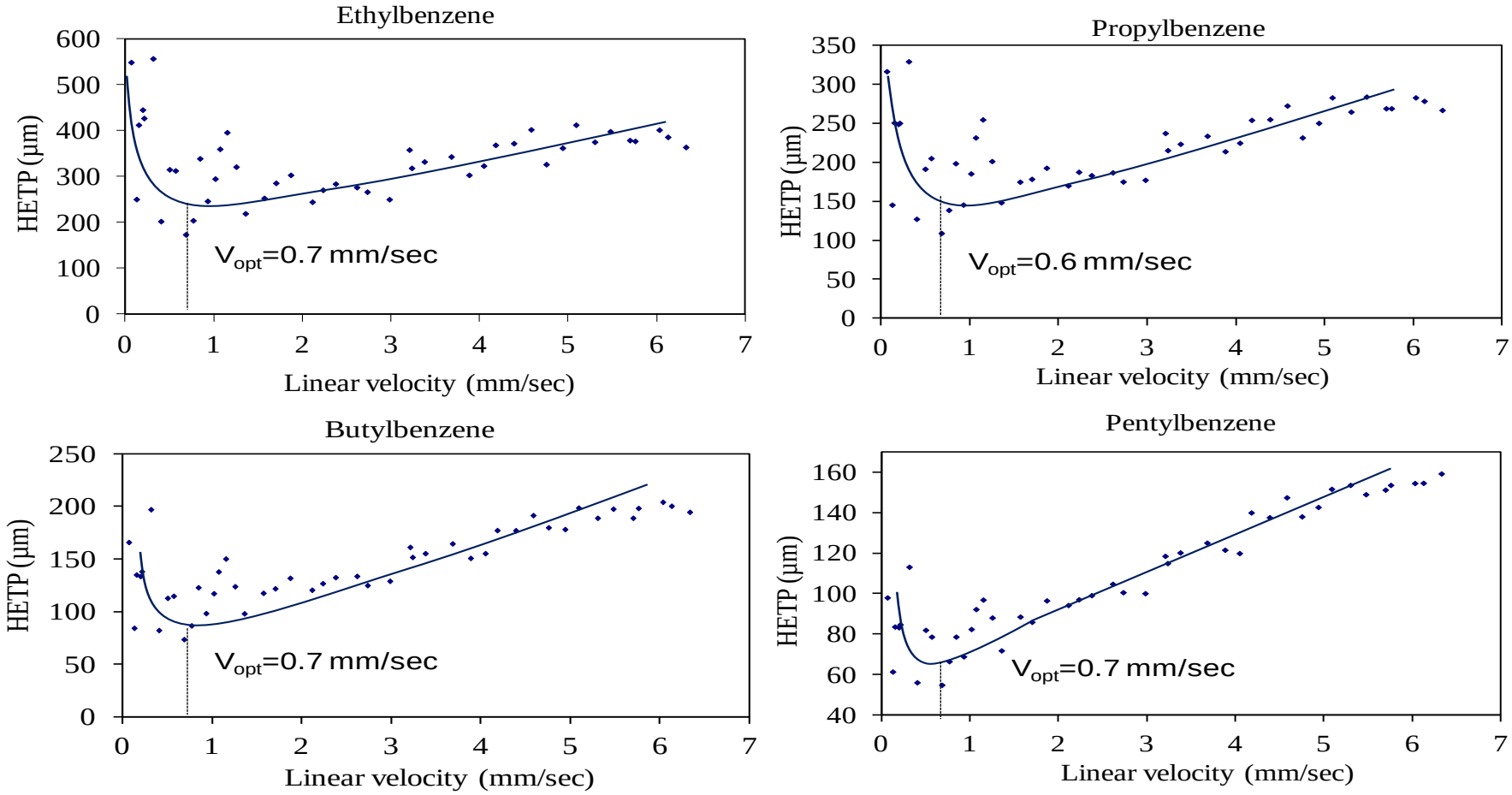

***Figure 5.6**: Van Deemter curves for 100 ppm mixture of ethylbenzene, propylbenzene, butylbenzene and pentylbenzene. V_{opt}: optimal linear velocity.*

Table 5.1: *Chromatographic parameters (n=3) for the separation of alkylbenzenes on Au-NP functionalised LMA-co-EDMA monoliths before and after modification with alkyl chains. Retention factor: k', efficiency: N/m and resolution: R.*

	Bare LMA monolith			After modification with 16 nm AuNPs			After modification with 1 m*M* octadecanethiol			After modification with 1 m*M* octadecylamine		
	k'	N/m	R	k'	N/m	R	k'	N/m	R	k'	N/m	R
Ethylbenzene	2.0	3000	5.51	1.1	900	2.47	1.0	890	2.34	1.1	1070	2.56
Propylbenzene	3.3	4500	2.55	1.5	900	0.91	1.5	910	0.8	1.7	920	0.94
Butylbenzene	5.4	6400	3.5	2.4	960	1.15	2.3	980	1.16	2.5	1060	1.23
Pentylbenzene	8.8	8300	4.3	3.5	1050	1.21	3.5	1020	1.18	3.7	1130	1.31

However, the modification of the immobilised AuNPs with octadecylamines led to improvements in hydrophobicity as revealed by a slight increase in k' values as illustrated in Table 5.1, which indicated that the modification of the AuNPs with alkyl chains was not complete. The retention factor for pentylbenzene for example increased from 3.5 to 3.7 upon modification with octadecylamine representing an increase of 5.7%. These results confirmed the previously reported observations illustrated in Figure 5.4 for the phase transfer of citrate-stabilised AuNPs from aqueous solution to organic solution, where partial phase transfer of the citrate-stabilised AuNPs occurred only in the presence of amine-functionalised alkyl chains. The retention factor values obtained upon modification with octadecylamine however, were still below the originally reported values obtained with a bare LMA monolith.

A decrease in column hydrophobicity also led to poor efficiencies. For example at a k' value of 3.5 (which is the approximate retention factor of propylbenzene on a bare LMA monolith), a decrease in efficiency from 4500 to 1050 N/m was observed after the immobilisation of AuNPs on the stationary phase. At the same k' value (which corresponds for pentylbenzene after modification with AuNPs), no improvements in efficiency were observed after modification with octadecanethiol while slightly higher efficiencies were observed after modification with octadecylamine. For example 1130 N/m were observed for pentylbenzene from an original value of 1050 N/m. Efficiency values were determined based on the EP formula which involves using peak widths at half peak heights (calculated using Chromeleon software). These results confirmed that although the AuNP coverage was dense, as confirmed by FE-SEM images shown in Chapter 4, the GMA layer was still accessible for interacting with the analytes.

In summary, a test mixture of alkylbenzenes was used to evaluate the chromatographic properties of polymer monoliths functionalised with AuNPs in reversed-phase mode. The hydrophilic nature of the immobilised AuNPs resulted in decreased hydrophobicity and performance of the stationary phase as confirmed by the reduced retention factors of the target analytes. Finally the modification of the immobilised AuNPs with amino/thiol-functionalised alkyl chains was performed as an effort to restore the column hydrophobicity however, significant improvements in column performance were not observed.

5.3.1.3 Ion-exchange applications of AuNP-agglomerated polymer monoliths

The use of polymeric materials in ion-exchange chromatography is advantageous because of the resistance of these materials over a wide p*H* range, allowing compatibility with a wide selection of eluents. Previous reports have documented the preparation of porous polymer monoliths for ion-exchange applications either by direct co-polymerisation of functional monomers or by subsequent modification of the monolithic surface with ion exchange groups, either by chemical modification or grafting techniques. With co-polymerisation the relative density of charged functional groups is relatively low, however by availing of photo-grafting techniques extensive branching occurs along the surface leading ultimately to a much higher surface coverage of ion exchange groups. In order to improve the limited surface area of polymer monoliths, which results in low chromatographic efficiency for small molecules, recent development has been aimed at modifying the surface chemistry for the immobilisation of nano-particles due to the high surface to volume ratio of such materials. Reports which describe the use of AuNP-agglomerated monolithic stationary phases for ion-exchange however, have been quite limited [13]. Among the interesting properties of these nano-materials, their stability over a large p*H* range, between p*H* 1-12 [9], would be particularly advantageous for applications in ion-exchange chromatography as well as the known affinity of Au for thiol functional groups which can be used to tailor the surface chemistry for specific applications.

In the work here described, the modification of the AuNP-agglomerated polymer monoliths with negatively charged sulphonate groups was performed to allow cation-exchange applications. These stationary phases were prepared as described in Section 5.2.3 and subsequently functionalised by flushing a solution of mercaptoethanesulphonate in both directions as described in Section 5.2.7, allowing the formation of Au-S bonds which led to free negatively charged sulphonate functional groups on the surface. Based on previous observations described in Section 5.3.1.1 regarding the functionalisation of citrate-stabilised AuNPs with octadecanethiol, it was hypothesised that in the current scenario the formation of Au-S bonds would be more favourable since at a p*H* of 9.5 (which is the p*H* value for

the citrate-stabilised AuNPs) the deprotonation of the thiol group occurs (pK_a of mercaptoethanesulphonate is 9.2) resulting in strong covalent bonds between the resulting thiol groups and gold.

The first step of characterisation of the prepared monolith involved the measurement of the ion-exchange capacity, as described in Section 5.2.7.1. This was measured using a method which involved the adsorption of Ca^{2+} ions, which were then eluted with a 0.5 m*M* $CuSO_4$ eluent. Because $CuSO_4$ absorbs in the UV, a negative dip was observed when a non-UV absorbing species, such as Ca^{2+}, moved along the detector.

As it can be seen from Figure 5.7, the time taken to remove the adsorbed Ca^{2+} on a 12 cm long sulphonated AuNP monolith was roughly 4.2 minutes compared to 2.2 minutes for the blank AuNP-monolith.

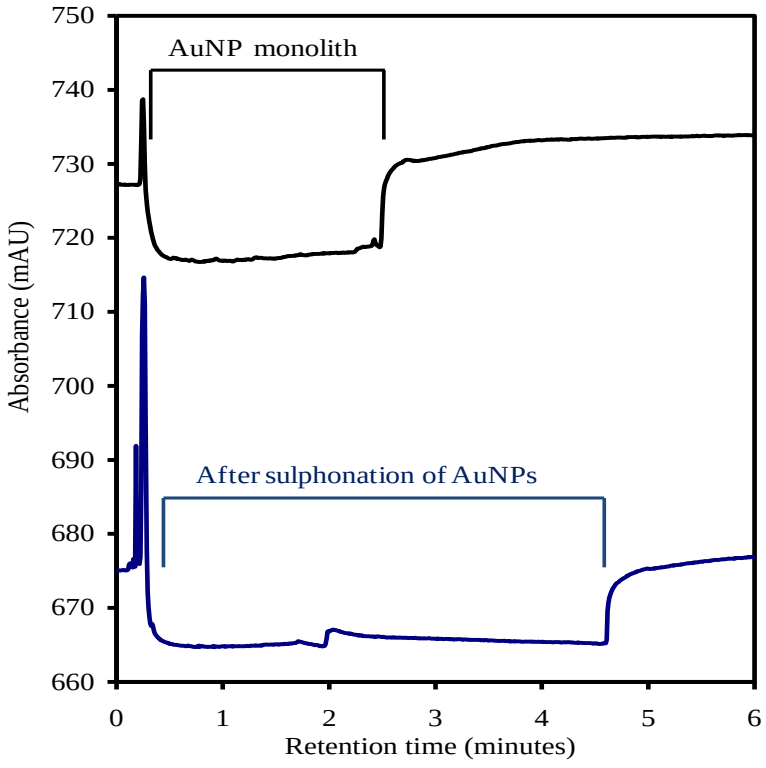

Figure 5.7: *Determination of the ion-exchange capacity of an AuNP-agglomerated monolith before and after modification with sulphonate groups. Eluent: 0.5 mM $CuSO_4$, UV detection at 210 nm, flow-rate 1µL/min. Column length: 12 cm.*

It was found that the capacity was 1.1 nequiv/column for the AuNP-monolith prior to sulphonation and 4.2 nequiv/column after modification with sulphonate groups. The ion-exchange properties of the sulphonated AuNP-agglomerated stationary phase were then evaluated by injecting 2.5 m*M* solutions of Ca^{2+} and Mg^{2+}. Among these analytes, only Ca^{2+} was retained as demonstrated by the presence of a negative peak in Figure 5.8, using a $CuSO_4$ eluent (0.5-5 m*M)* with efficiencies of up to 1730 N/m.

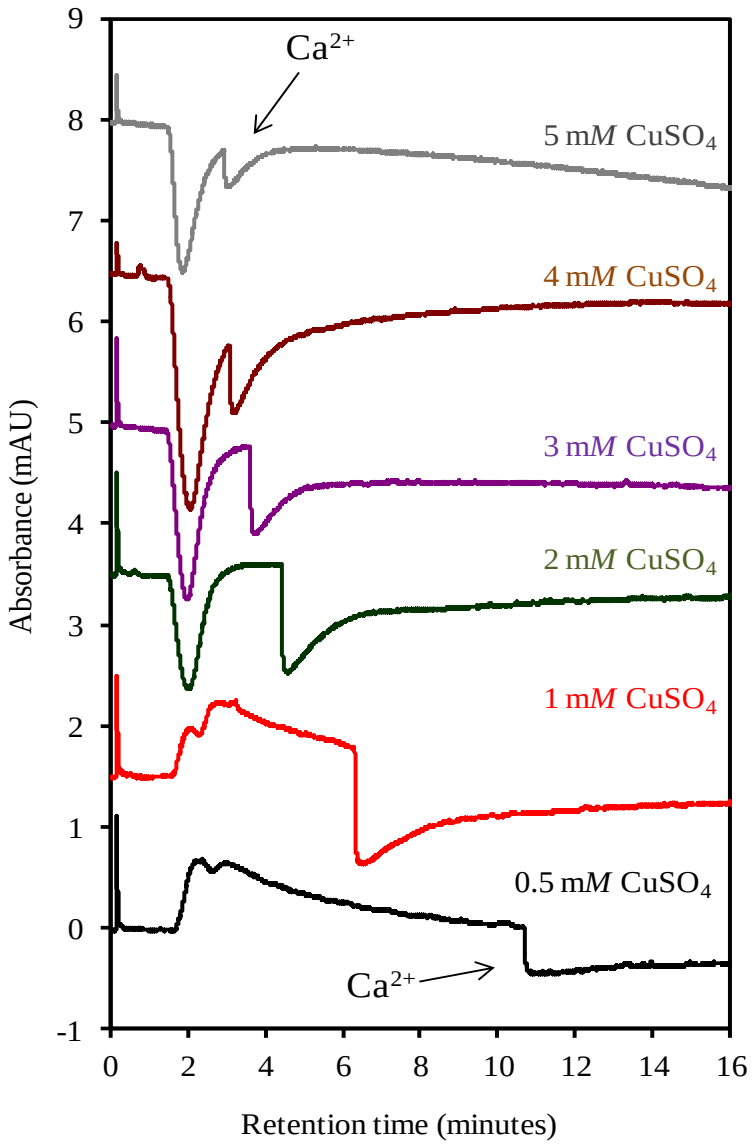

Figure 5.8: *Image showing the retention of 2.5 mM Ca^{2+} on a AuNP functionalised monolith modified with sulphonate groups. Eluent: 0.5 mM to 5.0 mM $CuSO_4$, UV detection at 210 nm, flow-rate 1 µL/min, 100 nL injections. Column length: 12 cm.*

No retention for Mg^{2+} was observed since according to the order of elution in cation-exchange, Mg^{2+} would elute before Ca^{2+} (hence it would appear in the void). As summarised in Table 5.2, a decrease in $CuSO_4$ concentration led to longer retention times and decreased efficiencies.

Table 5.2: *Retention factor and efficiency values for the retention of Ca^{2+} on sulphonated AuNP-agglomerated LMA-co-EDMA monoliths.*

$CuSO_4$ concentration (m*M*)	Retention factor ($k^{'}$) (*n*=3)	Efficiency values (N/m) (*n*=3)
5	0.6	1730
4	0.6	1400
3	0.9	800
2	1.3	770
1	2.1	750
0.5	3.9	700

Poor column performance was attributed to the low ion-exchange capacity of the stationary phase which was considerably lower than what had been previously reported for similar polymer monoliths which had been modified with latex nano-particles. In this case ion-exchange capacities between 9-24 nequiv/30 cm column were reported [23].

The relationship between retention factor for Ca^{2+} and the eluent concentration was also investigated. In ion chromatography the migration rate of a sample ion (Ca^{2+} in this case) is dependant on the magnitude of the distribution constant (*K*). The equilibrium present will be determined by the eluent ion (E), a sample ion (S) and the ion-exchange stationary phase (R) and will be defined as:

$$R.E + S \leftrightharpoons R.S + E \qquad \text{(Equation 5.1)}$$

The distribution constant *K* can then be expressed as:

$$K = [R.S][E] / [R.E][S] \qquad \text{(Equation 5.2)}$$

The retention factor (k') is the ratio of the sample ion in the stationary phase to that in the eluent and is defined as:

$$k' = [R.S] / S \qquad \text{(Equation 5.3)}$$

By expressing R.E as the ion-exchange capacity (C), the relationship between retention factor and distribution constant can be simplified to:

$$k' = KC / E \qquad \text{(Equation 5.4)}$$

This can be converted to the logarithmic form which is expressed as:

$$\text{Log } k' = -\log E + \log K + \log C \qquad \text{(Equation 5.5)}$$

The relationship illustrated above in Equation 5.5 indicated that a linear decrease of log k' occurs as log E is increased and the slope of this line can be used to reveal important information on the behaviour of the ion-exchange process. A slope of -1 will be present if both the sample ion (S) and the eluent ion (E) have the same charge. If however, S is divalent and E is monovalent, the slope of the line will be -2 [24]. As shown in Figure 5.9, the slope of the line for Ca^{2+} using a $CuSO_4$ eluent was found to be -0.8 which is in agreement with the mechanism illustrated above since both sample and eluent ions are divalent. It must be stated however, that the ion-exchange properties of the AuNP-agglomerated stationary phase here used were dictated by a combination of sulphonate groups present on the surface, due to the modification of the immobilised AuNPs with mercaptoethanesulphonate, as well as the residual negatively charged citrate functionalities which were originally present on the surface of the AuNPs.

The results illustrated above demonstrate that AuNP-agglomerated monolithic stationary phases can be further functionalised to perform as ion-exchangers by availing of the affinity of AuNPs for thiol moieties. The ion-exchange capacity was increased (from 1.1 to 4.2 nequiv/column) by modification of the citrate-stabilised AuNPs with sulphonate groups by availing of the affinity of gold for thiol functionalities.

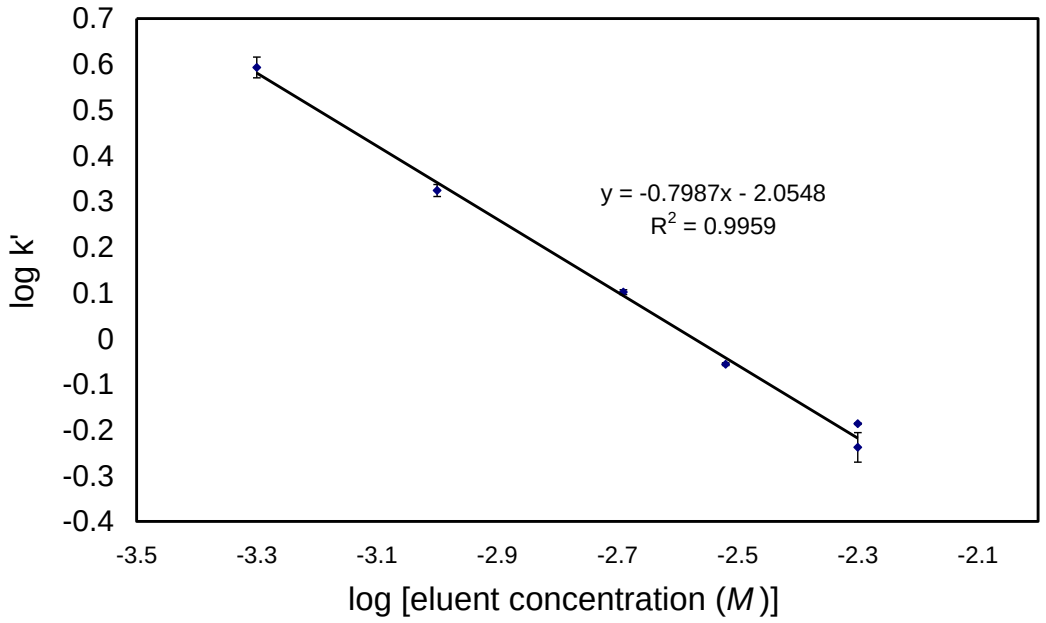

Figure 5.9: *Plot showing the relationship between the log of the retention factor (k') and the log of $CuSO_4$ concentration for the separation of Ca^{2+} on the sulphonated AuNP-agglomerated monolith.*

5.3.2 Chromatographic evaluation of PAA-grafted SiNP-agglomerated polymer monoliths

5.3.2.1 Characterisation of PAA-grafted SiNPs

A further evaluation of the ion-exchange properties of nano-agglomerated monolithic stationary phases was performed by functionalising the surface of polymer monoliths with PAA-grafted SiNPs which were prepared by a collaborator in DCU. The modification of polymer monoliths with charged nano-particles for ion-exchange chromatography has been previously documented in the literature [23, 25-27] however, the vast majority of these reports focus on the use of positively charged latex nano-particles for anion-exchange applications as previously illustrated in Section 1.8.1. In this instance however, the presence of PAA chains on the surface of a SiNP core allows applications in cation-exchange mode since at p*H* values above 4.3, which is the pK_a value of PAA [28], the carboxylic groups become de-protonated. It was also hypothesised that by grafting PAA chains on the surface on the SiNPs, an increased ion-exchange capacity would be achieved due to the high presence of carboxylic groups. The materials here described hence demonstrated

potential for the preparation of novel nano-agglomerated monolithic stationary phases suitable for cation-exchange chromatography.

As shown from the FE-SEM image in Figure 5.10, a PAA brush was grafted around a silica core leading to overall particle sizes of 106 ± 1.2 nm (*n*=3). Since these nano-particles were dispersed in water, the negatively charged carboxylate groups created a repulsive force around the surface which allowed the formation of a stable suspension. Zeta potential studies revealed a γ value of -40.0 ± 1.8 mV (*n*=3) which is approximately two-times the γ value for citrate stabilised AuNPs reported in Section 4.3.2.

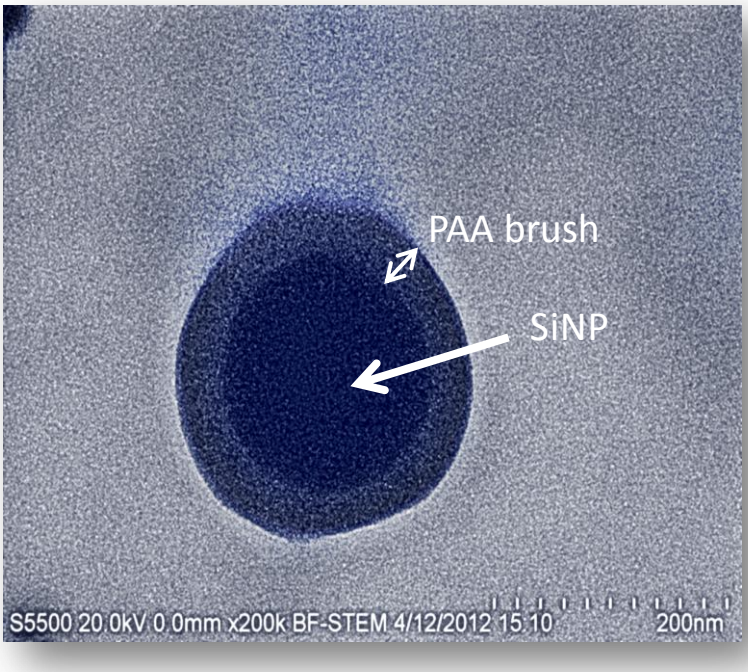

Figure 5.10: *SEM image of a PAA-grafted SiNP (magnification: 200,000x).*

5.3.2.2 Immobilisation of PAA-grafted SiNPs on polymer monoliths

The functionalisation of monoliths with charged nano-particles for the preparation of ion-exchange stationary phases has been traditionally performed by electrostatic interactions. For example, Hilder *et al.* [25] described the preparation of a BuMA-*co*-EDMA-*co*-AMPS monolith for modification with positively charged latex nano-particles which were electrostatically attached via the negatively charged sulphonate groups. Since not all of these sulphonate groups were available to react on the

surface of the monolith, the coverage of latex nano-particles was not maximised (although still leading to a 30% increase in surface area values). Here a monolith with quaternary ammonium functionalities was prepared as described in Section 5.2.10 and used as a solid support for the immobilisation of the previously described PAA-grafted SiNPs. Photografting techniques were used to maximise the presence of GMA functional groups on the surface of the monolith which contain reactive epoxy functionalities that were subsequently functionalised in order to achieve quaternary ammonium groups. The negatively charged nano-particles were electrostatically attached on the positively charged surface of the monolith. Initial confirmation of the presence of nano-particles was obtained by FE-SEM analysis. Similarly as shown by Hilder *et al.*[25] for latex nano-particles (see page 28), FE-SEM images of both blank and modified monoliths revealed the presence of PAA-grafted SiNPs on the latter samples (see Figure 5.11) where they appeared as small dots on an otherwise smooth surface.

FE-SEM however does not provide any information on the distribution of ion-exchange functionalities along the axial length of monolithic capillary columns. For this purpose sC^4D was here used as a novel methodology for characterising non-invasively the nano-agglomerated ion-exchange stationary phases prepared, using a similar approach as previously documented for the immobilisation of AuNPs on polymer monoliths in Chapter 4, Section 4.3.7. Here the benefits of sC^4D were further emphasised since the PAA-grafted SiNP suspension was colourless hence a visual inspection of the monolith was not sufficient to verify if a successful immobilisation on the surface had occurred.

The functionalisation of the monolith with quaternary ammonium groups was initially verified using sC^4D, where a sevenfold increase in conductive response was observed relative to a blank column as shown in Figure 5.12 (a). Upon modification with the PAA-grafted SiNPs, it was possible to visualise the functionalisation of the surface at 2, 6 and 10 cm intervals. The subsequent attachment of these nano-materials resulted in a considerable decrease in conductive response due to the interaction of the negatively charged PAA-grafted SiNPs with the NR_4^+ sites. The C^4D response for a SiNP-functionalised monolith was found to be very similar to the original profile obtained with a bare monolith. The sC^4D characterisation was performed simultaneously as the functionalisation with nano-particles occurred,

since the SiNP suspension was in pure water without any other ionic species present (such as citrate ions in the case of AuNPs) which would prevent a stable conductive response and would require a further washing step with water prior to obtaining C^4D measurements.

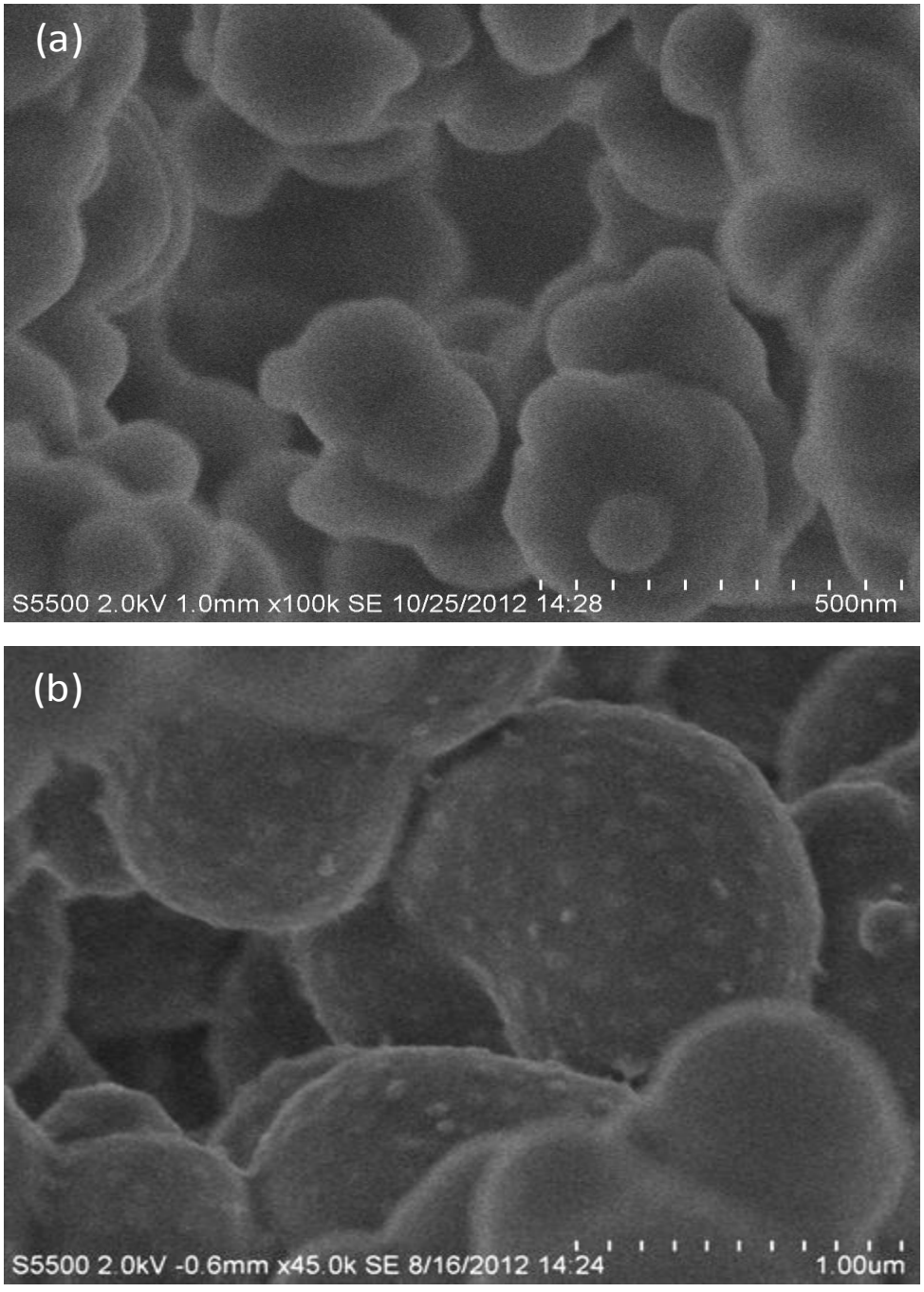

Figure 5.11: *FE-SEM images showing (a) a blank quaternary ammonium functionalised monolith (magnification: 100,000x) and (b) immobilised PAA-grafted SiNPs on the surface of a quaternary ammonium functionalised polymer monolith (magnification: 45,000x).*

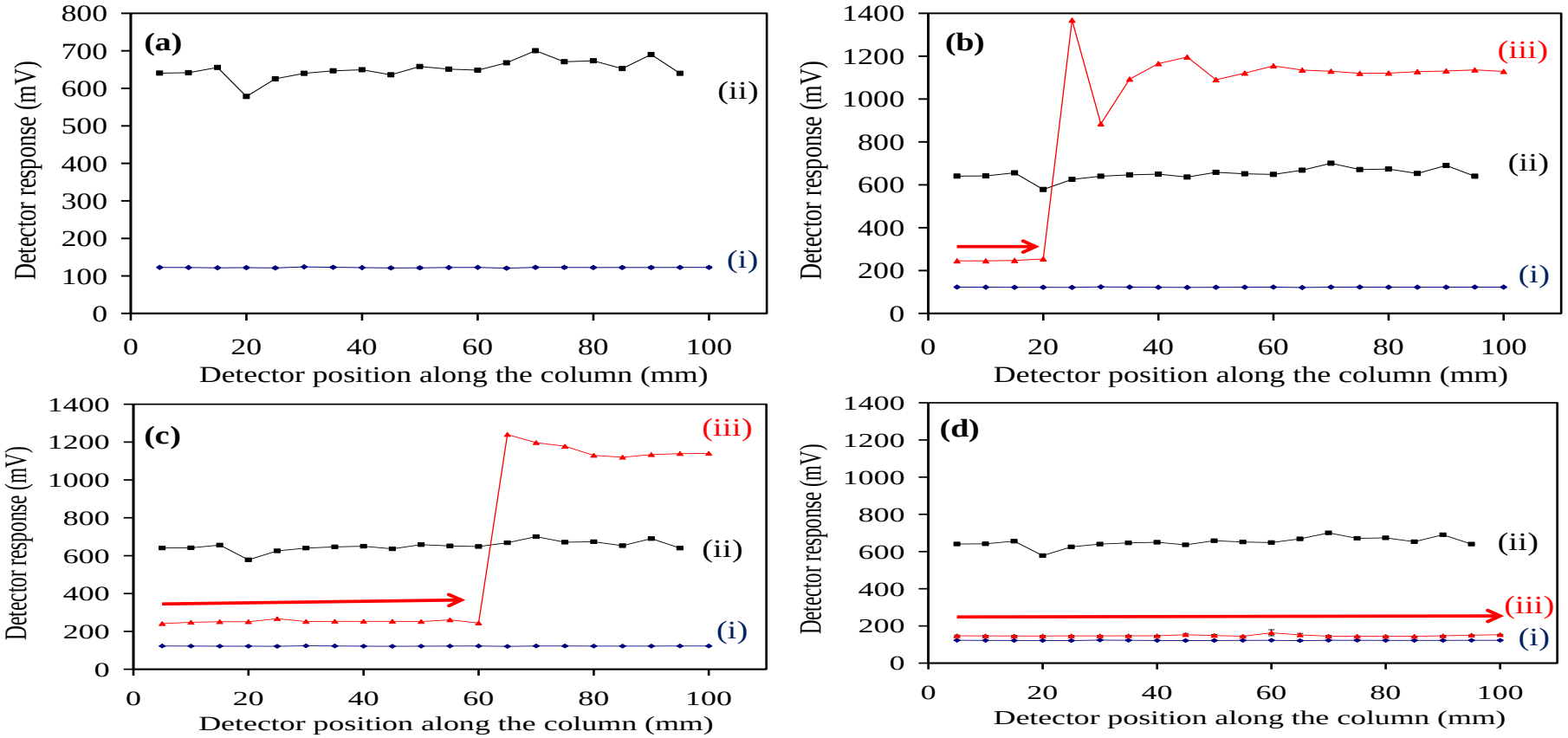

***Figure 5.12**: sC^{4}D profiles showing the immobilisation of PAA-grafted SiNPs on the surface of a quaternary ammonium functionalised (NR_4^+) polymer monolith (a) before any modification, (b) after 2 cm, (c) 6 cm and (d) 10 cm. Conductive responses of (i) bare LMA monolith, (ii) NR_4^+ functionalised monolith and (iii) the same monolith as the modification with PAA-grafted SiNPs occurred are shown.*

5.3.2.3 Ion-exchange applications of PAA-grafted SiNP-agglomerated polymer monoliths

The chromatographic characterisation of the stationary phase here prepared involved an initial evaluation of the anion-exchange properties of the quaternary ammonium functionalised polymer monoliths prior to the modification with the PAA-grafted SiNPs. The eluent chosen for this work was based on a combination of phthalic acid/ethylenediamine eluent which is suitable for both cation and anion-exchange applications [29]. Ethylenediamine is a divalent organic base which was titrated with phthalic acid, a diprotic organic acid, to achieve the desired p*H*. Ethylenediamine has a +2 charge below p*H* 6.99 (pK_{a2} of ethylenediamine) and phthalate has a -2 charge at p*H* values above 5.51 (pK_{a2} of phthalic acid) hence by operating at p*H* values in this region the eluting strength of the eluent is maximised. Another advantage of using this eluent was represented by the range of detection modes available. Phthalate allows the use of indirect UV as well as direct conductivity detection while ethylenediamine can be used for indirect conductivity detection of metals.

A mixture of 10 ppm Cl^- and 10 ppm $H_2PO_4^-$ was separated in 20 minutes using a 0.25 m*M* (p*H* 6.5) phthalic acid/ethylenediamine eluent and non-suppressed C^4D detection as shown in Figure 5.13 with $H_2PO_4^-$ being the most retained anion as expected. Sharp and well resolved peaks were observed, although with low efficiencies of 3,000 N/m for Cl^- and 10,000 N/m for $H_2PO_4^-$. Previously, efficiencies of up to 13,000 N/m for Cl^- have been reported on similar monolithic stationary phases [30].

As mentioned in Section 5.3.2.2, the attachment of the PAA-grafted SiNPs on the monolith's surface was initially verified using FE-SEM and sC^4D. Further confirmation of the successful modification with nano-particles was also obtained chromatographically by the loss of retention of the previously separated anions, as illustrated in Figure 5.14, due to a decrease in anion-exchange capacity of the monolith since the positively charged quaternary ammonium functionalities on the surface of the monolith are now interacting with the negatively charged nano-particles.

The injection of a 10 ppm Cl^- standard resulted in no visible peaks indicating that both chloride and sodium (from the sodium chloride salt used) were unretained. A negative peak was observed after the void by injecting a 10 ppm $H_2PO_4^-$ standard. It was hypothesised that this negative peak represented a system peak, since an identical peak was observed after a blank injection.

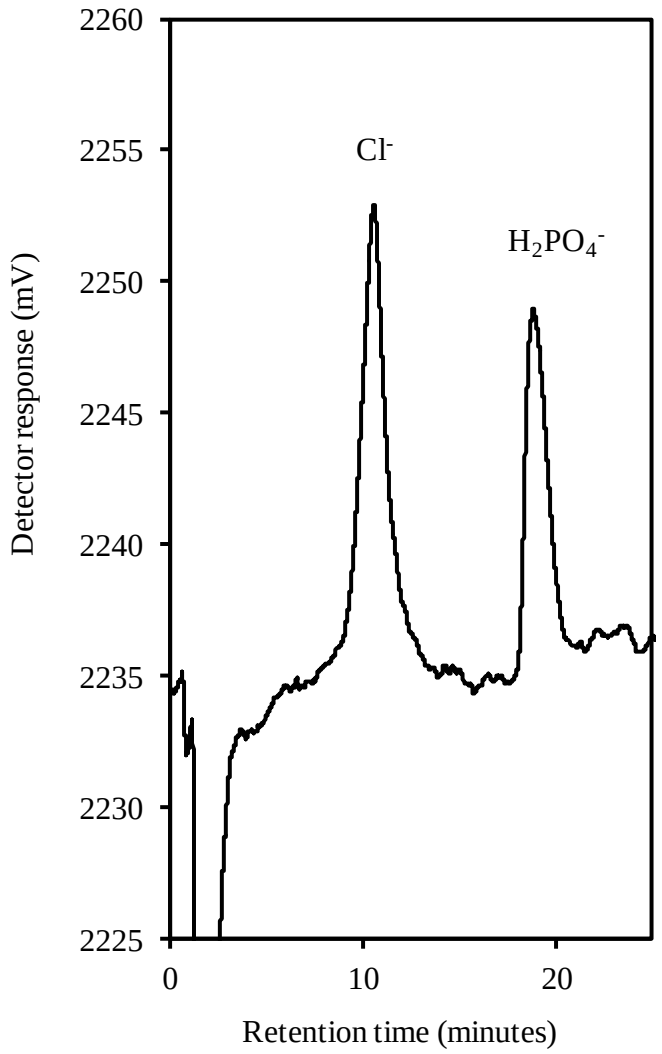

Figure 5.13: *Retention of 10 ppm Cl^- and $H_2PO_4^-$ on a quaternary ammonium functionalised monolith using a phthalic acid eluent (0.25 mM) adjusted to pH 6.5 using ethylenediamine. Conditions: on-column conductivity detection with settings: 2x high, -0dB, offset 000. Effective column length: 12 cm. Flow-rate: 1 µL/min. Injection volume: 100 nL.*

The appearance of system peaks could also be a plausible explanation. System peaks were originally discovered by Gjerde and Fritz [31] and they are the result to variations in column equilibrium upon the injection of a sample. In anion-exchange for example, an equilibrium is formed by the displacement of the the anions on the stationary phase by the anions in the eluent. In reality a further equilibrium exists where the eluent is sorbed by the ion-exchange matrix. If the p*H* of an injected sample is more basic than the p*H* of the sorbed eluent, part of this will be ionised and desorbed. A negative peak will then be visible due to the re-adsorption of the eluent on the ion-exchange stationary phase.

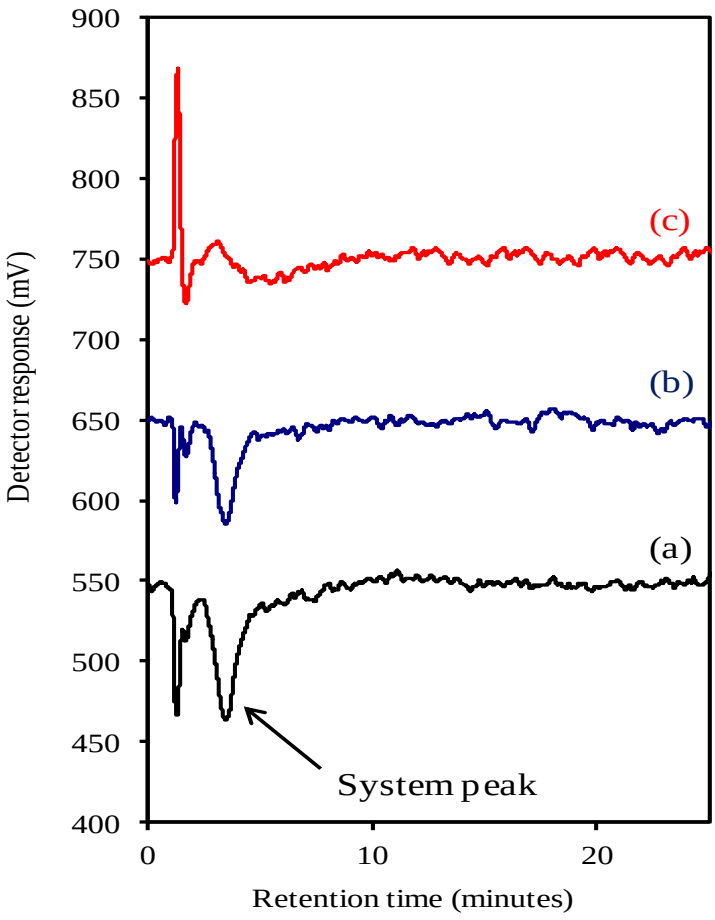

***Figure 5.14**: Injections of (a) a water blank, (b) 10 ppm $H_2PO_4^-$ and (c)10 ppm Cl^- on the PAA-grafted SiNP-functionalised monolith. Conditions: on-column C^4D detection with settings: 2x high, 0dB, offset 000. Phthalic acid eluent (0.25 mM) adjusted to pH 6.5 using ethylenediamine. Effective column length: 12 cm. Flow-rate: 1 µL/min. Injection volume: 100 nL.*

The reverse process occurs when a sample of more acidic p*H* is injected which results in a positive peak due to the desorption of the excess eluent from the ion-exchange stationary phase.

The cation-exchange properties of the SiNP-agglomerated stationary phase were evaluated using similar conditions as reported for the anion-exchange experiments. In this case, an eluent at p*H* 6.5 was required in order to preserve a negative charge on the PAA-grafted SiNPs and prevent their detachment from the positively charged surface. Also in order to prevent the possible deterioration of silica core, high p*H* eluents were avoided since silica notoriously dissolves under alkaline conditions.

Retention of 10 ppm Mg^{2+} and 100 ppm Ca^{2+} were observed as shown in Figure 5.15 with respective efficiencies of up to 7,800 N/m and 5,200 N/m which are well below the efficiency values reported by Ueki *et al.* [32] of 20,000 N/m for the separation of similar cations on sulphonated polymer monoliths. Negative peaks were observed due to negative conductance of the analytes relative to the ethylenediammonium ion from the eluent. No retention of Na^{+} was observed since traditionally Na^{+} has low retention in cation-exchange chromatography.

Similar retention times were observed between the two analytes with calcium being slightly more retained than magnesium (with retention factor values of 3 and 2.7 respectively) as would be expect from the typical order of elution of cations in ion-exchange.

A positive peak was also observed at 1.8 minutes after the injection of 100 ppm Ca^{2+} which can be attributed to the Cl^{-} anion. In this case a concentration of 180 ppm Cl^{-} was injected which is much higher than the 10 ppm Cl^{-} concentration which revealed no retention (see Figure 5.14). An increase in retention time to 2 minutes was observed by decreasing the concentration to 90 ppm Cl^{-} while no retention was observed after injecting 45 ppm Cl^{-}. This suggested that the stationary phase behaved as a mixed mode stationary phase due to the combined presence of the negatively charged PAA-grafted SiNPs and some residual NR_4^{+} groups present on the surface of the monolith. Similarly, a negative peak was observed at 2.1 minutes after the injection of 10 ppm Mg^{2+} which can be attributed to the ClO_4^{-} anion. However, a similar negative peak appeared after the injection of a blank hence, as previously suggested, the presence of system peaks represented another plausible explanation.

In order to improve the resolution between the two peaks, variations in eluent and sample concentrations could be performed. It is well known that in ion chromatography variations in concentration of the injected analyte would result in shifted retention times. For example it was observed that by decreasing the concentration of Ca^{2+} from 100 ppm to 50 ppm, the retention factor increased from 3 to 3.4 (showing very low cation-exchange capacity) as shown in Figure 5.16 however, at the expense of sensitivity since a decrease in concentration resulted in a decreased peak size Ca^{2+}.

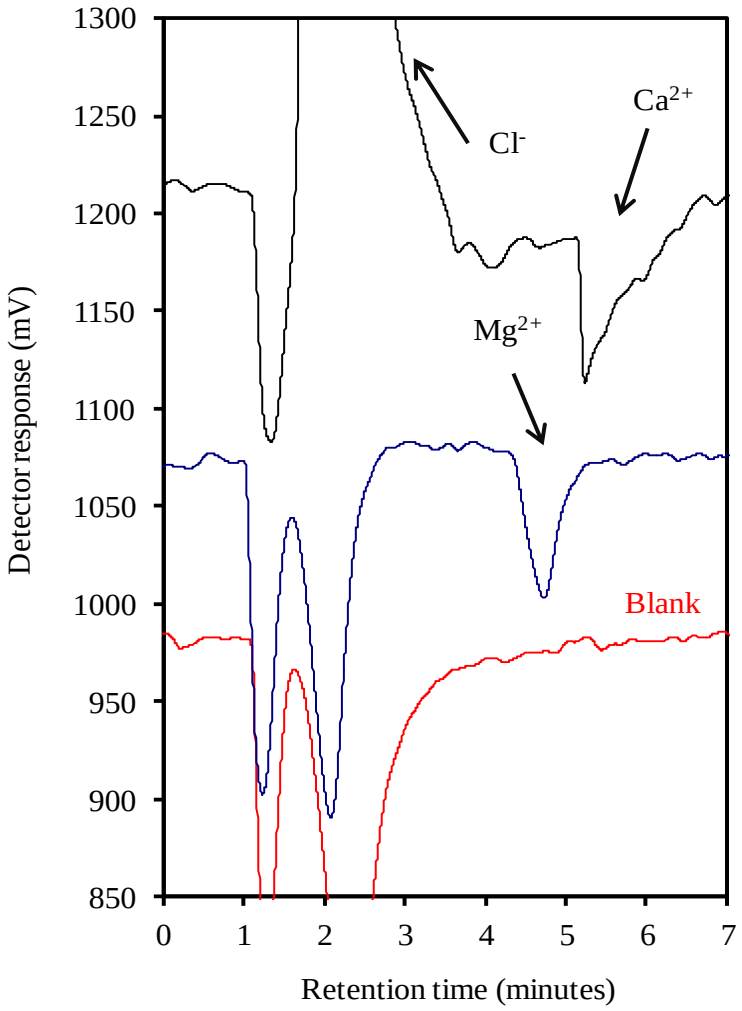

Figure 5.15: *Retention of 100 ppm Ca^{2+} and 10 ppm Mg^{2+} on the PAA-grafted SiNP-agglomerated monolith. Conditions: on-column C^4D detection with settings; 2x high, -0dB, offset 000. Eluent: ethylenediamine (0.5 mM) adjusted to pH 6.5 using phthalic acid. Effective column length: 12 cm. Flow-rate: 1 µL/min. Injection volume: 100 nL.*

A decrease in eluent concentration would also led to longer retention times however, issues related to column reproducibility prevented further evaluation of the properties of the stationary phase.

In summary, PAA-grafted SiNPs were immobilised on the surface of a quaternary ammonium functionalised polymer monoliths for ion-exchange applications. The immobilisation of the nano-particles allowed applications in both anion and cation-exchange modes by availing of a phthalic acid/ethylenediamine eluent.

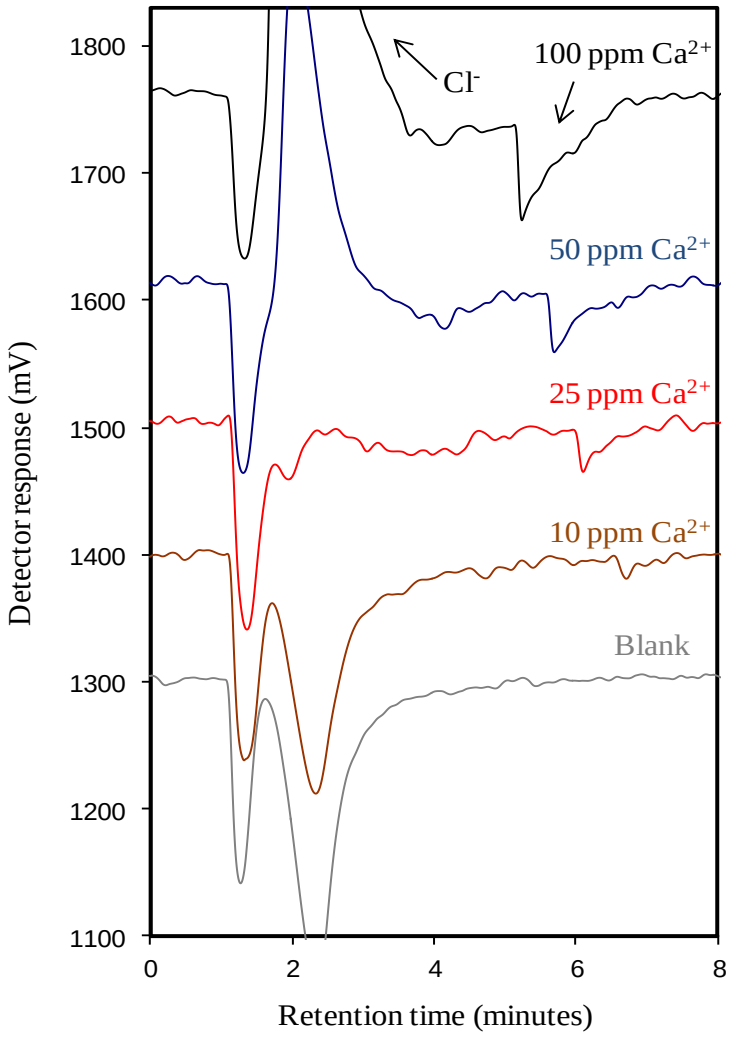

Figure 5.16: *Retention of Ca^{2+} at various concentrations (10-100 ppm) on the PAA-grafted SiNP-agglomerated monolith. Conditions: on-column C^4D detection with settings; 2x high, -0dB, offset 000. Eluent: ethylenediamine (0.5 mM) adjusted to pH 6.5 using phthalic acid. Effective column length: 12 cm. Flow-rate: 1µL/min. Injection volume: 100 nL.*

A low cation-exchange capacity was however observed after the modification with the PAA grafted-SiNPs. Further evaluation of the properties of these stationary phases would involve determining the effects of variations in eluent concentration and p*H* however issues regarding column reproducibility were observed which prevented these studies from being performed.

5.4 Conclusion

Polymer monoliths in capillary format were modified with AuNPs and PAA-grafted SiNPs for chromatographic applications in reversed-phase and ion-exchange modes. Poor column performance relative to a bare polymer monolith with strong hydrophobic character was visualised after agglomeration with AuNPs due to the co-elution of a previously separated test mix of alkylbenzenes on a bare monolith. The subsequent modification of the immobilised AuNPs with either thiol or amine functionalised hydrophobic chains did not improve significantly the hydrophobic character of the monolith. Similarly, the modification of the agglomerated AuNPs with sulphonate functionalities allowed applications in ion-exchange mode, although with limited selectivity towards Ca^{2+} ions despite an increase in ion-exchange capacity after sulphonation of the immobilised AuNPs (from 1.1 to 4.2 nequiv/column). Other quaternary ammonium functionalised polymer monoliths were used as solid supports for the immobilisation of negatively charged SiNPs. The electrostatic immobilisation of these materials was confirmed by FE-SEM, sC^4D and also chromatographically by the loss of retention of a previously separated anion mixture which was performed on quaternary ammonium functionalised monoliths. Cation-exchange applications were possible due to the negatively charged PAA brushes present on the surface of the SiNPs as confirmed by the retention of Ca^{2+} and Mg^{2+}. Further studies would be required on these nano-agglomerated stationary phases in order to evaluate the stability of these columns, to determine their ion-exchange capacity values and to evaluate the effects of variations in eluent p*H* and concentration.

5.5 References

1. Agui, L.; Yanez-Sedeno, P.; Pingarron, J. M. Role of carbon nanotubes in electroanalytical chemistry - A review. *Analytica Chimica Acta* **2008,** *622* (1-2), 11-47.

2. Huang, X. H.; Jain, P. K.; El-Sayed, I. H.; El-Sayed, M. A. Gold nanoparticles: interesting optical properties and recent applications in cancer diagnostic and therapy. *Nanomedicine* **2007,** *2* (5), 681-693.

3. Jacobs, C. B.; Peairs, M. J.; Venton, B. J. Review: carbon nanotube based electrochemical sensors for biomolecules. *Analytica Chimica Acta* **2010,** *662* (2), 105-127.

4. Luo, X. L.; Morrin, A.; Killard, A. J.; Smyth, M. R. Application of nanoparticles in electrochemical sensors and biosensors. *Electroanalysis* **2006,** *18* (4), 319-326.

5. Wang, F.; Hu, S. S. Electrochemical sensors based on metal and semiconductor nanoparticles. *Microchimica Acta* **2009,** *165* (1-2), 1-22.

6. Connolly, D.; Currivan, S.; Paull, B. Polymeric monolithic materials modified with nanoparticles for separation and detection of biomolecules: A review. *Proteomics* **2012,** *12* (19-20), 2904-2917.

7. Ortiz, Y.; Cintron, J. M.; Colon, L. A. Gold coated SiO_2 modified with self-assembled monolayers as a potential stationary phase for liquid chromatography. *Abstracts of Papers American Chemical Society* **2001,** *221* (1-2), U80-U80 74-ANYL.

8. Kobayashi, K.; Kitagawa, S.; Ohtani, H. Development of capillary column packed with thiol-modified gold-coated polystyrene particles and its selectivity for aromatic compounds. *Journal of Chromatography A* **2006,** *1110* (1-2), 95-101.

9. Qu, Q. S.; Peng, S. W.; Mangelings, D.; Hu, X. Y.; Yan, C. Silica spheres coated with C18-modified gold nanoparticles for capillary LC and pressurized CEC separations. *Electrophoresis* **2010,** *31* (3), 556-562.

10. Alwael, H.; Connolly, D.; Clarke, P.; Thompson, R.; Twamley, B.; O'Connor, B.; Paull, B. Pipette-tip selective extraction of glycoproteins with lectin modified gold nano-particles on a polymer monolithic phase. *Analyst* **2011,** *136* (12), 2619-2628.

11. Connolly, D.; Twamley, B.; Paull, B. High-capacity gold nanoparticle functionalised polymer monoliths. *Chemical Communications* **2010,** *46* (12), 2109-2111.

12. Guerrouache, M.; Mahouche-Chergui, S.; Chehimi, M. M.; Carbonnier, B. Site-specific immobilisation of gold nanoparticles on a porous monolith surface by using a thiol-yne click photopatterning approach. *Chemical Communications* **2012,** *48* (60), 7486-7488.

13. Cao, Q.; Xu, Y.; Liu, F.; Svec, F.; Frechet, J. M. J. Polymer monoliths with exchangeable chemistries: use of gold nanoparticles as intermediate ligands for capillary columns with varying surface functionalities. *Analytical Chemistry* **2010,** *82* (17), 7416-7421.

14. Lv, Y.; Lin, Z.; Svec, F. Hypercrosslinked large surface area porous polymer monoliths for hydrophilic interaction liquid chromatography of small molecules featuring zwitterionic functionalities attached to gold nanoparticles held in layered structure. *Analytical Chemistry* **2012,** *84* (20), 8457-8460.

15. Lv, Y.; Alejandro, F. M.; Frechet, J. M.; Svec, F. Preparation of porous polymer monoliths featuring enhanced surface coverage with gold nanoparticles. *Journal of Chromatography A* **2012,** *1261*, 121-128.

16. Thabano, J. R. E.; Breadmore, M. C.; Hutchinson, J. P.; Johns, C.; Haddad, P. R. Silica nanoparticle-templated methacrylic acid monoliths for in-line solid-phase

extraction-capillary electrophoresis of basic analytes. *Journal of Chromatography A* **2009,** *1216* (25), 4933-4940.

17. Karg, M.; Schelero, N.; Oppel, C.; Gradzielski, M.; Hellweg, T.; von Klitzing, R. Versatile phase transfer of gold nanoparticles from aqueous media to different organic media. *Chemistry-A European Journal* **2011,** *17* (16), 4648-4654.

18. Stober, W.; Fink, A.; Bohn, E. Controlled growth of monodisperse silica spheres in micron size range. *Journal of Colloid and Interface Science* **1968,** *26* (1), 62-&.

19. Krenkova, J.; Foret, F. Iron oxide nanoparticle coating of organic polymer-based monolithic columns for phosphopeptide enrichment. *Journal of Separation Science* **2011,** *34* (16-17), 2106-2112.

20. Hakkinen, H. The gold-sulfur interface at the nanoscale. *Nature Chemistry* **2012,** *4* (6), 443-455.

21. Krysinski, P.; Chamberlain, R. V.; Majda, M. Partial electron transfer in octadecanethiol binding to gold. *Langmuir* **1994,** *10* (11), 4286-4294.

22. Xie, S.; Allington, R. W.; Frechet, J. M. J.; Svec, F. Porous polymer monoliths: an alternative to classical beads. *Advances in biochemical engineering/biotechnology* **2002,** *76*, 87-125.

23. Zakaria, P.; Hutchinson, J. P.; Avdalovic, N.; Liu, Y.; Haddad, P. R. Latex-coated polymeric monolithic ion-exchange stationary phases. 2. Micro-ion chromatography. *Analytical Chemistry* **2004,** *77* (2), 417-423.

24. Staahlberg, J. Electrostatic retention model for ion-exchange chromatography. *Analytical Chemistry* **1994,** *66* (4), 440-449.

25. Hilder, E. F.; Svec, F.; Frechet, J. M. J. Latex-functionalized monolithic columns for the separation of carbohydrates by micro anion-exchange chromatography. *Journal of Chromatography A* **2004,** *1053* (1-2), 101-106.

26. Hutchinson, J. P.; Hilder, E. F.; Shellie, R. A.; Smith, J. A.; Haddad, P. R. Towards high capacity latex-coated porous polymer monoliths as ion-exchange stationary phases. *Analyst* **2006,** *131* (2), 215-221.

27. Hutchinson, J. P.; Zakaria, P.; Bowiet, A. R.; Macka, M.; Avdalovic, N.; Haddad, P. R. Latex-coated polymeric monolithic ion-exchange stationary phases. 1. Anion-exchange capillary electrochromatography and in-line sample preconcentration in capillary electrophoresis. *Analytical Chemistry* **2005,** *77* (2), 407-416.

28. Leaist, D. G. Coupled diffusion of weakly ionized poly-electrolytes - polyacrylic acids in water. *Journal of Solution Chemistry* **1989,** *18* (5), 421-435.

29. Connolly, D.; Victory, D.; Paull, B. Rapid, low pressure, and simultaneous ion chromatography of common inorganic anions and cations on short permanently coated monolithic columns. *Journal of Separation Science* **2004,** *27* (10-11), 912-920.

30. Connolly, D.; Paull, B. High-performance separation of small inorganic anions on a methacrylate-based polymer monolith grafted with [2(methacryloyloxy)ethyl] trimethylammonium chloride. *Journal of Separation Science* **2009,** *32* (15-16), 2653-2658.

31. Gjerde, D. T.; Fritz, J. S. Sodium and potassium benzoate and benzoic acid as eluents for ion chromatography. *Analytical Chemistry* **1981,** *53* (14), 2324-2327.

32. Ueki, Y.; Umemura, T.; Li, J. X.; Odake, T.; Tsunoda, K. Preparation and application of methacrylate-based cation-exchange monolithic columns for capillary ion chromatography. *Analytical Chemistry* **2004,** *76* (23), 7007-7012.

Chapter 6: Final conclusions and future work

In this Thesis nano-agglomerated polymer monoliths were prepared in capillary format for applications in catalysis and liquid chromatography. Photografting techniques were used to maximise the coverage of both spherical AuNPs and bimetallic Pd/Pt nano-flowers in an effort to improve the limited surface area of polymer monoliths. The grafting of either acrylates or methacrylates bearing reactive functionalities, followed by subsequent amination, resulted in the formation of free primary amine groups on the surface of the monoliths. Upon flushing nano-particle colloidal suspensions, a very dense and homogeneous metal nano-particle coverage was achieved which were retained via strong multi-point interations preventing the leaching of the nano-materials.

The catalytic conversion of NADH to NAD^+ was performed using Pd/Pt nano-flower agglomerated polymer monoliths using a ‘‘stopped flow’’ configuration demonstrating potential biological applications of these micro-reactors. Cells contain a limited supply of NAD^+ and NADH and unless this NADH is recycled to NAD^+, oxidative metabolism in this cell will cease for lack of an electron acceptor hence the nano-flower agglomerated monoliths could be used as efficient micro-reactors for this purpose. While a certain contact time between the nano-flowers and NADH is required for allowing the conversion to NAD^+, other catalytic reactions such as the reduction of ferrocyanide (III) were performed in direct flow-through mode at very high linear velocities (up to 50 mm/s). The complete reduction achieved demonstrated the high catalytic activity of the immobilised nano-flowers. Also C-C coupling reactions such as the Suzuki-Miyaura, Sonogoshira and Heck reactions, which are catalysed by palladium and platinum-based materials, are currently widely used in the pharmaceutical industry hence the micro-reactors here prepared could potentially be applied for performing these reactions in flow-through mode representing an advantage relative to currently adopted procedures which require the removal of catalyst after completion of the reaction for purifying the products.

Gold nano-particle agglomerated polymer monoliths were also prepared in capillary and pipette-tip formats and the catalytic properties were evaluated using the reduction of ferrocyanide (III) as a model reaction. The effect of nano-particle size was evaluated and related to catalytic efficiency since higher efficiencies were observed when smaller nano-particles were used. The ability to prepare these micro-

reactors in pipette-tip format could facilitate their integration with 96-well plate systems connected to robotic devices for high-throughput catalysis. Similarly capillary columns agglomerated with AuNPs can be integrated easily with LC systems for pre or post-column derivation if positioned upstream or downstream of an analytical column. For example the affinity of AuNPs for thiol or amino functionalities can be used for immobilising cysteine-based peptides which can then be derivatised and released, by flushing a solution of mercaptoethanol, towards the analytical column.

Quaternary ammonium functionalised polymer monoliths were also prepared as anion-exchange stationary phases and used as supports for facilitating the electrostatic immobilisation of silica nano-particles. These had been grafted with negatively charged poly(acrylic acid) groups allowing subsequent cation-exchange applications using a phthalic acid/ethyelenediamine eluent. Although limited ion-exchange capacities were achieved, nevertheless the modification with SiNPs allowed retention of cations such as Ca^{2+} and Mg^{2+} which demonstrated potential applications for environmental analysis of water samples. Previously the quaternary ammonium functionalised monoliths had been applied for the separation of Cl^- and $H_2PO_4^-$ which again could find similar environmental applications and, in the case of phosphate in particular, be applied towards the analysis of fertilizers. In any case further studies are required for evaluating the properties of these nano-agglomerated stationary phases upon variations in p*H* and concentration of the eluent.

In all instances, nano-agglomerated monoliths were characterised visually using FE-SEM. However, since FE-SEM requires the destruction of the sample, an alternative non-invasive technique, sC^4D, was applied as a characterisation tool to verify the presence of immobilised nano-particles on the surface. The ability to be operated in scanning mode, allowed the precise visualisation at mm intervals of the distribution of the immobilised nano-particles in the monolith. Recently C^4D has also been applied for the characterisation of monoliths in micro-fluidic channels hence the micro-reactors here prepared can be potentially integrated in such devices for the preparation of micro total analytical systems (μTAS) using sC^4D to verify the homogeneity of the nano-particle coverage.

In conclusion, the customisable chemical properties of polymer monoliths allowed the achievement of a very dense coverage of metal nano-particles on their surface by using photografting techniques. The nano-particle agglomerated polymer monoliths demonstrated applications as micro-reactors towards catalytic reactions by combining the catalytic properties of these nano-sized materials with the flow-through properties of polymer monoliths, due to their macro-porous structure, which make these types of stationary phases ideal supports for these materials. The interesting properties of metal nano-particles are currently being exploited in the areas of medicine, electronics and sensor devices hence the materials here developed have potential to be applied outside the confinements of catalysis and liquid chromatography.